Tampere University

MARKUS LAHIKAINEN

Advanced Control Strategies of Light-Responsive Polymers for Soft Robotics

MARKUS LAHIKAINEN

Advanced Control Strategies of Light-Responsive Polymers for Soft Robotics

ACADEMIC DISSERTATION
To be presented, with the permission of
the Faculty of Engineering and Natural Sciences
of Tampere University,
for public discussion in the auditorium Pieni sali 1 (FA032)
of the Festia building, Korkeakoulunkatu 8, Tampere,
on 1 October 2021, at 12 o'clock.

ACADEMIC DISSERTATION
Tampere University, Faculty of Engineering and Natural Sciences
Finland

Responsible supervisor and Custos	Professor Arri Priimägi Tampere University Finland	
Co-Supervisor	Dr. Hao Zeng Tampere University Finland	
Pre-examiners	Professor Yue Zhao Université de Sherbrooke Canada	Ph.D. Carlos Sanchez-Somolinos University of Zaragoza Spain
Opponent	Professor Jan Lagerwall University of Luxembourg Luxembourg	

The originality of this thesis has been checked using the Turnitin OriginalityCheck service.

Cover design: Roihu Inc.

ACKNOWLEDGEMENTS

ABSTRACT

Soft robotics is a rapidly developing research field that has triggered a significant amount of research effort during the past few years. The field aims at providing new technical innovations to overcome the challenges encountered in conventional hard-bodied robotic systems constructed using rigid joints and links, such as lack of flexibility and adaptability. Among the most promising materials for the fabrication of soft robots are smart stimuli-responsive polymers that can be triggered with external energy sources to undergo various chemical and physical changes such as mechanical motions like contraction or bending. Among different classes of stimuli-responsive polymers, photomechanical actuators are of particular interest as they provide a route to harness light energy to remotely fuel mechanical motions. Today, most photochemical actuators are based on reversible photochemical switching of photochromic molecules between two forms with distinct structural and photo-chemical properties. On the other hand, photoactuation can also be driven photothermally using light absorption by organic dyes or inorganic moieties for heat generation, which stimulates the shape changes of the polymer.

   In this thesis we use liquid crystal networks and hydrogels as materials platforms to devise photoactuators and soft robots that can be controlled and powered remotely with light producing reversible shape changes. Liquid crystal networks enable pre-programmable shape changes and hence several actuation modes can be achieved within one material. In hydrogels, complex shape changes can be programmed by tuning materials properties locally after fabrication. By utilizing both photothermal and photochemical effects, we use three advanced light control strategies to power photomechanical actuation: self-sustained motion, multicolor functions, and reconfigurability. By using these strategies, we demonstrate sophisticated photoactuators exhibiting self-oscillation, non-reciprocal motions, logic gate actuation, reconfigurable gripping, and shape-morphing between Gaussian curvatures. The results of this thesis deepen the understanding on the role of photothermal and photochemical effects in controlling photomechanical actuation, and present new pathways and control strategies for soft micro-robotics.

TIIVISTELMÄ

Pehmeä robotiikka on nopeasti kehittyvä tutkimusala, mikä pyrkii tuottamaan uusia pehmeisiin materiaaleihin pohjautuvia ratkaisuja nykyisin käytössä oleville metallikuorisille roboteille, joiden liikettä ohjataan sähköllä elektronisten komponenttien avulla. Lupaavimmat materiaalit pehmeiden robottien valmistuksessa ovat "älykkäät", ulkoisiin ärsykkeisiin reagoivat polymeerit, joiden liikettä voidaan ohjata käyttämällä polttoaineena valoenergiaa. Nämä niin sanotut valoaktuaattorit pystyvät absorboimaan valoenergiaa ja muuttamaan sen avulla muotoaan. Tyypillisen valoaktuaattorin toiminta perustuu valokemialliseen ilmiöön, eli ne sisältävät valoon reagoivia molekyylikytkimiä, joiden muotoa ja muita ominaisuuksia voidaan muuttaa valon avulla. Toinen tapa perustuu valotermiseen ilmiöön, jossa esimerkiksi orgaaniset molekyylit absorboivat valoa, muuttavat sen lämpöenergiaksi ja edelleen mekaaniseksi liikkeeksi.

Tässä väitöskirjassa valoaktuaattorien ja pehmeiden robottien valmistuksessa käytetään kahta erilaista materiaalia: nestekidepolymeerejä ja hydrogeelejä. Nestekidepolymeerit mahdollistavat ennalta ohjelmoitavan muodonmuutoksen, jolloin saman materiaalin avulla pystytään tuottamaan erilaista liikettä. Hydrogeeleissä monimutkaiset muodonmuutokset voidaan ohjelmoida muuttamalla materiaalin ominaisuuksia paikallisesti polymeerin valmistuksen jälkeen. Molemmat materiaalit kykenevät reversiibeliin muodonmuutokseen valoenergian avulla ja ovat siksi erinomaisia materiaaleja pehmeässä robotiikassa. Hyödyntämällä sekä valotermistä että valokemiallista ilmiötä, tässä väitöskirjassa tutkitaan kolmea ohjausstrategiaa valoaktuaation aikaan saamiseksi: 1) itse ylläpidettyä liikettä kuten valomekaanista oskillaatiota, 2) moniväriaktuaatioita, jossa käytetään valon eri aallonpituuksia tuottamaan erilaista liikettä, ja 3) uudelleenohjausta, jossa aktuaattori voidaan valmistuksen jälkeen ohjelmoida liikkumaan eri tavoin. Tämän väitöskirjan tulokset syventävät ymmärrystä valotermisen ja valokemiallisen ilmiöiden roolista valoaktuaatiossa ja tarjoavat uusia ohjausstrategioita pehmeille roboteille.

CONTENTS

ABBREVIATIONS AND SYMBOLS

AIBN	Azobisisobutyronitrile
azo	Azobenzene
CD	Cyclodextrin
DEA	Dielectric elastomers
DMD	Digital micromirror device
EAP	Electroactive polymers
GLCN	Glassy liquid crystal networks
IEP	Ionic electroactive polymer
LbL	Layer-by-Layer
LC	Liquid crystals
LCD	Liquid crystal display
LCE	Liquid crystal elastomer
LCN	Liquid crystal network
LCST	Lower critical solution temperature
LED	Light-emitting diode
Mc	Merocyanine spiropyran
McH^+	Protonated merocyanine spiropyran
NIR	Near infrared
PNIPAm	Poly(N-isopropylacrylamide)
POM	Polarized optical microscope
SCP	Shape-changing polymer
SMP	Shape-memory polymer
Sp	Spiropyran
UCST	Upper critical solution temperature
UV	Ultraviolet
a	Coefficient of thermal expansion
β	Angle between mesogen and the local director
ε	Dielectric permittivity
θ	Out-of-plane bending angle

Φ	Twisting angle
d	Displacements
E	Young's modulus
K	Gaussian curvature
$\boldsymbol{n}$	Local director of liquid crystals
P	Pitch length
S	Order parameter
T_g	Glass transition temperature

ORIGINAL PUBLICATIONS

Publication I   Zeng, H.; Lahikainen, M.; Liu, L.; Ahmed, Z.; Wani, O.M.; Wang, M.; Yang., H; Priimagi, A. Light-Fuelled Freestyle Oscillators. *Nature Communications*, **2019,** *10*, 5057.

Publication II Lahikainen, M.; Zeng, H; Priimagi, A. Design Principles for non-reciprocal photomechanical actuation. *Soft Matter*, **2020**, *16*, 5951-5958.

Publication III Lahikainen, M.; Zeng, H.; Priimagi, A. Reconfigurable Photoactuator Through Synergistic Use of Photochemical and Photothermal Effects. *Nature Communications*, **2018**, *9*, 4148.

Publication IV Lahikainen, M.; Kuntze, K.; Zeng, H.; Helantera, S.; Hecht, S.; Priimagi, A. Tunable Photomechanics in Diarylethene-Driven Liquid Crystal Network Actuators, *ACS Applied Materials & Interfaces*, **2020**, *12*, 47939-47947.

Publication V   Kuenstler, A.S.; Lahikainen, M; Zhou, H.; Xu, W.; Priimagi, A.; Hayward, R.C. Reconfiguring Gaussian Curvature of Hydrogel Sheets with Photoswitchable Host-Guest Interactions. *ACS Macro Letters*, **2020**, *9*, 1172-1177.

AUTHOR'S CONTRIBUTION

The thesis consists of five peer-reviewed articles. The main work for **Publications I-IV** was done at Hervanta Campus of Tampere University, while the work related to **Publication V** was done at the University of Massachusetts, Amherst, during a 3-month research internship by the author.

Publication I   This publication presents a light-fueled liquid crystal network which exhibits self-oscillation with multiple oscillation modes, including contraction-expansion, bending, twisting, and a "freestyle" mode. M. Lahikainen took part in an execution of experiments, fabrication of the samples, characterization of the materials used, analysis of oscillation behavior, and contributed to writing the manuscript.

Publication II   This publication deals with non-reciprocal motion, a characteristic central in locomotion of the various natural species, in light-fueled liquid crystal network actuators. We invoke photothermal and/or photochemical actuation strategies to distinctly control different parts of the actuators, yielding non-reciprocal motion patterns through sequential switching of different illumination wavelengths. M. Lahikainen took part in planning the research, performed all the experiments, analyzed the data, and wrote the first draft of the manuscript. The manuscript was finalized together with the coauthors.

Publication III   In this publication, we show that photothermal and photochemical effects can be used synergistically in stimuli-responsive liquid crystal networks, in order to fabricate photoactuators with reconfigurable shape morphing. The reconfigurable actuators are further utilized in devising a light-fueled smart gripper. M. Lahikainen took part in planning and execution of the experiments, fabricated and characterized all the samples, performed the data analysis, and contributed to writing the manuscript.

Publication IV   In this publication, we incorporate photochromic diarylethene crosslinkers into liquid crystal networks and devise a photomechanical actuator whose light responsivity can be tuned by the electrocyclization reaction. The actuator is demonstrated to exhibit AND gate logics, associating two optical inputs with a material deformation as an output. M. Lahikainen took part in planning the research, performed all the actuation experiments, fabricated the samples, analyzed the data, and wrote the first draft of the manuscript. The manuscript was finalized together with the coauthors. M. Lahikainen also supervised the laboratory work of an undergraduate student S. Helanterä.

Publication V   In this publication, we present a method to program and re-program curvatures in hydrogel sheets. Through controlling the interactions between pendent azobenzenes and free alpha-cyclodextrin macrocycles via photoisomerization, we locally pattern hydrophobicity/swelling endowing arbitrarily designed curvatures. M. Lahikainen took part in research planning and performed the sample fabrication and data analysis together with A. Kuenstler. M. Lahikainen and A. Kuenstler wrote first the draft of the manuscript. The manuscript was finalized together with the coauthors.

1 INTRODUCTION

"Robot", a term originating from science fiction, was first introduced in 1920.[1] In the past hundred years, engineers have brought the vision from machines which make our life easier into reality through the development of a vast range of applications. Today's robots are often associated with hard-bodied machines containing rigid joints and links. One advanced example is the *Atlas* robot from Boston Dynamics.[2] The robot is constructed with 28 hydraulic actuators, and it can walk, run, dance, and even perform a somersault with 360° turn. One of the important characteristics of present-day robots is the capacity of being programmed to perform tasks such as lifting objects, cutting sheets in factories, and growing crops in the farm. For a long time, engineers have dedicated their efforts to perfect the electronic elements in conventional robots, to build up more reliable and precise control strategies to reach a higher level of sophistication and to boost the movement speed of the robotic devices.[3]

However, because of the growing needs for human-robot interfacing, new concerns are raised. First, one great challenge for a hard-bodied robot is safety. Even a small malfunction or inaccuracy of the robotic movement can cause severe injuries to people nearby. Therefore, for example, human labor and the tasks executed by robots are often separated in factories to prevent accidents. Second, hard-bodied robots are typically of large size. Nowadays it is possible miniaturize the size of power sources, control circuits and sensors down to few centimes, but not to millimeter scale or below. Downscaling would be needed in actions where robot's small size is essential such as searching people from collapsed buildings or performing operations inside human body.[4,5] Third, in natural conditions, i.e., outside factory production lines, the environment of the robot is continuously changing, and the robotic action cannot be based on pre-programming. Instead of being only a "dull" labor alterative for human, robots must learn to adapt to their surrounding environment and take actions accordingly. This novel robotic concept is strongly inspired by biological species[6] — robots need to adapt, sense their environment, and even make decisions and learn. In other words, the robots of tomorrow must be "smart" and capable of advanced functionalities.

To overcome the above-mentioned challenges encountered in conventional hard-bodied robotic systems, scientists have tried to replace the hard parts with soft materials. As a result, soft robotics has been an emerging research field in the past decades.[7–9] According to Web of Science over 5500 scientific articles related to soft robots have been published in past ten years, collecting over 80,000 citations. Soft robots provide extra degrees of freedom for actuation, hence greatly simplifying many task executions that are very difficult for traditional robots, such as grasping a fragile object with a non-regular shape, squeezing into a narrow space, or passing obstacles. Getting rid of hard components also render soft robots safe for humans, unlike their hard-bodied counterparts. Regarding the materials used for soft robotic actuation, majority of the research focuses on pneumatic/hydraulic actuators that provide large shape changes and deformation flexibility determined by the amount of input pressure.[10,11] However, these methods rely on wire or tube connections in energy delivery and/or robotic control, posing great hurdles for device miniaturization. To realize a miniature soft robot, much effort is needed to scale down the actuators, control circuitry, and power sources, and to integrate all of them within the dimensions of a few centimeters or below.[12] Such miniaturized robots may have applications for instance in the fields of cell manipulation, drug delivery systems and microfluidics,[13,14] yet miniaturization remains as one of the grand challenges in soft robotics. To address this challenge, an attractive alternative is to use stimuli-responsive materials[15,16] which can alter their physical and chemical properties upon exposure to external energy sources. Stimuli-responsive materials can be powered with, *e.g.*, heat, magnetic, electric or acoustic field, humidity or light.[17–23] Using external stimulus to power the robotic movement removes the need for wires and integrated power sources in the robot's body, helping not only in robot miniaturization but also in making the robot more adaptive to the environment. As stimuli-responsive materials change their properties in response to changes in environmental conditions, they may allow robots to sense and adapt to their surroundings. Among the different stimuli that can be used to power stimuli-responsive materials, light has many attractive features as it is clean and non-toxic and provides a wireless powering approach with no physical contact between the energy source and the material.

In this work we develop new types of wireless soft actuator systems with an overall size in the millimeter-centimeter range. Using these materials, we realize micro-robotic systems that are endowed by rigorously designed actuation modes driven by external feedback received from the light field and built-in responsive function of the material.

Among different classes of light-responsive materials, polymers stand out as particularly attractive.[16,24] Polymer materials can be either hard or soft, glassy or elastic, depending on their physical properties and chemical structures, hence enabling great flexibility in material design and, in the context of soft actuators, the diversity of mechanical motions obtained. Photomechanical polymeric actuators offer an interesting route to harness light energy to fuel mechanical motions,[25] thus providing a solid pathway towards light-driven soft micro-robots. Among the variety of polymer materials that can deform under light stimulus, we have chosen two systems: liquid crystal networks (LCNs) and hydrogels. LCNs are crosslinked polymers containing liquid crystal molecules. They provide the orientational order of liquid crystals in highly deformable solid-state materials, allowing large light-induced anisotropic deformations to be achieved.[26] Hydrogels, on the other hand, are hydrophilic crosslinked polymers capable of holding a large amount of water in their network. The water-holding capacity of the hydrogels can vary in response to environmental change, leading to material swelling/shrinkage and thus 3D-deformation.[27] In this study, the stimuli-responsive behavior of both classes of materials are designed, programmed and utilized to obtain complex structural deformation and advanced control strategies for soft robotics.[28]

1.1   Aim and scope of this work

Fabrication of polymeric actuators capable of sophisticated stimuli-responsive movements when powering with light energy forms the core of this thesis. This thesis contributes to the field of soft micro-robotics by introducing advanced concepts and design principles based on 1) self-sustained oscillation, 2) distinct responses to different colors of light, and 3) reconfigurable photo-deformation. The connection between the advanced control strategies and the publications comprising this study is shown in Fig. 1.1.

Self-oscillator is a stimuli-responsive structure that can sustain periodic motion without a need to control the periodicity of the power source (Concept 1). In **Publication I**, we report light actuators exhibiting self-oscillation with three basic oscillation modes: contraction-expansion, bending and twisting. Particularly, we device a freestyle self-oscillator, that combines many oscillation modes within a single structure. The self-oscillation phenomenon is further studied in **Publication II** where we show that self-oscillation can be designed to occur non-reciprocally.
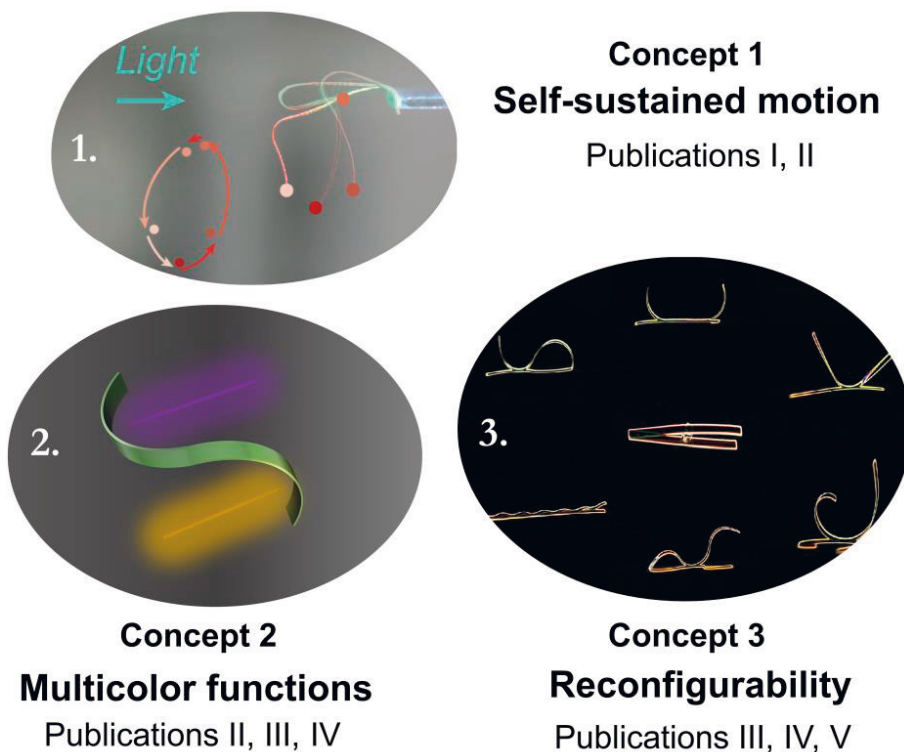
Figure 1.1 The three advanced control strategies to drive photoactuation used in this thesis, and their connections to the thesis publications.

To achieve advanced light-control strategies for soft robotics, we fabricated LCNs capable of distinct responses to different colors of light (Concept 2). In **Publication II**, actuators are fabricated with two segments responding to different wavelengths of light. Parallel control of these actuators resulted in non-reciprocal movements, which is essential for complex robotic locomotion. In **Publication III**, we utilize photothermal and photochemical effects in a monolithic actuator strip and show that these two mechanisms act synergistically and lead to enhanced deformability. In **Publication IV**, a novel light control method is achieved by using diarylethene crosslinkers in LCNs, where the light controllability in visible wavelengths is fine-tuned by UV-induced absorption changes of the material.

This work also studies one of the grand challenges in photoactuation and soft robotics: reconfigurability (Concept 3). Reconfigurable photoactuators can respond to an identical stimulus in different ways, through a re-programming process conducted after fabrication. In **Publications III** and **V,** we used patterned light field to control azobenzene isomer distribution to achieve distinct deformation

geometries in LCNs, and reconfigure arbitrary curvatures in hydrogel sheets, respectively. In **Publication IV**, the light sensitivity is reconfigured using all-optical control of the diarylethene photochrome.

1.2   Thesis structure

This thesis is divided into 5 chapters. Chapter 1 provides the introduction and motivation of this work, formulating the aims of the study. Chapter 2 provides background information on stimuli-responsive polymers used for the study. The focus lies in liquid crystal networks and stimuli-responsive hydrogels, covering common approaches for their preparation and characterization.

Chapter 3 deals with photomechanical deformation (actuation). The chapter starts with a discussion of the types of light-triggered LCN shape changes, followed by more detailed description of the mechanisms, i.e. photothermal actuation based on light-absorbing agents and photochemical mechanisms where azobenzene or other photochromic molecules are utilized. Moreover, a comparison between photothermal and photochemical actuation strategies is elaborated. Finally, light-induced shape-morphing is discussed from the hydrogel viewpoint.

Chapter 4 highlights the key results of the publications comprising this thesis. Detailed discussion is provided along the three key focal concepts outlined above: self-sustained photoinduced motions, distinct response to different wavelengths of light, and reconfigurability, attempting to address the advances these concepts can bring to the context of soft photoactuators.

Chapter 5 summarizes the results of the thesis and provides future prospects for the fields of photoactuation and soft robotics.

2 ARCHITECTURES OF STIMULI-RESPONSIVE POLYMERS

Stimuli-responsive polymers can respond reversibly to one or many stimuli like heat, pH, optical, electric or magnetic fields, humidity, chemical additives, and so on.[16] Polymeric materials offer a range of benefits such as the flexibility of polymer backbone (to form materials from hard plastics to soft elastomers), designable functional groups and possibility to incorporate different kinds of responsive elements into their structure. Stimuli-responsive polymers are considered to be excellent candidates in applications like controlled drug delivery, sensing, tissue engineering, responsive coatings, artificial muscles and soft robotic systems.[28,29] In this chapter, we introduce distinct classes of stimuli-responsive polymer systems and their key characteristics. We will particularly concentrate on two types of polymer systems capable of shape changes in response to external stimulus: liquid crystal networks and hydrogels. We will start from the historical background, followed by actuation mechanisms, and finally elaboration on relevant fabrication approaches.

2.1 Stimuli-responsive polymers

Polymers can be found everywhere, as each of us is dealing with plastics-containing daily products like water-bottles, cell phones, clothes, etc. Even though polymers are often used as a synonym for plastics, they widely exist also in living organisms. For instance, rubber and cellulose or DNA and proteins, responsible for life, are natural polymers. The utilization of polymers dates back all the way to ancient Egypt where people started using papyrus for writing. However, the chemical nature of polymers was unknown until the 20th century and the work of Hermann Staudinger.[30] Staudinger predicted that polymers contain smaller elementary units called monomers. These monomers can be polymerized, i.e., linked with covalent bonds to form long macromolecular chains, which can further associate with each other via chemical or physical interactions. Shortly after this discovery, the first synthetic polymer, Nylon, was fabricated in 1935 by Dupont.[31] Triggered by these pioneering findings, researchers have been making groundbreaking advances in the field of

polymer science and a huge amount of different polymers with diverse chemical, mechanical, electrical and optical properties have been synthesized. Polymers appear in various morphologies and they can be produced in the form of linear (homo- or co-) polymers, block copolymers or dendrimers; they can form micelles or capsules via self-assembly. Polymers may be anchored to a surface, generating single/mixed polymer brushes, films, and layer-by-layer (LbL) assemblies. 3D polymer networks can also be generated using chemical or physical crosslinking.

The fast growth of polymer research led also to the development of responsive polymers. Those materials can respond to their environment by altering their chemical and/or physical properties, referred as stimuli-responsive polymers from now on.[32,33] In these polymers, the stimuli-responsiveness arises from activation of the functional groups or other responsive elements/domains inside the polymer matrix. When stimuli-responsive polymers meet specific inputs, they undergo structural and conformational change which is then accompanied by variation in their physical properties. In the past decades, many stimuli-responsive polymer systems have been studied with fine-tuned morphologies, utilizing various inputs, and producing wide range of outputs, targeting various applications as illustrated in Fig. 2.1. Rather than giving a comprehensive overview, we direct readers to these reviews[16,33–35], and give here only some state-of-the-art examples of applications to show the multiplicity of the field of stimuli-responsive polymers.

Probably the most primitive example of stimuli-responsive polymers is the one exhibiting temperature dependence. A phase transition, a feature causing change in the polymer chain conformation at the solvation state,[36] was first demonstrated in the 1960s with Poly(N-isopropylacrylamide) (PNIPAm).[37] PNIPAm exhibits a lower critical solution temperature (LCST), above which de-mixing occurs between polymer chains and aqueous solution, yielding phase separation. Today, PNIPAm can be functionalized with various elements having responses to different stimuli (i.e. pH, ionic strength or light), and developed into materials exhibiting various outputs, such as changes of color, wettability, cell interfacing, etc.[33]

The stimuli-responsive polymers can convert stimulated inputs to readable outputs which makes them suitable to sensor applications. In this context, polymer surfaces with modified nanoparticles or nanocrystals have been attractive choices due to tunable quantum effects they possess.[35] Stimulated conformational change of the polymers modifies the chemical environment of the attached particles and therefore changes the optical properties of the polymer matrix. For example, polymers functionalized with pH-responsive molecules can change light absorption and/or emission through pH-modified surface plasmon resonance of gold

nanoparticles[38] or Förster resonance energy transfer of quantum dots.[39] Also, polymer sensors capable of detecting biological species have been demonstrated. In this case, enzymes produced from bacteria[40] or urea[41], are often involved in polymer responsiveness to detect the quantity of species.
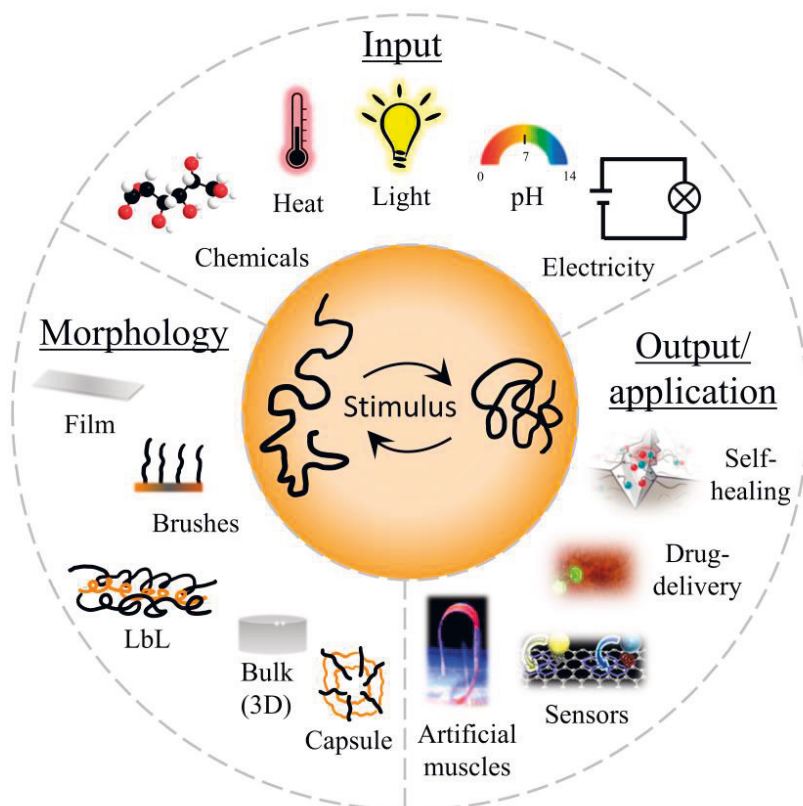
Figure 2.1 Stimuli-responsive polymers. Polymer structural and conformational change under specific stimulus leading different outputs/applications. Figures in Output/application reproduced with permission: Self-healing[42], Copyright 2010, Annual Reviews. Drug delivery[43], Copyright 2006, John Wiley and Sons. Sensors[39], Copyright 2014, ACS. Artificial muscles[44], Copyright 2009, RCS.

As stimuli-responsive polymers can also be made biocompatible, they have been used extensively in bio-medical applications like drug delivery.[24] In stimuli-controlled drug delivery, polymer structure is deemed to survive *in vivo* and *in vitro*, deliver the cargo and release the drug into the targeted cells. To this extent, polymer capsules and nanofibers have been extensively used. They can, for instance, grab the drug cargos, protect it inside the human body, and release the drug under specific stimuli

(temperature, pH, light)[43] or the presence of biological substances (high sugar or allergens level).[33]

Another interesting application is the capacity of self-healing. Self-healing polymers can recover their properties such as elasticity or surface smoothness, after the structure has been physically damaged.[45] This capacity is usually induced by re-formation of chemical bonds under stimulus, and it can be realized by several chemical mechanisms like interchain diffusion, covalent bond re-formation or post-curing of thermoplastic polymers.[42] For example, light input has been used to design optically healable supramolecular rubbery polymer, in which the polymer recovers after activating the metal-ligands by UV exposure.[46] In another example, a LbL assembly of polyelectrolytes on a metal surface provides a mechanism for corrosion protection: after detection of corrosive ions, the polymer releases inhibitors, buffering the pH of the corrosive area and self-curing of the polymer film, enabling self-healing activity.[47]

Finally, by targeting applications in the regime of soft robotics, stimuli-responsive polymers able to change their shape under an external stimulus, referred to soft actuators or artificial muscles, are of great interest. These polymers can produce similar or even higher stains and stresses than natural muscles, and provide sophisticated control over shape-morphology.[48] In the following, we will introduce macromolecular robotic actuator systems based on crosslinked polymers, and elaborate the topic of soft robotics in the next section.

2.2 Stimuli-responsive polymer actuators

Dynamic shape deformations are frequently observed in nature across both animal and plant kingdoms. In animals, the most distinct feature is the ability to move their limbs and create mass translocation (locomotion) powered by muscles that translate the energy received from biochemical fuels into mechanical output (contraction/expansion). Plants, in turn, can reversibly re-shape their geometry via, for example, osmotic pressurization or hygroscopic swelling; common example being Venus flytraps that close upon mechanical triggering.[49] Both animal and plant kingdoms have provided an endless source of inspiration for engineering stimuli-responsive polymer actuators and artificial muscles that can be further developed into concrete soft robotics applications.[49,50]

Conventionally, stimuli-responsive polymer actuators can be divided in two classes: shape-changing polymers (SCP) and shape-memory polymers (SMP).[51] The

main difference between SCP and SMP lies in the distinct shape-changing kinetics. SCPs usually deform gradually if they are subject to specific stimuli, heat being the most common one, and restore their original form when the stimulus is stopped. Such shape change is usually reversible and can be cyclically performed. Conversely, SMPs are programmable materials with temporary shapes (bent, twisted, or folded), by processing the polymer above its transition (glass transition or melting) temperature followed by a cooling process.[52] This temporary shape is maintained until the stimulus is applied (e.g. heated above transition temperature) to induce the recovery of structure. A major advantage of SMPs over SCP is their reversible and reconfigurable deformability, which enables them to deform in multiple shapes but usually deteriorate in response to repeated actuation cycles.

Many stimuli-responsive polymer systems are realized based on above mechanisms. In earliest demonstrations, polymer actuators with bilayer structures exhibited bending deformation due to different thermal expansion coefficients between the layers.[35] In this configuration, one layer can be stimuli-responsive while the other may be passive, and different thermal strains between the layers cause bending of the structure. Depending on the layer material, e.g. SCP or SMP, bending deformation can be performed in programmable or reversible fashion. However, this approach often suffers problems associated with poor adhesion between the layers and is limited in the forms of actuation. Thus, there is a need to investigate novel actuator systems with versatile shape morphing and prolonged mechanical stability.

Electroactive polymers (EAP) is one of the most popular class of soft actuators,[17] as they can generate large deformation and forces, thus mimicking the working mechanism of human muscles that are also triggered by electrical signals and induce contraction. EAPs can be divided into two categories: dielectric elastomers (DEA) and ionic electroactive polymers (IEP). The working mechanism of DEA is similar to capacitors – they can be fabricated by coating polymer surface with charged materials (carbon grease or graphite) or by deposition of compatible electrode to sandwich the polymeric film.[53] Under an electrical field, the polymer surfaces attract each other, pressing the structure and resulting in contraction along the thickness of the actuator. IEPs, on the other hand, are constructed in a way that the material itself is sensitive to the electric field. For instance, the polymer matrix can be swollen within ionic solution or doped with carbon nanotubes to attain the electric sensitivity and shape-deformation under the electric field.[54] However, even if used extensively in soft robotic applications, EAPs have an obvious problem: they rely on high

voltages which limits their tunability, working environment and miniaturization possibilities.

Two classes of specific stimuli-responsive actuators have been receiving significant attention these days: liquid crystal networks (LCN) and hydrogels. They can produce large, complex, and controllable deformation by reacting to a wide variety of stimuli like heat, pH, light, and humidity. Moreover, controlled deformation can be achieved in various environments like in air, water or even inside the human body. These two actuator systems form the focus of this thesis and are discussed in more detail in the following sections.

2.3   Liquid crystal networks

In this section, the most relevant class of stimuli-responsive polymer actuators for the thesis, liquid crystal networks (LCNs), is discussed. Before going to details of the shape-changing mechanism and fabrication process of LCNs, liquid crystals (LCs) are briefly introduced.

2.3.1   Liquid Crystals

Liquid crystals are common to every household because of the liquid crystal displays (LCD) used nowadays on smart phones and TV screens. As the name implies, LCs possess properties that are intermediate to those of liquids and crystalline solids. This is the reason why the LC phases are often denoted as mesophases. Liquid crystals can flow like liquids, but still have orientational anisotropy, meaning that their physical (optical, electrical) properties are direction-dependent.[55] The LC mesophases can exist at a specific concentration (lyotropic) or temperature (thermotropic) range. Molecules forming lyotropic mesophases are usually amphiphilic (one end is hydrophobic and another hydrophilic), and the LC phase arises from the interaction between the LC molecules with a suitable solvent. As thermotropic LCs are the focus in this work, lyotropic LCs are not covered further.

Molecules which can form thermotropic LC phases are called mesogens. The most typical forms of the mesogens are rod-like (calamitic), as used in this work, and disc-like (discotic) shapes.[56] Today, hundreds of molecules can form LC phases, however they are sharing some basic characteristics and some common structural features, as shown in Fig. 2.2a. A typical rod-shape mesogen (Fig 2.2b) have two or

three rings (often six-membered ring, e.g., phenyl-ring) connecting directly to each other or through a linking group. This structure provides rigidity and linearity, both important factors for formation of LC phases. The linking groups increase the length of the molecules, while preserving the linear shape. Some linking groups (e.g. azo) can be photo-switched, enabling their use for optically controlled LC phases (Fig. 2.2c). Second important factor is the end-group. Long alkyl (C_nH_{2n+1}) or alkoxy ($C_nH_{2n+1}O$) chains or polar groups (CN, Cl, F) stabilize the anisotropy of the structure and affect the melting point. Moreover, the end-group can contain functional groups (e.g. acrylates) which can be polymerized to form liquid crystal polymers (Fig. 2.2c), discussed further in the next section.
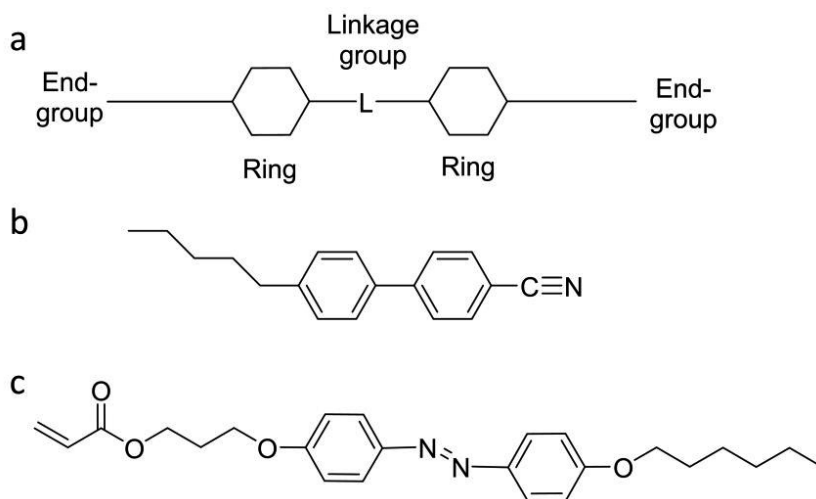
Figure 2.2 a) A basic structure of the rod-shaped LC molecule; b) chemical structure of a common LC molecule, 5CB; c) LC molecule having azo linkage group and an acrylate end-group.

In thermotropic liquid crystals, the LC phase occurs within specific temperature range below isotropic but above crystalline state, depending on chemical nature and physical properties of the mesogens. Thermotropic LCs can be divided into different categories, depending on the type of molecular orientation, and whether positional order of the molecules is present. In a general case, when elevating the temperature, smectic mesophases firstly appear, followed by nematic and eventually isotropic phase (Fig. 2.3).[57] A material can have one or more LC phases. In Smectic LC phase, molecules have both long-range positional order in the parallel direction to the layers' normal, and orientational order, while in nematic LCs only orientational order is present.[58] Smectic phase is also divided into subcategories according to how the mesogens are oriented with respect to the layers' normal or the plane. For instance,

Smectic A shows molecular director in the direction of the layer normal, and in Smectic C the molecules are tilt with respect to the layer normal. The scalar order parameter (S) states about the orientational order present in the material, providing an average over the orientation of all the molecules in the assembly. It can be defined by the following equation:

$$S = \frac{1}{2} <3 \cos^2 \beta - 1> , \qquad (1)$$

where β is angle between the local director (n) and the long axis of LC molecule, and $<.>$ is the average sign. The order parameter can vary between 0 (amorphous material) and 1 (perfectly ordered material). Typical value for nematic LCs is around 0.6. The order parameter of nematic LCs decrease gradually with increasing temperature and drops to zero when nematic-isotropic phase transition occurs, as predicated by Landau-de Gennes theory.[58]
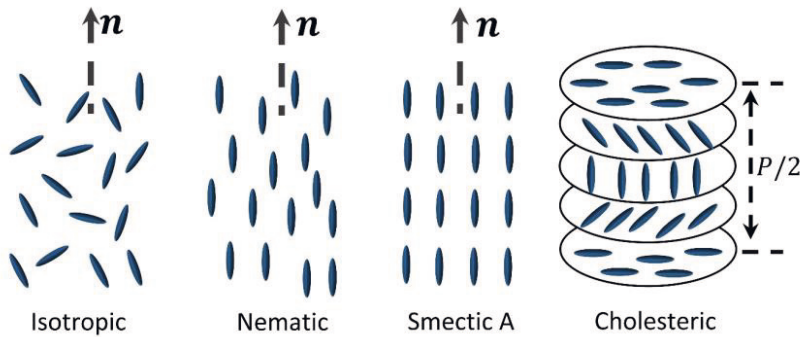
Figure 2.3 A schematic showing orientation of the molecules in isotropic liquid and common liquid crystal phases.

One special LC phase is the cholesteric mesophase, which is formed when nematic LC is doped with chiral molecules. Chirality causes a helical rotation of the molecules along an axis perpendicular to n. Along the helical axis the cholesteric mesophase shows periodic behavior. The periodicity is dictated by the length in which the helix completes a full 360° rotation, known as the pitch, P. The pitch determines the wavelength of light that is reflected through Bragg conditions. Typical cholesteric LCs have a pitch length of hundreds of nanometers, comparable to wavelengths of visible light.[59] As the pitch length can also vary with temperature, cholesteric LCs exhibit distinct colors at different temperatures.

As LC orientation is anisotropic, its dielectric, magnetic and optical (birefringence, dichroism) properties are direction-dependent.[60] Dielectric anisotropy allows different values of dielectric permittivity in directions parallel ($\varepsilon_{\parallel}$) and perpendicular ($\varepsilon_{\perp}$) to $\boldsymbol{n}$. If the LC has positive dielectric anisotropy ($\varepsilon_{\parallel} > \varepsilon_{\perp}$) the molecules align their long axis parallel to the electric field direction. Materials with negative dielectric anisotropy would align perpendicular to the electric field. In terms of optical properties, anisotropic features result to the refractive index of the material differing for the light polarized in directions parallel or perpendicular to $\boldsymbol{n}$.[61] Therefore, light polarization can be modulated when passing through LC assemblies when not parallel or perpendicular to the director $\boldsymbol{n}$. The anisotropic electrical and optical properties lie behind the basic working principles for LCDs and other electro-optic devices.

Orientational order and anisotropy of LCs are also responsible for their elastic properties. Because of their low viscosity, the LC order can be destructed with external stimulus (electric, magnetic, and light fields), but once the stimulus is removed, the mesogens return to their initial state to release the stored elastic energy. This property can be translated to the macroscopic mechanical deformation of the material in liquid-crystalline polymers, a feature which will be elaborated in the next section.

2.3.2   Construction of LCNs from LC molecules

To translate the anisotropic properties of LCs into solid polymers, the LC phase must be "frozen-in" by polymerization of the LC mixture to form solid, stimuli-responsive materials (Fig. 2.4a). To achieve this, LC mesogens must contain chemical groups that allow polymerization, e.g. acrylates, methacrylates, thiols or epoxy groups. Historically, (meth)acrylate polymerization was firstly predicted by de Gennes[62] in 1975 and synthesized by Finkelman[63] in the beginning of the 80s, about 100 years after the discovery of the liquid crystals. Polymer networks which exhibit liquid crystallinity have been referred by many names, depending on the crosslinking density, Young's modulus (E) and glass transition temperature (T_g) of the polymer.[68] The most common ones are glassy liquid crystal networks (GLCNs, densely crosslinked, $E > 0.2$ GPa) and liquid crystal elastomers (LCEs, loosely crosslinked, $E \sim 1$ MPa).[26] In this thesis we will use the term LCN to refer to both polymer types unless otherwise stated.
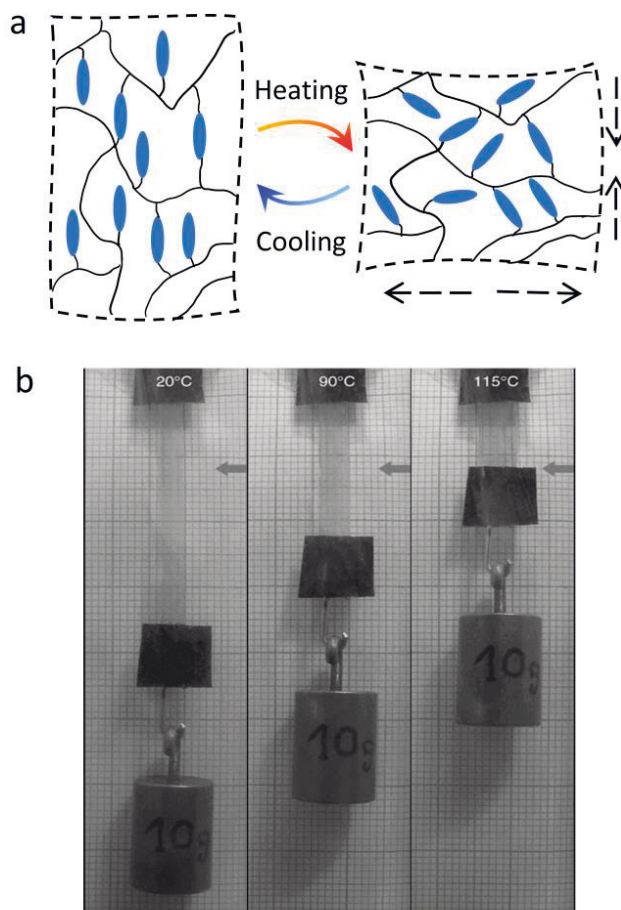
Figure 2.4 a) A schematic illustration of heat-responsive elongation-contraction of a uniaxially aligned LCE. **b)** Thermomechanical contraction of the LCE along the director lifting 10 g weight.[64] Figures reproduced with permission: **b)** Copyright 2010, John Wiley and Sons.

LCNs are crosslinked polymer networks that combine polymer elasticity with the orientational anisotropy of LC phases. After crosslinking, the polymer chain conformation correlates directly with the macroscopic shape of the entire structure which can be changed upon external stimuli such as heat, pH, light, moisture and electric or magnetic field.[65] All LCNs are naturally thermoresponsive but their shape-changing mechanisms upon heating/cooling may differ.[66] In rubbery LCN (or LCE), the T_g is below room temperature and the LC mesogens and polymer chains are coupled, leading to an ability of large-magnitude reversible shape change upon heating-cooling cycles.[67] At low temperature (in LC phase, usually nematic), the LC mesogens are aligned in a specific direction pre-determined during the fabrication,

and the polymer chains are elongated and connected to each mesogen. An increase in temperature elevates the average β, and thus lowers S (Eq. 1), until the molecular order is lost, and the isotropic state reached. At this state, the polymer chains exhibit random-coil conformation driven by entropy (Fig. 2.4a),[64] which leads to the macroscopic deformation. This muscle-like shape change is called thermomechanical actuation, and a substantial strain is often observed parallel to the LC director (Fig. 2.4b).[68] Conversely, for densely crosslinked LCNs (or GLCNs) that have T_g above room temperature (typically 40-120 °C), the LC moieties mostly maintain their orientation/alignment upon even substantial heating.[69] Here, thermomechanical actuation arises from anisotropic thermal expansion, characterized by the coefficient of thermal expansion (α).[26] In aligned GLCNs, α depends strongly on the alignment direction, being positive perpendicular to the director and negative parallel to it. Upon heating, the GLCN expands perpendicular to $\textbf{\textit{n}}$, thus by controlling the LC alignment distribution through the thickness of the material or inscribing in-plane variations, significant bending and other 3D shape deformations can be observed, as will be discussed in more detail in Chapter 3. It is worth noting that in some cases it might be difficult to distinguish between LCE and GLCN, as both phase transition and thermal expansion may contribute to the overall deformation, due to the fact that the material is often thermally actuated across a broad temperature range (from room temperature to above two hundred degrees Celsius).[70,71]

Conventionally, LCNs are prepared via two different approaches: 1) two-step reaction utilizing polymeric (typically siloxane based) and/or monomeric precursors and 2) one-step method using only monomeric precursors. The two-step method was invented by the Finkelmann Group.[63] In this method, the prepared precursors are loosely crosslinked, and some amount of mechanical stretching (Fig. 2.5a), or sometimes use of electric/magnetic fields,[72] is needed to align the mesogens. The created LC alignment is then fixed by secondary crosslinking step to form stabilized polymer structure. While the first polymerization step takes place on the surface of a catalyst upon heating, the second one can be obtained by heat- or photo-polymerization.[73]

The one-step method was first demonstrated by Broer and co-workers in Philips Research Center in late 1980s.[74] In this method, low-molecular-weight reactive mesogens, usually diacrylates, are polymerized in a single-step (Fig. 2.5b). Because the polymerization needs to be conducted at the LC phase to attain well-controlled molecular-level orientation, photopolymerization is often more favorable than the thermal one. Prior to the polymerization, the mesogen mixture (isotropic phase) is

infiltrated between two surfaces of a cell with specific treatments, which align the molecules when cooling down to LC phase. This surface alignment technique, benefitting from surface anchoring mechanism, is similar to the commonly used techniques in fabricating LC-based electro-optical devices like LCDs.[75,76] In most cases, and also in our studies, thin polymer layers (polyvinyl alcohol, polyimide) are spin-coated on the substrates and rubbing of these layers introduces nanogrooves that orient the LCs near the surface to planar configuration (Fig. 2.6a) and the orientation is translated into other liquid crystal molecules via intermolecular interactions, leading to controlled LC alignment across the sample thickness.[77] Related approaches may also produce homeotropic orientation, where molecules are oriented perpendicularly to the substrate (Fig. 2.6b). However, to have good alignment throughout the material thickness, the method is usually limited fairly thin films, in the range of tens of microns. Complex 2D alignment can be obtained with photoalignment techniques where the dichroic materials coating, or photoalignment layer, can pattern the LC director as dictated by polarized light irradiation with a resolution well below a micron.[78,79]
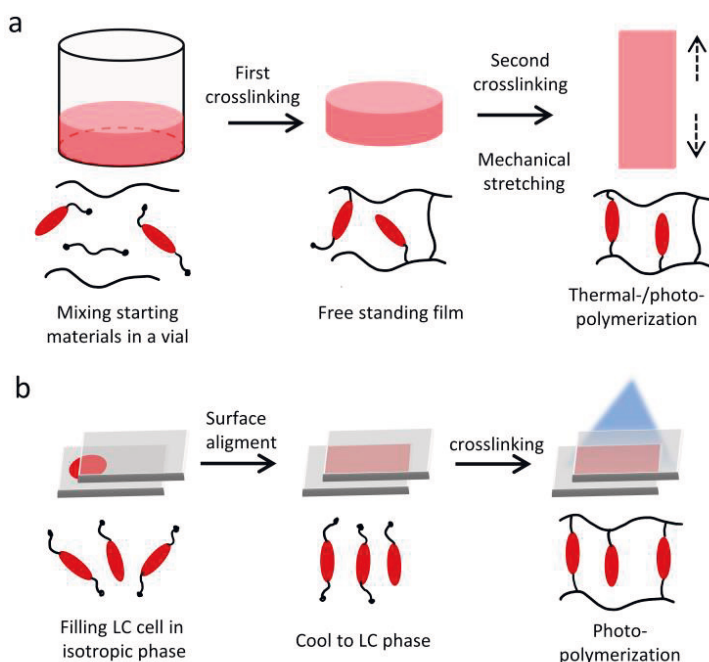

Figure 2.5 Two main approaches for the preparation of LCNs. **a)** A two-step process where material is first loosely crosslinked followed by mechanical stretching to align LC molecules and second polymerization. **b)** A one-step method where mesogens are first aligned in an LC cell and then crosslinked via photopolymerization.
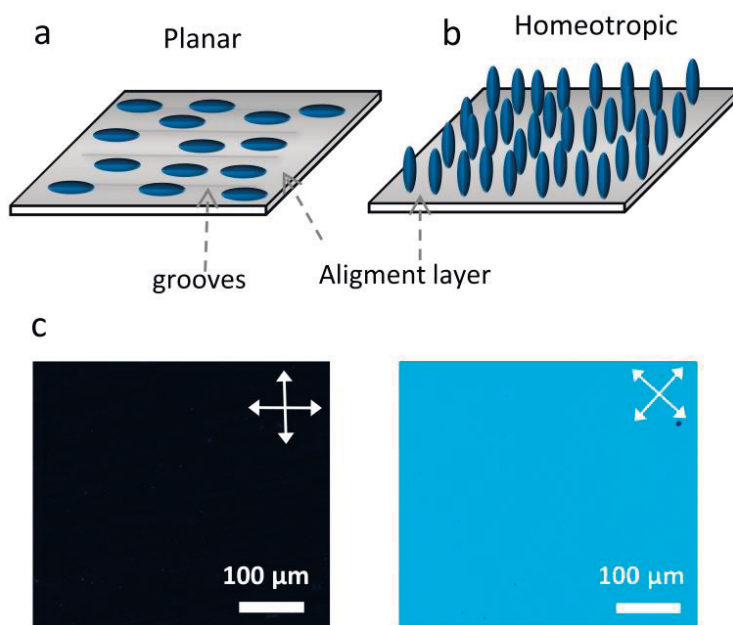
Figure 2.6 Schematic representation of basics LC alignment: planar **(a)** and homeotropic **(b)** of mesogens. c) POM images of planar-aligned LCN film with polarizers parallel/perpendicular (left) and at ±45° angle to **n**.

After polymerization, the LCN can be characterized by polarized optical microscope (POM). POM consists of a light source and two crossed polarizers placed on the light path and therefore no light cannot transmit through the microscope to the image plane. However, when a birefringent sample, such as LCN, is placed between the polarizers, the polarization is modulated, and light can transmit through to the second polarizer. In planar-aligned LCN films, the sample quality can be assessed by comparing the brightness and uniformity of POM images when **n** is parallel/perpendicular to the polarizers (no polarization modulation, dark image) and when **n** is at ±45° angle to the polarizers (large polarization modulation, bright image) as shown in Fig. 2.6c.

When making the choice between the LCN fabrication approaches, one should consider their properties from the perspective of application they are targeting. For example, in **Publication I,** we study light-fueled oscillation with different oscillation modes and for that, fabrication of LCNs that exhibit different deformation modes is needed. For the bending and twisting deformation, we adopted a typical molecular composition from Broer and co-workers,[80] which leads to glassy end-on side-chain polymer structure (Fig. 2.7a). These materials are stiff and can generate relatively low

level of strain and limited deformability. Usually, the deformability can be enhanced by decreasing the crosslinking density or using mesogens forming side-on polymer structure,[81,82] where rod-shaped mesogens are connected to the polymer backbone from the middle (Fig. 2.7b). This improved deformability was utilized to realize contraction-expansion oscillation mode, and we used a composition slightly modified from the one reported by Keller and co-workers.[82] As main-chain LCNs (Fig. 2.7c) have been proven to be capable of greater deformation performance,[64] we chose the material provided by Prof. H Yang's Group,[83] for the so-called freestyle oscillator, where multiple oscillation modes are simultaneously achieved.
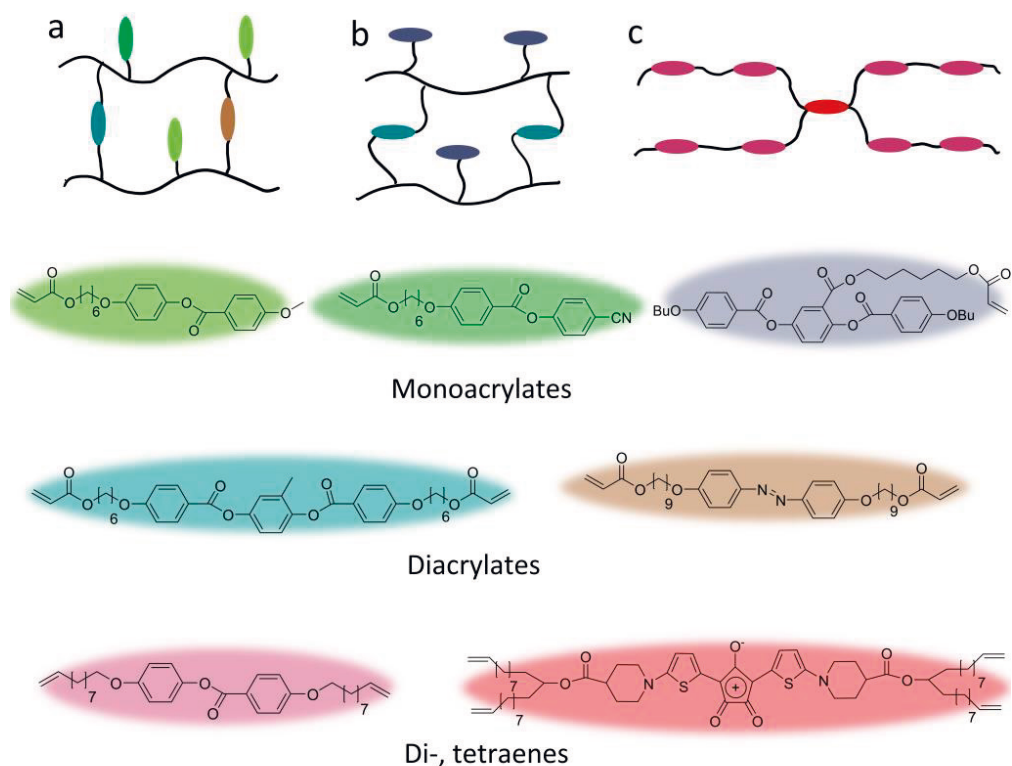

Figure 2.7 Different LCN architectures based on connectivity of the mesogens to a main polymer chain: **a)** end-on side chain, **b)** side-on side chain and **c)** main-chain, and monomers from **Publication I** for construct those.

Beyond the conventional methods, researchers have recently developed novel fabrication method by using chain-extension reactions.[84–86] In this method LC molecules with two reactive groups are first co-polymerized with small molecules having amine or thiol groups. These monomers undergo a chain-extension reaction through thiol-ene reaction or Michael addition to form a main-chain polymer (or oligomer) structure. After the chain extension, the material is crosslinked by photopolymerization. The chain-extension combines the advantages of the two-step main-chain LCNs (large deformability) and the one-step side-chain ones (facile molecular alignment control and patterning).[87,88] In particular, chain-extended LCNs can be produced using extrusion-based printing with a 3D printer because of their high viscosity. During the printing process, the LC alignment is induced by the monomer-mixture flow through the nozzle, and the complex 3D architecture can be fixed by UV curing.[89] These 3D printed structures can morph between predetermined shapes under thermal[90,91] or light[92,93] stimuli, while the deformability can be possibly programmed. As a result, 3D printing of responsive materials is often referred to also as 4D printing. This chain-extended LCN based 4D printing technique has received huge attention these days, because it fits well into the interface between soft robotics and stimuli-responsive materials.[94]

2.4   Thermoresponsive hydrogels

Hydrogels are chemically or physically crosslinked polymers holding a large amount of solvent in their network without dissolving them.[95] Commonly hydrogel systems are working in an aqueous environment and upon thermal stimulus their water-absorbing capability can change. As a result, the gel undergoes a reversible swelling-deswelling process (Fig. 2.8). In contrast to LCNs, hydrogels are usually isotropic, and the deformation is homogenous along all directions. Hydrogels can be fabricated to respond to several stimuli such as pH, electric and light fields.[96] Due to prerequisite of aqueous environment, operation temperatures around 35 °C (close to human body temperature), and tissue-like mechanical properties, hydrogels are often prepared for bioengineering applications, for example, drug delivery, tissue regeneration, and soft underwater robotics.[97]
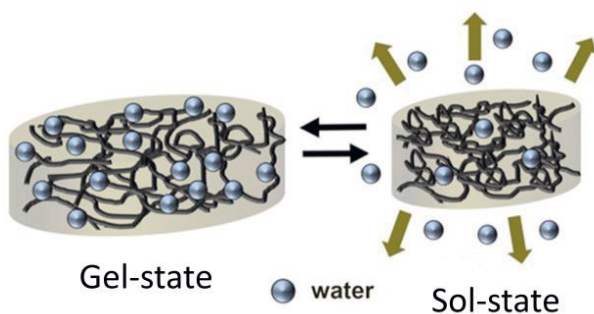
Figure 2.8 Swelling-deswelling of the hydrogel results 3D-shape deformation.[28] A figure reproduced with permission: Copyright 2020, John Wiley and Sons.

Hydrogels can be prepared from many natural (collagen, chitosan) and synthetic (poly(ethylene glycol), polyvinyl alcohol)[98] materials, but synthetic covalently crosslinked PNIPAm based hydrogels are by far the most popular ones. We have also adopted this material in **Publication V**. Similar to LCNs, polymerization of the PNIPAm hydrogels can be done either in one-step (*in situ* crosslinking) by mixing monomers, crosslinkers and free-radical initiators (Fig. 2.9),[99] or in two steps (post-synthetic) through first forming linear (co)-polymer and then crosslinking.[100] In both cases, thermal- and photo-polymerization can be used.[101,102] The key difference compared to LCN polymerization is that with hydrogels, polymerization is solvent-based. The solvent can be water or combination of water and polar organic solvent. Polymerization of the hydrogels can occur in a vial to form bulky gels, or in a spin-coated thin layer on substrates or inside a glass cell for thin film configuration.[101,103]

Figure 2.9 Synthesis of PNIPAm based hydrogels with free-radical thermal polymerization using azobisisobutyronitrile (AIBN) as an initiator (**Publication V**).

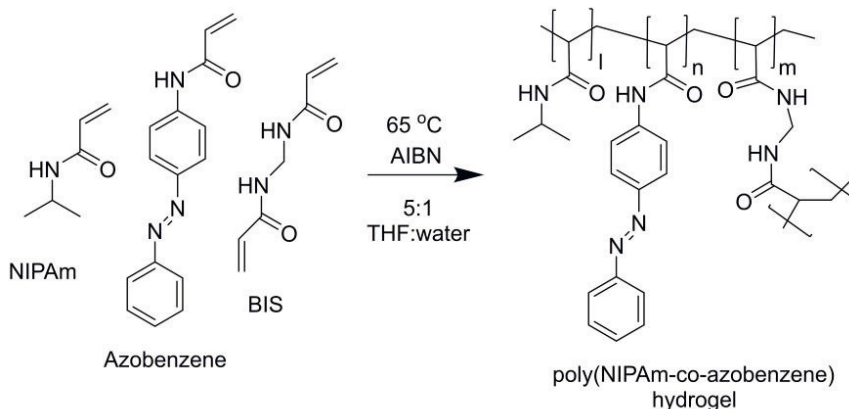PNIPAm hydrogels are thermoresponsive in the way that heat alters the water content inside the polymer network, resulting in drastic volume change. PNIPAm hydrogels have a lower critical solution temperature (LCST) of about 32-34 °C.[104] When the environmental temperature is below the LCST, PNIPAm hydrogel is in a swollen state (gel-state) and hydrogen-bonding interactions with adjacent water molecules dominate over the interactions between the polymer chains.[105] Upon heating, the hydrogen bonds are gradually broken and intra- and inter-molecular hydrogen bonding/hydrophobic interactions between the polymer chains prevail. Above LCST, these interactions result in a collapsed conformation of the polymeric chains (sol-state).[106] This collapse leads to a significant volume shrinkage of the material. In some other hydrogel systems this mechanism is reversed, and they become soluble when heating above upper critical solution temperature (UCST).[96] Based on this critical transition process, precisely adjustable temperature-controllable mechanical properties by swelling/deswelling of material can be attained.[107] Besides the volume deformability, the optical properties of hydrogels can vary dramatically after the sol-gel transitions, leading to transitions between transparent and opaque, highly scattering states.

Since the temperature-driven swelling of hydrogels depends on the solvent interaction with the molecules and the hydrophilic/hydrophobic balance within the polymer network, additives in the gel matrix or solvent can influence the LCST. By co-polymerizing hydrophilic (e.g. acetic acid) or hydrophobic (e.g. azobenzene) additives to the hydrogels, LCST can be shifted to higher or lower temperatures, respectively.[108,109] Furthermore, incorporation of photoactive units or photoacids into the hydrogels enables light and pH sensitivity, respectively.[110,111] Tuning of LCST can also be done by adding salts, surfactants or co-solvent, which alter the solvent polarity and therefore adjust the polymer-solvent interactions.

The amount of swelling of the hydrogels can be characterized by measuring the weight change between the swollen and dry hydrogel and thus determining the swelling ratio. Temperature-dependent swelling can be quantified by measuring the weight of the swollen gel at different temperatures. Swelling ratio in specific temperature can be controlled with crosslinking density of the hydrogels and swelling ratio usually decreases when the crosslinker concentration increases as material becomes stiffer or more plastic.[95] Kinetics of volume change is based on poro-elastic mass transport and is therefore affected by the crosslinking density and hydrophilicity of the gel.[98] The solvent diffusion time is directly proportional to second power of the smallest spatial dimension of the gel network.[112] As a result, bulky hydrogels typically exhibit slower speed in volume change than thin films. This

scaling-accelerated actuation process has benefited the investigation of thin film hydrogels for miniaturized devices with fast response and high environmental sensitivity.[113]

3 CONTROLLING PHOTOMECHANICAL DEFORMATION

Among different classes of stimuli-responsive materials, photomechanical actuators are of great interest as they provide a route to harness light energy to fuel mechanical motions. Light is a highly attractive energy source, as it delivers photons (energy) rapidly and wirelessly over long distances. It is also versatile as its wavelength, intensity, and polarization can be controlled/programmed with high temporal and spatial resolution. Hence, light offers many possibilities for actuation control and pathways for sophisticated robotic movements.

To obtain photomechanical deformation, light-sensitive elements need to be incorporated into the responsive polymer.[25] Depending on the specific mechanism, the actuation can occur either photothermally or photochemically. In photothermal actuation, organic dyes or nanoparticles are often used as light absorbing units to convert light into heat.[64,114] The heat serves as a driving force to change the LC alignment or causes thermal expansion in LCNs or change swelling metrics in hydrogels, leading to shape morphing.[115] Deformation via photochemical effect is based on reversible photoswitching of photochromic molecules, most typically azobenzene.[116] The photochromic units can switch between two states with distinct structural and physical properties, triggering a certain degree of disorder to the oriented LCNs or changing hydrophilicity of hydrogels,[87,116] thus yielding macroscopic deformation.

In this Chapter, we first illustrate the diversity of shape changes that have been obtained in LCNs. Then, photomechanics will be discussed in more detail by elaborating photochemical and photothermal effects, in both LCNs and hydrogels. Other alternatives for light stimulus *e.g.* electric or magnetic fields, chemical-stimulus or pH, will not be included but the reader is referred to following reviews for more elaborate discussions.[7,16,33,117] This Chapter is partly based on ref. [3].

3.1   Complex shape morphing in LCNs

The mechanism of light-induced shape changes in LCNs relies on the specific form of built-in molecular alignment. As described in the previous chapter, uniaxially aligned LCNs exhibits a contraction-expansion deformation, and different 3D-deformation modes like bending or twisting can be induced tuning the LC alignment or crosslinking density across the sample thickness.[118] Similar to other actuators, bending is the most studied actuation mode in LCNs. However, conversely to bi-layer structures,[119] bending LCNs can be fabricated in the form of a single monolithic layer with homogenous chemical compositions, while the "bilayer-like" behavior is dictated by different molecular alignment between the two surfaces. There are two main types of alignment to induce bending actuation, 1) splay alignment, where LC molecules tilt from in-plane to out-of-plane and 2) twisted alignment, where LC molecules make 90° rotation through the film thickness as schematically shown in Fig. 3.1. In both cases the bending occurs because of anisotropic thermal expansion within the material – contraction along the director axis and expansion in the other directions – always resulting in bending towards the planar-aligned side.[120] However, the bending of splayed and twisted LCNs upon identical stimulus are different.[121] The twisted film would also contract along the short axis, thus creating a curvature, the signs being opposite to those along the long axis and the film morphs into saddle-like shape, which decreases its bending strength compared to the splay-aligned sample. The bending deformation is commonly, and in this thesis as well, chosen to characterize and quantify the photomechanical response of LCN actuators under different irradiation (wavelength, intensity) conditions.
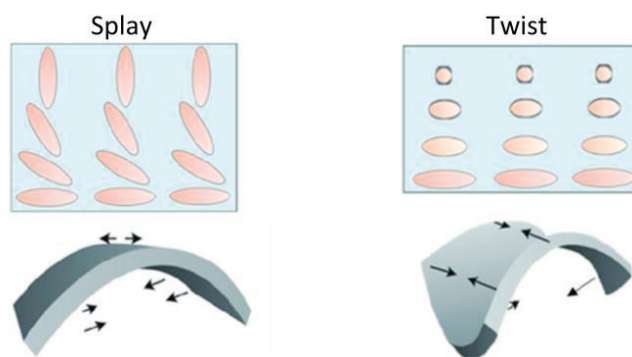

Figure 3.1 Schematic illustration of splay and twisted alignment and their different bending behavior.[65] A figure adapted with permission under terms of CC BY 4.0, Copyright 2020, The Authors.

Besides bending deformation, splay and twisted alignments can also produce coils and helicoids, depending on the stripe-cutting angle between the director $\boldsymbol{n}$ and the long axis of the film. In bending actuator, the cutting angle should be near zero, but having it $\pm 45^{0}$ yields helicoidal deformation.[122] More complex shape changes can be obtained by less conventional in-plane molecular alignment. For example, azimuthal and radial alignments can be obtained using photoalignment technique, leading to conical deformation (Fig. 3.2a).[86,123,124] Moreover, regional patterning of twisted[125] or splay[126] alignment with alternating orientation segments can cause adjacent LCN segments to bend in opposite directions, yielding accordion-like configuration (Fig. 3.2b). Radial-splay alignment has been used to devise an artificial iris, which can open and close upon blue/green light illumination (Fig. 3.2c).[127] An alternative approach for complex shape morphing is through spatial control of crosslinking density which generates different contraction-expansion ratio and thus different shape changes.[128] However, all the above examples, no matter how sophisticated, exhibit only one pre-determined geometry of deformation under identical heat- or light-stimulus. Using reconfigurable actuation strategy can allow re-programming the shape morphing under identical stimulus, as will be discussed in Chapter 4.4.
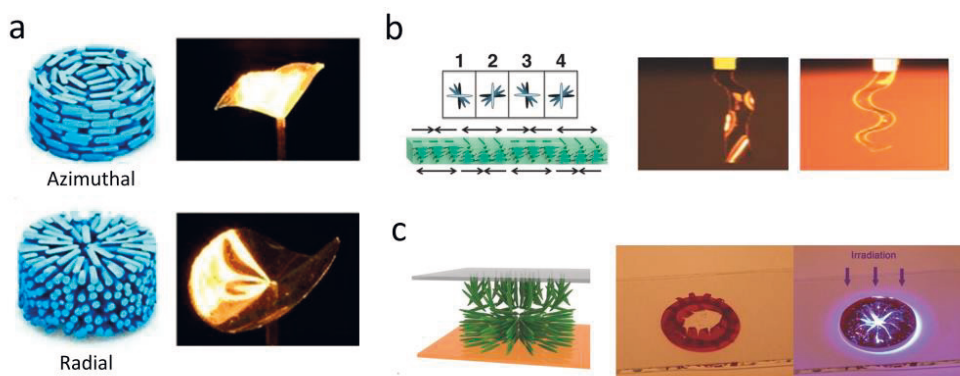
Figure 3.2 Complex LCN alignment and shape deformation: **a)** Azimuthal and radial alignments produce conical shapes.[124] **b)** Alternating patterning of twist orientation leads to accordion-like motion.[125] **c)** Radial-splay alignment and artificial iris.[127] Figures reproduced with permission: **a)** Copyright 2021, John Wiley and Sons. **b)** Copyright 2013, John Wiley and Sons. **c)** Copyright 2017, John Wiley and Sons.

3.2   Photothermal effect using photo absorbers

In photothermal actuators, light is absorbed by organic or inorganic dopants and converted to heat by non-radiative thermal relaxation processes.[25,129] The heat dissipates to the whole polymer matrix and induces macroscopic shape deformation in the same manner as direct heating (Fig. 3.3).[114] However, compared to direct heating, optical heating preserves all the desirable features of light stimuli, i.e. allowing localized and remote stimulation. Again, the shape morphing is dictated by the pre-designed molecular alignment,[130] thus the extent of deformation can be changed by controlling the heat released from the light-absorbing moieties, or in other words, varying the illuminating light intensity. Shape deformation kinetics is mostly determined by heat capacity and thermal conductivity of the polymer, being usually in the range of seconds (Fig. 3.3) in an actuator with millimetre-to-centimetre length and tens of microns thickness.[12] Relaxation to the initial shape usually occurs within roughly the similar time span after ceasing the light.
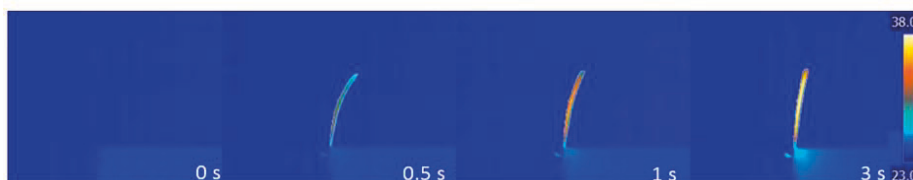
Figure 3.3 Photothermal actuation with constant intensity, showing a time series of thermal camera images for photothermal bending of a splay aligned LCN strip (**Publication III**).

The light-active elements used for photothermal actuation in LCNs can be roughly divided into three categories: 1) organic dyes, 2) carbon-based nanomaterials, and 3) plasmonic nanoparticles.[115] The key selection criterion between these is that the doping agents must be soluble into the LC mixture. For organic dyes, this is straightforward because of the similarities between dyes and LC monomers. Many suitable dyes are commercially available or easy to synthesize (Fig. 3.4).[131,132] Moreover, organic dyes can also be added in the polymer network after the LCN has been polymerized, using heat-driven diffusion.[133] Organic dyes exhibit different absorption properties depending on their chemical structures, allowing the photomechanical deformation to be driven by light within the whole ultraviolet (UV), visible, and near infrared (NIR) spectrum, depending on the targeted application.

Besides organic dyes, some inorganic materials are also suitable for photoactuation. Carbon materials like carbon black, carbon nanotubes and graphene absorb light from UV to IR, being highly efficient photothermal materials.[134,135] For example, carbon nanotubes can be oriented along the direction of LC mesogens, and controlled by both light and electrical fields.[136,137] Plasmonic nanoparticles, on the other hand, are versatile photothermal heaters due to their high molar extinction coefficient and high quantum yield of photothermal conversion.[138] Especially gold nanorods stand out as they can be synthesized with many sizes and aspect ratios which determine the surface plasmon resonances of the particles, and therefore the photothermal activation wavelength.[139,140] For example, LCNs containing very low amount (~0.05 w%) of gold nanorods can lead a temperature rise over 150 °C under moderate light intensities.[141,142] However, inorganic particles are usually difficult to disperse into organic polymer matrixes, as they aggregate during the polymerization, resulting in decrease in the LC order parameter and deteriorating the mechanical and optical properties of the film.
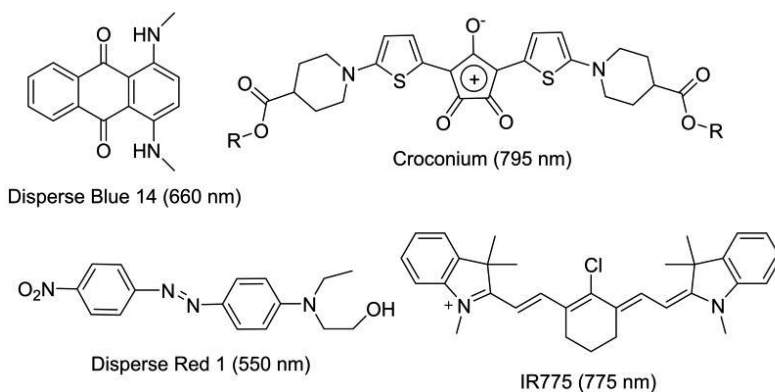
Figure 3.4 Organic dyes used in this thesis to trigger photothermal actuation and their peak wavelengths.

As photothermal heating often leads to fast photomechanical deformation, it has been used to realize micro-devices capable of locomotion, as shown in Fig. 3.5a. Here, one conventional method is to use LCNs as a light-responsive layer combined with asymmetric surface(s) to create movement tendency. Upon spatial[143,144] (Fig. 3.5a) or temporal[145] light excitation control, LCNs deform the body cyclically, and locomote due to the asymmetric friction between structure and the surface. Locomotion has been demonstrated also with monolithic stripe-like LCNs with patterned in-plane alignment. Directional movement can be induced by a local shape

deformation and asymmetric friction bias with laser scanning along the stripe (Fig. 3.5b)[146] or under cyclic spatially uniform light illumination (Fig. 3.5c).[126] By placing viscous liquid under the robot, snail-like upward walker have been demonstrated as shown in Fig. 3.5d.[147]
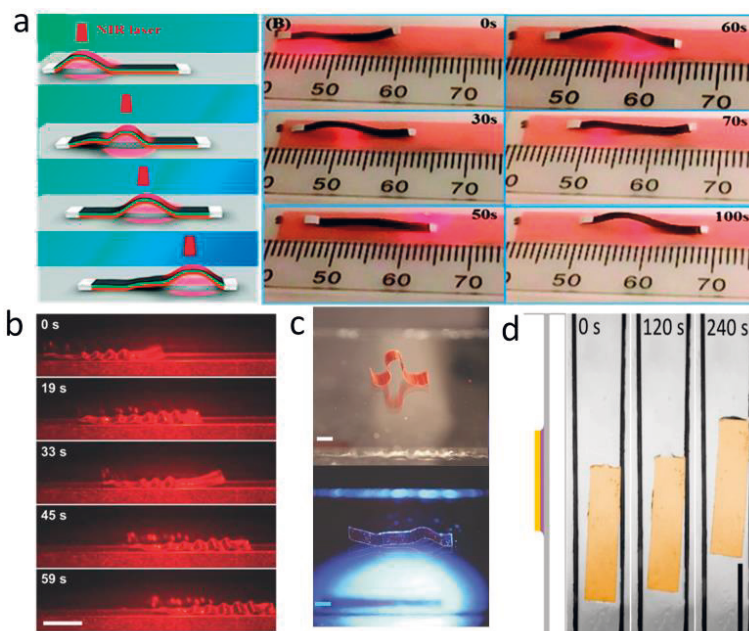
Figure 3.5 Walking LCN robots utilizing the photothermal effect: **a)** Locomotion of trilayer cantilever through NIR laser scanning.[143] **b)** Traveling-wave deformation of a monolithic robot.[146] **c)** Locomotion under spatially uniform blue light.[126] **d)** Adhesive climbing on a vertical glass surface.[147] Figures reproduced with permission: **a)** Copyright 2018, RCS. **b)** Copyright 2016, John Wiley and Sons. **c)** Copyright 2017, John Wiley and Sons. **d)** Copyright 2019, John Wiley and Sons.

3.3   Photochemical effect using photochromic switches

Photochromic switches are organic molecules that can reversibly change their structural, optical or electronic properties in response to light stimuli.[148] These molecules have at least two thermodynamically (meta)stable states, and they are capable of reversible phototriggered interconversion between them. To effectively translate the molecular-level deformation into macroscopic mechanical motions, i.e. photochemically induced actuation, the switching have to take place in the solid state, and the switched molecules must act in concert. Here, the phototriggering of molecular photoswitches has yielded large shape morphing in anisotropic LCNs.[26,149]

By far, the most popular photoswitches to drive photochemical actuation of LCNs are photoisomerizable azobenzene (azo) derivatives.[64] They are aromatic compounds, having two phenyl rings bridged by an -N=N- group. Azobenzene and their derivatives can undergo reversible shape changes (i.e. photoisomerization) between a thermally stable *trans*-state and a metastable *cis*-state when absorbing a photon (Fig. 3.6a). Depending on the molecular structure and environment, isomerization occurs either through out-of-plane rotation or in-plane inversion of -N=N- bond.[150] *Trans*-azobenzenes absorb light strongly in the UV region due to $\pi \rightarrow \pi^*$ electronic transition and in blue wavelengths due to weak $n \rightarrow \pi^*$ transition (Fig. 3.6b). In *cis*-form $\pi \rightarrow \pi^*$ transition becomes weaker and blue-shifted while the $n \rightarrow \pi^*$ transition is enhanced. Isomerization causes a huge change in the molecular length from about 9.0 Å in the rod-shaped *trans*-form to 5.4 Å in the bent *cis*-form.[151] Also the dipole moments of these two isomers differ (0 D in *trans*- and 3 D in the *cis*-form for the unsubstituted azobenzene). *Trans*-azobenzenes are often mesogenic and align together with LC molecules along the director. However, isomerization of azobenzene to the bent *cis*-form disrupts the LC ordering, reducing the order parameter and triggering isothermally induced order-to-disorder transition in the LC and free volume changes in the solid state, which may trigger macroscopic shape deformation of the polymer.[152–155]

The deformation of LCN actuator is associated with a *cis*-isomer population, hence the lifetime of *cis*-isomer determines the stability of the deformed structure. A long *cis*-lifetime (~hours) guarantees that the actuated shape can be maintained for a reasonably long period (~tens of minutes) after ceasing light stimulus. To restore the original state, one can apply *cis*-to-*trans* isomerization through visible illumination or with (photo)heating for a thermal relaxation.[20] *Cis*-lifetime of azobenzenes depends strongly on its chemical structure. In **Publications I-III** we used a conventional azobenzene having alkoxy chain substitution with *cis*-lifetime of several hours. When an azobenzene is para-substituted with strong electron-donating and -withdrawing groups, that provide strongly asymmetric electron distribution (the push–pull effect), the *cis*-lifetime can be reduced to seconds or less. Conversely, by introducing halogen atoms, like fluorine, to *ortho*-position, *cis*-lifetime can be increased to even years.[156] Substitution can also significantly red-shift the $\pi \rightarrow \pi^*$ band, allowing photoswitching with visible light.[157]
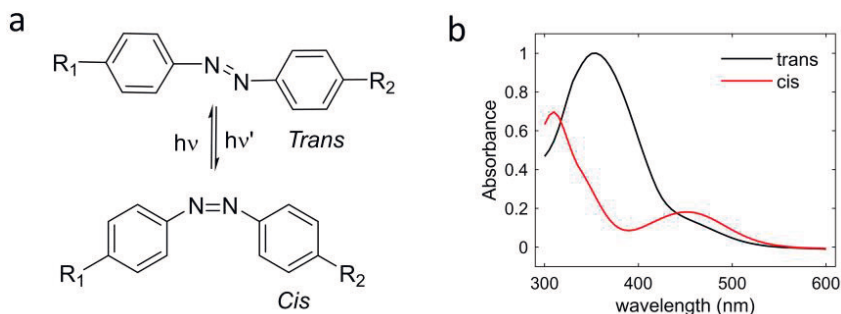
Figure 3.6 a) Azobenzene photoisomerization and **b)** UV-Vis absorption spectrum of *trans*- and *cis*-isomers.

Planar-aligned azo-LCN actuators often exhibit photoinduced bending. This is because the typically used relatively high azobenzene concentrations and high molar extinction coefficient of the *trans*-isomer lead to absorption gradient through the material thickness. Light cannot penetrate through the whole sample and photoisomerization occurs within a thin layer near the sample surface.[158] This creates a different light-induced strain across the film thickness, and the film bends towards the light source. The photochemically induced strain can also have a strongly non-linear response over a longer time span. *Trans-cis* isomerization induces major spectral changes and reduces the absorption coefficient at an excitation wavelength and more light would penetrate through the sample, yielding a planar-aligned bent sample to gradually unbend.[152,159,160]

Azobenzene-LCN actuators have received a lot of attention in the past two decades. After the pioneering work of Finkelman[161], Ikeda and co-workers reported on polarization sensitive bending in azo-LCNs,[154] and robotic demonstrations such as light-driven plastic motor[162], inchworm-type locomotion, and a robotic arm (Fig. 3.7a)[44]. In the past few years, many other complex shape-morphing structures have been achieved, such as buckling[87] (Fig. 3.7b), helical twisting[163] (Fig. 3.7c), a helical roller (Fig. 3.7d)[164], and kirigami deformations[165]. Moreover, Broer and co-workers have shown many photoswitchable topographical surface textures based on substrate-constrained films and azo-containing polymeric coatings.[166,167]

Conventional azobenzene actuators have some limitations as they lack long-term deformed shape stability, because in most cases, the *cis*-isomer relaxes thermally back to the *trans*-form with relatively short time (minutes to hours).[168] Moreover, wavelengths to control *trans*-to-*cis* and *cis*-to-*trans* isomers are close together, in many cases even overlapping, which prevents orthogonal wavelength control of the isomerization.[150] To overcome these problems, researchers have studied alternative

photochemical molecules to drive photochemical actuation.[169,170] One strategy is to utilize substituted azobenzenes which can have longer *cis*-lifetime and red-shifted activation wavelength. For example, *ortho*-fluorinated azobenzene can lead to truly bi-stable actuation in LCN.[171] Another strategy seeks to use a large library of photochromic molecules and select a molecule that has better properties and which do not disturb an elegant balance of orientation of LCN. Recently, hydrazone[172], diarylethene[173] and stilbene[174] -based photoswitches have been shown to lead to thermally bi-stable actuation in LCNs.
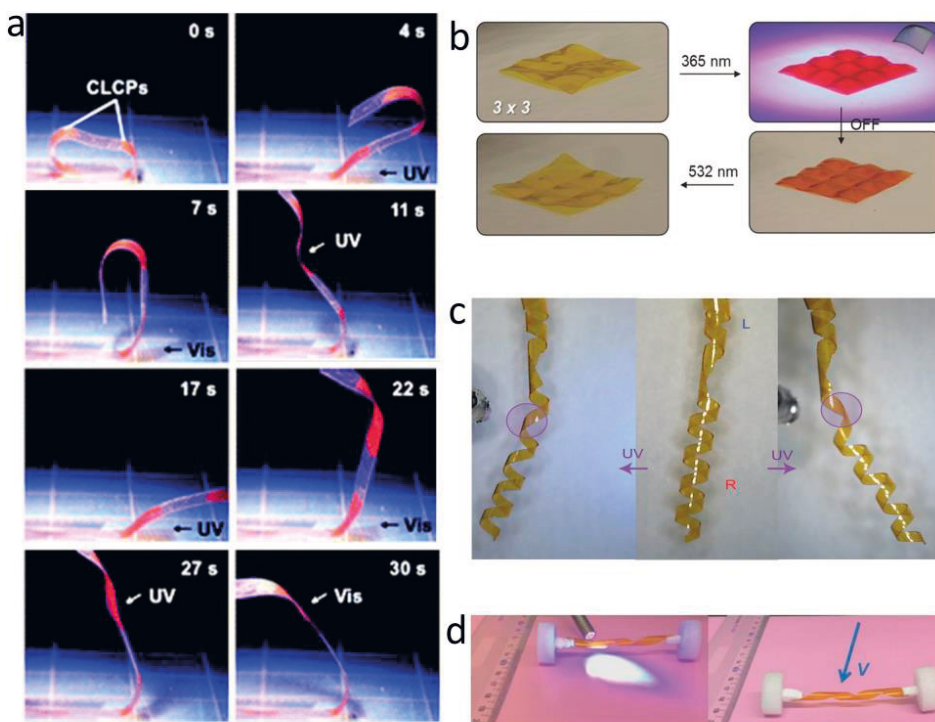
Figure 3.7 Photochemical actuation using azobenzenes: **a)** Robotic arm movements.[44] **b)** LCN film with buckling deformation induced by UV light.[87] **c)** A LCN spring with two oppositely handed helixes connected by a kink.[163] **d)** Spring-like "motor" for locomotion.[164] Figures reproduced with permission: **a)** Copyright 2009, RCS. **b)** Copyright 2016, John Wiley and Sons. **c)** Copyright 2014, Springer Nature. **d)** Copyright 2017, John Wiley and Sons.

3.4   Photochromic molecules as heat generators

Optical irradiation of samples containing photochromic molecules brings together photothermal and photochemical strategies and sometimes the photothermal effect suppresses the photochemical one. For example, irradiation of azobenzenes with short *cis*-isomer lifetime or simultaneous activation of *trans-cis* and *cis-trans* isomerization can create distinct isomerization-driven heating.[175–177] In **Publication I** we used Disperse Red 1 (see Fig. 3.4), a 'push-pull' azobenzene with strong electron-accepting and -donating groups in the *para* positions (having *cis*-lifetime in the second range), as an effective heat generator. Even in the cases when photochemical processes are believed to be the main mechanism for driving the actuation, photoheating can rarely be completely avoided and it may contribute to the final deformation.[178,179]

Other photochromic molecules, like hydrazone[180] and *ortho*-fluorinated azobenzenes[181] are also used as photothermal agents. Moreover, stilbene photoswitches capable of rotation via an alkene double bond have been showed to translate absorbed light energy to heat when isomerization reaction is forbidden by crosslinking.[182] In **Publication IV**, we incorporated photochromic diarylethene (DAE) crosslinker into LCNs and used it as a photothermal heat generator. Diarylethene can undergo reversible ring-closing and ring-opening via 6π electrocyclization when illuminated with UV and visible light, respectively (Fig. 3.8a). DAE derivatives have thermally bi-stable isomers with half-life in the order of hundreds of years in room temperature in organic solvents.[183,184] Another superior feature of DAE compared to azobenzene is that its π-electronic conjugation changes considerably upon photoinduced electrocyclization, resulting in huge spectral change (spectral shift of > 200 nm) between the isomers – ring-open form absorbing UV and ring-closed form green-red light (Fig. 3.8b). The switching reaction is reversible and repeatable with light irradiation and photoconversion rate is up to 99%.[185,186] We utilized these features to power a DAE-LCN actuator photothermally, by first generating color via UV-induced electrocyclization of DAE and subsequently actuating the material with green-light-induced thermal effect. In our system, the electrocyclization of the DAE could not induce visible macroscopic deformation of the LCN film, as DAE undergoes only a small structural change when illuminated with UV light.
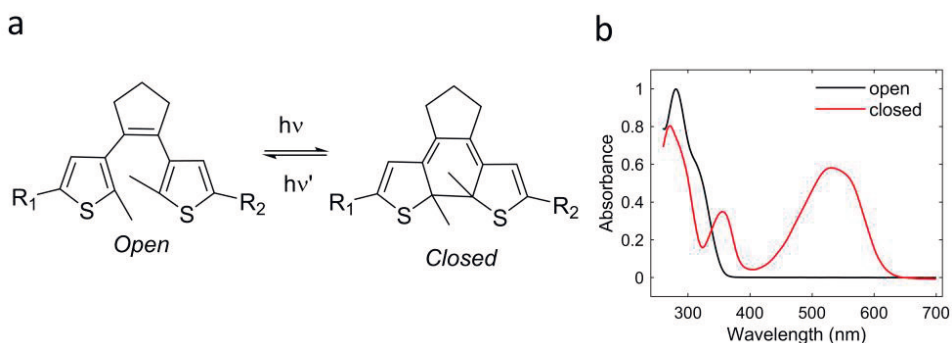
Figure 3.8 a) Diarylethene electrocyclization and **b)** a UV-Vis absorption spectrum of the ring open and closed forms

3.5 Comparison between photochemical and photothermal actuation

As described above, both photothermal and photochemical effects can be used to fabricate actuators, for potential use for future soft robotic applications. Both mechanisms have their own strengths and weaknesses which need to be considered when devising light-fueled robots.[187] With the scope of the thesis, these differences can be grouped into three categories: 1) light-absorbing elements 2) photoactuation behavior and 3) photopatterned deformation (see Table 3.1).

A photothermal dye can absorb light within a specific spectral range. Due to the diversity of dye molecules, the absorption can be tuned across a broad wavelength range, from visible to NIR. This makes photothermal actuation appealing for human-safe interfacing, as photochemically driven LCNs typically utilize harmful UV irradiation.[25] Combining several photothermal dyes into a single network can extend the absorbing spectral range to cover the whole solar spectrum, leading to sunlight-driven actuation.[181] Regarding the sample preparation, photothermal elements can be easily doped into the LCN matrix. However, for efficient photochemical actuation the photoswitches need to be crosslinked to the polymer network, making them synthetically more challenging to work with. Finally, the molar concentration required for efficient actuation is different between the two mechanisms. For photothermal actuation, few weight percentages of organic dyes (even less for nanoparticles) is sufficient to trigger photoheating upon moderate light intensities (few hundreds mW/cm²). However, much higher concentrations (from 5 to 100 mol-%) are needed to invoke photochemical actuation, and as mentioned

earlier, such a high concentration result *cis*-isomer gradient through the material thickness.

Table 3.1 Comparison between photochemical and photothermal strategies in shape-morphing.

	Function	Photothermal	Photochemical
1) Light absorbing element	Absorbing wavelengths	UV to NIR	UV-blue
	Connection to the polymer	Doped/bonded	Covalently bonded
	Concentration	Few w%	Up to 100 w%
2) Actuation	Dynamics	Fast; relaxation when ceasing the irradiation	Slow; bi-stable
	Environment	Mostly air	Air, water
3) Photopatterning	Resolution	Lowered by heat transfer	Diffraction-limited

The actuation dynamics between these two mechanisms is also different. The speed of actuation/relaxation in photothermal actuators is dictated by thermal heat capacity of the structure. As such, a small sized actuator (small thermal capacity) often allows fast (within millisecond) actuation, the key feature for soft robotic applications. The actuation is also dynamic in the sense that it relaxes when light is turned off. Conversely, the macroscopic deformation of photochemical actuators lags behind the illumination and it often takes minutes to complete the deformation.[149] This may seem to be a drawback in robotic actuation, but if the photochromic molecules possess a long lifetime of the metastable state, the actuator's deformation can also persist for long, which suggests a useful pathway to bi-stable photoactuation that can be useful, e.g., in tunable photonics. Regarding the working environment, photochemical actuation can be efficient in both air and in aqueous environment.[188] However, photothermal actuators rarely show efficient actuation under water due to the high thermal dissipation.[12] One possible solution is to add plasticizers to reduce the temperature required for shape-morphing.[189]

It is a curiosity driven question what will happen if combining photochemical and -thermal mechanisms. In **Publication II**, we devised a single actuator composed with two photomechanical segments utilizing different kinetics of photochemical

and photothermal actuations. We show that this configuration can lead to non-reciprocal movement, one of the basic characteristic patterns of natural locomotion. The results presented in **Publication II** indicate that instead of looking for the pros and cons of the photothermal and photochemical mechanisms, it might be fruitful to seek for the best combination of both. In this context, other researchers have reported enhanced control strategies for soft robotic movements. Several strategies relying on the combination of azobenzene isomerization as the photochemical trigger and visible-NIR photothermal moieties have been utilized. For example, with bi-layer LCN structure having photochemical and -thermal dyes in separate layers, different actuation modes can be achieved by triggering the different mechanisms.[190] Separating the two mechanisms into different actuators can also bring about sophisticated soft-robotic movement control like photochemical gripping of an object and parallel photothermal control over the lifting motion.[141] Great effort has been dedicated to differentiate between these two photomechanical actuation schemes. The dominating mechanism can be detected by a measuring temperature change of the film under different illumination conditions.[191] In **Publication III**, we have elaborated a detailed pathway to differentiate these two mechanisms, and how to implement both to realize synergistically enhanced actuation and reconfigurable robotics. Further details on this will be given in Chapter 4.4.

Finally, comparison between the two actuation mechanisms can also be made from the perspective of photopatterning. In the context of this thesis, photopatterning is denoted as photothermal or -chemical deformation, which is triggered only in selected parts of the film using patterned light. In photothermal patterning, thermal broadening and heat dissipation due to convection or conduction limits the sharpness of the deformation.[192] Photochemical patterning can be applied with much higher resolution, even reaching the diffraction limit of light. In **Publications III** and **V**, we utilize photochemical patterning of *cis*-azo concentration in different parts of the LCN or hydrogel films, respectively. In **Publication III** photomask was fabricated by covering a glass slide with black tape followed by laser cutting. The photomask was placed on top of the film prior to illumination with light-emitting diode (LED). In **Publication V**, we use maskless lithography utilizing a digital micromirror device (DMD) connected to an inverted optical microscope. This technique enables the projection of any computer-designed pattern though microscope objective to the sample with high spatiotemporal resolution, using laser or LEDs illumination with desirable emission profile.[193]

3.6 Light-induced shape morphing of thermoresponsive hydrogels

In Chapter 2.5 we discussed the deformation mechanism of responsive hydrogels and noted that due to isotropic swelling/deswelling, anisotropic shape changes cannot be easily attained through molecular alignment control as with LCNs. However, complex shape changes can be induced through programming the swelling/deswelling properties locally.[194,195] Generally, swelling gradients generate in-plane stresses that are compensated with out-of-plane bending or buckling.[196,197] If the gradient appears in one dimension, e.g. across the thickness, it causes changes in the mean curvature of the gel (bending) as schematically shown in Fig. 3.9a. If such gradient is distributed across a two-dimensional plane, more complex shape-morphing can be produced.[198,199] For instance, centrosymmetric variation of the swelling ratio (higher swelling at the center) yields a spherical cap with positive Gaussian curvature: (Fig. 3.9b), while reversing the gradient results in a saddle-shape (Fig. 3.9c). [200]
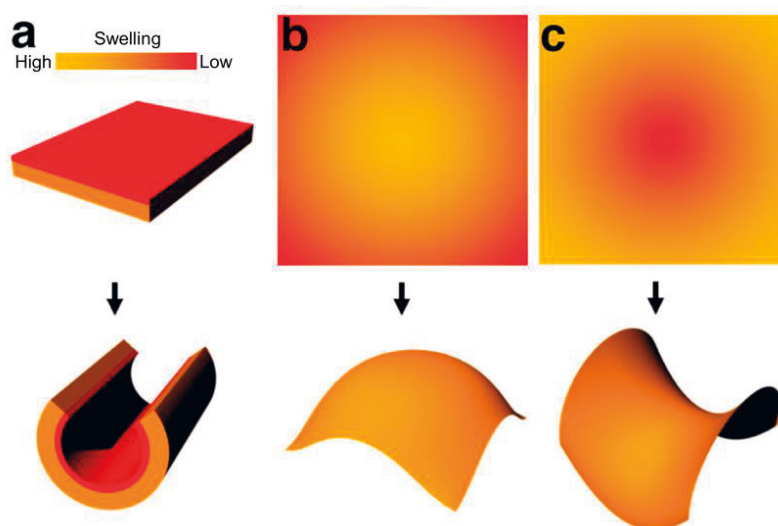

Figure 3.9 Shape-morphing of hydrogel thin films. A bilayer structure with swelling gradient leads bending on the film **(a).** In-plane gradients lead to more complex shapes with positive **(b)** or negative **(c)** Gaussian curvature.[200] Adapted with permission: Copyright 2017, ACS.

A conventional way to inscribe the swelling gradient in thermoresponsive hydrogels is to vary crosslinking density by controlling (photo)polymerization conditions.[201,202] Alternatively, the light absorption depth or spatial illumination can be used to tune the photothermal heating across the sample thickness or in-plane, yielding built-in gradients for swelling. For this, gold nanoparticles and carbon nanomaterials are the most used photoheating agents.[203] Based on such gradient-driven actuation, many shape-morphing devices upon localized light stimuli have been demonstrated,[204–207] including a NIR-light-driven micro-hand (Fig. 3.10a) and a gel sheet with various out-of-plane buckling motions under patterned white light illumination (Fig. 3.10b). To harness photodeformation for hydrogel-based soft robotics, one must overcome the barrier of slow actuation speed. The limited swelling kinetics and slow response time of hydrogels (hours for cm-scale robots),[196] in principle, can be enhanced by using porous hydrogels, which facilities fast water diffusion into and out from the hydrogel network.[208,209] For example, porous cm-scale hydrogel pillars deform within seconds, enabling octopus-like swimming locomotion under laser irradiation (Fig. 3.10c).[208]
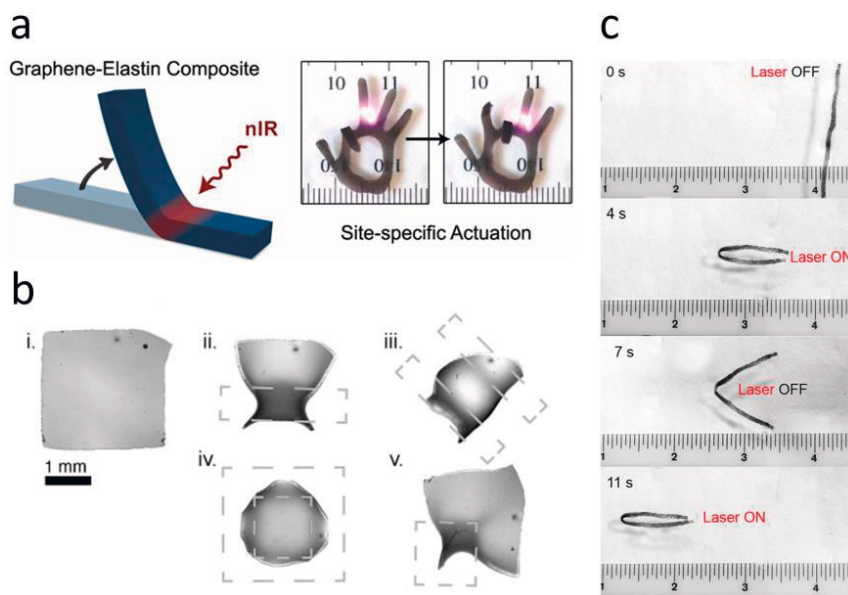
Figure 3.10 Photothermal actuation in hydrogels. **a)** A bilayer-type hydrogel actuator bends under NIR laser irradiation.[204] **b)** Out-of-plane buckling of a thin hydrogel sheet using patterned white light.[206] **c)** Forward-moving porous hydrogel driven by laser irradiation.[208] Figures reproduced with permission: **a)** Copyright 2013, ACS. **b)** Copyright 2015, John Wiley and Sons. **c)** Copyright 2015, John Wiley and Sons

In thermoresponsive hydrogels, photochemically-induced shape deformation can be achieved through covalent attachment of photochromic molecules. If the dipole moment of the photochrome changes upon isomerization, the gel will change its hydrophilicity, and thus tune the LCST/UCST temperatures. Hence, at a fixed temperature, swelling and sol-gel transition can be controlled isothermally with photoswitching. The resulting light-induced shape change is often attributed to the change in polarity rather than the shape of photochromic molecules. In this context, two most used photochromic switches are spiropyrans and azobenzenes. Spiropyrans, alike DAE derivatives, can undergo photocatalyzed electrocyclization from unpolar spiro-form (Sp) to highly polar merocyanine-form (Mc). In acidic conditions, spiropyran forms thermally stable protonated merocyanine-form (McH$^+$). The system exhibits negative photochromism: McH$^+$ can be converted to Sp form with blue light and the back reaction occurs in the dark.[210] Dipole moment difference between McH$^+$ and Sp forms is usually higher than 10 D. Due to such dramatic polarity change, hydrogels functionalized with spiropyran can swell and shrink under light illumination,[211,212] being useful for microfluidic applications.[213] However, for soft robotics, spiropyran-based hydrogels have two major limitations. First, they must operate in acidic conditions, limiting their working environment. Second, gels have a slow rate of re-swelling as the isomerization of Sp to McH$^+$ depends on a spontaneous ring-opening reaction which usually requires hours, thus posing hurdles for fast robotic movements.[214,215]

Conversely, azobenzene-based hydrogels can operate in a solution with wide range of pH, while both *trans*-to-*cis* and *cis*-to-*trans* isomerization can be controlled with light. The drawback is that isomerization of azobenzene can only cause relatively small polarity change, yielding only a moderate actuation in hydrogel.[111,216] To improve the shape-morphing and deformation speed of azo-hydrogels, one possibility is to harness reversible host-guest interactions of azobenzene with cyclodextrin (CD). Cyclodextrins are cyclic oligosaccharides which consist of glucose subunits joined by α-1,4 glycosidic bonds. The most studied ones are α-, β- and γ-cyclodextrins, which are comprised of six, seven and eight glucose subunits, respectively. Cyclodextrins have a frustum structure, with hydroxyl groups placed at the outer surface, making them water-soluble but simultaneously creating a hydrophobic inner cavity that is an excellent host for hydrophobic guest groups. In azo-CD host-guest systems, *trans*-azo can fit into the hydrophobic cavity of CD while the *cis*-isomer is expelled from it as schematically shown in Fig. 3.11.[217] The binding constant of CD with *trans*-azo is over 50 times higher than that with *cis*-azo.[218] Utilizing this scheme, azobenzene- and CD-functionalized hydrogels have been used

to modify the crosslink density and drive swelling change of the gel. In their pioneering work, Harada and co-workers polymerized PNIPAm hydrogel having pendant azobenzene and CD units forming host-guest bonding and therefore acting as additional crosslinkers (Fig. 3.12). Upon irradiation with UV light, *trans*-to-*cis* isomerization occurs, destroying the host–guest complexes and decreasing the crosslinking density, which in turn gives rise to swelling of the gel. By irradiation with visible light, back isomerization occurs, the host-guest complexes are restored, and the gel shrinks. Using this mechanism, also photoinduced bending could be obtained: irradiation of thick strip-like gel actuator with UV light leads to a gradient of light intensity and host-guest crosslink density, and the gel bends away from the light source (Fig. 3.12). By illumination with visible light, the stripe relaxed back to its initial shape. After this work, many follow-up studies have detailed the mechanism and improved the actuation strength and speed of the guest-host hydrogels.[219–221]
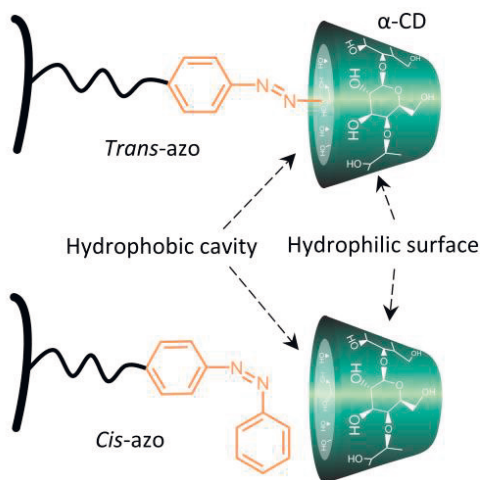
Figure 3.11 Schematic of supramolecular complexation between azobenzene and α-cyclodextrin. The *trans*-azo fits into the hydrophobic inner cavity of the CD but the *cis*-azo does not.

Instead of tuning the crosslinking density, azo-CD host-guest interaction can be also used to tune the hydrophilicity of the hydrogel. As *trans*-azo-CD complexes are much more hydrophilic than free *cis*-azo, reversible host-guest interactions offer a simple way to modulate hydrophilicity of the polymer on-demand. This on-demand technique for controlling the material hydrophilicity has been widely used to tune the solubility and stiffness of linear macromolecules.[222–224] In **Publication V**, we adapted similar concept and combined it with shape-programmable thin hydrogels. We use azobenzene-functionalized polymer and free α-CD molecules to form

reversible host-guest interaction, thus enabling controllable polymer hydrophilicity and deformability upon light excitation.

Figure 3.12 Photochemical azo-CD hydrogel actuator based on reversible host-guest interaction between azo and α-CD under UV/Visible light.[225] Adapted with permission: Copyright 2014, ACS.

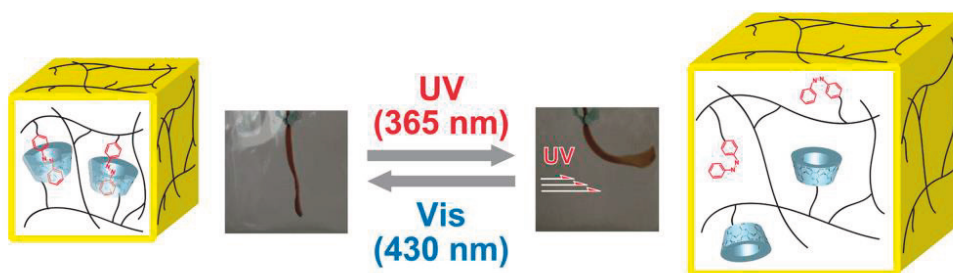# 4   ADVANCED CONTROL STRATEGIES FOR PHOTOACTUATION

Soft photoactuators can convert light signals into mechanical work without complex circuits or electronic control found in conventional hard machine systems. In this context, the word "photoactuator" does not only imply a design which can deform under light illumination but rather a structure that can sense and process the optical signals received and respond accordingly.[226] To attain this goal, much research effort in regard to 3D fabrication, chemical composition, and soft robotic design, has been devoted to light-responsive LCNs and hydrogels to endow them with ever-increasing functionalities and complexity. Particularly, the photoactuation behavior of these materials has been fine tuned for high environmental sensitivity, capability of processing the information received, and subsequent response. During the past decades several concepts have been proposed for pursuing such high level of sophistication, as treated in many recent reviews.[29,226–228] Among those examples, LCN- or hydrogel-based light robots can perform versatile movements like walking, swimming, jumping and gripping, but also possess more sophisticated skills, such as self-regulation[127,229], object recognition[176,230], self-healing[231] and learning[232,233]. The key concepts behind such advanced functions lie in optimized use of the photothermal and photochemical effects, clever material engineering including controlling the LC alignment and crosslinking density, and finally, proper temporal and/or spatial control of the light source.

This chapter focuses on three advanced control strategies for photoactuation that are used in the publications comprising this thesis: self-sustained motion, multicolor response, and reconfigurable action. The elaboration starts by a brief review of previous studies. After that, the most relevant findings from the thesis publications are presented and the improvements they bring to the controllability of photoactuators and light-driven soft robots, are highlighted.

4.1 Review of previous studies

Usually, soft robotic movement, like locomotion, needs cyclic actuation of the light-responsive material, which is attained with spatially and/or temporally modulated light source. Recent studies have suggested a more advanced strategy, where the cyclic shape change is self-sustained and the structure can maintain its motion without a need to control the properties or spatial location of the power source. Coincidentally, such self-sustained motion is also ubiquitous in nature, for instance, heartbeat, pulsation, and cell cycling being some examples.

The self-sustained motion, most widely studied in LCNs, is based on photomechanical-bending-induced oscillation, which was firstly observed in azobenzene-containing cantilevers.[155,234] Those cantilevers were irradiated with a focused laser beam, triggering the bending motion towards the light source due to combination of photothermal and photochemical effects. Bending of the film exposed one of the surfaces to light, which subsequently caused bending to opposite direction and exposure of the other surface, as schematically shown in Fig. 4.1a. This caused alternated activation of both cantilever surfaces and oscillation at high frequency (up to 270 Hz). By adjusting parameters such as cantilever dimensions, laser intensity and polarization direction, different oscillation amplitudes and frequencies could be obtained. Also, by tuning the angle between the director $\boldsymbol{n}$ and the cantilever long axis, out-of-plane twisting was obtained.[235] Bending-type oscillation can also be achieved by self-shadowing effects as schematically illustrated in Fig. 4.1b.[131,144,209,236] In this case, LCN or hydrogel cantilevers comprise photothermal agents that cause light-induced heating and yield photothermal bending from specific position defined as a hinge. Once the cantilever bends, the structure itself sweeps across the beam path and shadows the hinge. Finally, the hinge cools down, cantilever relaxes and simultaneously exposes the hinge to light, and the whole process repeats.

Self-sustained motion has been used to realize LCN-based micro-devices, in which the light energy is converted to the mechanical energy to provide work output.[162,164,180,237,238] For example, a self-sustained plastic motor can rotate upon simultaneous irradiation from two sides using different wavelengths (Fig. 4.2a).[162] Self-sustained walker was fabricated by confining an LCN cantilever into a rigid support structure, and photothermal wave-like oscillator was used to propel locomotion of the structure (Fig. 4.2b).[177] In hydrogels, a pillar structure capable of 0.7 Hz oscillation upon continuous irradiation was demonstrated, and such self-

sustained motion was further developed into a swimming protype on top of water surface (Fig. 4.2c).[209]
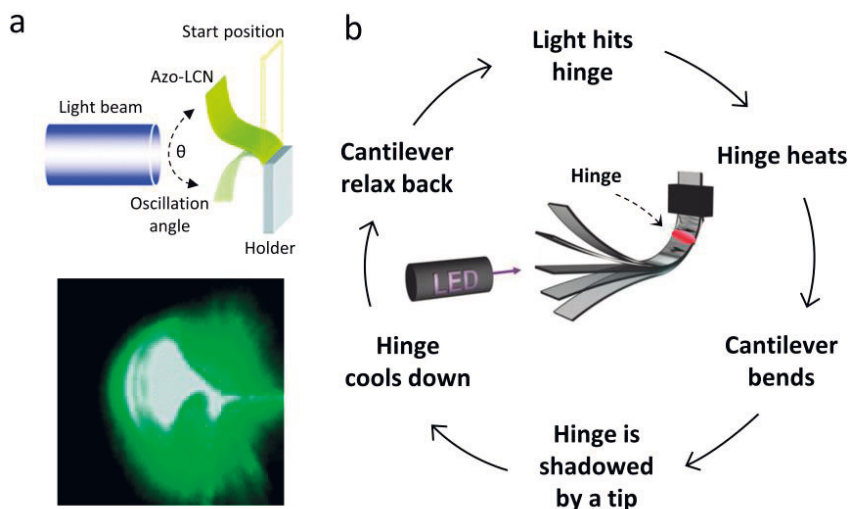
Figure 4.1 Self-sustained oscillation based on bending-induced exposure of different sides of the cantilever to light **(a)**[155], and self-shadowing **(b)**[131]. Figures reproduced with permission: **a)** Copyright 2005, RCS. **b)** Copyright 2017, John Wiley and Sons.
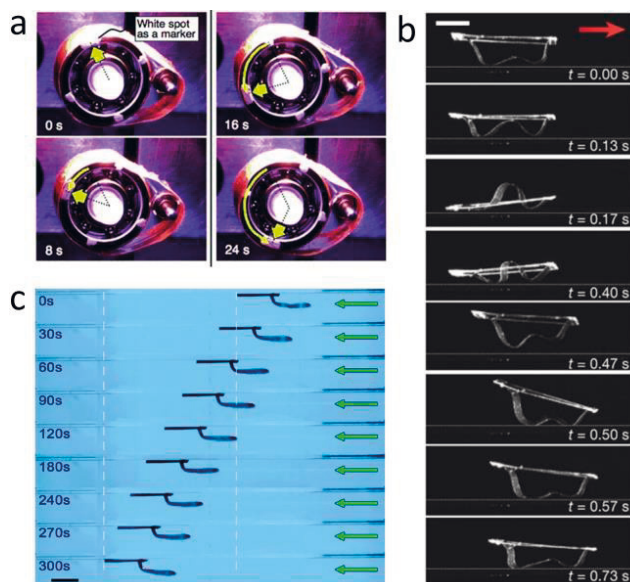
Figure 4.2 Self-sustained locomotion under light illumination. **a)** LCN motor[162], **b)** LCN wave-machine[177], **c)** hydrogel swimmer[209]. Figures reproduced with permission: **a)** Copyright 2008, John Wiley and sons. **b)** Copyright 2017, Springer Nature. **c)** Copyright 2019, AAAS.

Being responsive or even responding autonomously to a constant stimulus is just the beginning of the advanced photo-control of smart soft actuators. An advanced robot should be capable of reacting to multiple stimuli from the environment. This is often inspired by nature, where numerous species can adapt to the environmental changes including temperature, light, humidity, chemicals, etc. However, obtaining this goal in synthetic material systems is still challenging. Usually, most LCN or hydrogel photoactuators are based on a single actuation mode upon irradiation with one specific light wavelength. To extend the actuating modes, multicolor actuation can be used, which enables orthogonal wavelength control through incorporation of photoactive molecules responding to different parts of the light spectrum. For example, splay-oriented LCNs having two regions with different absorbing azobenzenes have been fabricated with inkjet printing.[239] By controlling bending of each stripe in a sequence of different light pulses, non-reciprocal motion was produced mimicking the motion of natural cilia (Fig. 4.3a). An LCN actuator assembly was reported to exhibit robotic locomotion in air[240,241] (Fig. 4.3b) and under water, where the movement direction and other functions, like gripping, could be steered with different wavelengths.[242] PNIMPAm hydrogel with altering layers of nanospheres (absorbing at 546 nm) and nanoshells (absorbing at 785 nm) was reported to show different swelling behavior upon different light fields (Fig. 4.3c).[243] Through different chemical composition, one can include different controllability into the material. However, the above-listed examples are still restricted by the limited form of actuation that has been dictated during the fabrication, for instance, the fixation of LC molecular alignment.

In nature, many species possess various degrees of freedom in movement – they can change their body in many ways by reacting to one environmental stimulus – having a reconfigurable response. In artificial materials, to realize this kind of smartness has been one of the grand challenges. To achieve reconfigurability in photoactuation, one must be able to tune the material behavior after fabrication and re-program the actuation on demand for different applications.

This issue has been raised in some recent studies, and one extensively used approach is to adjust crosslinking density after sample fabrication by utilizing dynamic covalent chemistry. In this chemical architecture, a reconfigurable polymer system should contain elements that can reversibly form/cleave covalent bonds under specific stimuli, for instance, transesterification[244] or Diels-alder reactions[245] in LCN matrix. Another strategy is to utilize light-sensitive reactions based on disulfide metathesis[246,247] or reaction with allyl sulfide[248], to induce patterns of the bond-cleavage/forming across sample area. Recently, Zhao and co-workers

demonstrated reconfigurable photoactuator based on selective de-crosslinking of anthracene dimers controlled by light.[249] The LCN was crosslinked via anthracene dimers, but upon irradiation with UV light, anthracene undergoes photocleavage and decrosslinking occurs. Thus, the sample could be patterned with crosslinked (actuation domains) and uncrosslinked (non-actuation domains) regions. Upon heating the polymer directly or phothermally by activation of NIR absorbing dye, it undergoes reversible shape-morphing determined by the photopatterned regions (Fig. 4.4a).
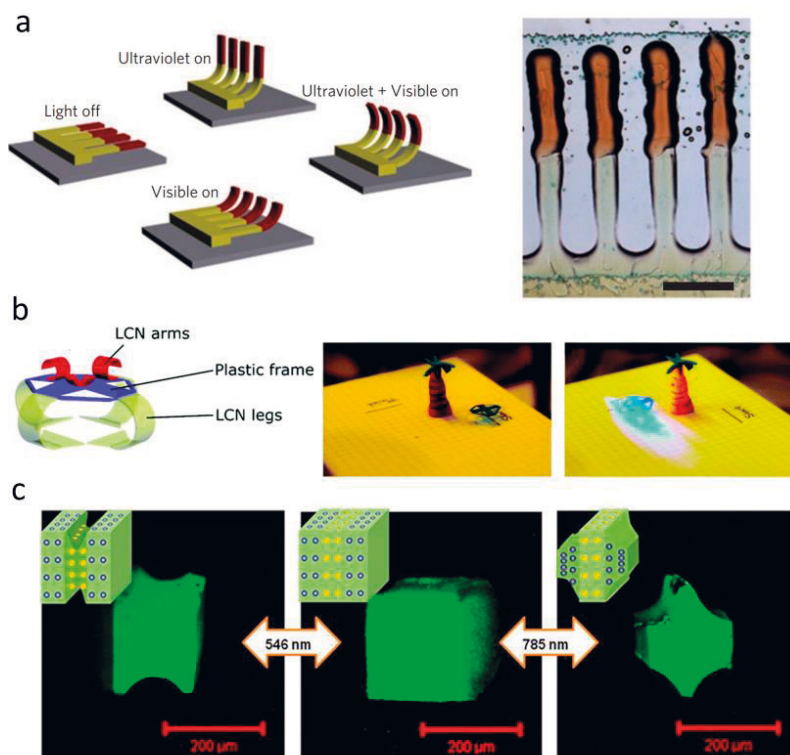
Figure 4.3 Multicolor actuation. **a)** Artificial LCN cilia producing non-reciprocal motion under distinct light illumination.[239] **b)** A soft robot made by LCN assemblies able to move and grip the cargo.[178] **c)** Wavelength-selective shaping of a PNIPAm structure containing gold nanospheres and -shells in alternating layers.[243] Figures reproduced with permission: **a)** Copyright 2009, Springer Nature. **b)** under terms of CC BY 3.0, Copyright 2020, The Authors. **c)** Copyright 2012, ACS.

Without influencing the crosslinking density, reconfigurability can be obtained by adjusting the properties of the mesogens locally. For example, LCNs containing azomerocyanine photoswitch, which can be converted to hydroxyazopyridinium-form locally with acid treatment (vice versa, with a base), have been used.[250] The two

forms have distinct absorption spectra and actuator cantilever can be designed to have hinges responding to specific wavelengths of light depending on the spatial distribution of state of the switches. The same LCN sample can be written, erased, and rewritten with different patterns, yielding different shape-morphing under identical illumination conditions (Fig. 4.4b).[250] Another study utilized a bilayer structure combing SMP and azo-LCN. Specific shapes could be programmed by processing the SMP above its T_g, while reversible bi-shape morphing was achieved by activating the azo-LCN layer with UV/blue light at room temperature.[165] In hydrogels, re-writable shape changes are also reported. For instance, activation of the photothermal agent locally using patterned light[206] or (re-)patterning photothermal agents locally via stamping approach can be used for distinct light actuation (Fig. 4.4c).[251]

In this thesis, approaches to all the above-mentioned challenges for controlling photoactuation have been proposed and are elaborated in detail in the next three sections.
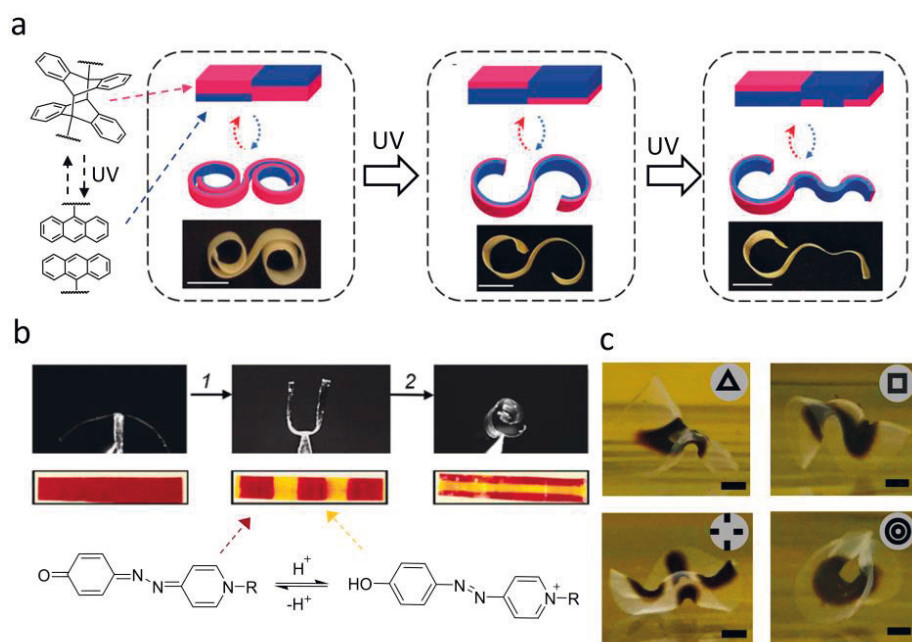
Figure 4.4 Reconfigurable photoactuators. **a)** Controlling dimerization of anthracene with UV light, LCN film can be patterned with light active (purple) and inert (blue) regions. Actuation is then possible by heat or light stimulus.[249] **b)** LCN actuator where light-active areas can be patterned with an acid.[250] **c)** A reconfigurable shape morphing of hydrogel thin film upon irradiation by varying the shape of the nanoparticle patterns (black areas).[251] Figures reproduced with permission: **a)** Copyright 2019, John Wiley and Sons, **b)** Copyright 2017, John Wiley and Sons. **c)** Copyright 2019, ACS

4.2   Self-sustained motion

To study the self-sustained motion, we have chosen three basic deformation modes: bending, contraction-expansion, and twisting, which have been elaborated in **Publication I**. Amplitude and oscillation frequency of the modes were quantified with out-of-plane bending angle (θ), displacement (d) and twisting angle (Φ) as schematically shown in Fig. 4.5a. The desired oscillation modes can be obtained through careful material engineering, i.e., alignment, mechanical properties, particular way of deformation, and a choice of illumination conditions including direction and intensity of the incident light (Fig. 4.5b). For **bending mode,** planar-aligned sample with n parallel to the cantilever long axis was used, while light was propagating along the cantilever axis. The bending mechanism was based on the combination of photothermal and photochemical effects, as described earlier (p. 43). This mechanism yielded a rapid deformation with a relatively high oscillation frequency of about ~80 Hz (Fig. 4.5c). For **contraction-expansion mode**, the same alignment was utilized, while the sample was illuminated from the top. Such deformation mode was based on photothermal effect: when the tip of the cantilever was exposed to the light spot, contraction occurred, and the tip moved out of the spot region. As light did not hit the cantilever, it cooled down, relaxed and re-exposed to the light spot. This mechanism yielded a relatively small oscillation frequency, about 0.5-18 Hz (Fig. 4.5d), as the heat produced needed to conduct along the cantilever axis to trigger deformation/relaxation. Oscillation frequency depend also on the position of the light beam. For **twisting mode**, the cantilever had LC alignment perpendicular to its long axis and it was illuminated from the side. The twisting of the actuator resulted in alternated exposure of the two surfaces and a continuous oscillation with frequency of about 1 Hz. Here, oscillation exhibited snapping between two stable states as soft material needed to accumulate stress to overcome the angular restriction. This resulted to rectangular waveform as shown in Fig. 4.5e.
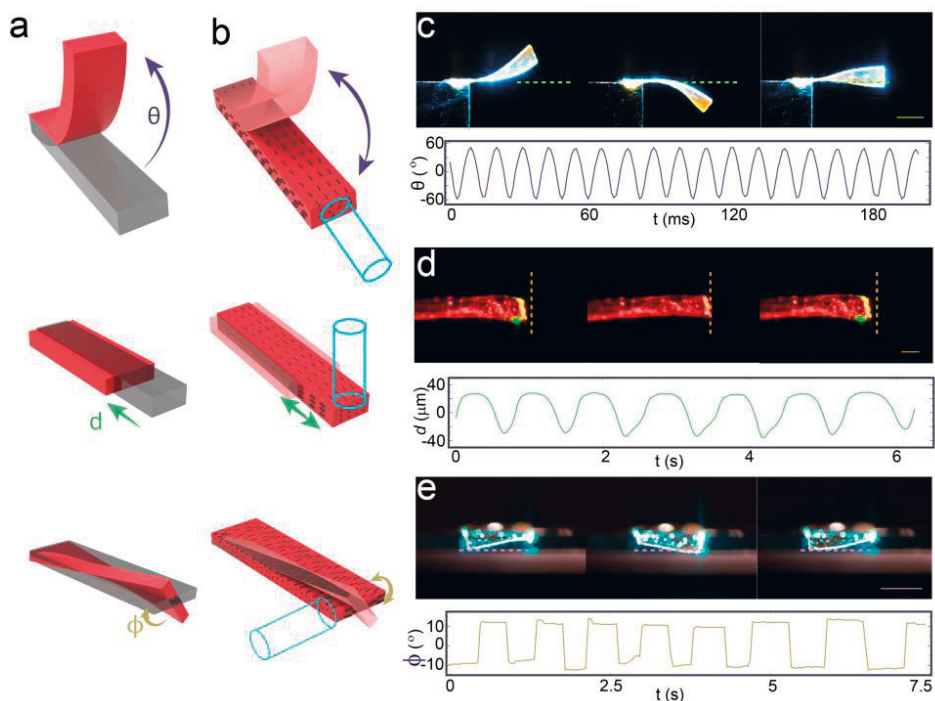
Figure 4.5 Three basic oscillation modes. **a)** Schematic of bending, contraction-expansion, and twisting modes. **b)** irradiation geometry and molecular alignment of the cantilever to initiate self-oscillation in each oscillation modes. **c-e)** Photographs of the oscillators and oscillation dynamics.

We also found that these basic deformation modes could be combined into one single actuator made of main-chain LCN with high deformability (Fig. 4.6a). Self-sustained oscillation was obtained by hanging the LCN cantilever on a hair thread. Upon photothermal excitation with a laser (532 nm), the localized strain builds up stress inside the LCN, causing it to deform and shift the gravity center. The cantilever rotated round the thread and went out of the excitation beam, followed by cooling in the dark and relaxation of structure. After relaxation, a new cycle could begin and self-sustained oscillation on the hair to be maintained. By small adjusting the position of the light spot, various stable oscillation modes (bending and/or contracting and/or twisting) were observed (Fig 4.6a). Also, self-evolution between the modes upon constant light irradiation was observed, coined as "freestyle oscillation". Different mode patterns were characterized by tracking the actuator position projected on x-y plane. Oscillation mostly occurred reciprocally, following the same path to both directions (Fig. 4.6b). However, sometimes trajectories with non-zero area were observed (Fig. 4.6c), indicating non-reciprocal motion with time-reversal asymmetry. Non-reciprocal motion is common to various natural species and is

essential for animal locomotion such as flying or swimming.[252] These natural examples have provided inspiration and control strategies also for the in soft micro robotics.[253]
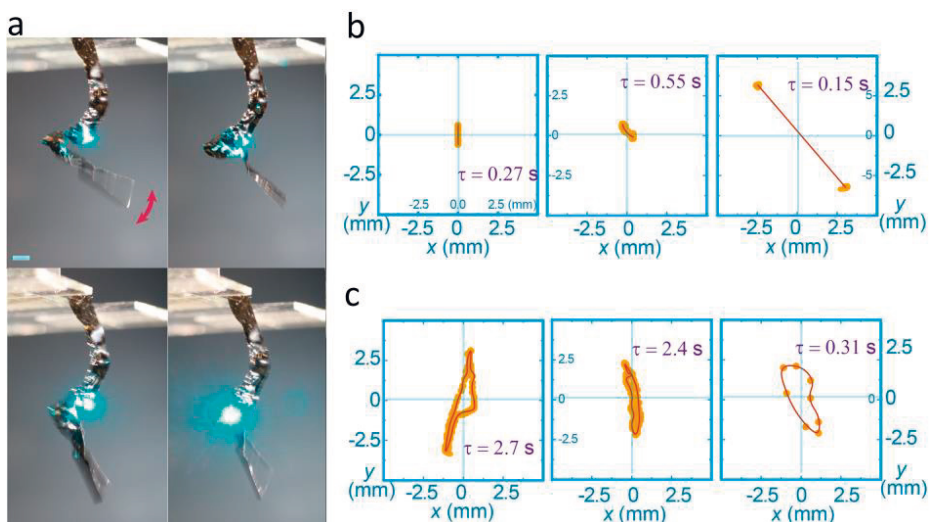

Figure 4.6 Snapshots **(a)** and *x–y* plane trajectory data for one oscillation cycle of different self-oscillation modes showing reciprocal **(b)** and non-reciprocal **(c)** movements.

In **Publication II,** we investigated non-reciprocal self-sustained oscillation in more detail. We utilized relatively long, flexible monolithic LCN cantilevers containing photothermal Disperse Red 1 dye (See Fig. 3.4 for chemical structure). The actuation was triggered with a 532 nm laser beam along the horizontal direction, and self-shadowing-induced oscillation was observed (Fig. 4.7a). Even though the chemical composition of the actuators was uniform, the cantilever could be divided into two parts: Part B being the area where light beam firstly hits, locating very close to place where cantilever was attached to the support, the rest being Part A. First, when the laser beam was hitting Part B, deformation caused Part A to shadow Part B. Part A, under light illumination, exhibited a dynamic change of cantilever's center of mass yielding gravity-induced torque on Part B. Change in torque of the cantilever led to the deformation of Part B and subsequently changed the position of Part A and closed the actuation cycle. Eventually, the movement trajectory of the cantilever exhibited a non-reciprocal pattern in the x–y plane (Fig. 4.7b) for > 50 oscillation cycles with frequency of about 0.1 Hz.
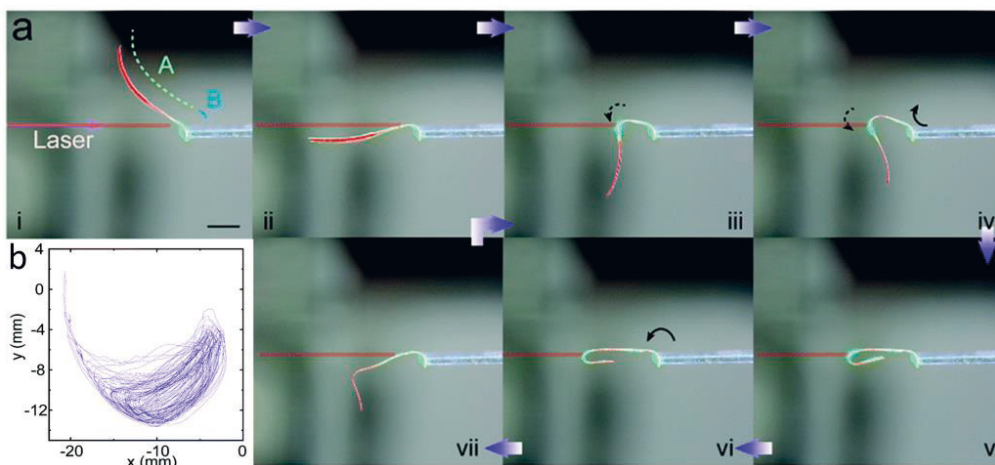
Figure 4.7 Non-reciprocal self-oscillation. **a)** Optical images of LCN self-oscillator under a constant light illumination. **b)** x-y movement trajectory of the cantilever position in 50 oscillation cycles.

4.3   Multicolor function

In **Publications II** and **III**, multicolor actuation with LCNs was studied by combining photothermal and photochemical actuation strategies either in different segments (parallel use) as shown in Fig. 4.8a or with the same film (synergistic use) as shown in Fig. 4.8b. In both cases, photochemical effect arises from the *trans-cis* isomerization of the azobenzene (Fig. 3.6) crosslinks, while Disperse Blue 14 (Fig. 3.4) was chosen for photothermal dye as its absorption wavelength is well separated from the azobenzene as illustrated in Fig. 4.8c, enabling orthogonal wavelength control of the two effects.

In **Publication II**, LCN actuators with two segments were fabricated by infiltrating two LCN mixtures through the opposite edges of an LC cell simultaneously, followed by photopolymerization. With this method, no additional adhesives between the two parts were needed. Non-reciprocal motion was obtained through distinct temporal control (Fig. 4.9a) of the two segments upon spatially uniform light fields with different wavelengths. The actuation kinetics was as follows: 1) UV light on → the bottom part (Fig. 4.9a yellow) bent because of *trans-cis* isomerization of the azobenzene crosslinks; 2) UV light off → the bottom part remained bent (due to the relatively long lifetime of *cis*-isomer, 3h) & red light on → the upper part (Fig. 4.9a blue) bent because of photothermal heating; 3) Blue light on → the bottom part relaxed due to *cis*-to-*trans* isomerization, while the upper part

remains bent; 4) Red light off → the upper part relaxed & blue light off → the system reset and a new cycle could start. The motion was studied by tracking the tip position in the x-y plane (Fig. 4.9b), where the trajectory pattern with non-zero area verified the non-reciprocity. In **Publication II**, we also demonstrated that similar non-reciprocal actuation behaviors could be achieved by different combinations of dyes and actuation wavelengths.
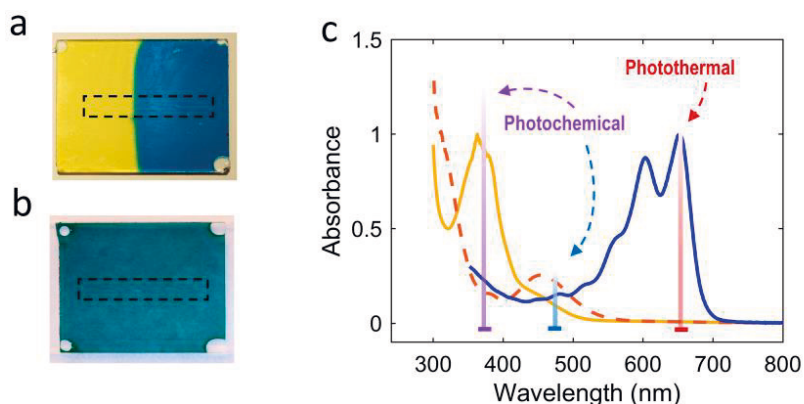
Figure 4.8 Multicolor function combining photothermal and photochemical actuation. Photograph of an LCN film with azobenzene crosslinker and DB14 in **a)** separate parts and **b)** same film. **c)** UV–Vis spectra of azobenzene crosslinker (yellow, orange) and DB14 (blue) used.
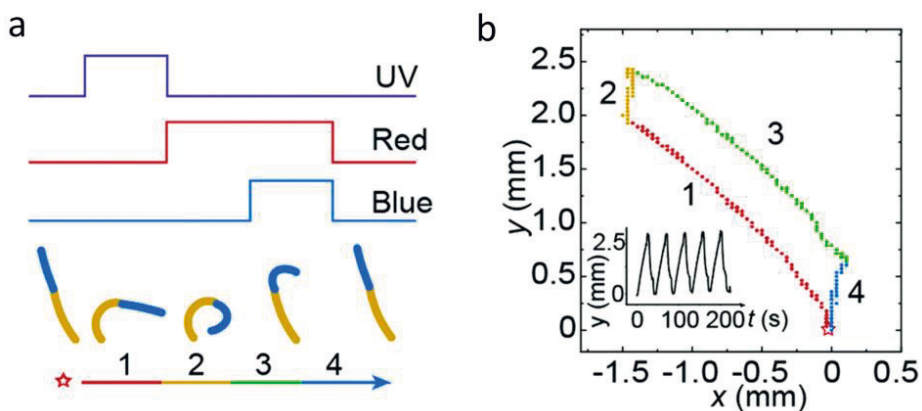
Figure 4.9 a) A light control sequence for non-reciprocal motion: 1) UV on 2) UV off, red light on 3) blue light on; 4) red and blue light off. Blue and yellow colors in the cantilever represent DB14- and azo-crosslinker -containing LCN segments, respectively. **b)** Non-reciprocal movement is characterized by a trajectory pattern with a non-zero area. Inset: displacement during repeated actuation cycles

In **Publication III**, the actuation was obtained in a chemically uniform LCN sample. The azobenzene crosslinker and DB14 were incorporate into the LCN film and the bending behavior of splay-aligned cantilevers under different illumination conditions was studied. Here, photochemical and photothermal actuation alone led to bending deformation toward the same direction (dictated by molecular alignment within the cantilever). Importantly, we observed a synergistic effect when combing both. With subsequent illumination of UV (photoisomerization) followed by red light (photothermal effect), the actuation strength was enhanced compared to the sum of photochemical and photothermal actuation being applied separately (Fig. 4.10). This was attributed to stress, induced by a photochemical isomerization, inside the polymer network, which could be later released by photothermal heating. Moreover, when ceasing the red light, the cantilever relaxed back only partially, indicating that the photochemically induced deformation could be preserved after photothermal actuation (Fig. 4.10a). When using both mechanisms simultaneously, cantilever attained its maximal deformation (Fig. 4.10b, purple). This actuation behavior also indicated that *cis*-azo concentration could be pre-patterned into the sample without significant actuation, but deformation could be obtained after applying photothermal heating later on. This gives access to reconfigurable photoactuation which will be further discussed in the next section.
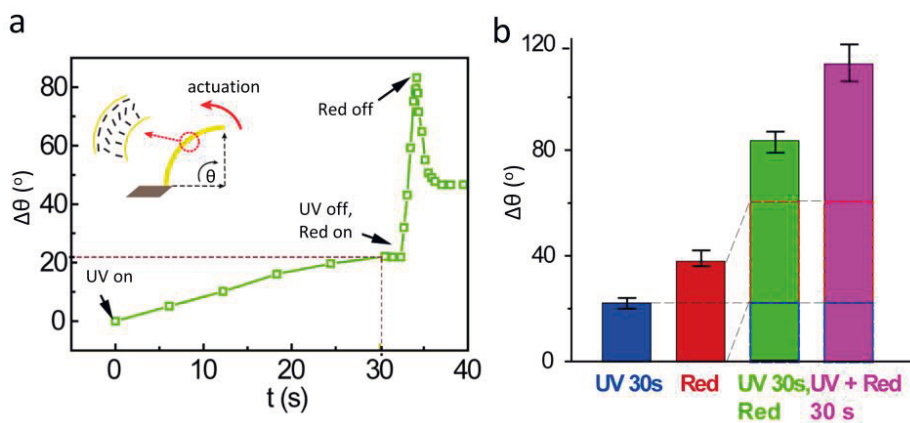
Figure 4.10 Enhanced photoactuation. **a)** Synergistic actuation using subsequent UV (isomerization) and red-light (photoheating) illumination. Inset: schematic of the bending direction. **b)** Maximum bending angle change upon different light stimuli

In **Publication IV,** a distinct wavelength control was achieved using only one photochromic dye, DAE (see Fig. 3.8a), crosslinked into the LCN. The actuation was based on photothermal effect since the electrocyclization of the DAE could not

induce observable photochemical deformation in our system (DAE undergoes only a small structural change upon illumination). The advantages of using DAE rather than azobenzene in photothermal actuation are the huge spectral change upon UV illumination (from 300 to 550 nm), and long thermal stability even under elevated temperatures. We utilized these features to realize a photoactuator (driven by visible light) with tunable light sensitivity (via UV). This advanced photo-control strategy enabled the demonstration of AND-gate logic operation. Logic gates are fundamental instruments for hard-bodied, electronically powered robots. However, incorporating similar logical operation concepts into soft robotics is a concern due to the mismatch between electronic components and compliant entities. Our DAE-LCN showed the AND-gate logic where UV and visible light served as inputs and photomechanical deformation (bending) as output (Fig. 4.11a). The AND logical table could be formulated as follows 1) if no light was used, the sample remained transparent, no heat was generated, and hence no deformation. 2) When only UV light was applied, the sample became absorbing, due to electrocyclization of DAE, and changed its color, but no photothermal heating took place due to relatively small illumination intensity and a high quantum yield of the ring closure of DAE. 3) If only visible light was used, the sample remained transparent (no absorption), thus no photoheating and again no deformation. 4) By using both light inputs simultaneously, the AND-gate was activated and photothermal deformation occurred. By tuning the UV dose and visible light intensity, the amount of photodeformation could be controlled, as showed in Fig. 4.11b.
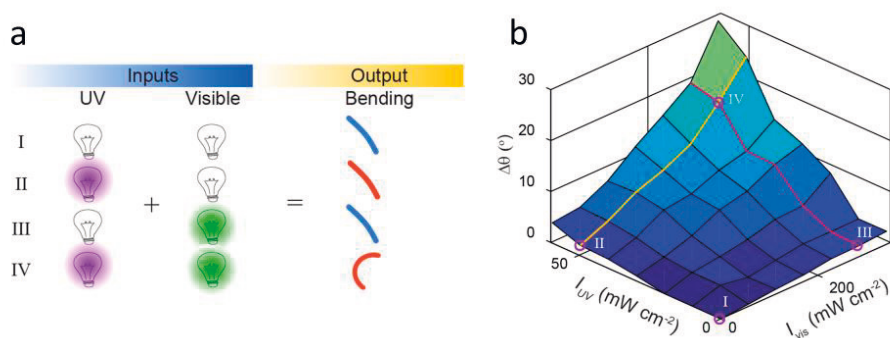

Figure 4.11 And-gate photoactuation: **a)** A logic table of the AND-gate photoactuator. Two inputs are UV and visible light irradiation while the output is the photomechanical bending. **b)** A bending angle of the DAE-LCN cantilever as a function of different UV and visible light intensities

4.4   Reconfigurable behavior

One of the main results of this thesis is to realize reconfigurable photoactuation. In **Publication III**, we demonstrated this through synergistic implementation of photochemical and photothermal effects. To obtain different kinds of deformation upon one identical stimulus, the spatial content of *cis*-azobenzene was patterned through UV mask exposure. This step enabled us to spatially program inner stresses into the LCN. The UV photopatterning did not yield significant shape change of the cantilever. Upon photothermal heating using red light, the cantilever quickly deformed into different geometries pre-determined by the *cis*-pattern as shown in Fig. 4.12. All shapes were obtained within the same LCN sample, and the initial flat geometry could be retained after illuminating with blue light (converting all the *cis*-azos back to the *trans*-form). Such reconfigurable actuation could be used to realize a soft robot with programmable performance. As shown in Fig. 4.13, a light driven gripper could grip the object (100 times heavier than a gripper itself) under red light and drop it when ceasing the light. However, if the gripper was pre-irradiated with UV light, it could still grip the object under red light but keep holding it for ca. 5 min after ceasing the red light. Again, the gripper could be restored to its original state by irradiating with blue light and commanded again (upon UV or not), to decide whether to grip-and-drop or grip-and-hold.
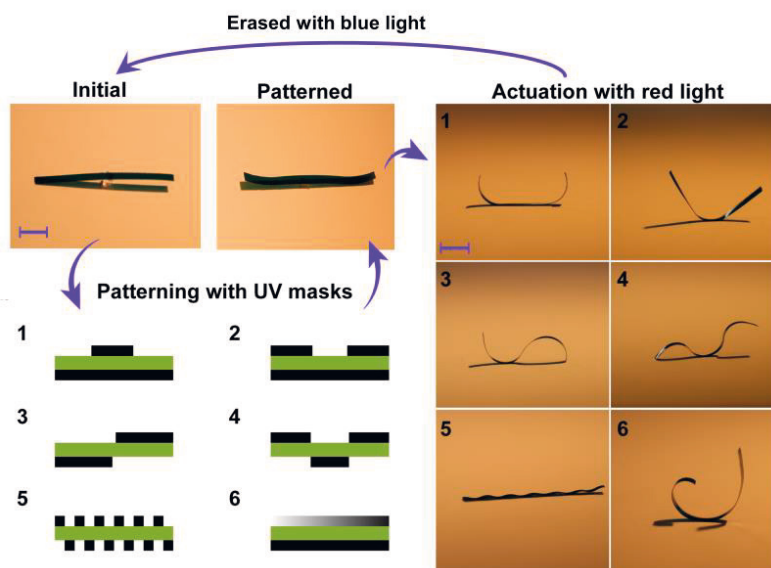
Figure 4.12 Reconfigurable shape-morphing using photochemical patterning and photothermal actuation. Scale bars: 5 mm.
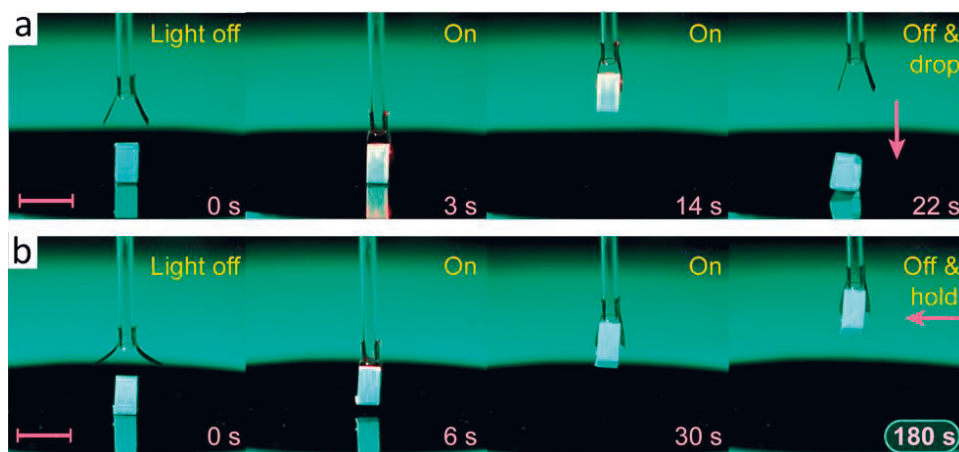
Figure 4.13 A reconfigurable micro-gripper with grip-and-release **(a)** and grip-and-hold **(b)** modes. Scale bar 5 mm.

In **Publication IV**, another reconfiguration strategy was proposed by showing that light-sensitive LCN could be tuned via optical control of the absorption level of the material. Thermally stable DAE allows the absorbance (at 550 nm) of the DAE-LCN film to be fixed at a desired level after illumination with different UV-Visible doses (Fig. 4.14a). Depending on the absorption, different photo-heating and thus actuation strengths upon identical visible light intensity can be achieved. The intensity-deformation curves under different UV intensities are shown in Fig. 4.14b.
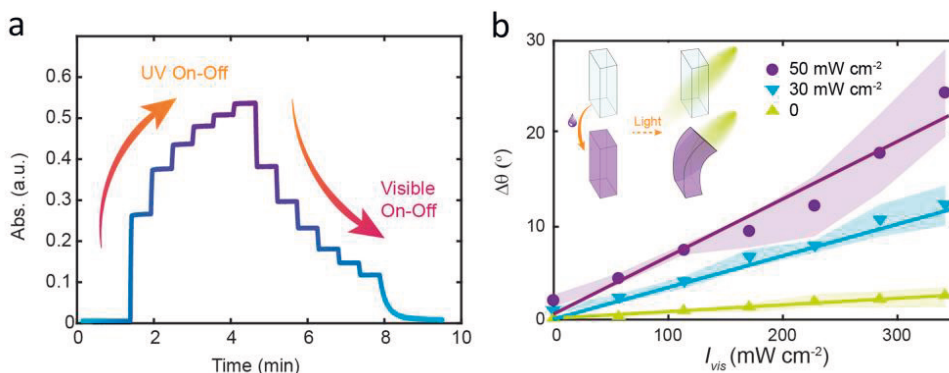
Figure 4.14 a) Increase and decrease of absorbance (at 550 nm) in the DAE containing LCN film by irradiation with UV and visible light, respectively **b)** A bending angle of the DAE-LCN cantilever upon irradiation with various intensities of UV and visible light. Actuator's sensitivity to visible light is estimated from the linear fit to the intensity-deformation data. Inset: Schematics of a reprogrammable actuator that shows minimal deformation initially but exhibits shape changes after color change.

In **Publication V,** the concept of reconfiguration was broadened to hydrogels utilizing reversible host-guest interactions between pendant azobenzene and a free α-CD inside PNIPAm. Under flood UV illumination of the thin hydrogel sheet (thickness ≈ 25 μm), immersed to the α-CD water solution, host-guest complexes were broken (Fig. 4.15a), leading to hydrophilicity-induced deswelling and macroscopic shrinking of the gel (Fig. 4.15b). To investigate how supramolecular complexation influences LCST behavior of the gel, areal swelling changes were monitored with the function of temperature in the dark and upon flood UV illumination. Prior to illumination, the gel showed a gradual de-swelling upon heating to 26 °C, followed by a sudden LCST transition (Fig. 4.15c, filled red circles). Illumination with 365 nm resulted in a decrease in swelling and a shift of the LCST transition to lower temperatures as the azo-α-CD complexes were destroyed (Fig. 4.15c, filled red squares). The percentage change in areal swelling showed a 50% increase in *cis*-azo-containing gel compared to *trans* samples in room temperature. To verify that swelling difference arose from the formation of host-guest complexes, areal swelling change was also measured in deionized water without α-CD, where only a small increase (≈5%) in swelling was observed upon *trans–cis* isomerization due to the small increase in polarity of the *cis*-isomer (Fig. 4.15c, black).
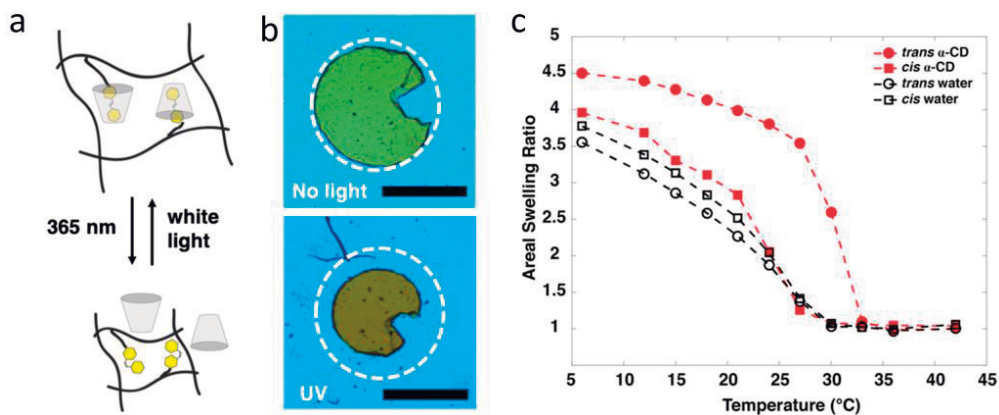
Figure 4.15 a) Schematic of reversible host-guest complexation between pendant azobenzene and free α-CD during *cis–trans* isomerization, leading to reversible changes in swelling. **b)** Optical micrographs of gels before and after UV illumination. Scale bar: 1 mm. **c)** A swelling difference of the gel before and after UV illumination in different temperatures in α-CD solution (red) and deionized water (black).

The controllable swelling upon UV illumination was utilized to program different Gaussian curvatures into the gel sheet. The gels were micro-patterned with UV light using a DMD integrated to an inverted microscope. When patterned in a circular

annulus such that the center of the gel remained unilluminated, de-swelling at the edges resulted in out-of-plane buckling into a spherical shape with positive Gaussian curvature (Fig. 4.16a). However, by illumination with white light, *cis*-to-*trans* isomerization occurred, and flat state was recovered (Fig. 4.16b). Another shape could be reprogrammed by shining a different pattern of UV light. For example, a saddle-like shape with negative Gaussian curvature was formed by patterning de-swelling in the center of the film (Fig. 4.16c). Photochemical patterning allowed shape persistency due to the relatively long thermal lifetime of the azobenzene (≈ 15 hour at room temperature), which is an improvement compared to photothermal strategies normally used, in which the gel retains an original shape after ceasing the light.[206] Moreover, this technique allowed reprogrammed shape deformation using only light without need of complex process like nanoparticle reduction.[251]
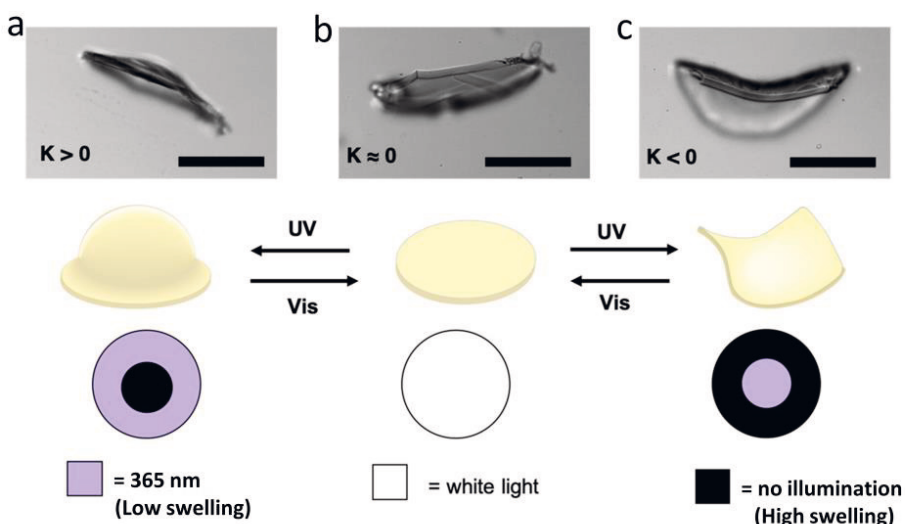
Figure 4.16 Reprogrammable hydrogel sheet between positive Gaussian curvature **(a)**, flat state **(b)** and negative Gaussian curvature **(c)** under UV/white light illumination. Scale bar: 1 mm.

5 CONCLUSION AND OUTLOOK

In this thesis we used LCNs (**Publications I-IV**) and thermoresponsive hydrogels (**Publication V**) to design soft polymers with advanced photoactuation behavior. We used three control strategies: self-sustained motion, multicolor functions and reconfigurability. Their connections to the publications are summarized in Table 5.1. Technically, we utilized photothermal and photochemical actuation mechanisms separately, in parallel, and synergistically to achieve complex actuation behavior like self-oscillation, non-reciprocal motion, AND-gate actuation, smart gripping, and Gaussian curvature control. To trigger the photochemical effect, we used photopolymerizable azobenzenes with thermal lifetime of several hours. For photothermal actuation we doped different organic dyes into polymer matrix, for instance, Disperse Blue 14, Disperse Red 1, and photochromic diarylethene. All the dyes and their absorption wavelengths were carefully chosen for their specific target.

Table 5.1 Summary of the advanced control strategies for photoactuation demonstrated in this thesis connected with the publications

Advanced Control Strategy	Publication				
	I	II	III	IV	V
1. Self-sustained motion	x	x			
2. Multicolor function		x	x	x	
3. Reconfigurability			x	x	x

Self-sustained oscillation, a phenomenon studied in **Publications I** and **II**, describes the interplay between light and the actuator: light absorption induces actuator's shape change, the deformed shape further modifies the absorption, causing the actuator to self-adjust its deformation. This is considered as a novel strategy to realize autonomous systems exhibiting self-propelled walking or swimming and may play significant roles in future soft robotics. We also demonstrated non-reciprocal self-

sustained oscillation and believe that in the future, this strategy may even lead to flying robots, which have not yet been realized using light responsive LCNs. However, to devise flying robots several parameters need to be improved like oscillation frequency and actuation speed. This not only requires careful optimization of the actuator's mechanical properties (stress, elastic modulus, density) and structure (size, shape), but also sophisticated control over the actuation kinetics to produce sufficient thrust via non-reciprocal trajectory (like bird's hovering). Special attentions on interaction between soft matter and unsteady aerodynamics is also required when designing responsive material based flying robots.

In **Publication II-IV** we showed that sophisticated control over LCN shape changes can be obtained using multiple wavelengths. The multicolor functions discussed in this thesis includes parallel use of photochemical and photothermal strategies for non-reciprocal actuation (**Publication II**), their synergistic use for enhanced photoactuation (**Publication III**) and separate use with one photochromic dye, DAE, enabling AND-gate actuation (**Publication IV**). Even though we concentrated on using different wavelengths for soft robotic control, coupling differently absorbing dyes in one single LCN and using photothermal and photochemical effects synergistically, might lead to soft robots which can be driven with very low light power, eventually obtained directly from the sun.

In **Publication III**, we studied reconfigurable actuation, in which a photo-active structure could shape-morph differently under identical light stimulus. We demonstrated LCN cantilever capable of distinct shape-morphing (six different shapes) using photochemical patterning and subsequent photothermal actuation. Moreover, smart gripper with either grip-and-drop or grip-and-hold performance, was reported. In **Publication IV,** reconfigurability was made by adjusting light sensitivity of the LCN with UV light stimulus, and therefore different actuation strength could be fine-tuned upon one identical visible light illumination. In **Publication V**, we used patterned light to reconfigure positive and negative Gaussian curvatures within the hydrogel sheets. The reconfigurability did not require any other programming but patterning light itself caused different swelling metric in hydrogel sheet providing an easy way to control the shape-morphing. Reconfigurability is one of the grand challenges for photoactuation and light responsive soft robotics, as future robots would need to possess capabilities of perceiving several signals from the environment, responding to environmental change and finally learn to change their own behaviour. In this thesis, we have taken some primitive steps toward these ultimate goals.

The field of photoactuation is growing rapidly, but there is still a long way to go before the soft shape-changing materials will be "normal" polymers in our everyday lives or make their way to real-world applications. Most accomplishments reported are "proof-of-concept" studies in laboratory environment. However, human-friendly interaction, flexibility, and ease of handling are the most significant points for robotics, which have steered the directions of robotic research from traditional bulky rigid machines to nascent small soft actuators. In longer term, it is foreseen that ever-increasing innovations and triggered applications will be brought to the field of soft robotics and other related frontiers, such as sensing, biotechnologies, and photonics.

In conclusion, this thesis has led to advancements in LCN- and hydrogel-based photoactuation by introducing novel and advanced control strategies. The value of the new information gained in this thesis lies in the added understanding of photochemical and photothermal effects and efficient implementation of both in controlling photomechanical deformation. The strategies presented here contribute new routes towards soft micro robotics that can be self-adapting and smart.

BIBLIOGRAPHY

1. Roberts, A. *The History of Science Fiction*. (Palgrave macmillan UK, 2016).
2. Boston Dynamic, ATLAS. https://www.bostondynamics.com/atlas (2021).
3. Zeng, H., Lahikainen, M., Wani, O. M., Berdin, A. & Priimagi, A. Liquid crystal polymer networks and elastomers for light-fueled robotics. in *Photoactive Functional Soft Materials: Preparation, Properties, and Applications* (ed. Li, Q.) 197–226 (Wiley Online Books, 2018).
4. Abbott, J. J., Nagy, Z., Beyeler, F. & Nelson, B. J. Robotics in the Small, Part I: Microbotics. *IEEE Robot. Autom. Mag.* **14**, 92–103 (2007).
5. Wood, R. J. The first takeoff of a biologically inspired at-scale robotic insect. *IEEE Trans. Robot.* **24**, 341–347 (2008).
6. Kim, S., Laschi, C. & Trimmer, B. Soft robotics: A bioinspired evolution in robotics. *Trends Biotechnol.* **31**, 287–294 (2013).
7. Hines, L., Petersen, K., Lum, G. Z. & Sitti, M. Soft Actuators for Small-Scale Robotics. *Adv. Mater.* **29**, 1603483 (2017).
8. Rus, D. & Tolley, M. T. Design, fabrication and control of soft robots. *Nature* **521**, 467–475 (2015).
9. Laschi, C., Mazzolai, B. & Cianchetti, M. Soft robotics: Technologies and systems pushing the boundaries of robot abilities. *Sci. Robot.* **1**, eaah3690 (2016).
10. Wehner, M. *et al.* An integrated design and fabrication strategy for entirely soft, autonomous robots. *Nature* **536**, 451–455 (2016).
11. Shepherd, R. F. *et al.* Multigait soft robot. *Proc. Natl. Acad. Sci.* **108**, 20400–20403 (2011).
12. Zeng, H., Wasylczyk, P., Wiersma, D. S. & Priimagi, A. Light Robots: Bridging the Gap between Microrobotics and Photomechanics in Soft Materials. *Adv. Mater.* **30**, 1703554 (2018).
13. Nelson, B. J., Kaliakatsos, I. K. & Abbott, J. J. Microrobots for Minimally Invasive Medicine. *Annu. Rev. Biomed. Eng.* **12**, 55–85 (2010).
14. Ceylan, H., Giltinan, J., Kozielski, K. & Sitti, M. Mobile microrobots for bioengineering applications. *Lab Chip* **17**, 1705–1724 (2017).
15. Mura, S., Nicolas, J. & Couvreur, P. Stimuli-responsive nanocarriers for drug delivery. *Nat. Mater.* **12**, 991–1003 (2013).
16. Stuart, M. A. C. *et al.* Emerging applications of stimuli-responsive polymer

materials. *Nat. Mater.* **9**, 101–113 (2010).

17. Umedachi, T., Vikas, V. & Trimmer, B. A. Softworms: The design and control of non-pneumatic, 3D-printed, deformable robots. *Bioinspiration and Biomimetics* **11**, 0 (2016).

18. Tottori, S. *et al.* Magnetic helical micromachines: Fabrication, controlled swimming, and cargo transport. *Adv. Mater.* **24**, 811–816 (2012).

19. Qiu, T. *et al.* Wireless actuation with functional acoustic surfaces. *Appl. Phys. Lett.* **109**, 191602 (2016).

20. Ikeda, T., Mamiya, J. I. & Yu, Y. Photomechanics of liquid-crystalline elastomers and other polymers. *Angew. Chemie Int. Ed.* **40**, 506–528 (2007).

21. Sitti, M. & Wiersma, D. S. Pros and Cons: Magnetic versus Optical Microrobots. *Adv. Mater.* **32**, 1906766 (2020).

22. Anderson, I. A., Gisby, T. A., McKay, T. G., O'Brien, B. M. & Calius, E. P. Multi-functional dielectric elastomer artificial muscles for soft and smart machines. *J. Appl. Phys.* **112**, 041101 (2012).

23. He, Q. *et al.* Electrically controlled liquid crystal elastomer-based soft tubular actuator with multimodal actuation. *Sci. Adv.* **5**, eaax5746 (2019).

24. Alarcón, C. H., de las, Pennadam, S. & Alexander, C. Stimuli responsive polymers for biomedical applications. *Chem. Soc. Rev.* **34**, 276–285 (2005).

25. Hu, Y., Li, Z., Lan, T. & Chen, W. Photoactuators for Direct Optical-to-Mechanical Energy Conversion: From Nanocomponent Assembly to Macroscopic Deformation. *Adv. Mater.* **28**, 10548–10556 (2016).

26. White, T. J. & Broer, D. J. Programmable and adaptive mechanics with liquid crystal polymer networks and elastomers. *Nat. Mater.* **14**, 1087–1098 (2015).

27. Hoffman, A. S. Hydrogels for biomedical applications. *Adv. Drug Deliv. Rev.* **64**, 18–23 (2012).

28. McCracken, J. M., Donovan, B. R. & White, T. J. Materials as Machines. *Adv. Mater.* **32**, 1906564 (2020).

29. Zhang, X. *et al.* The Pathway to Intelligence: Using Stimuli-Responsive Materials as Building Blocks for Constructing Smart and Functional Systems. *Adv. Mater.* **31**, 1804540 (2019).

30. Mülhaupt, R. Hermann staudinger and the origin of macromolecular chemistry. *Angew. Chemie - Int. Ed.* **43**, 1054–1063 (2004).

31. Carothers, W. H. Linear condensation polymers. US2071250A (1937).

32. Hoffman, A. S. "Intelligent" Polymers in Medicine and Biotechnology. **664**, 645–664 (1995).

33. Wei, M., Gao, Y., Li, X. & Serpe, M. J. Stimuli-responsive polymers and their applications. *Polym. Chem.* **8**, 127–143 (2017).

34. Aida, T., Meijer, E. W. & Stupp, S. I. Functional supramolecular polymers. *Science (80-.).* **335**, 813–817 (2012).

35. Hu, L., Zhang, Q., Li, X. & Serpe, M. J. Stimuli-responsive polymers for

sensing and actuation. *Mater. Horizons* **6**, 1774–1793 (2019).

36.   Gandhi, A., Paul, A., Sen, S. O. & Sen, K. K. Studies on thermoresponsive polymers: Phase behaviour, drug delivery and biomedical applications. *Asian J. Pharm. Sci.* **10**, 99–107 (2015).

37.   Schild, H. G. Poly(N-isopropylacrylamide): experiment, theory and application. *Prog. Polym. Sci.* **17**, 163–249 (1992).

38.   Tokareva, I., Minko, S., Fendler, J. H. & Hutter, E. Nanosensors based on responsive polymer brushes and gold nanoparticle enhanced transmission surface plasmon resonance spectroscopy. *J. Am. Chem. Soc.* **126**, 15950–15951 (2004).

39.   Paek, K., Yang, H., Lee, J., Park, J. & Kim, B. J. Efficient colorimetric pH sensor based on responsive polymer-quantum dot integrated graphene oxide. *ACS Nano* **8**, 2848–2856 (2014).

40.   Ebrahimi, M. M. S., Laabei, M., Jenkins, A. T. A. & Schönherr, H. Autonomously Sensing Hydrogels for the Rapid and Selective Detection of Pathogenic Bacteria. *Macromol. Rapid Commun.* **36**, 2123–2128 (2015).

41.   Noh, K. G. & Park, S. Y. Biosensor Array of Interpenetrating Polymer Network with Photonic Film Templated from Reactive Cholesteric Liquid Crystal and Enzyme-Immobilized Hydrogel Polymer. *Adv. Funct. Mater.* **28**, 1707562 (2018).

42.   Blaiszik, B. J. *et al.* Self-healing polymers and composites. *Annu. Rev. Mater. Res.* **40**, 179–211 (2010).

43.   Skirtach, A. G. *et al.* Laser-induced release of encapsulated materials inside living cells. *Angew. Chemie - Int. Ed.* **45**, 4612–4617 (2006).

44.   Yamada, M. *et al.* Photomobile polymer materials - Various three-dimensional movements. *J. Mater. Chem.* **19**, 60–62 (2009).

45.   Wang, S. & Urban, M. W. Self-healing polymers. *Nat. Rev. Mater.* **5**, 562–583 (2020).

46.   Burnworth, M. *et al.* Optically healable supramolecular polymers. *Nature* **472**, 334–337 (2011).

47.   Andreeva, D. V., Fix, D., Möhwald, H. & Shchukin, D. G. Self-healing anticorrosion coatings based on pH-sensitive polyelectrolyte/inhibitor sandwichlike nanostructures. *Adv. Mater.* **20**, 2789–2794 (2008).

48.   Mirfakhrai, T., Madden, J. D. W. & Baughman, R. H. Polymer artificial muscles. *Mater. Today* **10**, 30–38 (2007).

49.   Li, S. & Wang, K. W. Plant-inspired adaptive structures and materials for morphing and actuation: A review. *Bioinspiration and Biomimetics* **12**, 011001 (2017).

50.   Klute, G. K., Czerniecki, J. M. & Hannaford, B. Artificial Muscles: Actuators for Biorobotic Systems. *Int. J. Rob. Res.* **21**, 298–309 (2002).

51.   Behl, M., Zotzmann, J. & Lendlein, A. Shape-Memory Polymers and Shape-Changing Polymers. in *Shape-Memory Polymers* (Spinger, 2009).

52. Lendlein, A. & Kelch, S. Shape-Memory Effect. *Angew. Chemie - Int. Ed.* **41**, 2034–2057 (2002).

53. Brochu, P. & Pei, Q. Advances in dielectric elastomers for actuators and artificial muscles. *Macromol. Rapid Commun.* **31**, 10–36 (2010).

54. Kim, H. J., Chen, B., Suo, Z. & Hayward, R. C. Ionoelastomer junctions between polymer networks of fixed anions and cations. *Science (80-.).* **367**, 773–776 (2020).

55. Andrienko, D. Introduction to liquid crystals. *J. Mol. Liq.* **267**, 520–541 (2018).

56. Demus, D. Chemical Structure and Mesogenic Properties. in *Handbook of Liquid Crystals* (Wiley-VCH, 1998).

57. Blinov, L. *Structure and Properties of Liquid Crystals.* (Spinger, 2011).

58. Selinger, J. V. *Introduction to the Theory of Soft Matter From Ideal Gases to Liquid Crystals.* (Spinger, 2016).

59. Chilaya, G. Cholesteric Liquid Crystals: Optics, Electro-optics, and Photo-optics. in *Chirality in Liquid Crystals* (2006).

60. Gennes, P.-G. de & Prost, J. *The Physics of Liquid Crystals.* (Clarendon Press, 1993).

61. Dunmur, D. & Toriyama, K. Physical Properties: Optical Properties. in *Handbook of Liquid Crystals* (Wiley Online Books, 1998).

62. Gennes, D. P. Reflexions sur un type de polymeres nematiques. *C. R. Acad. Sci.* **281**, 101–103 (1975).

63. Finkelmann, H., Kock, H. J. & Rehage, G. Investigations on liquid crystalline polysiloxanes. *Macromol. Rapid Commun.* **2**, 317 (1981).

64. Ohm, C., Brehmer, M. & Zentel, R. Liquid crystalline elastomers as actuators and sensors. *Adv. Mater.* **22**, 3366–3387 (2010).

65. Xiao, Y.-Y., Jiang, Z.-C. & Zhao, Y. Liquid Crystal Polymer-Based Soft Robots. *Adv. Intell. Syst.* **2**, 2000148 (2020).

66. Kularatne, R. S., Kim, H., Boothby, J. M. & Ware, T. H. Liquid crystal elastomer actuators: Synthesis, alignment, and applications. *J. Polym. Sci. Part B Polym. Phys.* **55**, 395–411 (2017).

67. Broer, D., Crawford, G. & Zumer, S. Part II Weakly Cross-Linked Systems: liquid Crystal elastomers. in *Cross-linked Liquid crystalline systems - from Rigid Polymer Networks to Elastomers* (CRC Press, 2011).

68. Thomsen, D. L. *et al.* Liquid crystal elastomers with mechanical properties of a muscle. *Macromolecules* **34**, 5868–5875 (2001).

69. Broer, D., Crawford, G. & Zumer, S. Part I Densely Cross-Linked Systems. in *Cross-linked Liquid crystalline systems - from Rigid Polymer Networks to Elastomers* (CRC Press, 2011).

70. Ube, T. & Ikeda, T. Photomobile Polymer Materials with Complex 3D Deformation, Continuous Motions, Self-Regulation, and Enhanced

Processability. *Adv. Opt. Mater.* **7**, 1900380 (2019).

71. White, T. J. Light to work transduction and shape memory in glassy, photoresponsive macromolecular systems: Trends and opportunities. *J. Polym. Sci. Part B Polym. Phys.* **50**, 877–880 (2012).

72. Hong, Y. *et al.* Micron-sized main-chain liquid crystalline elastomer actuators with ultralarge amplitude contractions. *J. Am. Chem. Soc.* **131**, 15000–15004 (2009).

73. Brömmel, F., Kramer, D. & Finkelmann, H. Preparation of the liquid crystal elastomers. in *Liquid Crystal Elastomers: Materials and Applications* (Spinger, 2012).

74. Broer, D. J., Finkelmann, H. & Kondo, K. In-situ photopolymerization of an oriented liquid-crystalline acrylate. *Die Makromol. Chemie* **189**, 185–194 (1988).

75. Kahn, F. J., Taylor, G. N. & Schonhorn, H. Surface-Produced Alignment OF Liquid Crystals. *Proc. IEEE* **61**, (1973).

76. Ishihara, S. & Mizusaki, M. Alignment control technology of liquid crystal molecules. *J. Soc. Inf. Disp.* **28**, 44–74 (2020).

77. Stöhr, J. & Samant, M. G. Liquid crystal alignment by rubbed polymer surfaces: A microscopic bond orientation model. *J. Electron Spectros. Relat. Phenomena* **98–99**, 189–207 (1999).

78. Ichimura, K. Photoalignment of Liquid-Crystal Systems. *Chem. Rev.* **100**, 1847–1873 (2000).

79. Priimagi, A., Barrett, C. J. & Shishido, A. Recent twists in photoactuation and photoalignment control. *J. Mater. Chem. C* **2**, 7155–7162 (2014).

80. Harris, K. D., Bastiaansen, C. W. M., Lub, J. & Broer, D. J. Self-assembled polymer films for controlled agent-driven motion. *Nano Lett.* **5**, 1857–1860 (2005).

81. Li, M. H., Keller, P., Antonietti, M., Lacey, D. & Meyer, R. B. Artificial muscles based on liquid crystal elastomers. *Philos. Trans. R. Soc. A Math. Phys. Eng. Sci.* **364**, 2763–2777 (2006).

82. Li, M.-H., Keller, P., Li, B., Wang, X. & Brunet, M. Light-Driven Side-On Nematic Elastomer Actuators. *Adv. Mater.* **15**, 569–572 (2003).

83. Liu, L., Liu, M. H., Deng, L. L., Lin, B. P. & Yang, H. Near-Infrared Chromophore Functionalized Soft Actuator with Ultrafast Photoresponsive Speed and Superior Mechanical Property. *J. Am. Chem. Soc.* **139**, 11333–11336 (2017).

84. Hoyle, C. E. & Bowman, C. N. Thiol-ene click chemistry. *Angew. Chemie - Int. Ed.* **49**, 1540–1573 (2010).

85. Yoon, H. H., Kim, D. Y., Jeong, K. U. & Ahn, S. K. Surface Aligned Main-Chain Liquid Crystalline Elastomers: Tailored Properties by the Choice of Amine Chain Extenders. *Macromolecules* **51**, 1141–1149 (2018).

86. Ware, T. H., McConney, M. E., Wie, J. J., Tondiglia, V. P. & White, T. J. Voxelated liquid crystal elastomers. *Science (80-.).* **347**, 982–984 (2015).

87. Ahn, S. K., Ware, T. H., Lee, K. M., Tondiglia, V. P. & White, T. J. Photoinduced Topographical Feature Development in Blueprinted Azobenzene-Functionalized Liquid Crystalline Elastomers. *Adv. Funct. Mater.* **26**, 5819–5826 (2016).

88. Ware, T. H., Perry, Z. P., Middleton, C. M., Iacono, S. T. & White, T. J. Programmable Liquid Crystal Elastomers Prepared by Thiol-Ene Photopolymerization. *ACS Macro Lett.* **4**, 942–946 (2015).

89. Saed, M. O. *et al.* Molecularly-Engineered, 4D-Printed Liquid Crystal Elastomer Actuators. *Adv. Funct. Mater.* **29**, 1–9 (2019).

90. Ambulo, C. P. *et al.* Four-dimensional Printing of Liquid Crystal Elastomers. *ACS Appl. Mater. Interfaces* **9**, 37332–37339 (2017).

91. Zhang, C. *et al.* 4D Printing of a Liquid Crystal Elastomer with a Controllable Orientation Gradient. *ACS Appl. Mater. Interfaces* **11**, 44774–44782 (2019).

92. López-Valdeolivas, M., Liu, D., Broer, D. J. & Sánchez-Somolinos, C. 4D Printed Actuators with Soft-Robotic Functions. *Macromol. Rapid Commun.* **39**, 3–9 (2018).

93. Ceamanos, L. *et al.* Four-dimensional printed liquid crystalline elastomer actuators with fast photoinduced mechanical response toward light-driven robotic functions. *ACS Appl. Mater. Interfaces* **12**, 44195–44204 (2020).

94. Yang, G. Z. *et al.* Ten robotics technologies of the year. *Sci. Robot.* **4**, eaaw1826 (2019).

95. Ahmed, E. Hydrogel: Preparation, characterization, and applications: A review. *J. Adv. Res.* **6**, 105-121 (2015).

96. Echeverria, C., Fernandes, S. N., Soares, P. I. P. & Godinho, M. H. Functional Stimuli-Responsive Gels: Hydrogels and Microgels. *Gels* **4**, 54 (2018).

97. Peppas, N. A., Hilt, J. Z., Khademhosseini, A. & Langer, R. Hydrogels in biology and medicine: From molecular principles to bionanotechnology. *Adv. Mater.* **18**, 1345–1360 (2006).

98. Drury, J. L. & Mooney, D. J. Hydrogels for tissue engineering: Scaffold design variables and applications. *Biomaterials* **24**, 4337–4351 (2003).

99. Harmon, M. E., Jakob, T. A. M., Knoll, W. & Frank, C. W. A surface plasmon resonance study of volume phase transitions in N-isopropylacrylamide gel films. *Macromolecules* **35**, 5999–6004 (2002).

100. Mateescu, A., Wang, Y., Dostalek, J. & Jonas, U. Thin hydrogel films for optical biosensor applications. *Membranes (Basel).* **2**, 49–69 (2012).

101. Kuckling, D., Harmon, M. E. & Frank, C. W. Photo-cross-linkable PNIPAAm copolymers. 1. Synthesis and characterization of constrained temperature-responsive hydrogel layers. *Macromolecules* **35**, 6377–6383

(2002).

102. Matsukuma, D., Yamamoto, K. & Aoyagi, T. Stimuli-responsive properties of N-isopropylacrylamide-based ultrathin hydrogel films prepared by photo-cross-linking. *Langmuir* **22**, 5911–5915 (2006).

103. Nash, M. E. *et al.* Ultra-thin spin coated crosslinkable hydrogels for use in cell sheet recovery - Synthesis, characterisation to application. *Soft Matter* **8**, 3889–3899 (2012).

104. Otake, K., Inomata, H., Konno, M. & Saito, S. Thermal Analysis of the Volume Phase Transition with N-Isopropylacrylamide Gels. *Macromolecules* **23**, 283–289 (1990).

105. Sponchioni, M., Capasso Palmiero, U. & Moscatelli, D. Thermo-responsive polymers: Applications of smart materials in drug delivery and tissue engineering. *Mater. Sci. Eng. C* **102**, 589–605 (2019).

106. Roy, D., Brooks, W. L. A. & Sumerlin, B. S. New directions in thermoresponsive polymers. *Chem. Soc. Rev.* **42**, 7214–7243 (2013).

107. Jaspers, M. *et al.* Ultra-responsive soft matter from strain-stiffening hydrogels. *Nat. Commun.* **5**, 5808 (2014).

108. Boutris, C., Chatzi, E. G. & Kiparissides, C. Characterization of the LCST behaviour of aqueous poly(N-isopropylacrylamide) solutions by thermal and cloud point techniques. *Polym. J.* **38**, 2567–2570 (1997).

109. Liu, R., Fraylich, M. & Saunders, B. R. Thermoresponsive copolymers: From fundamental studies to applications. *Colloid Polym. Sci.* **287**, 627–643 (2009).

110. Chen, G. & Hoffman, A. S. Graft copolymers that exhibit temperature-induced phase transitions over a wide range of pH. *Nature* **373**, 49–42 (1995).

111. Li, L., Scheiger, J. M. & Levkin, P. A. Design and Applications of Photoresponsive Hydrogels. *Adv. Mater.* **31**, (2019).

112. Yoon, J., Cai, S., Suo, Z. & Hayward, R. C. Poroelastic swelling kinetics of thin hydrogel layers: Comparison of theory and experiment. *Soft Matter* **6**, 6004–6012 (2010).

113. Tokarev, I. & Minko, S. Stimuli-responsive hydrogel thin films. *Soft Matter* **5**, 511–524 (2009).

114. Dong, L. & Zhao, Y. Photothermally driven liquid crystal polymer actuators. *Mater. Chem. Front.* **2**, 1932–1943 (2018).

115. Kuenstler, A. S. & Hayward, R. C. Light-induced shape morphing of thin films. *Curr. Opin. Colloid Interface Sci.* **40**, 70–86 (2019).

116. Russew, M. M. & Hecht, S. Photoswitches: From molecules to materials. *Adv. Mater.* **22**, 3348–3360 (2010).

117. Montero De Espinosa, L., Meesorn, W., Moatsou, D. & Weder, C. Bioinspired Polymer Systems with Stimuli-Responsive Mechanical Properties. *Chem. Rev.* **117**, 12851–12892 (2017).

118. Mehta, K. *et al.* Design and applications of light responsive liquid crystal polymer thin films. *Appl. Phys. Rev.* **7**, 041306 (2020).

119. Zhang, X. *et al.* Photoactuators and motors based on carbon nanotubes with selective chirality distributions. *Nat. Commun.* **5**, (2014).

120. Van Oosten, C. L., Harris, K. D., Bastiaansen, C. W. M. & Broer, D. J. Glassy photomechanical liquid-crystal network actuators for microscale devices. *Eur. Phys. J. E* **23**, 329–336 (2007).

121. Warner, M., Modes, C. D. & Corbett, D. Curvature in nematic elastica responding to light and heat. *Proc. R. Soc. A Math. Phys. Eng. Sci.* **466**, 2975–2989 (2010).

122. Sawa, Y. *et al.* Shape selection of twist-nematic-elastomer ribbons. *Proc. Natl. Acad. Sci.* **108**, 6364–6368 (2011).

123. Modes, C. D., Bhattacharya, K. & Warner, M. Gaussian curvature from flat elastica sheets. *Proc. R. Soc. A Math. Phys. Eng. Sci.* **467**, 1121–1140 (2011).

124. De Haan, L. T., Sánchez-Somolinos, C., Bastiaansen, C. M. W., Schenning, A. P. H. J. & Broer, D. J. Engineering of complex order and the macroscopic deformation of liquid crystal polymer networks. *Angew. Chemie - Int. Ed.* **51**, 12469–12472 (2012).

125. De Haan, L. T. *et al.* Accordion-like actuators of multiple 3D patterned liquid crystal polymer films. *Adv. Funct. Mater.* **24**, 1251–1258 (2014).

126. Zeng, H., Wani, O. M., Wasylczyk, P. & Priimagi, A. Light-Driven, Caterpillar-Inspired Miniature Inching Robot. *Macromol. Rapid Commun.* **39**, 201700224 (2017).

127. Zeng, H., Wani, O. M., Wasylczyk, P., Kaczmarek, R. & Priimagi, A. Self-Regulating Iris Based on Light-Actuated Liquid Crystal Elastomer. *Adv. Mater.* **29**, 1701814 (2017).

128. Yang, R. & Zhao, Y. Non-Uniform Optical Inscription of Actuation Domains in a Liquid Crystal Polymer of Uniaxial Orientation: An Approach to Complex and Programmable Shape Changes. *Angew. Chemie - Int. Ed.* **56**, 14202–14206 (2017).

129. Bisoyi, H. K., Urbas, A. M. & Li, Q. Soft Materials Driven by Photothermal Effect and Their Applications. *Adv. Opt. Mater.* **6**, 1800458 (2018).

130. De Haan, L. T., Schenning, A. P. H. J. & Broer, D. J. Programmed morphing of liquid crystal networks. *Polym. J.* **55**, 5885–5896 (2014).

131. Gelebart, A. H., Vantomme, G., Meijer, B. E. W. & Broer, D. J. Mastering the Photothermal Effect in Liquid Crystal Networks: A General Approach for Self-Sustained Mechanical Oscillators. *Adv. Mater.* **29**, 1606712 (2017).

132. Guo, L.-X. *et al.* A calamitic mesogenic near-infrared absorbing croconaine dye/liquid crystalline elastomer composite. *Chem. Sci.* **7**, 4400–4406 (2016).

133. Zeng, H., Zhang, H., Ikkala, O. & Priimagi, A. Associative Learning by Classical Conditioning in Liquid Crystal Network Actuators. *Matter* **2**, 194–206 (2020).

134. Yang, L., Setyowati, K., Li, A., Gong, S. & Chen, J. Reversible infrared actuation of carbon nanotube-liquid crystalline elastomer nanocomposites. *Adv. Mater.* **20**, 2271–2275 (2008).

135. Ji, Y., Marshall, J. E. & Terentjev, E. M. Nanoparticle-liquid crystalline elastomer composites. *Polym. J.* **4**, 316–340 (2012).

136. Ahir, S. V., Squires, A. M., Tajbakhsh, A. R. & Terentjev, E. M. Infrared actuation in aligned polymer-nanotube composites. *Phys. Rev. B* **73**, 085420 (2006).

137. Ahir, S. V., Huang, Y. Y. & Terentjev, E. M. Polymers with aligned carbon nanotubes: Active composite materials. *Polym. J.* **49**, 3841–3854 (2008).

138. Jain, P. K., Huang, X., El-Sayed, I. H. & El-Sayed, M. A. Noble metals on the nanoscale: Optical and photothermal properties and some applications in imaging, sensing, biology, and medicine. *Acc. Chem. Res.* **41**, 1578–1586 (2008).

139. Hauser, A. W., Liu, D., Bryson, K. C., Hayward, R. C. & Broer, D. J. Reconfiguring Nanocomposite Liquid Crystal Polymer Films with Visible Light. *Macromolecules* **49**, 1575–1581 (2016).

140. Liu, X. *et al.* Reversible and rapid laser actuation of liquid crystalline elastomer micropillars with inclusion of gold nanoparticles. *Adv. Funct. Mater.* **25**, 3022–3032 (2015).

141. Lu, X. *et al.* Liquid-Crystalline Dynamic Networks Doped with Gold Nanorods Showing Enhanced Photocontrol of Actuation. *Adv. Mater.* **30**, 1706597 (2018).

142. Yang, H. *et al.* Near-infrared-responsive gold nanorod/liquid crystalline elastomer composites prepared by sequential thiol-click chemistry. *Chem. Commun.* **51**, 12126–12129 (2015).

143. Dong, L., Tong, X., Zhang, H., Chen, M. & Zhao, Y. Near-infrared light-driven locomotion of a liquid crystal polymer trilayer actuator. *Mater. Chem. Front.* **2**, 1383–1388 (2018).

144. Ge, F., Yang, R., Tong, X., Camerel, F. & Zhao, Y. A Multifunctional Dye-doped Liquid Crystal Polymer Actuator: Light-Guided Transportation, Turning in Locomotion, and Autonomous Motion. *Angew. Chemie - Int. Ed.* **57**, 11758–11763 (2018).

145. Kohlmeyer, R. R. & Chen, J. Wavelength-Selective, IR Light-Driven Hinges Based on Liquid Crystalline Elastomer Composites. *Angew. Chemie* **125**, 9404–9407 (2013).

146. Rogóż, M., Zeng, H., Xuan, C., Wiersma, D. S. & Wasylczyk, P. Light-Driven Soft Robot Mimics Caterpillar Locomotion in Natural Scale. *Adv.*

Opt. Mater. **4**, 1689–1694 (2016).

147. Rogó, M. *et al.* A Millimeter-Scale Snail Robot Based on a Light-Powered Liquid Crystal Elastomer Continuous Actuator. *Macromol. Rapid Commun.* **40**, 1900279 (2019).

148. Dattler, D. *et al.* Design of Collective Motions from Synthetic Molecular Switches, Rotors, and Motors. *Chem. Rev.* **120**, 310–433 (2020).

149. Yu, H. & Ikeda, T. Photocontrollable liquid-crystalline actuators. *Adv. Mater.* **23**, 2149–2180 (2011).

150. Bandara, H. M. D. & Burdette, S. C. Photoisomerization in different classes of azobenzene. *Chem. Soc. Rev.* **41**, 1809–1825 (2012).

151. Jiang, H., Li, C. & Huang, X. Actuators based on liquid crystalline elastomer materials. *Nanoscale* **5**, 5225 (2013).

152. Van Oosten, C. L. *et al.* Bending dynamics and directionality reversal in liquid crystal network photoactuators. *Macromolecules* **41**, 8592–8596 (2008).

153. Ikeda, T., Nakano, M., Yu, Y., Tsutsumi, O. & Kanazawa, A. Anisotropic bending and unbending behavior of azobenzene liquid-crystalline gels by light exposure. *Adv. Mater.* **15**, 201–204 (2003).

154. Yu, Y., Nakano, M. & Ikeda, T. Directed bending of a polymer film by light. *Nature* **425**, 145 (2003).

155. Serak, S. *et al.* Liquid crystalline polymer cantilever oscillators fueled by light. *Soft Matter* **6**, 779–783 (2010).

156. Bléger, D., Schwarz, J., Brouwer, A. M. & Hecht, S. O -fluoroazobenzenes as readily synthesized photoswitches offering nearly quantitative two-way isomerization with visible light. *J. Am. Chem. Soc.* **134**, 20597–20600 (2012).

157. Bléger, D. & Hecht, S. Visible-Light-Activated Molecular Switches. *Angew. Chemie - Int. Ed.* **54**, 11338–11349 (2015).

158. Kondo, M. *et al.* Effect of concentration of photoactive chromophores on photomechanical properties of crosslinked azobenzene liquid-crystalline polymers. *J. Mater. Chem.* **20**, 117–122 (2010).

159. Corbett, D. & Warner, M. Linear and nonlinear photoinduced deformations of cantilevers. *Phys. Rev. Lett.* **99**, (2007).

160. Shimamura, A. *et al.* Simultaneous Analysis of Optical and Mechanical Properties of Cross-Linked Azobenzene-Containing Liquid-Crystalline Polymer Films. *ACS Appl. Mater. Interfaces* **3**, 4190–4196 (2011).

161. Finkelmann, H., Nishikawa, E., Pereira, G. G. & Warner, M. A new opto-mechanical effect in solids. *Phys. Rev. Lett.* **87**, 015501 (2001).

162. Yamada, M. *et al.* Photomobile polymer materials: Towards light-driven plastic motors. *Angew. Chemie - Int. Ed.* **47**, 4986–4988 (2008).

163. Iamsaard, S. *et al.* Conversion of light into macroscopic helical motion. *Nat. Chem.* **6**, 229–235 (2014).

164. Lu, X., Guo, S., Tong, X., Xia, H. & Zhao, Y. Tunable Photocontrolled

Motions Using Stored Strain Energy in Malleable Azobenzene Liquid Crystalline Polymer Actuators. *Adv. Mater.* **29**, 1606467 (2017).

165. Verpaalen, R. C. P., Pilz da Cunha, M., Engels, T. A. P., Debije, M. G. & Schenning, A. P. H. J. Liquid Crystal Networks on Thermoplastics: Reprogrammable Photo-Responsive Actuators. *Angew. Chemie - Int. Ed.* **59**, 4532–4536 (2020).

166. Liu, D., Bastiaansen, C. W. M., Den Toonder, J. M. J. & Broer, D. J. Photo-switchable surface topologies in chiral nematic coatings. *Angew. Chemie - Int. Ed.* **51**, 892–896 (2012).

167. Liu, D., Bastiaansen, C. W. M., Den Toonder, J. M. J. & Broer, D. J. Light-induced formation of dynamic and permanent surface topologies in chiral-nematic polymer networks. *Macromolecules* **45**, 8005–8012 (2012).

168. Harris, J. D., Moran, M. J. & Aprahamian, I. New molecular switch architectures. *Proc. Natl. Acad. Sci. U. S. A.* **115**, 9414–9422 (2018).

169. Boelke, J. & Hecht, S. Designing Molecular Photoswitches for Soft Materials Applications. *Adv. Opt. Mater.* **7**, 1900404 (2019).

170. Lancia, F., Ryabchun, A. & Katsonis, N. Life-like motion driven by artificial molecular machines. *Nat. Rev. Chem.* **3**, 536–551 (2019).

171. Iamsaard, S. *et al.* Fluorinated Azobenzenes for Shape-Persistent Liquid Crystal Polymer Networks. *Angew. Chemie - Int. Ed.* **55**, 9908–9912 (2016).

172. Ryabchun, A., Li, Q., Lancia, F., Aprahamian, I. & Katsonis, N. Shape-Persistent Actuators from Hydrazone Photoswitches. *J. Am. Chem. Soc.* **141**, 1196–1200 (2019).

173. Mamiya, J. I., Kuriyama, A., Yokota, N., Yamada, M. & Ikeda, T. Photomobile polymer materials: Photoresponsive behavior of cross-linked liquid-crystalline polymers with mesomorphic diarylethenes. *Chem. - A Eur. J.* **21**, 3174–3177 (2015).

174. Hou, J. *et al.* Photo-responsive helical motion by light-driven molecular motors in a liquid crystal network. *Angew. Chemie Int. Ed.* (2021).

175. Kumar, K., Schenning, A. P. H. J., Broer, D. J. & Liu, D. Regulating the modulus of a chiral liquid crystal polymer network by light. *Soft Matter* **12**, 3196–3201 (2016).

176. Wani, O. M., Zeng, H. & Priimagi, A. A light-driven artificial flytrap. *Nat. Commun.* **8**, 15546 (2017).

177. Gelebart, A. H. *et al.* Making waves in a photoactive polymer film. *Nature* **546**, 632–636 (2017).

178. Pilz Da Cunha, M., Debije, M. G. & Schenning, A. P. H. J. Bioinspired light-driven soft robots based on liquid crystal polymers. *Chem. Soc. Rev.* **49**, 6568–6578 (2020).

179. Lee, K. M. & White, T. J. Photochemical mechanism and photothermal considerations in the mechanical response of monodomain, azobenzene-

functionalized liquid crystal polymer networks. *Macromolecules* **45**, 7163–7170 (2012).

180. Vantomme, G., Gelebart, A. H., Broer, D. J. & Meijer, E. W. A four-blade light-driven plastic mill based on hydrazone liquid-crystal networks. *Tetrahedron* **73**, 4963–4967 (2017).

181. Kumar, K. *et al.* A chaotic self-oscillating sunlight-driven polymer actuator. *Nat. Commun.* **7**, 11975 (2016).

182. Lan, R. *et al.* Light-Driven Liquid Crystalline Networks and Soft Actuators with Degree-of-Freedom-Controlled Molecular Motors. *Adv. Funct. Mater.* **30**, 2000252 (2020).

183. Irie, M. & Mohri, M. Thermally Irreversible Photochromic Systems. Reversible Photocyclization of Diarylethene Derivatives. *J. Org. Chem.* **53**, 803–808 (1988).

184. Irie, M., Fukaminato, T., Matsuda, K. & Kobatake, S. Photochromism of diarylethene molecules and crystals: Memories, switches, and actuators. *Chem. Rev.* **114**, 12174–12277 (2014).

185. Tian, H. & Yang, S. Recent progresses on diarylethene based photochromic switches. *Chem. Soc. Rev.* **33**, 85–97 (2004).

186. Matsuda, K. & Irie, M. Diarylethene as a photoswitching unit. *J. Photochem. Photobiol. C Photochem. Rev.* **5**, 169–182 (2004).

187. Pilz Da Cunha, M., Van Thoor, E. A. J., Debije, M. G., Broer, D. J. & Schenning, A. P. H. J. Unravelling the photothermal and photomechanical contributions to actuation of azobenzene-doped liquid crystal polymers in air and water. *J. Mater. Chem. C* **7**, 13502–13509 (2019).

188. Ma, S., Li, X., Huang, S., Hu, J. & Yu, H. A Light-Activated Polymer Composite Enables On-Demand Photocontrolled Motion: Transportation at the Liquid/Air Interface. *Angew. Chemie - Int. Ed.* **58**, 2655–2659 (2019).

189. Shahsavan, H. *et al.* Bioinspired underwater locomotion of light-driven liquid crystal gels. *Proc. Natl. Acad. Sci.* **117**, 5125–5133 (2020).

190. Wang, M., Lin, B. P. & Yang, H. A plant tendril mimic soft actuator with phototunable bending and chiral twisting motion modes. *Nat. Commun.* **7**, 13981 (2016).

191. Cheng, Z., Wang, T., Li, X., Zhang, Y. & Yu, H. NIR-Vis-UV Light-Responsive Actuator Films of Polymer-Dispersed Liquid Crystal/Graphene Oxide Nanocomposites. *ACS Appl. Mater. Interfaces* **7**, 27494–27501 (2015).

192. Wang, M. *et al.* Multi-Stimuli Responsive Carbon Nanotube Incorporated Polysiloxane Azobenzene Liquid Crystalline Elastomer Composites. *Macromolecules* **49**, 663–671 (2016).

193. Allen, J. Application of patterned illumination using a DMD for optogenetic control of signaling. *Nat. Methods* **14**, 1114–1114 (2017).

194. Tang, L. *et al.* Poly(N-isopropylacrylamide)-based smart hydrogels: Design, properties and applications. *Prog. Mater. Sci.* **115**, 100702 (2020).

195. So, S. & Hayward, R. C. Tunable Upper Critical Solution Temperature of Poly(N-isopropylacrylamide) in Ionic Liquids for Sequential and Reversible Self-Folding. *ACS Appl. Mater. Interfaces* **9**, 15785–15790 (2017).

196. Ionov, L. Hydrogel-based actuators: possibilities and limitations. *Mater. Today* **17**, 494–503 (2014).

197. Ionov, L. Biomimetic hydrogel-based actuating systems. *Adv. Funct. Mater.* **23**, 4555–4570 (2013).

198. Na, J. H. *et al.* Programming reversibly self-folding origami with micropatterned photo-crosslinkable polymer trilayers. *Adv. Mater.* **27**, 79–85 (2015).

199. Jamal, M. *et al.* Bio-origami hydrogel scaffolds composed of photocrosslinked PEG bilayers. *Adv. Healthc. Mater.* **2**, 1142–1150 (2013).

200. Jeon, S. J., Hauser, A. W. & Hayward, R. C. Shape-Morphing Materials from Stimuli-Responsive Hydrogel Hybrids. *Acc. Chem. Res.* **50**, 161–169 (2017).

201. Kim, J., Hanna, J. A., Byun, M., Santangelo, C. D. & Hayward, R. C. Designing responsive buckled surfaces by halftone gel lithography. *Science (80-.).* **335**, 1201–1205 (2012).

202. Huang, L. *et al.* Ultrafast Digital Printing toward 4D Shape Changing Materials. *Adv. Mater.* **29**, 1605390 (2017).

203. Suzuki, A. & Tanaka, T. Phase transition in polymer gels induced by visible Light. *Nature* **346**, 345–347 (1990).

204. Wang, E., Desai, M. S. & Lee, S. W. Light-controlled graphene-elastin composite hydrogel actuators. *Nano Lett.* **13**, 2826–2830 (2013).

205. Zhang, X. *et al.* Optically- and thermally-responsive programmable materials based on carbon nanotube-hydrogel polymer composites. *Nano Lett.* **11**, 3239–3244 (2011).

206. Hauser, A. W., Evans, A. A., Na, J.-H. & Hayward, R. C. Photothermally Reprogrammable Buckling of Nanocomposite Gel Sheets. *Angew. Chemie - Int. Ed.* **127**, 5524–5527 (2015).

207. Peng, X. *et al.* Complex shape deformations of homogeneous poly(: N - isopropylacrylamide)/graphene oxide hydrogels programmed by local NIR irradiation. *J. Mater. Chem. B* **5**, 7997–8003 (2017).

208. Luo, R., Wu, J., Dinh, N. D. & Chen, C. H. Gradient porous elastic hydrogels with shape-memory property and anisotropic responses for programmable locomotion. *Adv. Funct. Mater.* **25**, 7272–7279 (2015).

209. Zhao, Y. *et al.* Soft phototactic swimmer based on self-sustained hydrogel oscillator. *Sci. Robot.* **4**, eaax7112 (2019).

210. Klajn, R. Spiropyran-based dynamic materials. *Chem. Soc. Rev.* **43**, 148–184

(2014).

211. Ziółkowski, B., Florea, L., Theobald, J., Benito-Lopez, F. & Diamond, D. Self-protonating spiropyran-co-NIPAM-co-acrylic acid hydrogel photoactuators. *Soft Matter* **9**, 8754–8760 (2013).

212. Sumaru, K., Ohi, K., Takagi, T., Kanamori, T. & Shinbo, T. Photoresponsive Properties of Poly (N -isopropylacrylamide) Hydrogel Partly Modified with Spirobenzopyran. *Langmuir* **22**, 4353–4356 (2006).

213. Schiphorst, J. *et al.* Molecular Design of Light-Responsive Hydrogels, For in Situ Generation of Fast and Reversible Valves for Micro fluidic Applications. *Chem. Mater.* **27**, 5925–5931 (2015).

214. Satoh, T., Sumaru, K., Takagi, T. & Kanamori, T. Fast-reversible light-driven hydrogels consisting of spirobenzopyran- functionalized poly(N-isopropylacrylamide). *Soft Matter* **7**, 8030–8034 (2011).

215. Francis, W., Dunne, A., Delaney, C., Florea, L. & Diamond, D. Spiropyran based hydrogels actuators—Walking in the light. *Sensors Actuators, B Chem.* **250**, 608–616 (2017).

216. Moniruzzaman, M., Fernando, G. F. & Talbot, J. D. R. Synthesis and characterization of an azobenzene- and acrylamide-based photoresponsive copolymer and gel. *J. Polym. Sci. Part A Polym. Chem.* **42**, 2886–2896 (2004).

217. Wang, D., Zhao, W., Wei, Q., Zhao, C. & Zheng, Y. Photoswitchable Azobenzene/Cyclodextrin Host-Guest Complexes: From UV- to Visible/Near-IR-Light-Responsive Systems. *ChemPhotoChem* **2**, 403–415 (2018).

218. Yamaguchi, H. *et al.* Photoswitchable gel assembly based on molecular recognition. *Nat. Commun.* **3**, 603 (2012).

219. Takashima, Y. *et al.* Expansion-contraction of photoresponsive artificial muscle regulated by host-guest interactions. *Nat. Commun.* **3**, 1270 (2012).

220. Zheng, Z. *et al.* Dynamic Softening or Stiffening a Supramolecular Hydrogel by Ultraviolet or Near-Infrared Light. *ACS Appl. Mater. Interfaces* **9**, 24511–24517 (2017).

221. Iwaso, K., Takashima, Y. & Harada, A. Fast response dry-type artificial molecular muscles with [c2]daisy chains. *Nat. Chem.* **8**, 625–632 (2016).

222. Tamesue, S., Takashima, Y., Yamaguchi, H., Shinkai, S. & Harada, A. Photoswitchable supramolecular hydrogels formed by cyclodextrins and azobenzene polymers. *Angew. Chemie - Int. Ed.* **49**, 7461–7464 (2010).

223. Schmidt, B. V. K. J., Hetzer, M., Ritter, H. & Barner-Kowollik, C. Modulation of the thermoresponsive behavior of poly(N,N-diethylacrylamide) via cyclodextrin host/guest interactions. *Macromol. Rapid Commun.* **34**, 1306–1311 (2013).

224. Guan, Y., Zhao, H. B., Yu, L. X., Chen, S. C. & Wang, Y. Z. Multi-stimuli sensitive supramolecular hydrogel formed by host-guest interaction

between PNIPAM-Azo and cyclodextrin dimers. *RSC Adv.* **4**, 4955–4959 (2014).

225. Harada, A., Takashima, Y. & Nakahata, M. Supramolecular polymeric materials via cyclodextrin-guest interactions. *Acc. Chem. Res.* **47**, 2128–2140 (2014).

226. Hu, J., Wang, W. & Yu, H. Endowing Soft Photo-Actuators with Intelligence. *Adv. Intell. Syst.* **1**, 1900050 (2019).

227. Li, J., Zhou, X. & Liu, Z. Recent Advances in Photoactuators and Their Applications in Intelligent Bionic Movements. *Adv. Opt. Mater.* 2000886 (2020).

228. Qin, L., Liu, X. & Yu, Y. Soft Actuators of Liquid Crystal Polymers Fueled by Light from Ultraviolet to Near Infrared. *Adv. Opt. Mater.* 2001743 (2021).

229. Li, C., Liu, Y., Huang, X. & Jiang, H. Direct sun-driven artificial heliotropism for solar energy harvesting based on a photo-thermomechanical liquid-crystal elastomer nanocomposite. *Adv. Funct. Mater.* **22**, 5166–5174 (2012).

230. Martella, D., Nocentini, S., Nuzhdin, D., Parmeggiani, C. & Wiersma, D. S. Photonic Microhand with Autonomous Action. *Adv. Mater.* **29**, 1704047 (2017).

231. Ni, B., Xie, H. Lou, Tang, J., Zhang, H. L. & Chen, E. Q. A self-healing photoinduced-deformable material fabricated by liquid crystalline elastomers using multivalent hydrogen bonds as cross-linkers. *Chem. Commun.* **52**, 10257–10260 (2016).

232. Zhang, H., Zeng, H., Priimagi, A. & Ikkala, O. Viewpoint: Pavlovian Materials—Functional Biomimetics Inspired by Classical Conditioning. *Adv. Mater.* **32**, 1906619 (2020).

233. Zhang, H., Zeng, H., Priimagi, A. & Ikkala, O. Programmable responsive hydrogels inspired by classical conditioning algorithm. *Nat. Commun.* **10**, 3267 (2019).

234. White, T. J. *et al.* A high frequency photodriven polymer oscillator. *Soft Matter* **4**, 1796–1798 (2008).

235. Lee, K. M. *et al.* Photodriven, flexural-torsional oscillation of glassy azobenzene liquid crystal polymer networks. *Adv. Funct. Mater.* **21**, 2913–2918 (2011).

236. Lan, R. *et al.* Near-Infrared Photodriven Self-Sustained Oscillation of Liquid-Crystalline Network Film with Predesignated Polydopamine Coating. *Adv. Mater.* **32**, 1906319 (2020).

237. Cheng, Y. C., Lu, H. C., Lee, X., Zeng, H. & Priimagi, A. Kirigami-Based Light-Induced Shape-Morphing and Locomotion. *Adv. Mater.* **32**, 1906233 (2020).

238. Wie, J. J., Shankar, M. R. & White, T. J. Photomotility of polymers. *Nat. Commun.* **7**, 13260 (2016).

239. Van Oosten, C. L., Bastiaansen, C. W. M. & Broer, D. J. Printed artificial cilia from liquid-crystal network actuators modularly driven by light. *Nat. Mater.* **8**, 677–682 (2009).

240. Zuo, B., Wang, M., Lin, B. P. & Yang, H. Visible and infrared three-wavelength modulated multi-directional actuators. *Nat. Commun.* **10**, 4539 (2019).

241. Pilz da Cunha, M. *et al.* A Soft Transporter Robot Fueled by Light. *Adv. Sci.* **7**, 1902842 (2020).

242. Huang, C. *et al.* Miniaturized swimming soft robot with complex movement actuated and controlled by remote light signals. *Sci. Rep.* **5**, 17414 (2015).

243. Zhu, Z., Senses, E., Akcora, P. & Sukhishvili, S. A. Programmable light-controlled shape changes in layered polymer nanocomposites. *ACS Nano* **6**, 3152–3162 (2012).

244. Ube, T., Kawasaki, K. & Ikeda, T. Photomobile Liquid-Crystalline Elastomers with Rearrangeable Networks. *Adv. Mater.* **28**, 8212–8217 (2016).

245. Jiang, Z., Xiao, Y., Yin, L., Han, L. & Zhao, Y. "Self-Lockable" Liquid Crystalline Diels–Alder Dynamic Network Actuators with Room Temperature Programmability and Solution Reprocessability. *Angew. Chemie* **132**, 4955–4961 (2020).

246. Wang, Z., Tian, H., He, Q. & Cai, S. Reprogrammable, Reprocessible, and Self-Healable Liquid Crystal Elastomer with Exchangeable Disulfide Bonds. *ACS Appl. Mater. Interfaces* **9**, 33119–33128 (2017).

247. McBride, M. K. *et al.* A readily programmable, fully reversible shape-switching material. *Sci. Adv.* **4**, eaat4634 (2018).

248. McBride, M. K. *et al.* Photoinduced Plasticity in Cross-Linked Liquid Crystalline Networks. *Adv. Mater.* **29**, 1606509 (2017).

249. Jiang, Z. C., Xiao, Y. Y., Tong, X. & Zhao, Y. Selective Decrosslinking in Liquid Crystal Polymer Actuators for Optical Reconfiguration of Origami and Light-Fueled Locomotion. *Angew. Chemie - Int. Ed.* **58**, 5332–5337 (2019).

250. Gelebart, A. H., Mulder, D. J., Vantomme, G., Schenning, A. P. H. J. & Broer, D. J. A Rewritable, Reprogrammable, Dual Light-Responsive Polymer Actuator. *Angew. Chemie - Int. Ed.* **56**, 13436–13439 (2017).

251. Guo, H. *et al.* Programming the Shape Transformation of a Composite Hydrogel Sheet via Erasable and Rewritable Nanoparticle Patterns. *ACS Appl. Mater. Interfaces* **11**, 42654–42660 (2019).

252. Dickinson, M. H. *et al.* How animals move: An integrative view. *Science (80- .).* **288**, 100–106 (2000).

253. Hu, W., Lum, G. Z., Mastrangeli, M. & Sitti, M. Small-scale soft-bodied robot with multimodal locomotion. *Nature* **554**, 81–85 (2018).

PUBLICATIONS

Publication I   Zeng, H.; Lahikainen, M.; Liu, L., Ahmed, Z.; Wani, O.M.; Wang, M.; Yang., H; Priimagi, A. Light-Fuelled Freestyle Oscillators. *Nature Communications*, **2019**, *10*, 5057.

Publication II   Lahikainen, M.; Zeng, H; Priimagi, A. Design Principles for non-reciprocal photomechanical actuation. *Soft Matter*, **2020**, *16*, 5951-5958.

Publication III   Lahikainen, M.; Zeng, H.; Priimagi, A. Reconfigurable Photoactuator Through Synergistic Use of Photochemical and Photothermal Effects. *Nature Communications*, **2018**, *9*, 4148.

Publication IV   Lahikainen, M.; Kuntze, K.; Zeng, H.; Helantera, S.; Hecht, S.; Priimagi, A. Light Tunable Photo-Mechanics in Diarylethene Liquid Crystal Network Actuators, *ACS Applied Materials & Interfaces*, **2020**, *12*, 47939-47947.

Publication V   Kuenstler, A.S.; Lahikainen, M; Zhou, H.; Xu, W.; Priimagi, A.; Hayward, R.C. Reconfiguring Gaussian Curvature of Hydrogel Sheets with Photoswitchable Host-Guest Interactions. *ACS Macro Letters*, **2020**, *9*, 1172-1177.

PUBLICATION
I

Light-Fuelled Freestyle Oscillators

Zeng, H.; Lahikainen, M.; Liu, L., Ahmed, Z.; Wani, O.M.; Wang, M.; Yang., H; Priimagi, A.

Light-fuelled freestyle self-oscillators

Hao Zeng [1]*, Markus Lahikainen[1], Li Liu[2], Zafar Ahmed[1], Owies M. Wani[1], Meng Wang [2], Hong Yang [2] & Arri Priimagi [1]*

Self-oscillation is a phenomenon where an object sustains periodic motion upon non-periodic stimulus. It occurs commonly in nature, a few examples being heartbeat, sea waves and fluttering of leaves. Stimuli-responsive materials allow creating synthetic self-oscillators fuelled by different forms of energy, e.g. heat, light and chemicals, showing great potential for applications in power generation, autonomous mass transport, and self-propelled micro-robotics. However, most of the self-oscillators are based on bending deformation, thereby limiting their possibilities of being implemented in practical applications. Here, we report light-fuelled self-oscillators based on liquid crystal network actuators that can exhibit three basic oscillation modes: bending, twisting and contraction-expansion. We show that a time delay in material response dictates the self-oscillation dynamics, and realize a freestyle self-oscillator that combines numerous oscillation modes simultaneously by adjusting the excitation beam position. The results provide new insights into understanding of self-oscillation phenomenon and offer new designs for future self-propelling micro-robots.

[1] Smart Photonic Materials, Faculty of Engineering and Natural Sciences, Tampere University, P.O. Box 541FI-33101 Tampere, Finland. [2] School of Chemistry and Chemical Engineering, Southeast University, 211189 Nanjing, China. *email: hao.zeng@tuni.fi; arri.priimagi@tuni.fi

Leaves oscillate in response to wind flow. Intriguingly, the frequency of such oscillation can be almost constant, even if driven by a gust of wind that lacks the corresponding periodicity. Leaf oscillation, together with a broad range of phenomena including heartbeat, bridge swaying, sea waves, etc., exemplify naturally occurring self-oscillatory processes[1]. The cause of such self-oscillation is the interplay between the oscillator motion and the force that triggers the oscillation. In the case of leaves, torsional galloping of the leaf shades the aerodynamic vortex generated behind the surface, thus providing positive feedback to the motion that sustains the vibration with a defined periodicity[2]. Generally, the onset of self-oscillation needs to meet critical conditions[3]. This is evident from daily observations: only one or few leaves with specific orientation with respect to the wind flow direction oscillate under a breeze, while the neighbouring leaves with different orientation remain stationary.

Passive oscillating elements in nature rely on an external driving force, such as wind. Stimuli-responsive soft materials allow realizing externally fuelled, man-made self-oscillators, the motion of which is sustained by inner forces that arise due to stimuli-induced changes in material properties. Self-oscillators fuelled by, e.g. light[4,5], heat[6], and chemical reactions[7] have been generated, offering a possibility towards self-sustained motions without the need of human control. Towards this goal, several device functions are demonstrated, including electric power generation[6,8], mass transport[9,10], mill[11], and self-propelling locomotion[5,7,12]. Among the different stimuli, light is particularly promising, due to its sustainability, precise controllability, and omnipresence, the Sun being the ultimate energy source. However, most of the light-driven self-oscillators reported to date are using bending deformation as the main degree of freedom of movement or, in few cases, the combination of bending and twisting[13,14]. The broader the range of available oscillation modes, the more sophisticated autonomous devices one can potentially construct. Therefore, there is a need for self-sustained actuators with versatile motion and complex oscillation modes.

Liquid crystal elastomers and polymer networks (LCNs) are an important class of soft actuators that have been widely used in micro-robotics[15–19]. Their utility is based on coupling between elasticity due to the crosslinked network and anisotropic molecular orientation arising from the LC character. As a result of this combination, LCNs may exhibit pronounced macroscopic shape changes in response to external stimuli. By embedding light-sensitive dyes into the LCN, the material can reversibly and rapidly deform upon light excitation[20]. The photoactuation can be triggered either photothermally[21] or photochemically[22] (or by a combination of these), both leading to light-induced control over the degree of molecular alignment. Programming the molecular alignment in LCNs leads to diverse forms of shape changes[23], enabling the desired deformation mode, and in some cases self-oscillation[4,5,13,14], to be realized.

Typically, light-fuelled self-oscillators rely on a bending LCN strip, in which the oscillation is triggered by alternate activation of the two surfaces[4], or an optical configuration that provides self-shadowing within the motion cycles[24]. Being based on cantilever-type or strip-like geometries, the oscillation has been explained with a model connecting the self-oscillation frequency with their harmonic resonances[24,25]. However, there are some complications in this approach. First, the photomechanical oscillators experience significant damping during the fast motion because of the small mass/inertia compared to the friction/drag. Such damping causes large energy loss and requires compensation from the external stimulus, different to conventional harmonic oscillation. Second, the energy flow into the material by light absorption is oscillating during the cyclic movement, which in turn gives rise to oscillating temperature in the LCN. The change

in intensity/temperature leads to change in modulus[26] and thus to a non-constant resonance frequency.

Owing to the above considerations, several important issues need to be addressed, such as the possibility of obtaining versatile oscillating modes, understanding the feedback mechanism that actually fuels the motion and compensates for the damping loss, and the differences between LCN self-oscillation and conventional cantilever oscillation.

Here we try to address the above questions by exploring the mechanism of self-oscillation in LCN photoactuators. We first theoretically point out that the time delay in the material response provides a positive feedback to the motion, serving as the key to self-sustained oscillation. Then we devise three cantilever-type photoactuators capable of exhibiting the three basic oscillation modes: bending, twisting, and contraction–expansion. We show that the oscillation frequencies of the latter two diverge from the expected natural frequencies. Finally, we demonstrate a freestyle self-oscillator by hanging an LCN photoactuator on a thread, in which all the above degrees of freedom can be combined. The freestyle oscillator has numerous stabilized oscillation modes upon light excitation at different sample positions and is able to evolve spontaneously between different modes upon irradiation with a constant light beam. We believe that the generalized model provided, together with the freestyle self-oscillator demonstrated, can give new insights into soft matter mechanics.

Results

Origin of light-fuelled self-oscillation. While tree leaves oscillate in response to wind flow (Fig. 1a, b), the photoresponse of a soft actuator results from its mechanical deformability upon light illumination. Taking a bending LCN actuator as an example (Fig. 1c), the bending angle increases when increasing the light intensity I (Fig. 1d), which can be qualitatively described as a linear dependence between the deformation (D) and the energy absorbed (E) by the actuator (Fig. 1f, g). Note that the deformation does not have to be bending as exemplified here but any combination of twisting/bending/contraction is illustrated later. Owing to the directionality of the incident light field, the effective light-absorbing area A depends on the deformed geometry. This can be noticed from Fig. 1e, illustrating that the higher the bending angle, the smaller the light-absorbing area. The relation between A and D can be qualitatively described as a linear curve (Fig. 1g), in which the axis of A can be linked to E through a simple relationship: $E = A \cdot I$. Imposing the two curves gives an intersection, determined by the light intensity, at which the equilibrium occurs (Fig. 1h).

Around this equilibrium, the most familiar case is the harmonic oscillator, where an object experiences a restoring force proportional to its displacement x. The equation of motion can be written as:

$$\ddot{x} + \omega_o^2 x = 0, \qquad (1)$$

where ω_o is the angular frequency of the system. Solving Eq. (1) yields harmonic oscillation with a constant amplitude and periodicity $2\pi/\omega_o$, defined by its natural frequency, as shown by the solid line in Fig. 1i. However, in most cases, the oscillator experiences damping from its environment, a restoring force proportional to the velocity of its motion:

$$\ddot{x} + \varsigma\dot{x} + \omega_o^2 x = 0, \qquad (2)$$

where ς is the damping ratio. Accounting for the damping, the amplitude gradually decreases, due to energy dissipation from the system to the environment (the dashed line in Fig. 1i).

For a light-responsive mechanical cantilever, the restoring force arises from a sequence of processes: light absorption by the
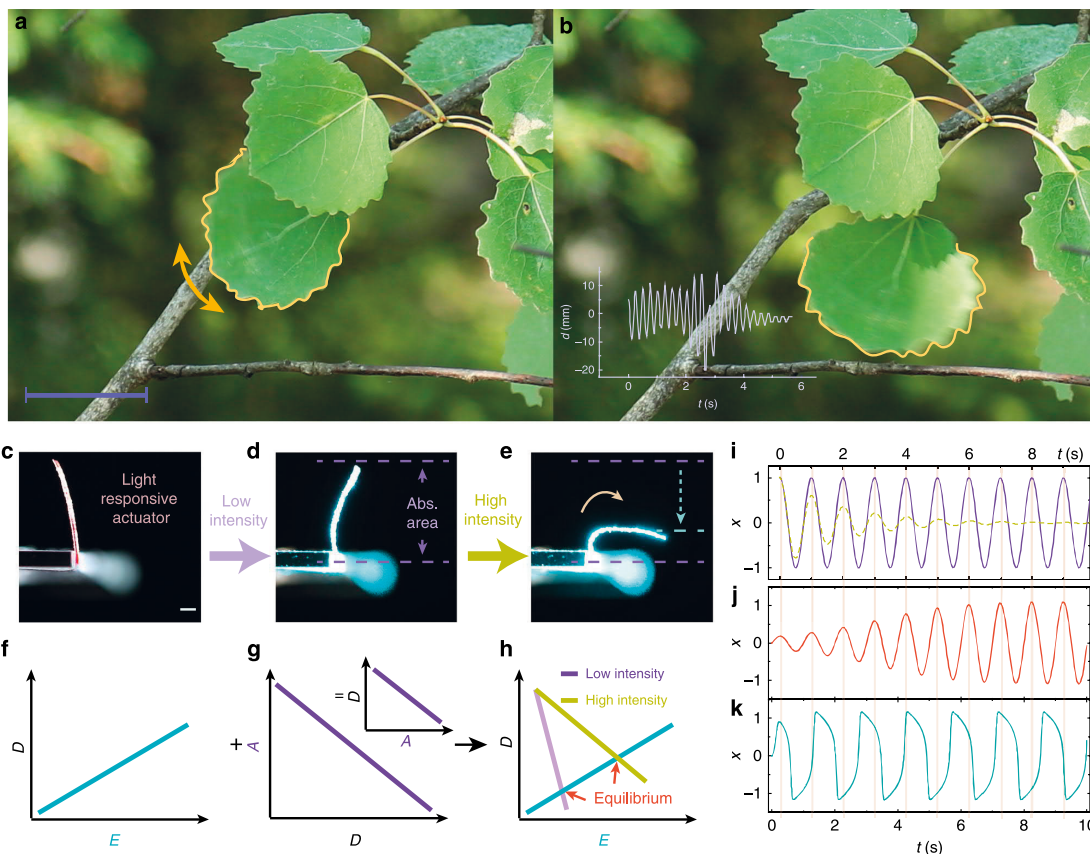
Fig. 1 The origin of self-oscillation in natural and in artificial light-fuelled systems. **a**, **b** Photographs of a leaf self-oscillating under a breeze. Inset of **b** shows time-dependent displacement of the centre of mass of the leaf, indicating periodic movement with well-defined frequency. Scale bar is 5 cm. A free-standing LCN actuator (**c**) bends slightly upon low-intensity irradiation (50 mW cm^{-2}, **d**) and more pronouncedly when the intensity is increased (200 mW cm^{-2}, **e**). **f–h** Schematic drawings showing the qualitative dependence between absorbed energy E, deformation D, effective light-absorbing area A, and equilibrium position upon illumination. **i** Harmonic oscillator (solid line, numerical solution to equation, $\ddot{x} + \omega_o^2 x = 0$) and an oscillator experiencing damping (dashed line, numerical solution to equation, $\ddot{x} + \varsigma\dot{x} + \omega_o^2 x = 0$), where $\omega_0 = 2\pi$, $\dot{x}(0) = 0$, $x(0) = 1$, $\varsigma = 0.1$. Self-oscillation induced by **j** a minor time delay σ and **k** a large σ. Numerical solutions to equation $\ddot{x} - (\sigma\omega_o^2 - \varsigma - \eta x^2)\dot{x} + \omega_o^2 x = 0$, where $\varsigma = 0.1$, $\omega_0 = 2\pi$, $\dot{x}(0) = 1$, $x(0) = 0$, and $\sigma\omega_o^2 = 1$, $\eta = 3$ in **j** and $\sigma\omega_o^2 = 20$, $\eta = 60$ in **k**

photoactive molecules, conversion of light energy into heat, heat transport across the sample area, and finally, build-up of the inner stress needed for deformation. All these contribute to a time delay σ in the actuation. Thus the equation of motion can be written as

$$\ddot{x}(t) + \varsigma\dot{x}(t) + \omega_o^2 x(t - \sigma) = 0. \qquad (3)$$

The value of σ may vary significantly depending on the material system, and it may also depend on the exact position of the LCN within the oscillation cycle. In order to reveal the contribution of this delay into the motion kinetics, we have simplified the model and consider only an invariant σ in the motion equation. We use Taylor expansion of Eq. (3), yielding

$$\ddot{x} + \varsigma\dot{x} + \omega_o^2\left(x - \sigma\frac{\dot{x}}{1!} + \sigma^2\frac{\ddot{x}}{2!} - \sigma^2\frac{\dddot{x}}{3!}\cdots\right) = 0 \qquad (4)$$

In this equation, the damping term $-\sigma\omega_o^2\dot{x}$ has a negative value, indicating that the oscillation amplitude increases to a certain extent, until the response becomes nonlinear. For example, air drag would significantly increase at large oscillation amplitudes, leading to amplitude saturation. Herein we adopt a

nonlinear positive damping term $\eta x^2\dot{x}$ (where η is a positive constant) based on van der Pol model[27] and simplify Eq. (4) using first-order approximation. The equation of motion for a light-responsive actuator at the equilibrium then appears as

$$\ddot{x} - (\sigma\omega_o^2 - \varsigma - \eta x^2)\dot{x} + \omega_o^2 x = 0. \qquad (5)$$

Numerical solution to Eq. (5) when σ is small is given in Fig. 1j, showing an exponential growth of the oscillation amplitude until reaching saturation. Comparing Fig. 1i, j one may notice that all these oscillations exhibit very similar periodicity, matching the conventional cantilever natural frequency, $\omega_o/2\pi$. However, when σ increases, the periodicity increases and the form of oscillation becomes non-sinusoidal, as shown in Fig. 1k. Numerical calculations on the oscillation frequency and the waveform upon increasing σ are given in Supplementary Fig. 1.

The key to self-oscillation is the time delay in the material response[1]: while an oscillator passes through the equilibrium ($x = 0$), the delayed force remains in the system showing the same direction as the velocity, thus pushing the object out of the equilibrium and providing positive feedback to the motion. Such
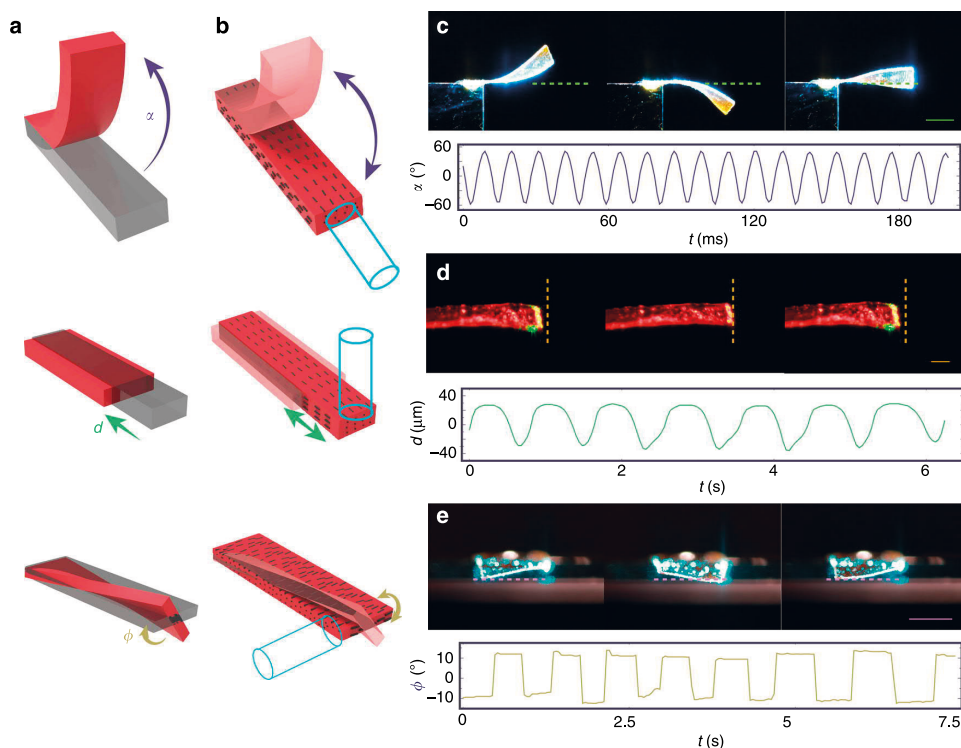
Fig. 2 Light-fuelled self-oscillators based on three basic deformation modes. **a** Schematic drawing of the three basic deformation modes in a cantilever: bending, contraction, and twisting. The deformation can be quantified through out-of-plane bending angle α, displacement d, and twisting angle Φ for each mode. **b** Molecular alignment and irradiation geometry to initiate self-oscillation in each deformation mode. **c** Photographs of bending actuator with size $5.5 \times 1.5 \times 0.05$ mm^3 upon 180 mW laser beam (spot size 2.2 mm) and the corresponding oscillation dynamics. **d** Photographs of cylindrical actuator (100 μm diameter) upon 100 mW focused laser excitation (spot size 20 μm) and the contracting–expanding oscillation dynamics. **e** Twisting self-oscillator (size: $3.5 \times 3.5 \times 0.05$ mm^3, laser: 180 mW, spot 2.2 mm) and the corresponding oscillation dynamics. The scale bars are 2 mm in **c**, **e**, 100 μm in **d**

feedback extracts the energy from the external energy source (light), fuelling the oscillator to sustain the motion. In the following, we explore the relation between the deformation degrees of freedom and the equilibrium positions in different light-fuelled self-oscillators and connect the observed oscillation modes to the material delay.

Basic oscillation modes. The three basic deformation modes in a cantilever—bending, contraction–expansion, and twisting—are schematically shown in Fig. 2a. Their amplitudes can be quantified as out-of-plane bending angle α, displacement d, and twisting angle Φ around the cantilever axis, respectively. To realize the basic deformations, we used planar-aligned LCN cantilevers, with a director along the cantilever for bending and contraction and perpendicular to it for twisting (Fig. 2b). The bending/twisting and contracting actuators are based on different LCN materials, as further elaborated in "Methods" and the Supplementary Methods.

The photoactuation is triggered with a 488 nm continuous-wave laser beam, using different irradiation geometries for the different modes as depicted in Fig. 2b. Bending is obtained by light propagation along the cantilever axis, in which case the laser alternately activates both surfaces during the cyclic motion. The photoactuation results from light absorption gradient across the thickness, which in turn gives rise to photoinduced stress on the irradiated surface, and bending towards the illuminating light

source. Combination of photochemical and photothermal effects is likely responsible for this type of oscillation[13]. Contraction occurs when the beam is focused on the tip of the cantilever, heating up the material, followed by subsequent cooling and expansion once the cantilever has moved away from the laser spot. Thus photothermal effects are responsible for this actuation mode. Twisting/torsional deformation takes place when the strip is illuminated from the side, causing an angular displacement around the cantilever axis and alternate exposure of the two cantilever surfaces, driven by similar mechanism as in the case of bending. Further details on photoactuation and the experimental arrangements are given in "Methods" and Supplementary Methods, respectively.

Equilibrium positions, where $\alpha = d = \Phi = 0$, can be found for each mode. When driven out of equilibrium (initiated by air fluctuation or a mechanical trigger), the cantilever returns to the equilibrium position due to elastic force, and the delay in the material response causes the self-oscillation as explained earlier. The frequency of the self-oscillation depends on the desired mode. The bending oscillation shown in Fig. 2c has the highest frequency of 80 Hz among the three basic modes (see the slow-motion video, Supplementary Movie 1), well matching with the calculated natural resonance frequency of the cantilever (about 90 Hz, see natural frequency calculations in Supplementary Methods for further details). This indicates a minimal time delay σ in such mode, yielding self-oscillation dominated by ω_o (Eq. (5), Fig. 1j). The natural resonance frequency is determined by

the cantilever geometry and the material rigidity, as has been systematically studied in several LCN self-oscillators[24,25]. In contrast, the contraction–expansion oscillator as well as the twisting one exhibit much longer periodicities, and resonance frequencies in the range of 0.5–18 Hz for contraction and about 1 Hz for twisting can be observed (Fig. 2d, e; Supplementary Movies 2 and 3). By comparing the observed frequencies to the natural resonances, estimated to be >20 kHz for the longitudinal vibration mode and ca. 170 Hz for the torsional one (see natural frequency calculations in Supplementary Methods), the frequencies of light-fuelled self-oscillations are 2–4 orders of magnitude lower. We ascribe this to significant increase in σ in those modes. During contraction–expansion, the light energy is absorbed within the focused spot area located at the tip of the cantilever. After the light absorption, heat has to be conducted along the cantilever axis to trigger deformation, thus posing a huge time delay. This delay strongly depends on the amount of energy being absorbed by the material. A set of stable oscillations with a broad range of frequencies, from 0.5 to 18 Hz, are observed by slightly tuning the laser spot position (same power) on the sample (Supplementary Fig. 2). We attribute this to differences in light scattering due to inhomogeneity and hence different amount of light being absorbed, which in turn yields different contraction length and time delay in the material response. In the twisting-mode oscillator, the time delay arises from the stress accumulation required for the material to switch its angular orientation. In this case, there seem to be two stable states, as indicated by the rectangular waveform shown in Fig. 2e.

More detailed analysis on the contraction–expansion and twisting self-oscillation modes have been conducted, with results shown in Supplementary Figs. 3 and 4. By maintaining the same excitation beam position but changing the input power, the frequency of the contraction–expansion mode varies between 16 and 20 Hz (see the Fourier transform in Supplementary Fig. 3b). However, no direct relation between the oscillation frequency and the excitation power can be deduced. The twisting actuator, instead, maintains the same oscillation amplitude irrespective of the laser power, but its oscillation frequency increases from 0.7 to 2 Hz (Supplementary Fig. 4b, c). Such findings seem to contradict conventional conceptions about cantilever mechanics, where the structural rigidity determines the natural resonance frequency, while the input power may affect only the oscillation amplitude. These observations, together with the non-sinusoidal waveforms and the considerably low oscillation frequencies compared to the natural resonance frequencies, indicate that the time delay becomes the dominating factor in the contracting and twisting self-oscillators. Note that, for large time delays, the simplified model given by Eq. (5) will no longer be accurate and more elaborate numerical calculation methods would be needed for solving the corresponding kinetic equations.

A freestyle self-oscillator. The actuators described above exhibit only one selected oscillation mode. In order to combine the different modes into a single actuator, we use a main-chain LCN with high degree of deformability[28] (>50% contraction upon order–disorder phase transition; thermal actuation and mechanical properties between different LCNs given in Supplementary Figs 5 and 6). Material details are given in "Methods"; for further information about sample preparation, see the Supplementary Methods. Upon excitation with a laser spot, the localized strain builds up stress inside the material, causing additional degrees of freedom for the entire deformed structure, as schematized in Fig. 3a and experimentally demonstrated in Fig. 3b–e. The strip (Fig. 3b) bends when illuminated with a laser spot (100 mW) at the centre of the cantilever (Fig. 3c). Moving the laser spot

horizontally, close to the edge of the cantilever, triggers combined twisting and bending deformation (Fig. 3d). By increasing the light intensity from 100 to 140 mW, a larger extent of deformation can be triggered, and bending and contraction occur simultaneously (Fig. 3e). To better visualize the twisting, we attached a weight to the end of the actuator (1.4 g, 250 times the weight of the actuator) to suppress bending (Fig. 2f). When the laser spot deviates from the centre of the actuator, contraction and twisting can be observed (Fig. 2g).

To trigger self-oscillation, the excitation beam orientation and spot location need to meet critical conditions. We realize this by puncturing a hole into the LCN (inset of Fig. 3j) and hanging it vertically on a thread (human hair), thereby providing freedom to swing around the thread axis, as schematically illustrated in Fig. 3h. Under such configuration, any kind of light-induced deformation (bending and/or contraction and/or twisting) shifts the centre of mass of the actuator (Fig. 3h; 1 → 2). In return, gravity imposes a torque to rotate the deformed structure around the thread axis (2 → 3), and the strip moves out of the illuminating area, cools down, and relaxes back to the original position (3 → 1′), and the cycle restarts.

Triggered by subsequent sequences of the above-described cycles, the strip oscillates continuously upon a constant laser beam excitation. By slightly changing the position of the laser spot, different oscillation modes can be obtained (Fig. 3i–k and Supplementary Movie 4). Each mode has a well-defined periodicity, as exemplified in the inset of Fig. 3k. During the distinct stable oscillation modes, the laser beam is not spatially or temporally modified. However, by slightly adjusting the laser spot position along the LCN strip, the actuator may exhibit fast-varying geometry, oscillating like a dancer on a thread (Supplementary Movie 5), which we coin as light-fuelled freestyle self-oscillation.

Stabilized oscillations and evolution between the modes. For more detailed characterization of the oscillating modes, we labelled the free end of the LCN strip with fluorescent particles (Fig. 4a, and further details are given in data collection in Supplementary Methods). With the help of the fluorescent markers, we can track the trajectory of oscillation in the x–y plane, offering a distinct fingerprint for each oscillation mode. Each mode prevails for a relatively long time, typically at least 5 s, maintaining the same amplitude and frequency (Supplementary Fig. 7). However, the oscillation frequency may significantly vary for the different modes, e.g. from 0.4 to 6.7 Hz between examples shown in Fig. 4b–g, and no connection between the oscillation frequency and amplitude seems to exist. The trajectories with zero area correspond to reciprocal oscillation (Fig. 4e–g) while those with non-zero area indicate non-reciprocal motion during the oscillation cycle (Fig. 4b–d).

Figure 4h presents an intriguing oscillation behaviour under constant irradiation conditions: spontaneous evolution between different oscillation modes. In short term, the periodicity of each mode is constant (Fig. 4k) but varies somewhat over extended time periods, e.g. from 0.35 to 0.45 s within 3 min (Supplementary Fig. 8). The spontaneous evolution between the modes (Fig. 4i, j) without changing the excitation beam position is ascribed to irreversibility of the actuating material, which is quantified by monitoring a freestanding LCN upon cyclic excitation (Supplementary Fig. 9). The cyclic actuation shows that the material maintains its deformability, i.e. the maximum strain obtained upon constant irradiation, while the relaxation process shows certain degree of reduction with a decay constant of about 80 cycles. The reason for such photomechanical irreversibility may be attributed to kinetic deformation driven
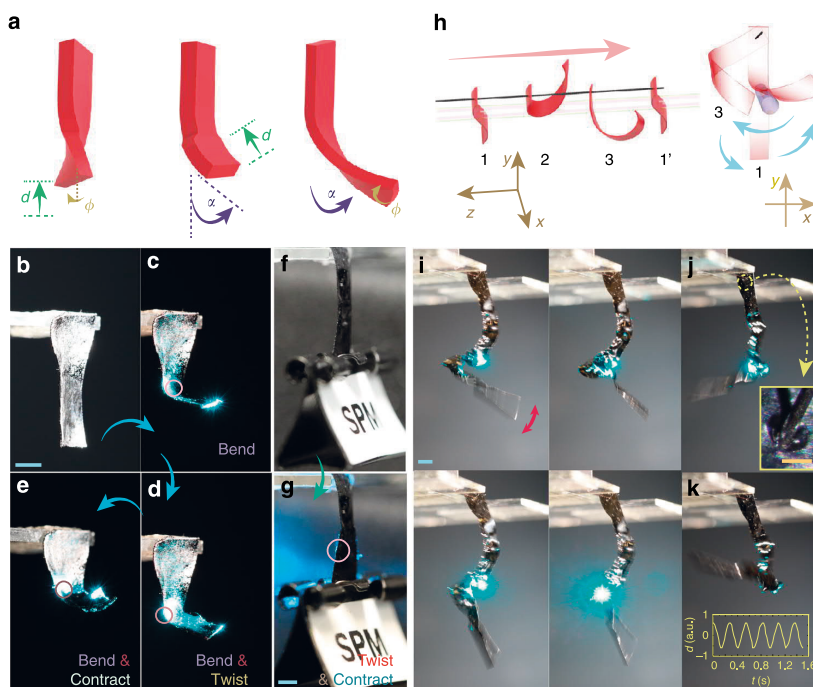
Fig. 3 A freestyle self-oscillator. **a** Schematic drawing of a soft actuator combining the three basic deformation modes (twisting, bending, and contraction). An LCN actuator (**b**) that bends (**c**), bends and twists (**d**), bends and contracts (**e**), upon changing the irradiation conditions. The circle marks the position of the laser spot. With an external load that prevents bending (**f**), the actuator contracts and twists simultaneously when excited from one side as indicated in **g**. **h** Schematics of a light-driven self-oscillator swinging on a thread. **i**–**k** Snapshots of the freestyle oscillator with different oscillation modes upon laser excitation (488 nm, 160 mW) at different positions. LCN strip size: $3 \times 25 \times 0.1$ mm^3. Inset of **j** shows the microscopic image of the hole punctured in the LCN actuator (scale bar 200 μm). Inset of **k** shows the displacement of the end of the strip during the oscillation process. All scale bars: 2 mm

by elastic entropy, where cyclic stretching–coiling gives rise to friction between the polymeric chains, and photobleaching of the dyes. During the oscillation, the actuator undergoes hundreds of deformation–relaxation cycles. Hence, even slight changes in material response may shift the deformation mode and lead to spontaneous evolution between the oscillation modes. At about 190 s, the oscillator stops at a stable position, where the negative damping condition is no longer met ($\sigma\omega_o^2 > \varsigma$, Eq. 5), possibility due to the irreversibility of the material response.

The prediction and control of the evolution between different modes during the freestyle oscillation is difficult to attain, due to the multiple degrees of freedom in deformation and complexity of light–matter interactions in responsive soft materials, resulting in different time delay in material response at different stages of the oscillation cycle. Despite the lack of control, the intriguing freestyle self-oscillation phenomenon provides insight into the process that, we believe, can be generalized into different kinds of responsive materials with arbitrary geometry, deformability, and stimulus responsivity, as long as a feedback mechanism has been established for sustaining the periodic motion.

From general material concept towards practical applications. The above light-driven system combines the basic oscillation modes—bending, contraction, and twisting—into a single free-style oscillator. Although the movements are complex, the free-style oscillator is governed by the same physics as conventional oscillators with simpler movements. We believe that similar principles can be applied also to other types of stimuli-responsive

systems. For example, thermoresponsive nylon fibres[9], carbon-nanotube-based bi-layer actuators[29], thermoactive elastomer rods[10], hydrogels[30], and azobenzene crystals[31] have all shown self-sustained cyclic movements. Different from approaches in systems chemistry[32,33], which aim at programming positive/negative feedback between reversible chemical reactions to induce oscillating behaviours, the approach demonstrated here focuses on photomechanical response in macroscopic samples, driven by time delay in material response and not restricted in few specific materials. Also note that the self-oscillation discussed in this study is different from the phenomenon of fluctuation, which, however, in some cases has been coined as chaotic self-oscillation[34]. A well-defined frequency component in the Fourier transform can serve as a good indicator for the occurrence of self-oscillation.

To combine self-oscillators into locomotive devices to achieve self-sustained micro-robots is challenging. First, most of the actuators used in self-oscillation studies are free-standing strips lacking external loading. Upon devising a linkage between the motor (the oscillator) and the robot body (the moving element), the mechanical conditions change. Upon locomotion, the oscillator's position with respect to the illumination source, as well as its geometry and mechanical properties, change, affecting the equilibrium conditions crucial for sustaining the oscillation. Thus a conventional mechanical design, e.g. biking the wheel[35], may lead to a failure in long-time conversion of oscillating motion into mechanical work. Second, efficient translocation often requires a nonreciprocal deformation, which in turn requires temporal coordination of a series of self-oscillation
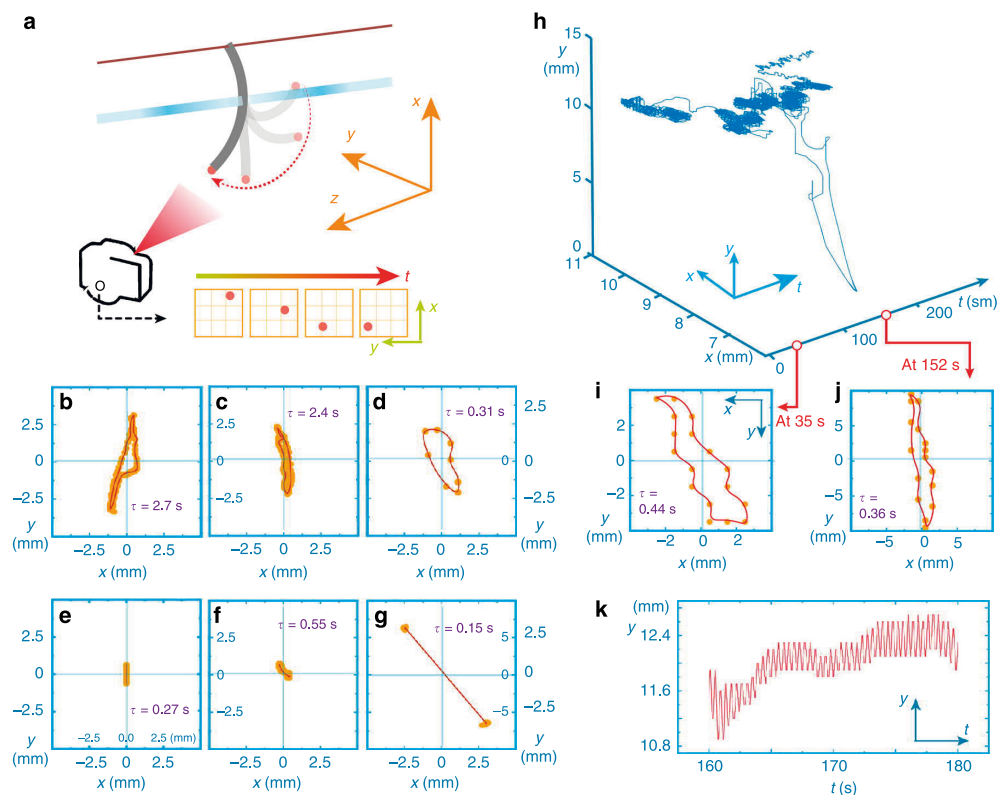
Fig. 4 Stabilized modes and evolution between the modes. **a** Schematic drawing of the arrangement for tracking the oscillator position. **b–g** Examples of different self-oscillation modes upon excitation with a laser spot at different positions. Data shows the tracking trajectory on x–y plane for one oscillation cycle. **h** Evolution between modes upon a constant laser excitation. The x–y trajectory spontaneously changes upon prolonged excitation (**i**, **j**), while maintaining the similar oscillating periodicity (**k**) until 190 s when the oscillation vanishes

events or within different sequences of a self-oscillation cycle with certain phase delays[36,37]. However, coupling between different self-oscillators sets extra hurdles. Third, light-responsive materials may not provide enough force to overcome the friction/drag experienced during the robotic motion, hence other soft mechanic properties like snapping and instabilities[37] need to be further investigated in self-oscillating systems, in order to reach their full potential. Although challenges exist, pioneering examples have shed light on device integration, e.g. mass transportation[9,10] and self-propelled walking[5]. We hope more self-sustained devices will be reported in the future, and that self-sustained robots can be integrated with more sophisticated functions by the joint scientific development in this field.

A useful application can be foreseen in realizing self-oscillator within fluidic environment, which may eventually give birth to self-sustained pumping and cilia-like collective movement for efficient microfluidic manipulation. However, the dragging force (large ς) may pose great hurdle to meet the required negative damping condition ($\sigma\omega_o^2 > \varsigma$). A possible solution could be to investigate stimuli-responsive materials with a large delay σ in material response, such as light/heat-responsive hydrogels[38].

Beyond the above-mentioned robotic applications that aim to transfer input light energy into mechanical work output, there is a frontier of optical applications to be investigated. A self-oscillator is essentially an optical chopper. However, compared to the conventional electronic motorized chopping system, it has many

advantages, such as compact size, light weight, and, being remotely powered, possibility towards integration into micro-devices. An oscillating strip can modulate a signal beam (635 nm) periodically in its transmission, as shown in Fig. 5a: during the down-bending stage, the beam is transmitted, while the up-bending stage blocks the beam. In other words, the signal beam transmission is controlled and modulated by the self-oscillator (Fig. 5b). Furthermore, one single strip can even control two signal beams simultaneously. As shown in Fig. 5c, the two signal beams can be in phase, when propagating along the same side of the strip, or 180° out-of-phase, when propagating from the opposite sides of the strip (Fig. 5d).

Discussion

We study the mechanism of light-driven self-oscillation and show that a time delay due to the material response is the key to sustain the periodicity of oscillation. By interplay between the equilibrium position upon irradiation and specific form of light-induced deformation pre-programmed into the LCN by molecular-alignment control, three basic oscillation modes—bending, contraction, and twisting—are demonstrated. A main-chain LCN actuator combines the basic oscillation modes, yielding freestyle oscillation when hung on a thread. Such freestyle oscillator exhibits different stabilized modes upon continuous laser excitation at different sample positions and evolution between the modes across a relatively long period under
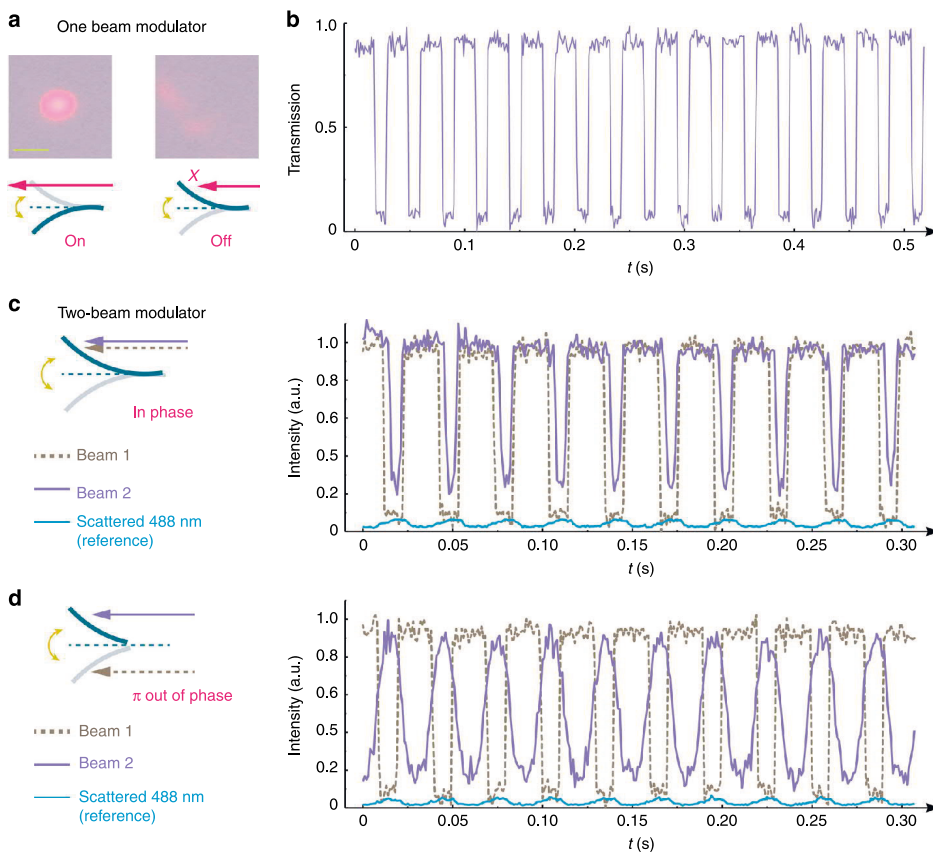
Fig. 5 Self-oscillator-based beam modulator. **a** A self-oscillating strip (bending mode, driven by a continuous 488 nm, 190 mW) can modulate the transmission of a signal beam (635 nm). The signal beam is focused on the upper part of the oscillator as shown by the schematic drawing, while the transmitted beam profiles are shown in the photos. Scale bar: 1 cm. **b** Transmission measurement of the beam being modulated by the self-oscillator. **c** Two signal beams are propagating along the same side of the oscillator and the measured transmission intensities being modulated in phase. **d** Two signal beams are propagating along the opposite sides of the oscillator and the measured transmission intensities being modulated 180° out-of-phase. Blue curves in **c**, **d** show the scattered 488 nm light intensity for phase reference. Strip size: $1 \times 10 \times 0.05$ mm^3

a constant light field. The results provide insight into light-driven self-oscillation in soft materials and may in longer term open up new approaches to realize light-driven motors for self-sustained soft micro-robotics.

Methods
Materials in brief. The LCN photoactuators demonstrated here are photopolymerized from monomer mixtures containing liquid crystalline mesogens, crosslinkers, light-sensitive dyes, and photoinitiators, via one-step or two-step fabrication strategies. Different materials were used for different deformation/oscillation modes. For bending and twisting, a side-chain LCN with 28 mol% crosslinker (of which 6 mol% are azobenzene crosslinkers) is used[39]; for contraction–expansion, we used a side-chain LCN polymerized from different LC mesogens and reduced crosslinker concentration (10 mol%)[40] to render the LCN softer; for freestyle actuator, we used a main-chain LCN synthesized through two-step fabrication process[28]. All details about material preparation procedures are given in Supplementary Methods.

Photoactuation in brief. An unfocused, continuous-wave 488 nm laser beam was propagated along the axis of the LCN cantilever in case of bending-mode oscillation and perpendicular to the axis for the twisting mode. Upon laser excitation, the azobenzene moieties in the LCN undergo repeated *trans-cis-trans* isomerization. Owing to limited light-penetration depth, isomerization gradient across the film thickness is formed, which, together with photothermal heating, gives rise to

cantilever deformation towards the light source. As a result, the laser beam illuminates alternately both cantilever surfaces, yielding periodic bending/twisting. Further details on the optical configuration are given in Supplementary Methods. For contraction–expansion mode oscillation, we used a purely photothermally driven actuator, where light was absorbed at a tip of an LCN fibre and the energy was transferred into heat and conducted along the cantilever to the rest of the actuator body. The temperature difference between illuminated and non-illuminated surfaces is negligible due to fast thermal transport occurring at microscopic scale. Bending and twisting actuators are film like, with length-to-thickness ratio about 100. For contraction–expansion mode, a microscopic fibre with 100 μm diameter was used, with length-to-thickness ratio around 1. Because of the low length-to-thickness ratio, the bending of the fibre was suppressed. The LCN used for freestyle oscillation was also a photothermal actuator. Because of its large deformability, multiple degrees of freedom of deformation can be activated by impinging the light beam at different sample positions and/or by changing the excitation power. In all cases, the excitation beam position needs to be finely tuned in order to reach the stable self-oscillating movement. Once it self-oscillates, the duration can last for typically >30 min for bending and twisting modes, >50 min for contacting–expanding mode, and >30 s for the freestyle mode. More details about photomechanics and optical configurations are given in Supplementary Methods.

Data availability
The data that support the findings of this study are available from the corresponding authors upon request.

References

1. Jenkins, A. Self-oscillation. *Phys. Rep.* **525**, 167–222 (2013).
2. Leclercq, T., Peake, N. & de Langre, E. Does flutter prevent drag reduction by reconfiguration? *Proc. R. Soc. A* **474**, 20170678 (2018).
3. Tadrist, L., Julio, K., Saudreau, M. & de Langre, E. Leaf flutter by torsional galloping: experiments and model. *J. Fluids Struct.* **56**, 1–10 (2015).
4. White, T. J. et al. A high frequency photodriven polymer oscillator. *Soft Matter* **4**, 1796–1798 (2008).
5. Gelebart, A. H. et al. Making waves in a photoactive polymer film. *Nature* **546**, 632–636 (2017).
6. Wang, X. Q. et al. In-built thermo-mechanical cooperative feedback mechanism for self-propelled multimodal locomotion and electricity generation. *Nat. Commun.* **9**, 3438 (2018).
7. Maeda, S., Hara, Y., Sakai, T., Yoshida, R. & Hashimoto, S. Self-walking gel. *Adv. Mater.* **19**, 3480–3484 (2007).
8. Tang, R. et al. Optical pendulum generator based on photomechanical liquid-crystalline actuators. *ACS Appl. Mater. Interfaces* **7**, 8393–8397 (2015).
9. Baumann, A. et al. Motorizing fibres with geometric zero-energy modes. *Nat. Mater.* **17**, 523–527 (2018).
10. Ahn, C., Li, K. & Cai, S. Light or thermally-powered autonomous rolling of an elastomer rod. *ACS Appl. Mater. Interfaces* **10**, 25689–25696 (2018).
11. Vantomme, G., Gelebart, A. H., Broer, D. J. & Meijer, E. W. A four-blade light-driven plastic mill based on hydrazone liquid-crystal networks. *Tetrahedron* **73**, 4963–4967 (2017).
12. Wie, J. J., Shankar, M. R. & White, T. J. Photomotility of polymers. *Nat. Commun.* **7**, 13260 (2016).
13. Lee, K. M. et al. Photodriven, flexural–torsional oscillation of glassy azobenzene liquid crystal polymer networks. *Adv. Funct. Mater.* **21**, 2913–2918 (2011).
14. Ge, F., Yang, R., Tong, X., Camerel, F. & Zhao, Y. A multifunctional dye-doped liquid crystal polymer actuator: light-guided transportation, turning in locomotion, and autonomous motion. *Angew. Chem. Int. Ed.* **57**, 11758–11763 (2018).
15. Zeng, H., Wasylczyk, P., Wiersma, D. S. & Priimagi, A. Light robots: bridging the gap between microrobotics and photomechanics in soft materials. *Adv. Mater.* **30**, 1703554 (2018).
16. Ohm, C., Brehmer, M. & Zentel, R. Liquid crystalline elastomers as actuators and sensors. *Adv. Mater.* **22**, 3366–3387 (2010).
17. Nocentini, S., Parmeggiani, C., Martella, D. & Wiersma, D. S. Optically driven soft micro robotics. *Adv. Opt. Mater.* **6**, 1800207 (2018).
18. Ambulo, C. P. et al. Four-dimensional printing of liquid crystal elastomers. *ACS Appl. Mater. Interfaces* **9**, 37332–37339 (2017).
19. López-Valdeolivas, M., Liu, D., Broer, D. J. & Sánchez-Somolinos, C. 4D printed actuators with soft-robotic functions. *Macromol. Rapid Commun.* **39**, 1700710 (2018).
20. Ikeda, T., Mamiya, J.-I. & Yu, Y. Photomechanics of liquid-crystalline elastomers and other polymers. *Angew. Chem. Int. Ed.* **46**, 506–528 (2007).
21. Yang, Y., Pei, Z., Li, Z., Wei, Y. & Ji, Y. Making and remaking dynamic 3d structures by shining light on flat liquid crystalline vitrimer films without a mold. *J. Am. Chem. Soc.* **138**, 2118–2121 (2016).
22. Li, M. H., Keller, P., Li, B., Wang, X. & Brunet, M. Light-driven side-on nematic elastomer actuators. *Adv. Mater.* **15**, 569–572 (2003).
23. White, T. J. & Broer, D. J. Programmable and adaptive mechanics with liquid crystal polymer networks and elastomers. *Nat. Mater.* **14**, 1087–1098 (2015).
24. Gelebart, A. H., Vantomme, G., Meijer, B. E. W. & Broer, D. J. Mastering the photothermal effect in liquid crystal networks: a general approach for self-sustained mechanical oscillators. *Adv. Mater.* **29**, 1606712 (2017).
25. Serak, S. et al. Liquid crystalline polymer cantilever oscillators fueled by light. *Soft Matter* **6**, 779–783 (2010).
26. Kumar, K., Schenning, A. P. H. J., Broer, D. J. & Liu, D. Regulating the modulus of a chiral liquid crystal polymer network by light. *Soft Matter* **12**, 3196–3201 (2016).
27. van der Pol, B. On relaxation-oscillations. *Philos. Mag.* **2**, 978–992 (1926).
28. Liu, L., Liu, M. H., Deng, L. L., Lin, B. P. & Yang, H. Near-infrared chromophore functionalized soft actuator with ultrafast photoresponsive speed and superior mechanical property. *J. Am. Chem. Soc.* **139**, 11333–11336 (2017).
29. Zhang, X. et al. Photoactuators and motors based on carbon nanotubes with selective chirality distributions. *Nat. Commun.* **5**, 2983 (2014).
30. He, X. et al. Synthetic homeostatic materials with chemo-mechano-chemical self-regulation. *Nature* **487**, 214–218 (2012).
31. Uchida, E., Azumi, R. & Norikane, Y. Light-induced crawling of crystals on a glass surface. *Nat. Commun.* **6**, 7310 (2015).
32. Leira-Iglesias, J., Tassoni, A., Adachi, T., Stich, M. & Hermans, T. M. Oscillations, travelling fronts and patterns in a supramolecular system. *Nat. Nanotechnol.* **13**, 1021–1027 (2018).
33. Novák, B. & Tyson, J. J. Design principles of biochemical oscillators. *Nat. Rev. Mol. Cell Biol.* **9**, 981–991 (2008).
34. Kumar, K. et al. A chaotic self-oscillating sunlight-driven polymer actuator. *Nat. Commun.* **7**, 11975 (2016).
35. Ge, F. & Zhao, Y. New function for thermal phase transition-based polymer actuators: autonomous motion on a surface of constant temperature. *Chem. Sci.* **8**, 6307–6312 (2017).
36. Duncan, P. N., Nguyen, T. V. & Hui, E. E. Pneumatic oscillator circuits for timing and control of integrated microfluidics. *Proc. Natl Acad. Sci.* **110**, 18104–18109 (2013).
37. Preston, D. J. et al. A soft ring oscillator. *Sci. Robot.* **4**, eaaw5496 (2019).
38. Zhao, Y. et al. Soft phototactic swimmer based on self-sustained hydrogel oscillator. *Sci. Robot.* **4**, eaax7112 (2019).
39. Lahikainen, M., Zeng, H. & Priimagi, A. Reconfigurable photoactuator through synergistic use of photochemical and photothermal effects. *Nat. Commun.* **9**, 4148 (2018).
40. Nocentini, S., Martella, D., Wiersma, D. S. & Parmeggiani, C. Beam steering by liquid crystal elastomer fibres. *Soft Matter* **13**, 8590–8596 (2017).

Author contributions

H.Z. and A.P. conceived the project. H.Z. carried out experiments with the help of M.L. and O.M.W. M.L. prepared LCN for bending and twisting oscillation mode. Z.A. synthesized side-chain LCN for contracting oscillation mode. L.L. synthesized the main-chain LCN under supervision of M.W. and H.Y. All authors contributed in writing the manuscript.

Competing interests

The authors declare no competing interests.

Additional information

Supplementary information is available for this paper at https://doi.org/10.1038/s41467-019-13077-6.

Correspondence and requests for materials should be addressed to H.Z. or A.P.

Peer review information *Nature Communications* thanks the anonymous reviewers for their contribution to the peer review of this work. Peer reviewer reports are available.

Reprints and permission information is available at http://www.nature.com/reprints

Publisher's note Springer Nature remains neutral with regard to jurisdictional claims in published maps and institutional affiliations.

PUBLICATION
II

Design Principles for non-reciprocal photomechanical actuation.

Lahikainen, M.; Zeng, H; Priimagi, A.

Check for updates

Design principles for non-reciprocal photomechanical actuation†

Markus Lahikainen, [ID] Hao Zeng* and Arri Priimagi [ID] *

Non-reciprocal motions are a sequence of movements exhibiting time-reversal asymmetry. Such movements are common among various natural species, being adopted as a typical strategy for achieving efficient locomotion. Generally, the realization of non-reciprocal motions in man-made robotic devices requires synchronous control of at least two individual actuators, hence posing challenges to soft micro-robotics where the miniaturization limits integration of different mechanical components and the possibility of using onboard batteries. Here, we introduce general concepts for achieving non-reciprocal movements in wirelessly controlled soft actuators made of photomechanically responsive liquid crystal networks. The monolithic actuators are composed of two segments that can be actuated photochemically and photothermally, and the non-reciprocal motion is obtained by a control sequence that temporally modulates light sources of different wavelengths. Through proper selection of photoactive compounds, the number of modulated light sources can be decreased, from three to two, and eventually to one. Finally, we demonstrate non-reciprocal self-oscillation by self-shadowing effect in a flexible strip under a constant light field with no temporal modulation. This study provides general guidelines to light-controlled non-reciprocal actuation, offering new strategies for the control of wireless soft micro-robotics.

Introduction

Animals cyclically change their body shapes to generate net displacements in order to translocate their centre of mass. A typical trajectory of such movements is such that the body part deforms into a certain configuration and then returns to the original one through another sequence of motions. In other words, the motion is non-reciprocal, exhibiting time-reversal asymmetry.[1] Many natural species have polished the non-reciprocal movements to perfection, in order to maximize the efficiency of their motions. Fig. 1 shows a prominent example: a bird flapping its wings by following different pathways during upward and downward strokes, to produce aerodynamic forces for lifting the mass. As other examples, the tails of many fish vibrate non-reciprocally to get maximum thrust,[2] caterpillar squirms by following a travelling-wave-like pattern,[3] and bacterial flagella move non-reciprocally in low-Reynolds-number liquids.[4] These natural examples have inspired a significant amount of research in man-made devices, providing design tools for soft micro-robotics driven by different actuation mechanisms[5–7] and locomotion strategies,[8,9] over various dimensional scales.[10–12]

Fig. 1 Non-reciprocal movement of a bird. The wings flip upward and downward by following different pathways, exhibiting time-reversal asymmetry.

In principle, non-reciprocal motions in man-made devices require synchronous control of shape change of at least two individual actuators. Conventionally, this has been achieved by electronic motors/actuators synchronized by a control circuit,[13] or pneumatic actuators powered by a sequence of pressurized tubes.[14] In soft-materials-based micro-robotics, significant challenges emerge. First, miniaturization limits the overall dimensions of the device, rendering the integration of multiple electric actuators, onboard batteries, and electronic circuitry, highly complex. Second, wire-connection poses restrictions on the spaces the soft robot is able to enter and causes additional drag for the locomotion. Thus, there is a strong demand to devise stimuli-responsive materials that can replace conventional wire-based actuators for robotic motion.[15–18] Light-responsive liquid crystal polymer networks (LCNs) have recently emerged as

Smart Photonic Materials, Faculty of Engineering and Natural Sciences, Tampere University, P. O. Box 541, FI-33101 Tampere, Finland. E-mail: hao.zeng@tuni.fi, arri.priimagi@tuni.fi

a powerful class of materials for advanced soft actuators.[19,20] Through light-induced changes in molecular packing within the crosslinked network, LCNs can exhibit large deformations under moderate-intensity illumination, resulting in sophisticated control over shape changes[21] and, in some cases, locomotion.[22,23] Two distinct photomechanical effects can drive the actuation of LCNs: (i) (meta)-stable deformation *via* photochemical processes such as *cis–trans* isomerization,[24–26] and (ii), photothermally driven processes invoked by light-induced heat generation.[27,28] Utilizing these two provides great opportunities and freedom in the realization of light-fuelled soft micro-robots.[29–32]

Using light energy to fuel the robot has several advantages over other stimuli sources such as electric, magnetic and acoustic fields.[33–36] As the most significant advantage from the perspective of the present work, by selecting photoactive units with different absorption properties, one can fabricate an actuator with multiple degrees of freedom of deformation, each being controlled by different wavelength.[37–39] Such multi-wavelength actuation constitutes the basis for obtaining non-reciprocal movements in light-responsive LCNs. As a pioneering example, non-reciprocal movement has been obtained in printed artificial cilia composed of two LCN segments with different photomechanical properties and responding to different wavelengths of light.[40] Alternatively, different moving speed between two parts of the same actuator driven by the same wavelength,[41] or sequential deformations along the material triggered by a scanning laser beam[42] could also lead to non-reciprocal motions. These approaches, however, require either specific attention in material design to obtain a visible non-reciprocal pattern, or a sophisticated optical set up in order to trace the position of the object during the beam scanning. In microactuator research, there is a need to obtain non-reciprocal motion by an easily achievable optical control strategy and using easily available materials.

In this article, we report different ways of obtaining non-reciprocal movements in strip-like, photomechanical LCN actuators. The monolithic strips are made of two distinct segments that undergo photochemical and photothermal actuations. We focus on light control schemes of the simplest form: temporal modulation (on–off switching) of spatially uniform light beams. Through sequential on–off switching of different wavelengths, we invoke photochemical or photothermal actuation in different parts of the strip, and as a result, non-reciprocal motion patterns. We present a strategy to reduce the number of modulated light sources from three to two and even to one, which is important for increasing the simplicity and reducing the cost of the wireless actuation control. Finally, we demonstrate a long LCN strip that exhibits non-reciprocal self-oscillation under illumination with a constant light field. The non-reciprocal oscillation is governed by the interplay between self-shadowing effect and the flexibility of the actuating strip, yielding non-reciprocal movement without any temporal light modulation. The results presented are expected to provide new design principles for soft robotic movement and strategies of light control in future microactuator devices.

Materials and methods

Materials rationale

The LCN actuators are made from monomer mixtures containing liquid crystalline mesogens, photoinitiator and photo-sensitive elements (Fig. 2a). The LCNs combine liquid-crystalline order and elasticity of polymer networks, rendering the material inherently thermo-responsive, possessing the capability of reversible shape changes. We employ different photoactive units in the polymer networks to trigger actuation by different parts of the UV-visible spectrum. The absorption spectra and excitation wavelengths of the photoactive molecules used are shown in Fig. 2b and c. The azobenzene crosslinker (Fig. 2b) activates photochemical actuation and light-induced bending in response to UV irradiation *via trans–cis* isomerization, while unbending arising from *cis–trans* isomerization can be invoked with 450–500 nm irradiation. Other photoactive units employed are Disperse Red 1 (DR1) and Disperse Blue 14 (DB14), shown in Fig. 2c, which are responsible for transferring light energy into
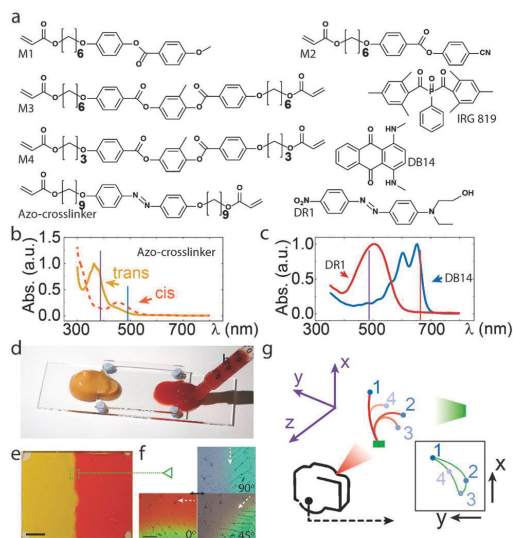

Fig. 2 (a) Chemical structures of the molecules used to fabricate the LCNs. The LCN films contain azobenzene crosslinks (b) and light-absorbing dyes (c), which invoke photochemical and photothermal actuation, respectively. The spectra in b and c are measured from 10 μm thick LCN films containing relevant photosensitive molecules. The vertical lines indicate the wavelengths used for excitation. (d) Illustration of the cell infiltration process for preparing the monolithic, dual-responsive photoactuator. (e) Photograph of an LCN film with azobenzene crosslinker (left) and DR1 (right). Scale bar: 5 mm. (f) Polarized optical micrographs at different angles at the boundary between the two parts of the LCN. Scale bar: 500 μm. The solid arrow indicates the microscope illuminating light polarization direction when arriving on the sample surface. The dashed arrow represents the alignment direction on the sample surface that is firstly exposed to the polarized light. (g) Schematic drawing of the optical setup used for tracking the non-reciprocal movements.

heat at different spectral regions, guaranteeing photothermally driven actuation alike in our previous studies.[11,29]

Actuator fabrication

The monomer mixture is dissolved in dichloromethane, filtered through PTFE syringe filter (Sigma Aldrich, pore size 0.2 μm) and magnetically stirred at 80 °C for 2 h to remove the solvent. To make the cell, two glass slides are spin coated with polyvinyl alcohol–water solution (1 wt% PVA, Sigma Aldrich) and rubbed uni-directionally using a satin cloth. The two rubbed slides are glued together using 30 μm spacers (silica micro-sphere, Thermo Scientific), such that the rubbing directions are aligned orthogonally with respect to each other. Such 90° twisted alignment gives rise to unidirectional bending, irrespective of the incident light direction.[43] During infiltration, the cell is set on a hot plate to 95 °C (at which temperature the mixture is in the molten, isotropic state), and two different monomer mixtures are infiltrated simultaneously through the opposite edges of the cell by capillary force (Fig. 2d). After cooling down to 50 °C (3 °C min⁻¹) to reach nematic phase, a blue LED (Prior Scientific; 420 nm, 11 mW cm⁻², 30 min) is used to polymerize the mixture. After that, the cell is opened, and a monolithic strip actuator composed of two halves of different responsive segments is cut from the film, matching the long axis of the strip with one of the rubbing directions. The strip dimension is $15 \times 1 \times 0.03$ mm³. A photograph of the resultant LCN film and polarized optical micrographs at the segment boundary are shown in Fig. 2e and f, respectively. For the self-oscillating strip, monomer mixture with DR1 is infiltrated into the glass cell with 50 μm gap following the same procedure. The film is polymerized with 375 nm LED (Prior Scientific, 7 mW cm⁻², 30 min) at room temperature. A strip with $20 \times 1 \times 0.05$ mm³ dimension is cut after opening the cell. A full list of chemical structures and composition for each fabricated actuator are given in Scheme S1 and Tables S1, S2 in ESI.†

Optical control

LED light sources with emission wavelengths 385 nm, 490 nm and 660 nm, are coupled into a liquid light guide equipped with a collimator lens (purchased through Prior Scientific). The intensities of the light sources are 8 mW cm⁻² (385 nm), 30 or 80 mW cm⁻² (490 nm) and 100 mW cm⁻² (660 nm) measured in front of the sample. The on–off time of each LED is controlled by a hardware and synchronized by a home-made LabVIEW program. Further details on the control strategies for the different non-reciprocal actuators are compiled to Tables S3 and S4 (ESI†).

Characterization method

The free-standing LCN strip is fixed on a support stage, and it deforms in the $X–Y$ plane, as schematically shown in Fig. 2g. The excitation light beams propagate along the Y-direction, while computer controls the sequence and timing of the light sources to be switched on and off. A camera is mounted along the Z-axis, capturing the movement of the actuator strip within the $X–Y$ plane. The photo-induced deformation is arranged to

bend towards the light source, unless mentioned otherwise. For tracking the position, a drop of fluorescent glue (containing Rhodamine 6G dyes, Merck) is used to mark the tip of the actuator. A weak UV light (365 nm, < 0.5 mW cm⁻²; does not contribute to photochemical actuation) is used to illuminate the whole area of the sample, and the fluorescence images were captured by the camera through an optical filter cutting off wavelengths below 500 nm. The tracking position was analysed by software "Kinovea", which extracts the trajectory during oscillation cycles, as schematically shown by the insert of Fig. 2g. The eventual trajectory pattern with non-zero area indicates the characteristic of non-reciprocal movement.

Results and discussion

Non-reciprocal motion *via* three-wavelength modulation

The premise for controlling two actuators (or in our case, the two parts of a monolithic LCN strip) individually upon a spatially uniform light field is that they must behave differently under identical illumination conditions. For this, we utilize the two well-recognized photomechanical actuation schemes in LCNs – the photothermal and photochemical effects. Fig. 3a
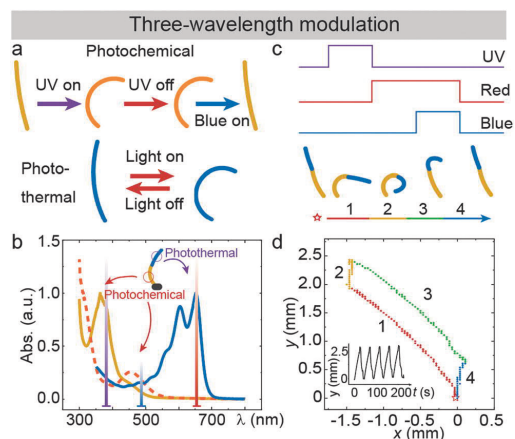

Fig. 3 (a) Schematic illustration of the photochemical and photothermal actuation. In both cases, the bending direction is dictated by the twisted alignment and is independent of the incident light direction. (b) Absorption spectra for the two LCN segments with orthogonal photomechanical responses. The inset shows the construction of the strip, of which the photochemically activated segment (bottom part) is fixed on the stage. The vertical lines indicate the wavelengths used for exciting the two segments. (c) Light control sequence for three-wavelength modulation: (1) UV on (0 s); (2) UV off, red light on (20 s); (3) blue light on (25 s); (4) red and blue light off (35 s). Yellow and blue colors in the stripe represent azobenzene crosslinker- and DB14-containing LCN strip segments, respectively. The color scheme serves to indicate the (in-)active actuator segments at different time sequences, not representing the actual deformation in the experiment. (d) The trajectory of the strip in the $X–Y$ plane. UV: 385 nm, 8 mW cm⁻²; blue: 490 nm, 30 mW cm⁻²; red: 660 nm, 100 mW cm⁻². Inset: Y-axis displacement during repeated actuation cycles. For details of chemical composition of the actuators, see Table S2 (ESI†).
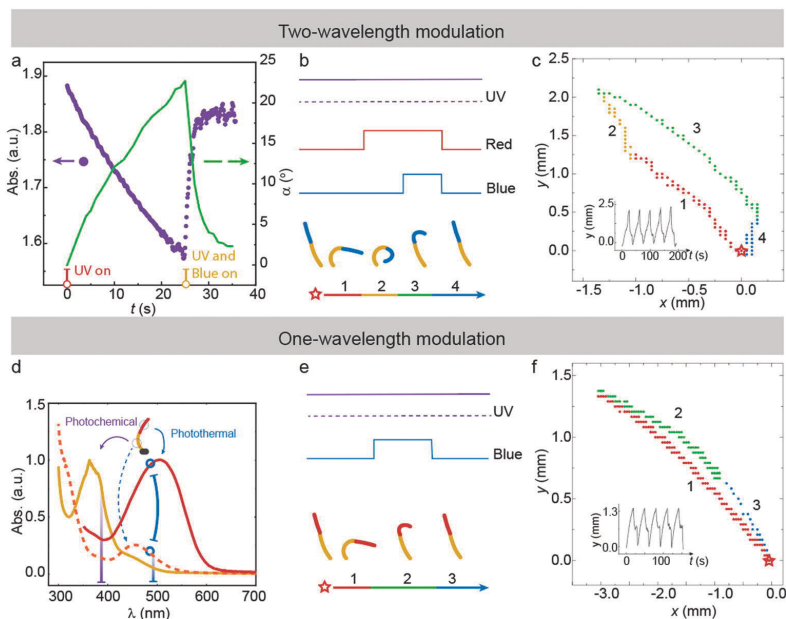
Fig. 4 Non-reciprocal motion *via* two- and one-wavelength modulation. (a) Isomerization and deformation kinetics upon UV and blue illumination. The isomerization kinetics was probed by monitoring the absorbance of the photochemical LCN containing azobenzene crosslinker at 400 nm, and the deformation was measured through the bending angle of the strip. (b) Light control sequence for two-wavelength modulation: (1) UV on through the entire cycle; (2) red light on (20 s); (3) blue light on (25 s); (4) red and blue light off (35 s). Yellow and blue colors in the stripe represent azobenzene crosslinker- and DB14-containing LCN segments, respectively. (c) The trajectory of the strip in the *X*–*Y* plane, indicating non-reciprocal movement. UV: 385 nm, 8 mW cm^{-2}; blue: 490 nm, 80 mW cm^{-2}; red: 660 nm, 100 mW cm^{-2}. Inset: *Y*-axis displacement during repeated actuation cycles. (d) The overlapping absorption bands of the n–π* transition of the azobenzene crosslinks in one segment, and the π–π* transition of DR1 in the other segment. Inset shows the construction of strip containing two individual segments, where the photochemical segment is fixed on the stage. The vertical lines indicate the wavelengths used for excitation. (e) Light control sequence for one-wavelength modulation: (1) UV on throughout the entire cycle; (2) blue light on (20 s); (3) blue light off (30 s). Yellow and red colors represent azobenzene crosslinker- and DR1-containing LCN strip segments, respectively. (f) The trajectory of the strip in the *X*–*Y* plane. UV: 385 nm, 8 mW cm^{-2}; blue: 490 nm, 80 mW cm^{-2}. Inset: *Y*-axis displacement during repeated actuation cycles. The color scheme in (b) and (e) serve to indicate the (in-)active actuator segments at different time sequences, not representing the actual deformation in the experiment. For details of chemical composition of the actuators, see Table S2 (ESI†).

schematically illustrates the differences between these two actuation modes. Photochemical actuation is based on *trans–cis* isomerization of azobenzene crosslinks, typically induced with UV light, which creates inner stress into the LCN to yield macroscopic deformation.[44] The deformation can sustain for a time period ranging from few minutes to several days after ceasing the UV illumination, depending on the *cis*-lifetime of the azobenzene used.[45,46] Alternatively, the original state can be retained using blue light to induce *cis–trans* isomerization. The photothermal effect is triggered by light-absorbing moieties (DR1 or DB14 dyes in our case) incorporated into the LCN, which convert the energy from absorbed photons into heat.[47,48] Heat causes the inner stress required for macroscopic deformation, which vanishes once the irradiation is ceased.

We fabricated an LCN actuator with two segments, one comprising the azobenzene crosslinks to invoke the photochemical effect, and the other with DB14 for triggering the photothermal effect. Fig. 3b shows the absorption spectra of

the two segments. Their activation wavelengths are well separated, allowing orthogonal control of the lower and upper parts of the actuator. Non-reciprocal motion can be obtained by the light control sequence depicted in Fig. 3c: (1) UV light on → the bottom part bends; (2) UV light off → the bottom part remains bent & red light on → the upper part bends; (3) blue light on → the bottom part unbends while the upper part remains bent; (4) red light off → the upper part unbends & blue light off → the system resets and a new cycle can start. The trajectory pattern in the *X*–*Y* plane is shown in Fig. 3d, indicating a clear non-reciprocal behaviour. Conversely, both photochemical and photothermal actuation modes separately lead to reciprocal motion, in which case the strip deforms and relaxes *via* the same path, as illustrated in Fig. S1 (ESI†). By repeating the light control sequence depicted in Fig. 3c, a cyclic non-reciprocal motion is obtained. The consistence between several successive actuation cycles is shown by the *Y*-axis displacement data, given in the inset of Fig. 3d.

Non-reciprocal motion *via* two-wavelength modulation

To reduce the number of light beams to be modulated, we use a strategy that makes use of different kinetics of photoinduced *trans–cis* and *cis–trans* isomerization of the azobenzene cross-linker. Fig. 4a shows the absorbance change and deformation kinetics of the LCN upon photochemical activation. Under UV irradiation (8 mW cm^{-2}), the azobenzene crosslinks undergo *trans–cis* isomerization, giving rise to a decrease in the absorbance of the π–π* band. Within 25 s, approximately 15% of the azobenzenes isomerize to the *cis*-state. By switching on the blue light (80 mW cm^{-2}) while maintaining the UV illumination, the absorbance rapidly recovers with a time constant of 1.2 s and saturates at a value slightly below the initial absorbance. From this we can deduce that the photostationary state upon simultaneous UV and blue irradiation comprises *ca.* 97% *trans*-isomers. The kinetics of absorbance change is in line with the photomechanical actuation: the strip bends slowly upon UV irradiation and rapidly unbends when the blue light is switched on. These observations indicate that photochemical *cis–trans* isomerization is the dominating effect when the actuator is activated within UV + blue spectral range.

The non-reciprocal motion using two-wavelength modulation can be obtained with the same actuator strip as was used for three-wavelength modulation, using the light control sequence shown in Fig. 4b: (1) for the entire cycle, UV light is on → the bottom part bends; (2) red light on → the upper part bends, while the bottom part remains bent; (3) blue light on → the bottom part unbends, while the upper part remains bent as the red light is on; (4) red light off → the upper part relaxes; the system resets when the blue light is ceased and a new cycle can start. The non-reciprocal behavior is shown by the *X–Y* trajectory pattern in Fig. 4c, while the inset of Fig. 4c confirms the repeatability of the cyclic actuation. Finally, we note that a strip composed of two segments that can be photothermally activated at different wavelengths can also perform non-reciprocal movements, as detailed in Fig. S2 (ESI†).

Non-reciprocal motion *via* one-wavelength modulation

To further reduce the number of modulating light beams, an overlap between the absorption bands that trigger *cis–trans* isomerization of the azobenzene crosslinks and the photothermal actuation in a different segment of the LCN strip, is adopted and illustrated in Fig. 4d. Hence, we invoke the photochemical *cis–trans* isomerization and the photothermal effect simultaneously with a single wavelength (490 nm), causing the different segments of the strip to bend (photothermal activation) and unbend (photochemical activation). We note that the photothermal dye used, DR1, also undergoes photoisomerization, but when doped to LCN, the actuation arises solely from the photothermal effect.[49] The following light control sequence is used (Fig. 4e): (1) for the entire cycle, UV light is on → the bottom part bends (20 s); (2) blue light on → the bottom part unbends and at the same time, the upper part bends; (3) blue light off → the upper part unbends, the system resets and a new cycle can start. The non-reciprocal trajectory

pattern is shown in Fig. 4f, and the *Y*-axis displacement is again used to monitor the reversibility of the actuation cycles (inset of Fig. 4f).

Non-reciprocal self-oscillation

To obtain non-reciprocal self-oscillation with spatially and temporally constant laser illumination (which we denote as zero-wavelength modulation in Fig. 5), the movement of the actuator should not only be non-reciprocal, but also cyclic and self-sustained.[50] Self-oscillation has been widely studied among light-driven actuators.[47,51–58] Most of the studies employ bending strips, however, non-reciprocal self-oscillation has rarely been reported.[52,54] Self-shadowing is an intriguing concept for achieving self-oscillation, which has been utilized in wave-like motion (a symbol of non-reciprocal motion) and autonomous locomotion in LCNs.[54]

We employ a strategy built on the combination of the self-shadowing effect and flexibility of the actuator body in a long, free-standing LCN strip. A continuous-wave 532 nm laser beam is used to excite the strip along horizontal direction (Fig. 5a), and the oscillation kinetics is followed to confirm the non-reciprocal motion. The monolithic strip can be divided into two parts, marked as A and B in Fig. 5a(i). Part B is defined by the area where the incident beam firstly hits, *i.e.*, it is confined close to the base the actuator is attached to. The rest of the strip forms Part A. Even if the chemical composition (Table S2, ESI†) of the two parts is identical, Part A dictates the photodeformation, yielding a dynamic change of centre of mass of the strip
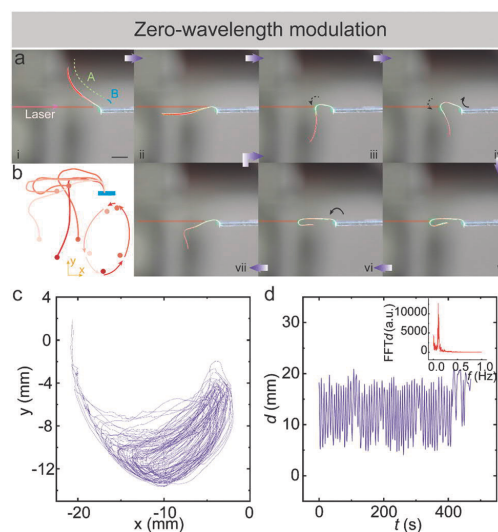
Fig. 5 Non-reciprocal self-oscillation. (a) Optical images of LCN self-oscillator under a constant laser beam excitation. Scale bar: 5 mm. Laser beam, 532 nm, 100 mW. Spot diameter: 2 mm. (b) Schematic drawing of the principle of oscillating kinetics. (c) *X–Y* movement trajectory of the trip position in 50 oscillation cycles. (d) Tip displacement during sequent oscillating cycles. Inset shows the Fourier transform of displacement data.

and the torque imposed on Part B due to the gravity, while Part B is responsible for mechanical relaxation but does not directly contribute to the cyclic photomechanical actuation. Any change in torque or modulus of the strip leads to bending of Part B in either clockwise or anticlockwise direction. When the laser beam is exciting Part B, it bends anticlockwise, causing Part A to shadow Part B (Fig. 5a(ii); Movie S1, ESI†). From thereon, only Part A is exposed to laser excitation. Fig. S3 (ESI†) presents top-view and bottom-view images of the LCN strip during the oscillation cycles.

The self-oscillation process is promoted by the following steps: initially, the beam hits Part A at the "bottom", *i.e.*, close to where it meets Part B (Fig. 5a(iii)). The photoinduced bending of the strip leads to a reduced torque raised by the gravity of Part A, and at the same time, the stiffness of Part B rebounds the cantilever by slightly bending to the clockwise direction (iv). This movement raises the height of Part A and brings about a continuous change of the spot where the laser hits the cantilever and hence its shape (iv–v–vi). While the cantilever is extending towards left (vi), the gravity-induced torque in Part A increases, forcing Part B to bend anticlockwise. The bending of Part B, in turn, reduces the height of Part A, allowing the incident beam to reach the "bottom" of Part A again (vii). At the same time, the deformed portion of Part A relaxes while the "bottom" of Part A starts to photodeform (vii-to-iii), and a new cycle can begin. The movement trajectory clearly exhibits a non-reciprocal pattern in the *X–Y* plane, as illustrated in Fig. 5b. Fig. 5c presents the evolution of *X–Y* plane trajectory over *ca.* 50 oscillation cycles. For more details, see the *X–Y* trajectory evolution data in Fig. S4 and Movie S2 (ESI†). The fact that subsequent trajectories follow different paths most likely arises from slight irreversibility in the properties of the polymer network upon photoactuation. However, the oscillation can self-sustain over extended periods of time, as confirmed by monitoring the oscillation of the strip over a time span of 400 s (Fig. 5d and Fig. S5, ESI†). The oscillation frequency is around 0.1 Hz, as indicated by the Fourier transform data shown in the inset of Fig. 5d.

Discussion

The non-reciprocal trajectory is sensitive to the experimental arrangement, *i.e.*, the positions of the two segments and their related deformation. For instance, reversing the photothermal and photochemical segments, such that the former is positioned to the bottom, or flipping the strip to reverse its bending direction, yield different non-reciprocal trajectories as illustrated in Fig. S6 and S7 (ESI†). Changing the ratio between the length of the photothermal and photochemical segments varies the pattern of the trajectory, yet the motion remains non-reciprocal (Fig. S8, ESI†). The efficiency of non-reciprocal motion, which can be visualized by the loop area under the *X–Y* trajectory within one oscillating cycle (*e.g.* Fig. 3d, 4c, f and 5c), can be improved by separately optimizing the deformation of each part of the actuator. More importantly, orthogonality of actuation, *i.e.*, separate addressability of the actuator segments, plays a significant role. For example, upon the three- and two-wavelength

modulation strategies, spectral separation allows individual control between the photochemically and photothermally actuated parts, yielding large non-reciprocal movement (Fig. 3d and 4c). However, when the two parts cross-talk, which is the case for the one-wavelength modulation strategy, the photochemical relaxation (unbending) and photothermal actuation occur simultaneously, yielding only minor non-reciprocal motion as observed in Fig. 4f.

It is important to study how to translate the cyclic movement of an actuator into robotic locomotion.[59,60] Along this direction, many pioneering results have been reported. To achieve walking on a surface, the conventional approach leans on friction bias during the cyclic deformation.[25,61] Non-reciprocal motion allows, for instance, a travelling-wave-like motion to induce locomotion without the need for friction asymmetry at the robot–substrate interface.[62,63] Non-reciprocal motion has also been exploited in creating micro-swimmers, especially in low-Reynolds-number liquids.[64–66] However, underwater actuation is hindered by quick heat dissipation in aqueous environment, rendering photothermal processes inefficient. Recent study on underwater actuation using liquid-crystal gels addressed this problem, pointing a way forward for underwater self-oscillation.[67]

To meet the capacities required for flying, the non-reciprocal motion speed has to be boosted in order to produce sufficient air thrust. At the same time, the density of the actuating device should be minimized. To meet those requirements, great effort has been recently dedicated towards improving the material properties, *e.g.*, the use of chain extenders to enhance the deformability,[68,69] and interpenetrating networks to increase the robustness.[70] Reconfigurability and programmability of the motions are also important in view of increasing the versatility of photoinduced motions.[71–73] These will lead to ever-more advanced robot realizations and non-reciprocal motions in the near future.

Conclusions

Different light-control strategies have been introduced to achieve non-reciprocal movements in photomechanical liquid-crystal network (LCN) actuators. By proper selection of the photoactive moieties, photochemical and photothermal actuation can be induced separately in two distinct segments of a monolithic LCN strip. Specific light control sequences, based on three-, two-, and one-wavelength modulation, are designed to bring about non-reciprocal motions. Finally, a non-reciprocal self-oscillator is demonstrated in a free-standing LCN strip. This actuator can sustain the non-reciprocal motion upon a spatially and temporally constant light field, benefitting from self-shadowing and the flexibility of the long, strip-like structure. The results provide general guidelines to simplify the modulation of the light fields, offering design principles for complex and non-reciprocal light-controlled movements and alternatives for wireless soft robotics.

Conflicts of interest

There are no conflicts to declare.

Acknowledgements

References

1 M. H. Dickinson, C. T. Farley, R. J. Full, M. A. R. Koehl, R. Kram and S. Lehman, *Science*, 2000, **288**, 100–106.

2 M. Sfakiotakis, D. M. Lane and J. B. C. Davies, *IEEE J. Oceanic Eng.*, 1999, **24**, 237–252.

3 L. I. van Griethuijsen and B. A. Trimmer, *Biol. Rev.*, 2014, **89**, 656–670.

4 E. M. Purcell, *Am. J. Phys.*, 1977, **45**, 3–11.

5 W. Hu, G. Z. Lum, M. Mastrangeli and M. Sitti, *Nature*, 2018, **554**, 81–85.

6 M. Wehner, R. L. Truby, D. J. Fitzgerald, B. Mosadegh, G. M. Whitesides, J. A. Lewis and R. J. Wood, *Nature*, 2016, **536**, 451–455.

7 C. Laschi, B. Mazzolai and M. Cianchetti, *Sci. Robot.*, 2016, **1**, aah3690.

8 K. Ma, P. Chirarattananon, S. Fuller and R. J. Wood, *Science*, 2013, **340**, 603–607.

9 Y. Wu, J. K. Yim, J. Liang, Z. Shao, M. Qi, J. Zhong, Z. Luo, X. Yan, M. Zhang, X. Wang, R. S. Fearing, R. J. Full and L. Lin, *Sci. Robot.*, 2019, **4**, eaax1594.

10 D. Martella, S. Nocentini, D. Nuzhdin, C. Parmeggiani and D. S. Wiersma, *Adv. Mater.*, 2017, **29**, 1704047.

11 O. M. Wani, H. Zeng and A. Priimagi, *Nat. Commun.*, 2017, **8**, 15546.

12 E. Diller and M. Sitti, *Adv. Funct. Mater.*, 2014, **24**, 4397–4404.

13 P. Liljebäck, K. Y. Pettersen, Ø. Stavdahl and J. T. Gravdahl, *Robot. Auton. Syst.*, 2012, **60**, 29–40.

14 R. F. Shepherd, F. Ilievski, W. Choi, S. A. Morin, A. A. Stokes, A. D. Mazzeo, X. Chen, M. Wang and G. M. Whitesides, *Proc. Natl. Acad. Sci. U. S. A.*, 2011, **108**, 20400–20403.

15 D. Rus and M. T. Tolley, *Nature*, 2015, **521**, 467–475.

16 L. Hines, K. Petersen, G. Z. Lum and M. Sitti, *Adv. Mater.*, 2017, **29**, 1603483.

17 S. Kim, C. Laschi and B. Trimmer, *Trends Biotechnol.*, 2013, **31**, 287–294.

18 J. M. McCracken, B. R. Donovan and T. J. White, *Adv. Mater.*, 2020, **32**, 1906564.

19 J. del Barrio and C. Sánchez-Somolinos, *Adv. Opt. Mater.*, 2019, **7**, 1900598.

20 H. Zeng, P. Wasylczyk, D. S. Wiersma and A. Priimagi, *Adv. Mater.*, 2018, **30**, 1703554.

21 T. Ube and T. Ikeda, *Adv. Opt. Mater.*, 2019, **7**, 1900380.

22 M. Pilz da Cunha, S. Ambergen, M. G. Debije, E. F. G. A. Homburg, J. M. J. den Toonder and A. P. H. J. Schenning, *Adv. Sci.*, 2020, **7**, 1902842.

23 L. Dong, X. Tong, H. Zhang, M. Chen and Y. Zhao, *Mater. Chem. Front.*, 2018, **2**, 1383–1388.

24 F. Lancia, A. Ryabchun and N. Katsonis, *Nat. Rev. Chem.*, 2019, **3**, 536–551.

25 M. Yamada, M. Kondo, R. Miyasato, Y. Naka, J. I. Mamiya, M. Kinoshita, A. Shishido, Y. Yu, C. J. Barrett and T. Ikeda, *J. Mater. Chem.*, 2009, **19**, 60–62.

26 S. K. Ahn, T. H. Ware, K. M. Lee, V. P. Tondiglia and T. J. White, *Adv. Funct. Mater.*, 2016, **26**, 5819–5826.

27 L. Liu, M. H. Liu, L. L. Deng, B. P. Lin and H. Yang, *J. Am. Chem. Soc.*, 2017, **139**, 11333–11336.

28 Y. Hu, Z. Li, T. Lan and W. Chen, *Adv. Mater.*, 2016, **28**, 10548–10556.

29 M. Lahikainen, H. Zeng and A. Priimagi, *Nat. Commun.*, 2018, **9**, 4148.

30 Z. Cheng, T. Wang, X. Li, Y. Zhang and H. Yu, *ACS Appl. Mater. Interfaces*, 2015, **7**, 27494–27501.

31 C. Huang, J. A. Lv, X. Tian, Y. Wang, Y. Yu and J. Liu, *Sci. Rep.*, 2015, **5**, 17414.

32 H. Zeng, P. Wasylczyk, C. Parmeggiani, D. Martella, M. Burresi and D. S. Wiersma, *Adv. Mater.*, 2015, **27**, 3883–3887.

33 M. Sitti and D. S. Wiersma, *Adv. Mater.*, 2020, 1906766.

34 I. A. Anderson, T. A. Gisby, T. G. McKay, B. M. O'Brien and E. P. Calius, *J. Appl. Phys.*, 2012, **112**, 041101.

35 T. Qiu, S. Palagi, A. G. Mark, K. Melde, F. Adams and P. Fischer, *Appl. Phys. Lett.*, 2016, **109**, 191602.

36 Q. He, Z. Wang, Y. Wang, A. Minori, M. T. Tolley and S. Cai, *Sci. Adv.*, 2019, **5**, eaax5746.

37 B. Zuo, M. Wang, B. P. Lin and H. Yang, *Nat. Commun.*, 2019, **10**, 4539.

38 A. H. Gelebart, D. J. Mulder, G. Vantomme, A. P. H. J. Schenning and D. J. Broer, *Angew. Chem., Int. Ed.*, 2017, **56**, 13436–13439.

39 M. Wang, Y. Han, L. X. Guo, B. P. Lin and H. Yang, *Liq. Cryst.*, 2019, **46**, 1231–1240.

40 C. L. Van Oosten, C. W. M. Bastiaansen and D. J. Broer, *Nat. Mater.*, 2009, **8**, 677–682.

41 D. Martella, D. Antonioli, S. Nocentini, D. S. Wiersma, G. Galli, M. Laus and C. Parmeggiani, *RSC Adv.*, 2017, **7**, 19940–19947.

42 S. Palagi, A. G. Mark, S. Y. Reigh, K. Melde, T. Qiu, H. Zeng, C. Parmeggiani, D. Martella, A. Sanchez-Castillo, N. Kapernaum, F. Giesselmann, D. S. Wiersma, E. Lauga and P. Fischer, *Nat. Mater.*, 2016, **15**, 647–653.

43 C. L. Van Oosten, K. D. Harris, C. W. M. Bastiaansen and D. J. Broer, *Eur. Phys. J. E: Soft Matter Biol. Phys.*, 2007, **23**, 329–336.

44 M. Yamada, M. Kondo, J. I. Mamiya, Y. Yu, M. Kinoshita, C. J. Barrett and T. Ikeda, *Angew. Chem., Int. Ed.*, 2008, **47**, 4986–4988.

45 M. Pilz Da Cunha, E. A. J. Van Thoor, M. G. Debije, D. J. Broer and A. P. H. J. Schenning, *J. Mater. Chem. C*, 2019, **7**, 13502–13509.

46 S. Iamsaard, E. Anger, S. J. Aßhoff, A. Depauw, S. P. Fletcher and N. Katsonis, *Angew. Chem., Int. Ed.*, 2016, **55**, 9908–9912.

47 A. H. Gelebart, G. Vantomme, B. E. W. Meijer and D. J. Broer, *Adv. Mater.*, 2017, **29**, 1606712.

48 Z. Wang, K. Li, Q. He and S. Cai, *Adv. Mater.*, 2019, **31**, 1806849.

49 H. Zeng, O. M. Wani, P. Wasylczyk, R. Kaczmarek and A. Priimagi, *Adv. Mater.*, 2017, **29**, 1701814.

50 A. Jenkins, *Phys. Rep.*, 2013, **525**, 167–222.

51 T. J. White, N. V. Tabiryan, S. V. Serak, U. A. Hrozhyk, V. P. Tondiglia, H. Koerner, R. A. Vaia and T. J. Bunning, *Soft Matter*, 2008, **4**, 1796–1798.

52 H. Zeng, M. Lahikainen, L. Liu, Z. Ahmed, O. M. Wani, M. Wang, H. Yang and A. Priimagi, *Nat. Commun.*, 2019, **10**, 5057.

53 F. Ge and Y. Zhao, *Chem. Sci.*, 2017, **8**, 6307–6312.

54 A. H. Gelebart, D. J. Mulder, M. Varga, A. Konya and G. Vantomme, *Nature*, 2017, **546**, 632–636.

55 R. Lan, J. Sun, C. Shen, R. Huang, Z. Zhang, L. Zhang, L. Wang and H. Yang, *Adv. Mater.*, 2020, **32**, 1906319.

56 G. Vantomme, A. H. Gelebart, D. J. Broer and E. W. Meijer, *Tetrahedron*, 2017, **73**, 4963–4967.

57 K. M. Lee, M. L. Smith, H. Koerner, N. Tabiryan, R. A. Vaia, T. J. Bunning and T. J. White, *Adv. Funct. Mater.*, 2011, **21**, 2913–2918.

58 Y. Kageyama, *ChemPhotoChem*, 2019, **3**, 327–336.

59 C. Ahn, K. Li and S. Cai, *ACS Appl. Mater. Interfaces*, 2018, **10**, 25689–25696.

60 J. J. Wie, M. R. Shankar and T. J. White, *Nat. Commun.*, 2016, **7**, 13260.

61 H. Zeng, O. M. Wani, P. Wasylczyk and A. Priimagi, *Macromol. Rapid Commun.*, 2017, **39**, 201700224.

62 M. Rogóż, K. Dradrach, C. Xuan and P. Wasylczyk, *Macromol. Rapid Commun.*, 2019, **40**, 1970036.

63 M. Rogóż, H. Zeng, C. Xuan, D. S. Wiersma and P. Wasylczyk, *Adv. Opt. Mater.*, 2016, **4**, 1689–1694.

64 S. Tottori, L. Zhang, F. Qiu, K. K. Krawczyk, A. Franco-Obregõn and B. J. Nelson, *Adv. Mater.*, 2012, **24**, 811–816.

65 H. Zhang, L. Koens, E. Lauga, A. Mourran and M. Möller, *Small*, 2019, **15**, 1903379.

66 A. M. Maier, C. Weig, P. Oswald, E. Frey, P. Fischer and T. Liedl, *Nano Lett.*, 2016, **16**, 906–910.

67 H. Shahsavan, A. Aghakhani, H. Zeng, Y. Guo, Z. S. Davidson, A. Priimagi and M. Sitti, *Proc. Natl. Acad. Sci. U. S. A.*, 2020, **117**, 5125–5133.

68 H. H. Yoon, D. Y. Kim, K. U. Jeong and S. K. Ahn, *Macromolecules*, 2018, **51**, 1141–1149.

69 T. H. Ware, M. E. McConney, J. J. Wie, V. P. Tondiglia and T. J. White, *Science*, 2015, **347**, 982–984.

70 H.-F. Lu, M. Wang, X.-M. Chen, B.-P. Lin and H. Yang, *J. Am. Chem. Soc.*, 2019, **141**, 14364–14369.

71 Y. Yang, E. M. Terentjev, Y. Wei and Y. Ji, *Nat. Commun.*, 2018, **9**, 1906.

72 T. Ube, K. Kawasaki and T. Ikeda, *Adv. Mater.*, 2016, **28**, 8212–8217.

73 Z. Wang, H. Tian, Q. He and S. Cai, *ACS Appl. Mater. Interfaces*, 2017, **9**, 33119–33128.

PUBLICATION
III

Reconfigurable Photoactuator Through Synergistic Use of Photochemical and Photothermal Effects.

Lahikainen, M.; Zeng, H.; Priimagi, A.

Reconfigurable photoactuator through synergistic use of photochemical and photothermal effects

Markus Lahikainen [1], Hao Zeng [1] & Arri Priimagi[1]

A reconfigurable actuator is a stimuli-responsive structure that can be programmed to adapt different shapes under identical stimulus. Reconfigurable actuators that function without control circuitry and are fueled remotely are in great demand to devise adaptive soft robotic devices. Yet, obtaining fast and reliable reconfiguration remains a grand challenge. Here we report a facile fabrication pathway towards reconfigurability, through synergistic use of photochemical and photothermal responses in light-active liquid crystal polymer networks. We utilize azobenzene photoisomerization to locally control the *cis*-isomer content and to program the actuator response, while subsequent photothermal stimulus actuates the structure, leading to shape morphing. We demonstrate six different shapes reconfigured from one single actuator under identical illumination conditions, and a light-fueled smart gripper that can be commanded to either grip and release or grip and hold an object after ceasing the illumination. We anticipate this work to enable all-optical control over actuator performance, paving way towards reprogrammable soft micro-robotics.

[1] Laboratory of Chemistry and Bioengineering, Tampere University of Technology, P.O. Box 541, FI-33101 Tampere, Finland. Correspondence and requests for materials should be addressed to H.Z. (email: hao.zeng@tut.fi) or to A.P. (email: arri.priimagi@tut.fi)

For the past decades, great efforts have been put into investigating stimuli-responsive soft materials and their use in designing soft actuators capable of complex, rapid, and reversible macroscopic movements[1,2]. The inspiration for the soft actuator research often times comes from natural species that are capable of adaptive shape changes, diverse geometric morphing, and highly efficient locomotion[3,4]. Stimuli-responsive soft actuators have proven their potential in realizing bio-inspired soft robots that are miniature in size and can be fueled remotely and wirelessly to yield complex movements[5–7]. Compared to synthetic, human-made devices, the sophistication of natural species is overwhelming: even the most primitive species can have multiple degrees of freedom in their movement, and reconfigurable response under the same environmental stimulus. Most artificial actuators, on the other hand, display only one specific kind of deformation under a specific stimulus (e.g., light, magnetic field, electric voltage)[8–10], and obtaining reconfigurable actuation under constant stimulus is a formidable challenge. Achieving this goal would pave way towards adaptive, reprogrammable soft micro-robotics.

Among different stimuli, light has arisen as a particularly attractive alternative, due to its high degree of spatial and temporal control over properties such as wavelength, intensity, and polarization. Several photoresponsive molecules[11,12] and material systems[13–15] such as hydrogels[7,16], carbon-nanotube-based actuators[17], and shape memory polymers[18] have been explored for devising soft actuators, yet photoresponsive liquid crystal elastomers and polymer networks (referred to as LCNs from hereon) are in many cases particularly intriguing[19]. LCNs combine the anisotropy of liquid crystals and the elasticity of loosely crosslinked polymeric materials, and by "programming" the molecular alignment pattern during the fabrication process (photopolymerization), an overwhelming variety of light-induced shape changes (e.g., contraction, bending, coiling, buckling, etc.) can be obtained[20–23]. In contrast to hybrid actuators relying on, e.g., bilayer structures to obtain efficient actuation[7,17], LCNs allow complex three-dimensional deformation in a monolithic film with uniformly distributed chemical composition[19].

The term reconfigurable actuation is often times used to refer to the ability to reversibly switch between different shapes upon external stimulus[14,15]. However, conventional stimuli-driven actuators, LCNs among other materials, even if reversible, typically exhibit only one pre-determined state of deformation under one specific stimulus. Hence, to obtain multiple shape changes, the stimulus has to be tuned, which in case of light-triggered actuation can refer to, e.g., changing the light intensity or its spatial/temporal distribution. Obtaining multiple shape changes upon an unchanged stimulus thus requires a programming step during fabrication (such as controlling the photo-polymerization process[24]) which eventually results in different samples with identical composition but distinct actuation modes. In contrast, reconfigurable actuators, as we define them, have the ability to obtain multiple shape changes from one single sample upon one identical stimulus. Previous reconfiguration strategies have been based on dynamic covalent bonds[25–29], acidic patterning[30], or base treatment[31]. All these methods rely on chemical processing to modify material properties like alignment, elastic modulus, and absorption, while the diversity of reconfigured shape change is limited. The lack of facile reconfiguration schemes is a significant drawback from the perspective of light-powered micro-robotics[32] which would benefit from fast and reliable control over actuation modes. A light-fueled soft actuator that would be reconfigurable, i.e., exhibit more than one type of shape change under the same light stimulus (same intensity, wavelength, polarization, etc.), and at the same time being fast and reliable, opens new horizons to realize flexible micro-devices with well adjustable performance.
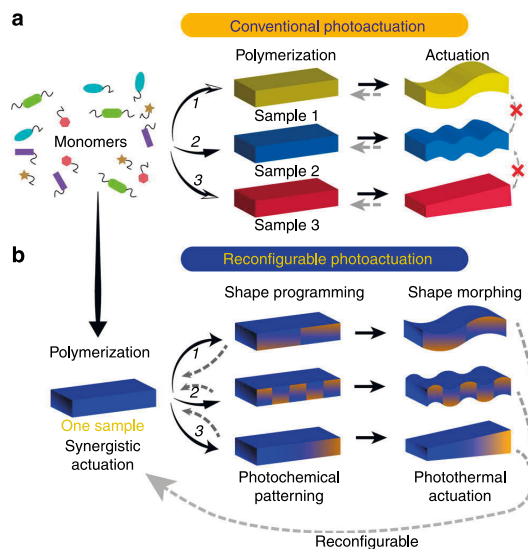

Fig. 1 Actuator concept. **a** Conventional stimuli-responsive actuators require a programming process in fabrication which eventually results in different samples with distinct actuation modes. **b** A reconfigurable photoactuator capable of multiple shape changes from one single sample upon one identical stimulus is achieved using photochemical trigger for shape programming and photothermal effect for shape morphing

Herein we present a fabrication strategy for solving this challenge through a facile pathway towards reconfigurable photo-actuation. Our concept is based on synergistic use of the photochemical and photothermal actuation schemes, a combination that we show to yield "actuation on command". The photochemical and photothermal effects play distinct roles in the synergistic photoactuation in a liquid crystalline polymer network, the former being used for shape programming and the latter for shape morphing. We demonstrate six different reversible shapes taken by the same actuator within a few seconds of irradiation under identical illumination conditions. The concept is further utilized to design a smart gripping device that can be commanded to either hold or release the object after ceasing the irradiation. These results offer an approach to reconfigurable micro-robotics with reversible, fully optical control over the shape programming and shape morphing.

Results

The design concept of synergistic photoactuator. Figure 1 shows the conceptual differences between conventional actuators and the reconfigurable actuation strategy proposed for the LCN actuator based on synergistic use of photochemical and photothermal effects. The light-induced deformations in LCNs can take place via two distinct mechanisms, being driven by either photochemical[33] or photothermal stimulus[20]. Photochemical LCN actuators rely on photoisomerization of azobenzene molecules[34], typically incorporated as crosslinks into the polymer network. The lifetime of the deformed shape is connected to the *cis*-isomer lifetime of the azobenzene used[35], and the actuator can be driven between two distinct states by irradiating it with two different wavelengths (see the schematic in Fig. 2a). Such systems allow for devising optically tunable photonic devices[36], and also enable efficient photoactuation in aqueous environment[37]. For soft robotic applications, the most efficient photoactuation scheme is
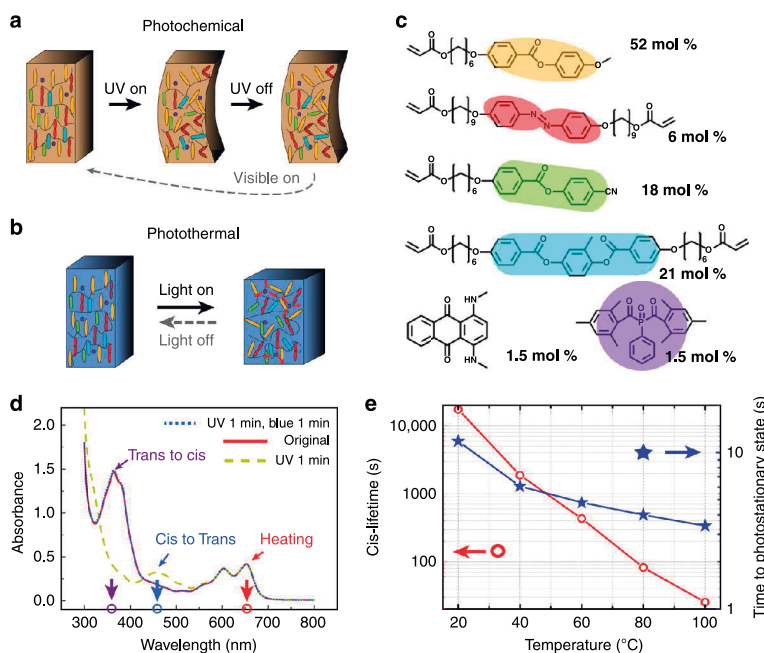
Fig. 2 Design of a synergistic photoactuator. Schematic drawing of **a** photochemical and **b** photothermal actuation. **c** Chemical composition of the liquid crystal monomer mixture. **d**, UV–Vis spectra of LCN film containing both DB14 and azobenzene crosslinks. The arrows indicate the excitation wavelengths used in the actuation: 365 nm for *trans–cis* isomerization (purple arrow), 460 nm for *cis–trans* isomerization (blue arrow), and 660 nm for photothermal heating (red arrow). **e** *Cis*-lifetime during the thermal relaxation in the dark (*cis–trans*) and time to reach photostationary state upon UV irradiation (*trans–cis*) at different temperatures

based on converting light energy into heat, which allows for fast and dynamic (i.e., the system rapidly relaxes back to the initial state once the irradiation is ceased, see Fig. 2b) motions and cyclically actuated, small-scale photomobile devices[38,39]. The different actuation dynamics of photochemically and photothermally driven strip-like LCN actuators is highlighted in Supplementary Figure 1. Both actuation mechanisms have yielded a wealth of fascinating demonstrations on light-fueled movements[40–42]. In the following, we demonstrate the synergistic use of these two mechanisms in order to design photoresponsive materials with characteristics not met in purely photochemical or photothermal actuators.

The materials used and their composition within the LCN actuator are shown in Fig. 2c (see Methods for fabrication details). The photoactive units were selected based on the following criteria. First, the wavelengths with which to trigger *trans–cis* isomerization, *cis–trans* isomerization, and the photothermal effect must be spectrally separated (see Fig. 2d and Supplementary Figure 2). Second, the lifetime of the *cis*-isomer of the azobenzene crosslinks at the operating temperature (accounting for the temperature rise due to the photothermal effect) must be long enough, such that thermal back isomerization within the experimental time frame would be minimized. The ultraviolet–visible (UV–Vis) spectra of the polymerized LCN actuator are shown in Fig. 2d, confirming the spectral separation and efficient, reversible isomerization of the azobenzene crosslinks. Figure 2e shows that the *cis*-lifetime (see Supplementary Figure 3 for further details) of the azobenzene used scales exponentially with temperature. For example, at 40 °C the *cis*-lifetime exceeds 30 min, which is long enough to be considered as bi-stable within the time frame of photothermal actuation, as will

be detailed later on. The fraction of *cis*-isomer in the photostationary state is ca. 80% even at elevated temperatures (see Methods for further details). However, the time to reach the photostationary state decreases significantly with increasing temperature (Fig. 2e). Therefore, certain degree of temperature increase due to photothermal effect serves to accelerate the photochemical actuation.

In our synergistic photoactuation scheme (Fig. 1b), the *trans–cis* isomerization of azobenzene moieties is used to locally control the mechanical properties of the actuator (yielding no shape changes), while photothermal effect triggers shape changes under red-light illumination by releasing the stress generated by inhomogeneous *cis*-azobenzene distribution. As the reverse *cis–trans* isomerization can be induced by blue-green irradiation, the system can be brought back to its initial state upon irradiation within these wavelengths, and subsequently reconfigured with UV light to adapt any other shape under red-light illumination.

Enhanced photoinduced bending in synergistic photoactuators. We studied the photoinduced bending of the synergistic photoactuators in splay-aligned films with 4 × 1 × 0.02 mm³ dimensions. In splay films, both photochemical and photothermal effects give rise to bending towards the same direction[43]—the planar-oriented side of the film—and can be easily characterized by measuring the bending angle as schematized in the inset of Fig. 3a. Upon photothermal heating (660 nm), the strip exhibits a gradual bending with magnitude increasing as a function of irradiation intensity (red circles in Fig. 3a), accompanied by a linear increase in temperature (blue dots in Fig. 3a). The speed of temperature increase/decrease upon light on/off does not depend
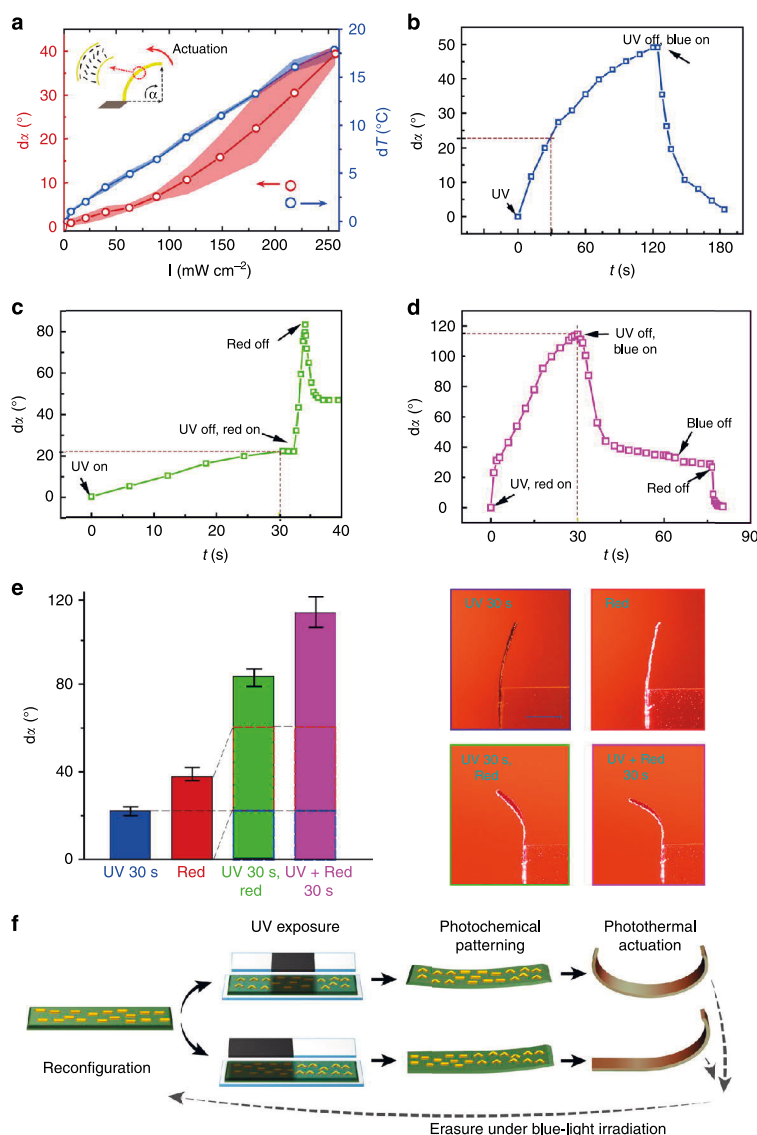
Fig. 3 Photoinduced bending upon photochemical and/or photothermal triggering. **a** Change of bending angle dα and maximum enhanced temperature as a function of red-light irradiation intensity. The error bars indicate standard deviation for $n = 3$ measurements. Inset shows the schematic drawing of the measured bending angle and actuation direction in respect to the molecular alignment. **b** Photochemically induced bending upon subsequent UV and blue light excitations. **c** Synergistic actuation using subsequent UV and red-light illumination. **d** Synergistic actuation under simultaneous UV and red-light illumination. **e** Bending angle change upon different stimuli. Error bars indicate standard deviation for $n = 3$ measurements. Photographs show the deformation of the same sample upon different illumination. Scale bar: 2 mm. **f** Schematic drawing of reconfiguration strategy by synergistically using photochemical and photothermal responses

on irradiation intensity (Supplementary Figure. 4), and both bending and unbending take place relatively fast, within less than 2 s once starting/ceasing the irradiation. As shown in Supplementary Fig. 5a–c, the response time is similar for samples with different thicknesses. In the experiments that follow, we adopt a moderate intensity of 260 mW cm^{-2}, corresponding to 18 °C temperature increase at the equilibrium stage and ca. 40° of photothermally induced bending.

For photochemical actuation, 365 nm (9 mW cm^{-2}) and 460 nm (18 mW cm^{-2}) were used for inducing *trans–cis* and *cis–trans* isomerization, respectively. The reason for using such low intensity is that we want to fully decouple the photochemical and photothermal actuation processes and as can be seen from Supplementary Fig. 6, heating induced by UV or blue irradiation is negligible, less than 1 °C. The photochemically induced bending is markedly slow compared to the photothermal actuation: within

2 min of UV exposure, the strip slowly bends to 50°, and 60 s irradiation with blue light retains the original shape (Fig. 3b). The slow bending speed is consistent with literature on photochemically driven actuators[8,21,35].

We next combined the photochemical and photothermal effects, first subsequently and then simultaneously. In Fig. 3c, 30 s UV irradiation, leading to bending of 22°, is followed by the photothermal excitation. Such subsequent UV → red illumination yields rapid bending up to 83°, i.e., much larger than the bending induced by red light only (40°), without prior UV exposure (Fig. 3a). We attribute this to photochemically induced stress inside the polymer network which can be released by photothermal heating. Interestingly, when the red light is ceased, the strip relaxes only partially and stabilizes to 47° angle (cf. 22° bending angle prior to red-light illumination). This indicates that the photochemically induced deformation can be preserved and even amplified by the photothermal actuation. Finally, when illuminating the film simultaneously with UV and red light to activate both the photochemical and photothermal mechanisms, the strip bends to 115° angle within 30 s (Fig. 3d), overwhelming the purely photochemical actuation (Fig. 3b) in both speed and magnitude.

The above-described experiments are summarized in Fig. 3e. Most importantly, combination of photochemical and photothermal actuation leads to a drastic increase in the bending angle—fivefold compared to the photochemically induced actuation and threefold compared to the photothermal one. Such enhanced photoinduced deformations are observed in samples with different thickness, as shown in Supplementary Figure 5d, which also illustrates that the bending angle increases with sample thickness. As a comparison, in carbon-nanotube-based photothermal actuators, both the degree of deformation and wavelength sensitivity decrease when increasing the thickness of the actuator[44]. Herein, we attribute the slightly enhanced actuation in thicker LCN strips (Supplementary Figure 5d) to changes in material rigidity upon changing the thickness. This is because the polymerization process itself depends on the sample thickness: the thicker the sample, the stronger the absorption due to the azobenzene units at the polymerization wavelength (420 nm; see Fig. 2d for the azobenzene absorption). Therefore, in thicker samples polymerization becomes less efficient, yielding softer samples with enhanced photoinduced bending. Figure 3e also reveals another interestingly fact: the enhancement arising from the photoisomerization and the photothermal heating can be achieved in different time domains. Therefore, photoisomerization-induced changes can be recorded/patterned into the polymer without introducing significant actuation, after which photothermal actuation can be applied to deform the structure without the need for further changes in isomerization (green column in Fig. 3e). The deformation is fully erasable by irradiation with blue light that induces cis-to-trans back isomerization. This mechanism immediately points towards an application in realizing light-driven reconfigurable actuators, based on the principle illustrated in Fig. 3f. Firstly, fully reversible photochemical pattering via mask exposure allows for local control over the cis-isomer content across the sample area, thus programming the actuator performance. Subsequently, photothermal heating stimulates the UV-encoded actuation capacity, leading to diverse shape morphing under identical light stimulus.

Reconfigurable shape changes and programmable microrobotics.
To demonstrate reconfigurability based on synergistic photoactuation, we fabricated a planar-aligned LCN strip with $25 \times 1 \times 0.05$ mm^3 dimensions and reshaped it into six different geometries under identical, spatially uniform red-light illumination (Fig. 4). This is achieved by spatially patterning areas with
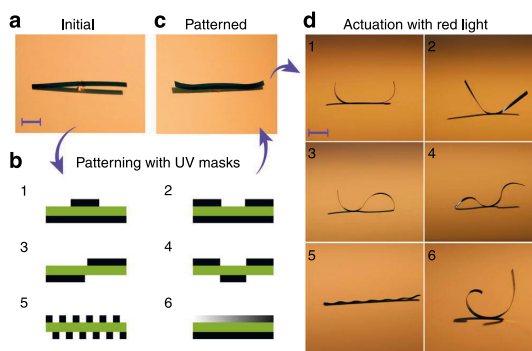

Fig. 4 Reconfigurable shape morphing. **a** Optical image of the actuator at the initial stage. **b** Schematic of mask patterns. **c** Optical image of the actuator after UV exposure using mask no.1. **d** Photothermally induced shape morphing upon red-light illumination after different mask exposure. Scale bars: 5 mm

high cis-isomer content by masked UV exposure from either one side or both sides of the sample (Fig. 4b). As shown in Fig. 4c, the UV preirradiation gives rise to negligible shape change of the strip, even if the cis-content within the actuator is significantly altered (i.e., the photochemically induced stress is "hidden" inside the LCN actuator). Upon red-light illumination, the strip quickly deforms into different geometries determined by the UV pre-irradiation (Fig. 4d, Supplementary Movie 1). We note that all the shapes are obtained within the same strip after retaining the initial flat state by exposure with blue light to convert all the cis-azobenzenes back to the trans-form (see in Methods).

In 2017, we reported on a light-fueled gripping device that can autonomously recognize and manipulate objects based on their reflection/scattering properties[45]. The concept proposed here opens up a strategy to design smart grippers with reconfigurable action. This is demonstrated by the device shown in Fig. 5. The gripper is fabricated by fixing two splay-aligned LCN actuators on a tip of a capillary, with photothermal excitation (red-light irradiation) coming from the back along the capillary direction (see Supplementary Fig. 7). The gripper is designed such that it is open in the dark (Fig. 5a), closes under red-light illumination (Fig. 5b), and retains the original shape when ceasing the irradiation. By such photothermally activated gripping action, the device is able to clamp and hold a 60 mg object, 100 times heavier than the actuator itself. If the device is preirradiated with UV, the gripper deformation is much more pronounced under identical red-light illumination, as shown in Fig. 5c and as expected based on Fig. 3c. In this case, the gripper remains closed even after ceasing the red-light illumination, due to the release of the photochemically induced stress (Fig. 5d). Therefore, synergistic photoactuation allows us to program the gripping device to adapt an operation mode in which the object is gripped, lifted up, and dropped immediately when the energy source is removed (Fig. 5e, also see Supplementary Movie 2), or gripped, lifted up, and held in place even after ceasing the irradiation (Fig. 5f, Supplementary Movie 3). Most importantly, the device can be reconfigured with irradiation with blue light and commanded whether to grip and release or grip and hold, which is a unique ability in LCN photoactuators.

Discussion
The demonstrated reconfigurable photoactuator is unique compared to other dual-responsive liquid crystalline polymer systems reported in the literature[46–48], and to wavelength-selective
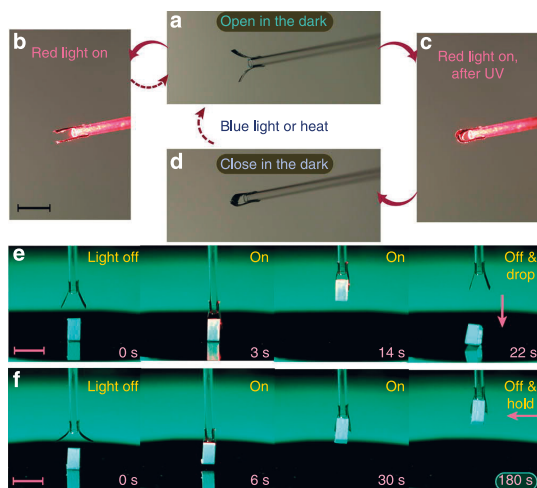
Fig. 5 A reconfigurable micro-gripper. A gripper in its initial, open stage (**a**) closes upon red-light illumination (**b**) and returns back to the original state when turning off the light. After UV exposure, the gripper closes upon red-light illumination (**c**) and maintains the closed state even after ceasing the irradiation (**d**). **e** Series of optical images of the gripper operated in a grip-and-release mode, and **f** the same device reprogrammed to operate in a grip-and-hold mode. Object being lifted up in (**e**, **f**) is 12 mg in weight. All scale bars: 5 mm

carbon-nanotube-based photothermal actuators[17,44]. To the best of our knowledge, our strategy is only one where the photochemical and photothermal stimuli act in concert in order to enhance the overall performance of the system and bring about new, unprecedented capacities. We use photochemistry for reconfigurability and photothermal effect for shape morphing, i.e., both serve their distinct, specific purposes. Even if playing distinct parts, they are inherently integrated, as shown by the actuation speed and deformation amplitude experiments of Fig. 3.

In many cases, quantitative analysis of purely photochemically driven actuation is complicated, due to the fact that it is often accompanied by a certain degree of photoinduced heat generation. We would like to draw attention to the fact that careful characterization and full decoupling of the effects arising from photoisomerization and photothermal heating is necessary for understanding the overall dynamics of photoactuation. In our case, photothermal heating of 18 °C (shown in Fig. 3a) brings about dramatic changes in the photochemical actuation in the LCN material with glass transition temperature at around room temperature (see differential scanning calorimetry measurement in Supplementary Fig. 8). It enhances the actuation speed by a factor of 12 (bending up to 50° takes 2 min upon UV irradiation but only 10 s upon simultaneous UV–red irradiation, see Fig. 3b, d), and the deformation amplitude by a factor of 5 (Fig. 3e). We attribute this to photothermally induced softening of the polymer matrix which allows the bent *cis*-isomers to transfer the deformation from molecular level into deformation of the whole polymer network with higher efficiency. Other researchers have shown that cyclic *trans–cis–trans* isomerization is able to soften the polymeric matrix[49] and enhance the topological actuation in photoresponsive cholesteric coatings[50]. Cyclic isomerization can also bring about significant mass migration of polymer chains, allowing for photoinduced surface patterning on amorphous polymer thin films[51]. We anticipate that the synergistic use of photochemical and photothermal effects and the results

explicated in Fig. 3 can contribute to elaborating the photo-actuation process for many azobenzene-containing polymer networks and elastomers.

The reconfigurability is based on the spatial control over the concentration of *cis*-isomers, thus the stability of the reconfigured state is inherently connected to the *cis*-lifetime of the azobenzene crosslinks. Therefore, the stability of the deformed structure depends on the environmental conditions, being longer in normal room lighting than outdoors under direct sunlight or at elevated temperatures (Supplementary Fig. 9). With the present material composition, the bent film recovers 50% of its original shape within 9 min under laboratory lighting (Supplementary Fig. 9a), revealing the time limit for preserving the reconfigured state. This weakens the sustainability of the reconfigurable robotics, and for instance the gripper shown in Fig. 5f can hold the object only for ca. 5 min after ceasing irradiation. This limitation can be overcome using azobenzenes with long *cis*-lifetime, such as the *ortho*-fluorinated ones demonstrated by Hecht and coworkers[52,53]. Improving the temporal and thermal stability of the reconfigured state is an important next step in our research.

We also emphasize that apart from LCNs, various types of materials exhibit light-induced shape changes, such as hydrogels[7,16], temperature-responsive and shape memory polymers[18,54] functional carbon-nanotube-based bilayers[17], photochromic crystals[55], etc. While chemists and material scientists continuously extend the diversity of materials and shape changes, engineers and micro-roboticists are dedicated to issues such as energy consumption[56] and integration of the photomechanical units as part of active circuits[2]. We note that the physical principles underlying light-driven device/robot realization using different materials are rather similar, as exemplified by, e.g., self-shadowing-induced oscillation[17,57], snapping motion[58,59], and rolling locomotion[17,60], all achieved in both LCNs and bilayer actuators. Keeping this in mind, we believe that the reconfigurability concept proposed herein can also be extended beyond LCNs, and synergies can be sought for by combining different types of light-responsive materials to simultaneously harness the strengths of each.

We have demonstrated a method to achieve reconfigurable actuation by combining photochemical and photothermal responses within a single LCN actuator. We highlight that photochemical actuation can be significantly boosted by photothermal heating, and synergistic use between these two actuation mechanisms can be used to realize reconfigurable shape morphing in the light-actuated LCN structures. We reconfigure a single actuator into six distinct geometries and apply this concept to build a light-fueled gripper which can be programmed to either release an object once irradiation is ceased, or keep it on hold. We anticipate that this facile, easy-to-prepare reconfigurable actuator paves way towards smart micro-robotics with adaptive motion and reprogrammable performance.

Methods
Materials. The LCN actuators are made by photopolymerization of a mixture containing 52 mol% of LC monomer 4-Methoxybenzoic acid 4-(6-acryloyloxyhexyloxy)phenyl ester (Synthon Chemicals), 18 mol% of LC monomer 4[4[6-Acryloxyhex-1-yl)oxyphenyl]carboxybenzonitrile (Synthon Chemicals), 21 mol% of di-acrylate crosslinker 1,4-Bis-[4-(6-acryloyloxyhexyloxy)benzoyloxy]-2-methylbenzene (Synthon Chemicals), 6 mol% of azo crosslinker 4,4′-Bis[9-(acryloyloxy)nonyloxy]azobenzene (Synthon Chemicals), 1.5 mol% of 1,4-Bis(methylamino)anthraquinone (Disperse Blue 14, Sigma Aldrich) and 1.5 mol% of photoinitiator Bis(2,4,6-trimethylbenzoyl)-phenylphosphineoxide (Sigma Aldrich). All molecules were used as received. The monomer mixture was dissolved in dichloromethane and filtered through PTFE syringe filter (Sigma Aldrich, pore size 0.2 μm), after which it was stirred at 80 °C (100 RPM) for 3 h in order to remove the solvent.

Photopolymerization. Glass substrates were cleaned by successive sonication in 2-propanol and acetone baths (20 min each), and dried under the flow of nitrogen gas. For planar alignment, two glass slides were spin coated with 1 wt% water solution of polyvinyl alcohol (PVA, Sigma Aldrich; 4000 RPM, 1 min) and rubbed uni-directionally using a satin cloth. After rubbing, the PVA substrates were blown with high-pressure nitrogen to remove dust particles from the surfaces. For splayed alignment, the glass slides were spin coated with PVA as before and a homeotropic alignment layer (JSR OPTMER, 5000 RPM, 1 min), and baked at 180 °C for 20 min. For cell preparation, two coated substrates were fixed together with UV glue (UVS 91, Norland Products Inc., Cranbury, NJ), using spacer particles (Thermo scientific, 10, 20, or 50 µm) to define the cell thickness. The mixture was then infiltrated into the cell on a heating stage at 90 °C and cooled down to 50 °C with a rate of 3 °C min^{-1}. An LED (Prior Scientific; 420 nm, 11 mW cm^{-2}, 30 min) was used to polymerize the LC mixture. A linear polarizer (Thorlabs, LPVISE100-A, extinction ratio >100) was placed in between the light source and the sample, with orientation perpendicular to the alignment direction in order to minimize the *cis*-isomer concentration induced by the polymerization. The polymerized film together with cross-polarized microscope images are shown in Supplementary Figure 10. The cell was opened, and strip-like LCNs were cut out from the film using a blade.

Characterization. Absorption spectra and isomerization kinetics were measured with a UV–Vis spectrophotometer (Cary 60 UV–Vis, Agilent Technologies) in a 10 µm splay-aligned LCN film. Photoexcitation experiments were conducted using wavelength of 365 nm (Prior Scientific, 18 mW cm^{-2}, 1 min) to trigger *trans–cis* isomerization, and 460 nm (26 mW cm^{-2}, 1 min) for *cis–trans* isomerization. A probe at 385 nm was used to determine the kinetics of *cis*-isomers. A Peltier thermostated cell holder (temperature accuracy ± 0.1 °C) was used to control the sample temperature. Optical images and movies were recorded using a Canon 5D Mark III camera (100 mm lens), and thermal images were recorded with an infrared camera (FLIR T420BX) equipped with a close-up (2×) lens. Cross-polarized microscope images were taken by Zeiss Axio Scope.A1. Differential scanning calorimetry measurement was performed with a Mettler Toledo Star DSC821e instrument, using heating/cooling speeds of 10 °C min^{-1}.

Actuation. A $4 \times 1 \times 0.02$ mm^3 splayed LCN strip was used for testing the photomechanical response upon UV (365 nm, 9 mW cm^{-2}), blue (460 nm, 18 mW cm^{-2}), and red (0–260 mW cm^{-2}) illumination (Prior Scientific). A $25 \times 1 \times 0.05$ mm^3 planar-aligned LCN was used for the reconfigurable shape morphing. UV masks were made by hand-cutting black tape and fixing it on a glass substrate. The sample was sandwiched between two masks (or a mask and a substrate) and exposed to UV light (365 nm, 50 mW cm^{-2}, 5 s). The shape morphing was induced upon red-light illumination (660 nm, ca. 300 mW cm^{-2} for 0–5 s). For erasing the shape change, the samples were exposed to the combination of blue (ca.100 mW cm^{-2}, 460 nm) and red (ca.300 mW cm^{-2}, 660 nm) light for 30 s.

Fabrication of light-fueled gripper. The gripper was made by fixing two pieces of $5 \times 1 \times 0.05$ mm^3 splay-aligned LCN strips onto a tip of a capillary tube using UV glue. Three-dimensional translation stage was used to manually control the position. A laser beam (635 nm, 3 W cm^{-2}, RLTMRL-635-1W-5, Roithner Lasertechnik) illuminated the LCN from the back along the capillary direction as shown in Supplementary Fig. 7. To change the gripper property, i.e., to command it to hold the object, the device was irradiated with UV light (365 nm, 50 mW cm^{-2}, 10 s).

Data analysis. The *cis*-isomer population was calculated from the absorption spectra shown in Supplementary Fig. 3, according to the Beer–Lambert law ($A = \varepsilon \times b \times c$; where A is absorbance, ε is molar absorption coefficient, b is thickness, and c is concentration), and assuming 1% *cis*-fraction at ambient conditions. The lifetime is calculated using a single exponential fitting in the kinetic data. The bending angle is measured by the central angle assuming the bent strip as a perfect arc of a circle.

Data availability

The data that support the findings of this study are available from the corresponding authors upon request.

References

1. Hines, L., Petersen, K., Lum, G. Z. & Sitti, M. Soft actuators for small-scale robotics. *Adv. Mater.* **29**, 1603483 (2017).
2. Rich, S. I., Wood, R. J. & Majidi, C. Untethered soft robotics. *Nat. Electron.* **1**, 102–112 (2018).
3. Palagi, S. & Fischer, P. Bioinspired microrobots. *Nat. Rev. Mater.* **3**, 113–124 (2018).
4. Kim, S., Laschi, C. & Trimmer, B. Soft robotics: a bioinspired evolution in robotics. *Trends Biotechnol.* **31**, 287–294 (2013).
5. Palagi, S. et al. Structured light enables biomimetic swimming and versatile locomotion of photoresponsive soft microrobots. *Nat. Mater.* **15**, 647–653 (2016).
6. Hu, W., Lum, G. Z., Mastrangeli, M. & Sitti, M. Small-scale soft-bodied robot with multimodal locomotion. *Nature* **554**, 81–85 (2018).
7. Zhang, H., Mourran, A. & Möller, M. Dynamic switching of helical microgel ribbons. *Nano Lett.* **17**, 2010–2014 (2017).
8. Li, M.-H., Keller, P., Li, B., Wang, X. & Brunet, M. Light-driven side-on nematic elastomer actuators. *Adv. Mater.* **15**, 569–572 (2003).
9. Lum, G. Z. et al. Shape-programmable magnetic soft matter. *Proc. Natl. Acad. Sci. USA* **113**, E6007–E6015 (2016).
10. Anderson, I. A., Gisby, T. A., McKay, T. G., O'Brien, B. M. & Calius, E. P. Multi-functional dielectric elastomer artificial muscles for soft and smart machines. *J. Appl. Phys.* **112**, 041101 (2012).
11. Seefeldt, B. et al. Spiropyrans as molecular optical switches. *Photochem. Photobiol. Sci.* **9**, 213–220 (2010).
12. Beharry, A. A. & Woolley, G. A. Azobenzene photoswitches for biomolecules. *Chem. Soc. Rev.* **40**, 4422 (2011).
13. Li, Q. (ed.). *Intelligent Stimuli-Responsive Materials. From Well-Defined Nanostructures to Applications* (John Wiley & Sons, Inc., New Jersey, 2013).
14. Liu, Y., Genzer, J. & Dickey, M. D. "2D or not 2D": shape-programming polymer sheets. *Prog. Polym. Sci.* **52**, 79 (2016).
15. Ko, H. & Javey, A. Smart actuators and adhesives for reconfigurable matter. *ACC Chem. Res.* **50**, 691–702 (2017).
16. Takashima, Y. et al. Expansion–contraction of photoresponsive artificial muscle regulated by host–guest interactions. *Nat. Commun.* **3**, 1270 (2012).
17. Zhang, X. et al. Photoactuators and motors based on carbon nanotubes with selective chirality distributions. *Nat. Commun.* **5**, 2983 (2014).
18. Na, J. H. et al. Programming reversibly self-folding origami with micropatterned photo-crosslinkable polymer trilayers. *Adv. Mater.* **27**, 79–85 (2015).
19. White, T. J. & Broer, D. J. Programmable and adaptive mechanics with liquid crystal polymer networks and elastomers. *Nat. Mater.* **14**, 1087–1098 (2015).
20. Ohm, C., Brehmer, M. & Zentel, R. Liquid crystalline elastomers as actuators and sensors. *Adv. Mater.* **22**, 3366–3387 (2010).
21. Yu, Y., Nakano, M. & Ikeda, T. Directed bending of a polymer film by light. *Nature* **425**, 145 (2003).
22. Iamsaard, S. et al. Conversion of light into macroscopic helical motion. *Nat. Chem.* **6**, 229–235 (2014).
23. Ware, T. H., McConney, M. E., Wie, J. J., Tondiglia, V. P. & White, T. J. Voxelated liquid crystal elastomers. *Science* **347**, 982–984 (2015).
24. Yang, R. & Zhao, Y. Non-uniform optical inscription of actuation domains in a liquid crystal polymer of uniaxial orientation: an approach to complex and programmable shape changes. *Angew. Chem. Int. Ed.* **56**, 14202–14206 (2017).
25. Pei, Z. et al. Mouldable liquid-crystalline elastomer actuators with exchangeable covalent bonds. *Nat. Mater.* **13**, 36–41 (2014).
26. Wang, Z., Tian, H., He, Q. & Cai, S. Reprogrammable, reprocessible, and self-healable liquid crystal elastomer with exchangeable disulfide bonds. *ACS Appl. Mater. Interfaces* **9**, 33119–33128 (2017).
27. Ube, T., Kawasaki, K. & Ikeda, T. Photomobile liquid-crystalline elastomers with rearrangeable networks. *Adv. Mater.* **28**, 8212–8217 (2016).
28. McBride, M. K. et al. Photoinduced plasticity in cross-linked liquid crystalline networks. *Adv. Mater.* **29**, 1606509 (2017).
29. Qian, X. et al. Untethered recyclable tubular actuators with versatile locomotion for soft continuum robots. *Adv. Mater.* **30**, 1801103 (2018).
30. Gelebart, A. H., Mulder, D. J., Vantomme, G., Schenning, A. P. H. J. & Broer, D. J. A rewritable, reprogrammable, dual light-responsive polymer actuator. *Angew. Chem. Int. Ed.* **56**, 13436–13439 (2017).
31. De Haan, L. T., Verjans, J. M. N., Broer, D. J., Bastiaansen, C. W. M. & Schenning, A. P. H. J. Humidity-responsive liquid crystalline polymer actuators with an asymmetry in the molecular trigger that bend, fold, and curl. *J. Am. Chem. Soc.* **136**, 10585–10588 (2014).
32. Zeng, H., Wasylczyk, P., Wiersma, D. S. & Priimagi, A. Light robots: bridging the gap between microrobotics and photomechanics in soft materials. *Adv. Mater.* **30**, 1703554 (2018).
33. Ikeda, T., Mamiya, J. I. & Yu, Y. Photomechanics of liquid-crystalline elastomers and other polymers. *Angew. Chem. Int. Ed.* **46**, 506–528 (2007).
34. Bandara, H. M. D. & Burdette, S. C. Photoisomerization in different classes of azobenzene. *Chem. Soc. Rev.* **41**, 1809–1825 (2012).
35. Iamsaard, S. et al. Fluorinated azobenzenes for shape-persistent liquid crystal polymer networks. *Angew Chem. Int. Ed.* **55**, 9908–9912 (2016).
36. Zhao, J., Liu, Y. & Yu, Y. Dual-responsive inverse opal films based on a crosslinked liquid crystal polymer containing azobenzene. *J. Mater. Chem. C* **2**, 10262–10267 (2014).
37. Gelebart, A. H., McBride, M., Schenning, A. P. H. J., Bowman, C. N. & Broer, D. J. Photoresponsive fiber array: toward mimicking the collective motion of cilia for transport applications. *Adv. Funct. Mater.* **26**, 5322–5327 (2016).

38. Nocentini, S., Martella, D., Parmeggiani, C., Zanotto, S. & Wiersma, D. S. Structured optical materials controlled by light. *Adv. Opt. Mater.* **6**, 180016 (2018).

39. Zeng, H. et al. Light-fueled microscopic walkers. *Adv. Mater.* **27**, 3883–3887 (2015).

40. Van Oosten, C. L., Bastiaansen, C. W. M. & Broer, D. J. Printed artificial cilia from liquid-crystal network actuators modularly driven by light. *Nat. Mater.* **8**, 677–682 (2009).

41. Lv, J. A. et al. Photocontrol of fluid slugs in liquid crystal polymer microactuators. *Nature* **537**, 179–184 (2016).

42. White, T. J. et al. A high frequency photodriven polymer oscillator. *Soft Matter* **4**, 1796 (2008).

43. Mol, G. N., Harris, K. D., Bastiaansen, C. W. M. & Broer, D. J. Thermo-mechanical responses of liquid-crystal networks with a splayed molecular organization. *Adv. Funct. Mater.* **15**, 1155–1159 (2005).

44. Wang, T., Torres, D., Fernández, F. E., Wang, C. & Sepúlveda, N. Maximizing the performance of photothermal actuators by combining smart materials with supplementary advantages. *Sci. Adv.* **3**, e1602697 (2017).

45. Wani, O. M., Zeng, H. & Priimagi, A. A light-driven artificial flytrap. *Nat. Commun.* **8**, 15546 (2017).

46. Wang, M., Lin, B. P. & Yang, H. A plant tendril mimic soft actuator with phototunable bending and chiral twisting motion modes. *Nat. Commun.* **7**, 13981 (2016).

47. Lu, X. et al. Liquid-crystalline dynamic networks doped with gold nanorods showing enhanced photocontrol of actuation. *Adv. Mater.* **30**, 1706597 (2018).

48. Cheng, Z., Wang, T., Li, X., Zhang, Y. & Yu, H. NIR-Vis-UV light-responsive actuator films of polymer-dispersed liquid crystal/graphene oxide nanocomposites. *ACS Appl. Mater. Interfaces* **7**, 27494–27501 (2015).

49. Kumar, K., Schenning, A., Broer, D. J. & Liu, D. Regulating the modulus of a chiral liquid crystal polymer network by light. *Soft Matter* **12**, 3196–3201 (2016).

50. Liu, D. & Broer, D. J. New insights into photoactivated volume generation boost surface morphing in liquid crystal coatings. *Nat. Commun.* **6**, 8334 (2015).

51. Mahimwalla, Z. et al. Azobenzene photomechanics: prospects and potential applications. *Polym. Bull.* **69**, 967–1006 (2012).

52. Bléger, D., Schwarz, J., Brouwer, A. M. & Hecht, S. *o*-fluoroazobenzenes as readily synthesized photoswitches offering nearly quantitative two-way isomerization with visible light. *J. Am. Chem. Soc.* **134**, 20597–20600 (2012).

53. Knie, C. et al. Ortho-fluoroazobenzenes: visible light switches with very long-lived Z isomers. *Chem. Eur. J.* **20**, 16492–16501 (2014).

54. Behl, M., Razzaq, M. Y. & Lendlein, A. Multifunctional shape-memory polymers. *Adv. Mater.* **22**, 3388–3410 (2010).

55. Naumov, P., Chizhik, S., Panda, M. K., Nath, N. K. & Boldyreva, E. Mechanically responsive molecular crystals. *Chem. Rev.* **115**, 12440–12490 (2015).

56. Kim, S. J., Kim, O. & Park, M. J. True low-power self-locking soft actuators. *Adv. Mater.* **30**, 1706547 (2018).

57. Gelebart, A. H., Vantomme, G., Meijer, E. W. & Broer, D. J. Mastering the photothermal effect in liquid crystal networks: a general approach for self-sustained mechanical oscillators. *Adv. Mater.* **29**, 1606712 (2017).

58. Hu, Y. et al. Electrically and sunlight-driven actuator with versatile biomimetic motions based on rolled carbon nanotube bilayer composite. *Adv. Funct. Mater.* **27**, 1704388 (2017).

59. Aßhoff, A. S. et al. High-power actuation from molecular photoswitches in enantiomerically paired soft springs. *Angew. Chem. Int. Ed.* **56**, 3261 (2017).

60. Lu, X., Guo, S., Tong, X., Xia, H. & Zhao, Y. Tunable photocontrolled motions using stored strain energy in malleable azobenzene liquid crystalline polymer actuators. *Adv. Mater.* **29**, 1606467 (2017).

Acknowledgements

Author contributions

H.Z. and A.P. conceived the project; M.L. and H.Z. performed experiments. All authors contributed in writing the manuscript.

Additional information

Supplementary Information accompanies this paper at https://doi.org/10.1038/s41467-018-06647-7.

Competing interests: The authors declare no competing interests.

Reprints and permission information is available online at http://npg.nature.com/reprintsandpermissions/

Publisher's note: Springer Nature remains neutral with regard to jurisdictional claims in published maps and institutional affiliations.

PUBLICATION
IV

Tunable Photomechanics in Diarylethene-Driven Liquid Crystal Network Actuators

Lahikainen, M.; Zeng, H.; Kuntze, K.; Helantera, S.; Hecht, S.; Priimagi, A.

Research Article

Tunable Photomechanics in Diarylethene-Driven Liquid Crystal Network Actuators

Markus Lahikainen, Kim Kuntze, Hao Zeng,* Seidi Helantera, Stefan Hecht, and Arri Priimagi*

Cite This: *ACS Appl. Mater. Interfaces* 2020, 12, 47939−47947

Read Online

ACCESS | Metrics & More | Article Recommendations | Supporting Information

ABSTRACT: The response of soft actuators made of stimuli-responsive materials can be phenomenologically described by a stimulus-deformation curve, depicting the controllability and sensitivity of the actuator system. Manipulating such stimulus-deformation curve allows fabricating soft microrobots with reconfigurable actuation behavior, which is not easily achievable using conventional materials. Here, we report a light-driven actuator based on a liquid crystal polymer network containing diarylethene (DAE) photoswitches as cross-links, in which the stimulus-deformation curve under visible-light illumination is tuned with UV light. The tuning is brought about by the reversible electrocyclization of the DAE units. Because of the excellent thermal stability of the visible-absorbing closed-form DAEs, the absorbance of the actuator can be optically fixed to a desired value, which in turn dictates the efficiency of photothermally induced deformation. We employ the controllability in devising a logical AND gate with macroscopic output, i.e., an actuator that bends negligibly under UV or visible light irradiation, but with profound shape change when addressed to both simultaneously. The results provide design tools for reconfigurable microrobotics and polymer-based logic gating.

KEYWORDS: *liquid crystal polymer network, photoactuation, diarylethene, photoswitch, logic gate, reconfiguration*
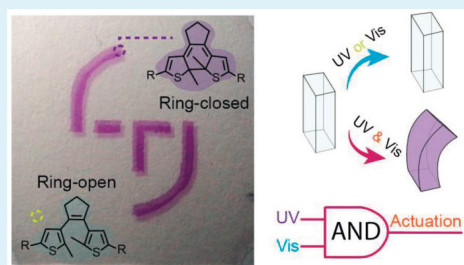
■ INTRODUCTION

Soft robotics is a research frontier dedicated to combine the flexibility of soft materials with the accurate control inherent to conventional rigid-bodied robots, anticipated to provide technological breakthroughs for human-friendly interfaces, controlled locomotion, and bioinspired robotic adaptation.[1] To apply the soft robots in single-cell manipulation, drug delivery/release, or microfluidics, their size has to be miniaturized.[2] For this, stimuli-responsive materials are often adopted,[3,4] allowing to activate robotic movements wirelessly using heat, magnetic or electric fields, humidity, or light.[5−9] Among the different classes of stimuli-responsive materials, light-driven liquid crystal polymer networks (LCNs) stand out due to their large shape-changes, versatile control over deformation (e.g., bending, coiling, and twisting), easy scalability from centimeter down to micrometer size, and high spatial and temporal resolution of the light activation.[10,11] Conventionally, the light-fueled actuation of LCNs is triggered by photoswitchable molecules incorporated into the polymer network.[12,13] Upon photon absorption, the photoswitches undergo reversible shape changes and induce disorder into the initially ordered polymer network, yielding photochemically induced macroscopic actuation.[14,15] An attractive alternative to trigger actuation is the use of the photothermal effect, i.e., the molecular disorder created by heat released during non-radiative relaxation of photoexcited moieties.[16−19] In the past

decade, many photothermally fueled LCN robotic movements have been demonstrated, including 3D kirigami/origami devices,[20] light steering motion by walking[21] and swimming,[22] object manipulation through gripping,[23,24] and self-sustainable oscillation.[25−27]

The inputs required by an operational actuator are control signal and powering source. For instance, the actuation force or displacement of an electromechanical actuator is controlled through current/voltage input.[28] In light-driven LCN robotics, the actuator performance is dictated by a complex interplay between molecular-level events (e.g., light absorption) and macroscopic properties of the polymer network (elastic modulus and alignment anisotropy).[29,30] For photothermal actuators, the performance can be described by an intensity-deformation curve, as schematically illustrated in Figure 1a. Increasing the illumination intensity increases the amount of deformation of the actuator, which in combination with predesigned shape morphing provides accurate light controllability over the robotic movements.[31] Typically, the intensity-
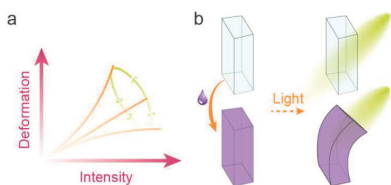
Figure 1. Concept of tunable photomechanics. (a) Performance of a photothermal actuator is described with a light intensity-deformation curve, and modification of the curve profile with an external stimulus allows reconfiguring the light response of the actuator. (b) Schematics of a reprogrammable photothermal actuator that shows minimal deformation initially and exhibits profound shape changes after color change (increased absorption).

deformation curve is fixed during the fabrication process; that is, a conventional photoactuator is responsive yet not reconfigurable. A possibility to tune the light response after fabrication allows reprogramming the performance of the actuator at will, paving way toward design strategies for reconfigurable and adaptive soft robotics.[32]

To manipulate the intensity-deformation curve (i.e., light controllability) and to obtain distinct actuation behavior upon identical light illumination conditions, recent studies have relied on chemical reconfiguration approaches such as the use of dynamic chemical bonds to rearrange the connectivity between polymer chains.[33−37] Only few studies have concentrated on obtaining reconfigurable photoactuation by purely optical methods. The power of optical methods is that in principle they can provide a noncontact reconfigurability platform. However, thus far they lack reversibility over multiple cycles of reconfiguration. For instance, optical de-cross-linking can be used to locally pattern the actuation across an LCN

film, but the obtained effect cannot be easily erased and patterned again.[38] While photochemical excitation allows to reversibly program the actuation behavior, subsequent photo-thermal actuation resembles the shape-memory effect and only yields few cycles of robotic actuation.[39]

To devise a photothermally driven actuator with light responsivity that can be reversibly tuned, control over light absorption of the photoactuator is the key parameter. By tuning the absorbance, one controls the photosensitivity, i.e., the minimum dose of input energy required for a desired shape change, as illustrated in Figure 1b. Reversible optical modification of absorption can most conveniently be achieved via photochromic molecules.[40,41] The challenge in harnessing photochromic molecules to control photothermal actuation lies in the fact that for the majority of the thus far exploited photochromic moieties—azobenzene[42,43] being the most frequently used—only one of the two states is thermally stable. The lack of bistability leads to inherent thermal relaxation from the metastable to the thermodynamically stable state and thus a continuously changing intensity-deformation relationship. While thermally stable photochromic molecules do exist and *ortho*-fluorinated azobenzenes[44] and hydrozones[45] have been used for bistable photoactuation in LCNs, their absorption changes upon isomerization are often limited. For instance, with an *ortho*-fluorinated azobenzene the absorbance in the visible range may increase upon UV illumination by about 50%,[44] which is insufficient for efficient tuning of the visible-light controllability through changes in material absorption.

Here, we introduce photochromic diarylethene (DAE) cross-links as effective tools toward optically reconfigurable light controllability in photothermal LCN actuators. The DAE units undergo ring-closing and ring-opening via a 6π electrocyclization when illuminated with UV (365 nm) and
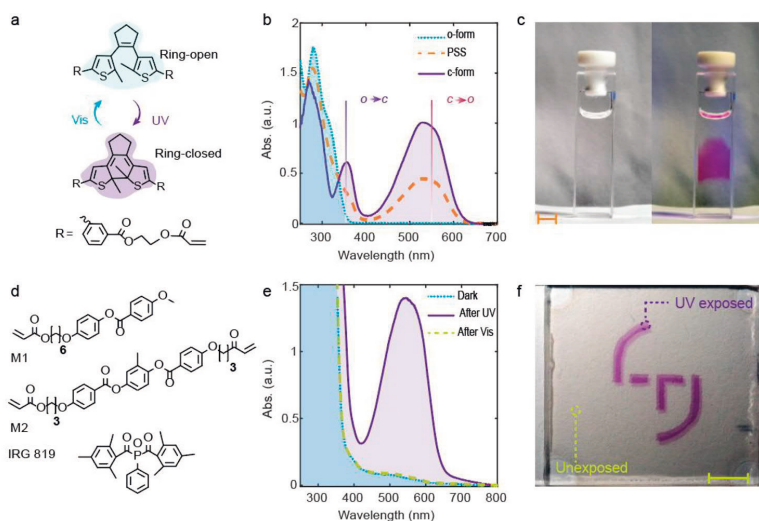

Figure 2. Diarylethene photoswitching. (a) Chemical structures of the ring-open and ring-closed forms of the DAE cross-linker. (b) UV−vis spectra of the DAE cross-linker in a 50 μM acetonitrile solution. (c) Photographs of DAE-containing acetonitrile solution before (left) and after (right) UV illumination. (d) Liquid crystal monomers and photoinitiator used to form LCN soft actuator. (e) UV−vis spectra of the DAE-LCN film before and after electrocyclization. UV: 365 nm, 50 mW cm^{-2}; vis.: 550 nm, 285 mW cm^{-2}. (f) Photograph of the DAE-LCN film after masked exposure to UV light. Scale bars: 5 mm.

visible light (550 nm), respectively, providing a convenient way to selectively address each switching state, i.e., ring-open and ring-closed DAE. Due to the outstanding thermal stability of the ring-closed DAE, the absorbance around 550 nm can be fixed to any value between 0.05 and 1.4 in a 20 μm LCN actuator strip. Hence, we make use of a control signal (UV irradiation) to tune the sensitivity of actuation to the powering source (visible-light irradiation). The DAE-based LCN (DAE-LCN) actuator exhibits AND gate logics: deformation is negligible when exposed only to UV or visible irradiation but pronounced shape changes are observed when exposed to both simultaneously.

■ **RESULTS**

Diarylethene Photoswitch. The DAE photoswitch used as the light-absorbing unit in the present study is shown in Figure 2a. It undergoes reversible open → closed (*o–c*) as well as closed → open (*c–o*) interconversion when illuminated with UV and visible light, respectively. As shown in Figure 2b, the open form absorbs strongly in the UV region while the closed form exhibits a band in the visible, centered at $\lambda = 540$ nm, leading to a significant color change from transparent to purple under UV irradiation (Figure 2c). The electrocyclization was studied with ^{1}H NMR, which under 365 nm irradiation yielded a photostationary state (PSS) consisting ca. 56% of the closed-form DAE, the quantum yield (QY) for the *o–c* conversion being $\Phi_{o\rightarrow c} = 0.54$. By irradiating the solution with 550 nm, *c–o* electrocyclization occurs and the process can be driven to completion, yet with a very low QY of $\Phi_{c\rightarrow o} = 0.009$. The low QY of the ring-opening accompared to the ring-closure is expected,[46] and in fact works for our benefit for maintaining the visible light actuation, as will be discussed later. Further details on the QY determination are given in the Supporting Information.

The core of the DAE molecules was extended with aryl groups, which serve to extend the conjugation and hence shift the absorption of the open as well as closed forms to higher wavelengths and enhance the rigidity of the DAE molecules, rendering them compatible with the polymerizable liquid crystal mixture constituting the actuator (Figure 2d).[47] The two acrylate groups attached to the DAE ensure their covalent attachment to the polymer network during photopolymerization. Details of the DAE synthesis and LCN sample preparation procedure are given in the Supporting Information and the Experimental Methods section, respectively. The electrocyclization of DAE is well preserved in the LCN: UV illumination enhances the absorption in the visible range (Figure 2e) and colorizes the exposed area in purple (Figure 2f). No photodegradation was observed for at least ten cycles of UV/visible irradiation (Figure S1). More details on the light-induced spectral changes and their kinetics in the LCN film are given in Figure S2. The polarized optical micrographs (Figure S3) reveal high homogeneity of the LCN, indicating no disruption of liquid crystalline alignment after incorporating the DAE into the network.

Spectral Stability. The temporal stability of the closed-form, visible-absorbing DAE, was investigated by monitoring the absorbance at 550 nm from a 10 μm thick LCN film containing 5 mol % of DAE at different temperatures (Figures 3a and S4). The half-life was estimated to be over 400 days at room temperature, which is 3 orders of magnitude longer than the *cis*-lifetime of typical azobenzene cross-linkers used in LCNs (Figure S5). The thermal stability decreases at elevated
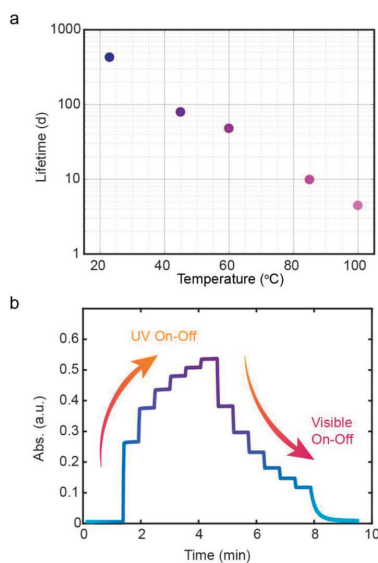

Figure 3. Spectral stability. (a) Thermal lifetime of the ring-closed DAE at different temperatures, measured for a 10 μm DAE-LCN film. (b) Stepwise change of absorbance (at 550 nm) in the DAE-LCN film by sequential irradiation with UV and visible light. UV: 365 nm, 120 mW cm^{-2}, 2 s; vis.: 550 nm, 300 mW cm^{-2}, 2 s.

temperatures, but even at 100 °C, the lifetime of the closed form exceeds 4 days (Figure 3a). Hence, the DAE-based LCN can be considered as a bistable system whose spectral properties can be purely controlled via optical excitations. This allows the absorbance to be fixed to a desired level, as demonstrated in Figure 3b where the LCN was periodically illuminated with UV irradiation, yielding a stepwise increase in the absorbance at 550 nm, whereas subsequent illumination at this wavelength allows controlled decrease in the absorbance in a similar stair-like fashion. This feature is not only useful for photomechanical actuation, but potentially also for applications in tunable photonics.[48]

Light-Tunable Photomechanics. For the photomechanical actuation studies, we fabricated a DAE-LCN actuator with $3 \times 0.5 \times 0.02$ mm^3 dimensions and 90° twisted molecular alignment. A tip-end bending angle is used to quantify the mechanical response under different irradiation conditions, as shown in the inset of Figure 4a. The bending is due to anisotropic thermal expansion within the strip, dictated by the molecular alignment and independent from the incident light direction.[49] Such bending occurs within the temperature range much below the nematic−isotropic phase transition of the LCN material, which is observed above 150 °C (Figure S6). Different molecular alignment or cutting direction would lead to different shape morphing such as twisting, coiling or contraction.[50] Bending-type deformation was chosen because it is easy to characterize by simply measuring the bending angle under different illumination conditions. We note also that the initial state of the actuator is bent, which is due to residual stress in the LCN generated during photopolymerization at elevated temperature.[51] Further details on the actuator fabrication are given in Experimental Methods, and a
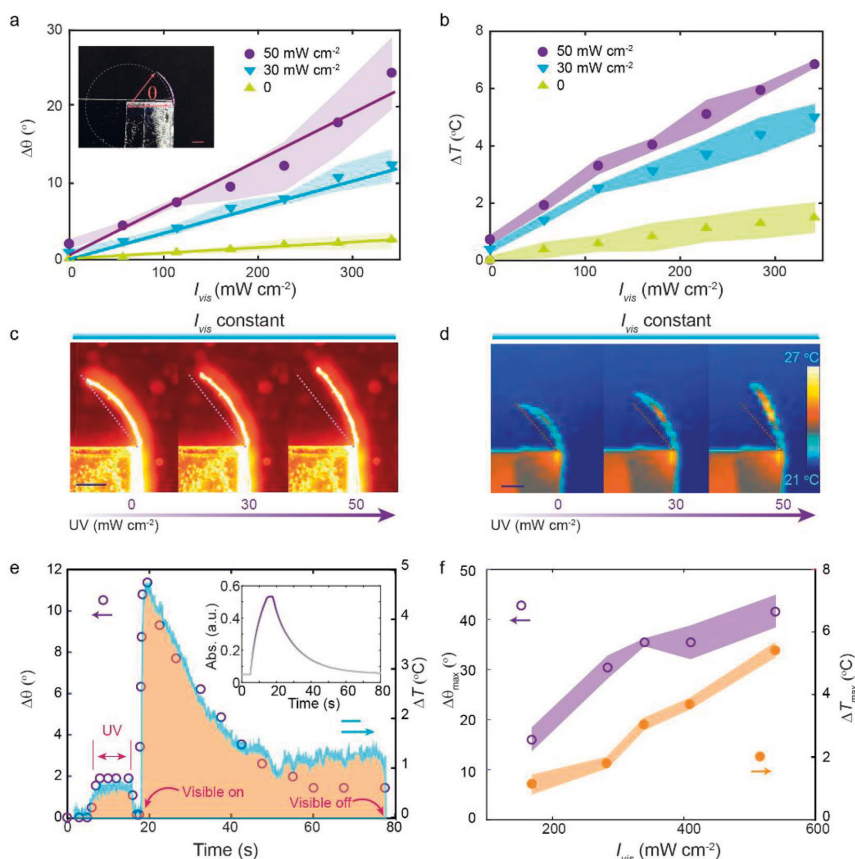
Figure 4. Light-tunable photomechanics. (a) Bending angle of the DAE-LCN strip upon irradiation with UV and visible light with different intensities. The sensitivity of the actuator to visible light (550 nm) is estimated from the linear fit to the intensity-deformation (bending) curve. Inset: optical image of the bending strip and indication of the strip bending angle for actuation measurements. (b) Temperature change of the actuator upon irradiation with UV and visible light with different intensities. (c and d) Optical and thermal images of the strip under 285 mW cm^{-2} visible-light illumination using UV exposure of different intensities. (e) Bending angle (purple dots) and temperature change (blue line) of the strip under subsequent illumination with UV (365 nm, 50 mW cm^{-2}, 10 s) and visible (550 nm, 285 mW cm^{-2}) light. Inset shows the corresponding absorbance changes of the strip. (f) Maximum bending angle (purple), and temperature change (orange) induced by different visible-light intensities after an identical UV pre-exposure (365 nm, 50 mW cm^{-2}, 10 s). Error bars in panels a, b, and f indicate standard deviation of $n = 3$ measurements.

schematic drawing of the characterization setup is shown in Figure S7.

The light sensitivity (absorbance) of the DAE-LCN actuator can be controlled by exposure with UV and visible light. As $\Phi_{o\rightarrow c} \gg \Phi_{c\rightarrow o}$, the PSS is rich of ring-closed DAE when applying UV and visible light simultaneously, and visible-light absorption is retained even under relatively strong visible excitation (Figure S2c,d). The intensity-deformation curves under different UV doses are shown in Figure 4a. Without using UV light, the actuator bends moderately under 550 nm, with sensitivity of 7.1° per W cm^{-2} (Figure 4b, green). The small deformation is due to small absorption ($A \approx 0.05$) of the ring-open DAE at 550 nm (Figure 2e). Even a small dose of UV significantly enhances the visible-light absorption and as a result, the deformation of the strip is boosted, the efficiency being 34.1° per W cm^{-2} and 62° per W cm^{-2} using UV

exposure of 30 mW cm^{-2} (Figure 4a, blue) and 50 mW cm^{-2} (Figure 4a, purple), respectively. We emphasize that the deformation under visible-light irradiation is due to the photothermal effect, driven by the closed-form DAE absorbing the photons, transferring the photon energy to heat, and subsequently triggering the actuation of the LCN. The photothermally induced temperature increase is shown in Figure 4b and the optical and thermal camera images of the actuator in Figure 4c,d.

We note that UV irradiation alone induces neither photothermal nor photochemical actuation. For example, UV exposure of 50 mW·cm^{-2} brings only 2° bending and <1 °C temperature elevation. This is explained by the high $\Phi_{o\rightarrow c}$ driving the o−c electrocyclization rather than converting light energy to heat. The absence of photochemical actuation (see Figure S8), different from the diarylethene-based photo-

chemical actuator reported by the Ikeda group,[52] is attributed to negligible shape change between the open-form and closed-form DAE[53] and to moderate concentration (5 mol %) of the DAE units. Different to many azobenzene-containing LCNs,[54−56] the Young's modulus of the DAE-LCN (~1.3 GPa at room temperature) was not affected by the electro-cyclization and the stress—strain behavior remains unchanged before and after UV illumination (Figure S9). Hence, in our actuator UV light acts as the "control signal" to modify the sensitivity of the actuator, while visible light takes the role of the "power source" that initiates the deformation. The mechanical response upon heating the actuator in a water bath (Figure S10a) is stable, as expected based on the thermosensitive nature of LCNs. Upon photothermal heating, the sample deformation reduces slightly over a time span of 60 min (Figure S10b). This may be due to slight degradation of diarylethene units upon moderate-intensity UV illumination (50 mW cm^{-2}).

When the UV and visible light are not applied simultaneously, the actuation is unsteady. Figure 4e shows the bending of the DAE-LCN strip upon sequential UV and visible irradiation. First, UV irradiation (10 s, 50 mW cm^{-2}) is used to raise the absorbance of the LCN from 0.05 to 0.5 (inset of Figure 4e). Then, the UV irradiation is ceased and visible light (550 nm, 285 mW cm^{-2}) is impinged on the strip, which quickly reaches the maximum bending angle (11° bending within 2 s) and then gradually retains the original shape. The photothermally induced deformation is driven by heat equilibrium, and the kinetics (Figure S11) is dictated by the heat capacity of the material. The extent of bending depends on the excitation power and the corresponding photoinduced temperature increase (Figures 4f and S12). The subsequent relaxation is due to ring-opening of the DAE cross-linker moieties upon visible-light illumination, which constantly reduces the absorption at 550 nm, thus gradually decreasing the photoinduced heating (Figure 4e, blue) and deformation. Exposure to visible-light illumination in the absence of UV leads to gradually decreasing actuation (Figure S13). Herein, pronounced differences between simultaneous and sequential UV—visible excitation can be observed. Upon simultaneous illumination, the population of the o- and c-forms of DAE reach an equilibrium, which stabilizes the actuation to a certain level (Figures 4a and S2d). Upon sequential illumination, the drop of absorption caused by visible-light excitation leads to continuous decrease in deformation (Figure 4e). We would like to note that rather than being a drawback, the dual wavelength dependence is a characteristic of the DAE-based LCN actuator which, as shown next, enables a proof-of-principle application of logical gating in photoactuation.

AND-Gate Photoactuation. Figure 5a shows the photo-induced bending under simultaneous UV (0 to 60 mW·cm^{-2}) and visible-light (0 to 342 mW·cm^{-2}) illumination. When the intensity of either of the irradiation sources is increased, the bending is boosted. On the other hand, if either of the irradiation sources is removed, the bending is negligible. Such behavior resembles the AND-gate logic, where an output signal is provided only when both input signals are applied simultaneously. In our notation the two light sources act as the input signals, while the deformation serves as the output. The AND logical table can be constructed as follows (Figure 5b): (1) If no light is applied, the DAE-LCN remains transparent and no heat is generated, hence no actuation; (2) when only UV light is used, the DAE-LCN becomes absorbing
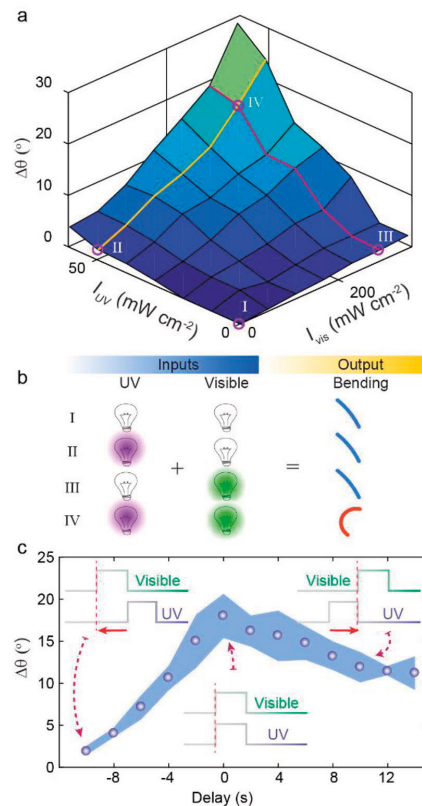

Figure 5. AND-gate photoactuation. (a) Bending angle of the DAE-LCN as a function of UV and visible light intensities. The numbers indicate the different gating status shown in panel b. (b) Logic table of the AND-gate photoactuator, the two inputs being the UV and Vis irradiation and the output being the bending of the strip. (c) The maximum bending of the strip upon changing the delay between UV and visible exposures. The error bar indicates standard deviation of n = 3 measurements.

but no photothermal heating takes place due to the lack of visible-light irradiation, hence no actuation; (3) if only visible light is used, the DAE-LCN remains transparent, hence no actuation (or to be more precise, only very minor actuation is observed); (4) by applying both light inputs simultaneously, the AND-gate is activated and the DAE-LCN deforms.

The bending angle of the AND-gate photoactuator is dictated by the absorbance and resultant photoinduced temperature increase (Figure S14a,b). If the visible-light intensity is kept constant (red line in Figure 5a), an increase in the UV intensity increases the population of closed-form DAE in the PSS, hence boosting the actuation (Figure S14c). By varying the visible-light intensity under constant UV illumination (yellow line in Figure 5a), the photothermal heating is boosted but the absorption of the film decreases as the conversion from the ring-closed to ring-open DAE is enhanced (Figure S14d). We also investigated the dependence of the AND gate actuation on the timing of the two inputs by applying UV light (10 s, 50 mW cm^{-2}) onto the DAE-LCN

and varying the time delay between the UV (10 s, 285 mW cm^{-2}) and visible inputs. The bending angles are recorded instantly after ceasing the visible light, and the results are plotted in Figure 5c. When the visible light precedes the UV input, only minimal actuation is observed as the sample is transparent and cannot absorb light energy. Deformation starts to appear when the two signals overlap, reaching the maximum when there is no delay between the two inputs. When visible light succeeds the UV illumination, the deformation decreases as the ring-opening reaction reduces the absorbance of the LCN in the absence of UV irradiation. When there is no overlap between the signals, the deformation persists as the UV-induced absorption remains due to the stability of closed-form DAE (Figure 3a). These dynamical responses to sequential illuminations could in the future provide a time-wise programming strategy for polymer-based logical circuits.

■ DISCUSSION

The light-tunable photoactuation presented relies on the photochromic properties of the DAE photoswitch, providing a unique linkage between two light stimuli: UV light is used for controlling the sensitivity (absorption) of the actuator in the visible range whereas visible light is driving shape deformation. Modifying the light absorption of the actuator after polymerization enables reconfigurable actuation where photothermal actuation strength in response to visible irradiation can be tuned. While many photochromic molecules have been used in shape-shifting LCNs,[57−61] they fall short to combine properties provided by the DAE, i.e., excellent thermal stability, large spectral separation of the isomers and thus significant absorption changes upon illumination, and low quantum yield of light-induced back isomerization to the thermodynamically stable state. This unique combination allows us to devise a logical-gate photoactuator using a single photochromic compound only. In addition, please note that the encoding of logical responsiveness can be processed through mask exposure on a 2D material sheet, which may bring opportunities in kirigami/origami-type devices with complex shape-morphing.[34,62]

We highlight once more that, in our system, DAE is used to invoke photothermal actuation. To achieve bistable, photochemically induced actuation, larger concentration of DAE in the LCN should be used, as has been demonstrated earlier.[52] Another versatile strategy for light-induced bistable actuation with DAE is based on single crystals, in which case shape deformation results from the changes in crystal packing caused by electrocyclization.[63,64] However, the AND-gate operation is possible in neither photochemically driven DAE-containing networks nor DAE crystals.

Logic gates and circuits are basic tools in hard-bodied, electronically driven rigid robots. Yet incorporating similar logical operation principles into soft robots is a challenge due to the mismatch between conventional rigid electronic components and compliant bodies.[31] Recently, different logic circuits have been incorporated into soft pneumatic systems leading to complex robotic movement.[65,66] However, the research on photomechanical logic gate -type operations are mostly limited to sol−gel transition of hydrogels,[67−69] where additional inputs (temperature, pH, and electric field) are often needed, increasing the complexity of these systems. The presented fully optically controlled AND-gate photoactuator is unique, and there are multitude of possibilities to extend our concept to other types of logic gates. Future studies may also

involve integration between different logic-gate photoactuators to build up polymer-based robots showing more sophisticated behavior than what can be achieved with a single logic-gate photoactuator. This may yield soft robots with automated task execution, taking action only when a combination of stimuli is met, making decisions through the designed logic circuitry. We anticipate that the paradigm of logic gates in the context of photoactuation may broaden the perspective of soft micro-robotics and intelligent microdevices.

■ CONCLUSIONS

We have devised a photothermally driven, diarylethene-based liquid crystal network photoactuator. The exceptional thermal stability of the closed-form diarylethene allows the visible-light absorbance of the actuator to be optically fixed to a desired value via suitable dose of UV irradiation, which acts as a control signal. This, in turn, enables all-optical control over the macroscopic deformation in response to visible light, which acts as the power source for the actuator. The diarylethene-based photoactuator allowed us to devise an AND logical gate with two optical inputs (UV and visible light) and a mechanical output (macroscopic bending). The photomechanical system presented gives new insights to set soft matter in motion via interplay between photochemical and photothermal effects, striving photoactuation toward logical gating and, in the longer term, even logical circuitry. We believe that such intelligent photoactuators may have a variety of applications in soft robotics, photonics and optoelectronics.

■ MATERIALS AND METHODS

LCN Monomer Mixture Preparation. The LCNs were made by photopolymerization of a mixture containing 72.5 mol % of LC monomer 4-methoxybenzoic acid 4-(6-acryloylox-yhexyloxy)phenyl ester (M1, Synthon Chemicals), 21 mol % of LC cross-linker 1,4-bis-[4-(3-acryloyloxypropyloxy)benzoyloxy]-2-methylbenzene (M2, Synthon chemicals), 5 mol % of diaylethene cross-linker (DAE), and 1.5 mol % of photoinitiator bis(2,4,6-trimethylbenzoyl)-phenylphosphineoxide (IRG 819, Sigma-Aldrich). DAE was synthesized in house (see the synthesis route in the Supporting Information). All other molecules were used as received. The monomer mixture was dissolved in dichloromethane and filtered through PTFE syringe filter (pore size 0.2 μm, Sigma-Aldrich). Finally, the solvent was evaporated at 80 °C for 2 h. The isotropic-to-nematic phase transition temperature of the mixture was ca. 47 °C, as determined with a polarized optical microscope (Zeiss Axio Scope.A1).

Photopolymerization. Glass substrates were cleaned by sonication in acetone and 2-propanol baths, 20 min each. The glass slides were spin coated with 1 wt % water solution of poly(vinyl alcohol) (PVA, Sigma-Aldrich; 4000 rpm, 1 min). Two glass slides were rubbed unidirectionally using satin cloth. Before and after rubbing, the coated glass slides were blown with high-pressure nitrogen gas to remove dust particles. The cells were glued from two glass slides with UV glue (UVS 91, Norland Products Inc., Cranbury, N) mixed with spacer particles (Thermo scientific) to define the cell thickness. The rubbing directions of the alignment layers on the glass slides were aligned to be parallel to form planar LC alignment or perpendicular to form 90° twisted alignment. The mixture was infiltrated into the cell on a heating stage at 70 °C (isotropic) and cooled down to 30 °C (nematic) with a rate of 2 °C min^{-1}. The sample was stabilized for 15 min before photopolymerization by using 11 mW cm^{-2} blue LED (420 nm, LED, Thorlabs, 30 min). After photopolymerization the temperature was elevated to 100 °C and the sample was illuminated with 550 nm light (20 mW cm^{-2} for 5 min), in order to convert the majority of DAE molecules to the ring-open form. The cell was opened, and strip-like LCNs were cut from the film using a blade. The fraction of unreacted monomers was ca. 2.5 wt %, as measured by

weighting the photopolymerized DAE-LCN sample before and after soaking in toluene for 5 min.

Characterization. Absorption spectra and isomerization kinetics were measured in a UV–vis spectrophotometer (Cary 60 UV–vis, Agilent Technologies) equipped with a Peltier-thermostated cell holder for temperature control (accuracy 0.1 °C). The 50 μM DAE-acetonitrile sample was measured in a 1 cm quartz cuvette, while the solid-state sample was a 10 μm thick film with planar alignment or a 20 μm thick film with 90° twisted alignment. Cross-polarized microscope images were taken with Zeiss Axio Scope.A1. An LCN strip with dimensions of $3 \times 0.5 \times 0.02$ mm^3 (90° twisted alignment) was used for studying the photomechanical response upon UV (365 nm) and visible (550 nm) illumination (Prior Scientific multiple LED light source). The light sources used were coupled into a liquid light guide equipped with a collimator lens before illuminating the sample. The intensities were measured in front of the sample position. Photographs and movies were recorded using a Canon 5D Mark III camera with a 100 mm objective lens, and thermal images were taken with an infrared camera (FLIR T420BX) equipped with a close-up (2×) lens. Stress–strain curves were determined by a homemade tensile tester in a 50 μm thick planar film with stretching speed of 0.1 mm s^{-1} and stretching direction in parallel with the LC director.

■ ASSOCIATED CONTENT

Supporting Information

The Supporting Information is available free of charge at https://pubs.acs.org/doi/10.1021/acsami.0c12735.

Synthesis protocol of DAE cross-linker, photokinetic studies of DAE cross-linker, additional UV–vis spectra and actuation data, and cross polarized optical micrographs (PDF)

■ AUTHOR INFORMATION

Corresponding Authors

Arri Priimagi — *Smart Photonic Materials, Faculty of Engineering and Natural Sciences, Tampere University, FI-33101 Tampere, Finland;* ● orcid.org/0000-0002-5945-9671; Email: arri.priimagi@tuni.fi

Hao Zeng — *Smart Photonic Materials, Faculty of Engineering and Natural Sciences, Tampere University, FI-33101 Tampere, Finland;* ● orcid.org/0000-0002-9150-214X; Email: hao.zeng@tuni.fi

Authors

Markus Lahikainen — *Smart Photonic Materials, Faculty of Engineering and Natural Sciences, Tampere University, FI-33101 Tampere, Finland;* ● orcid.org/0000-0002-4891-5352

Kim Kuntze — *Smart Photonic Materials, Faculty of Engineering and Natural Sciences, Tampere University, FI-33101 Tampere, Finland*

Seidi Helantera — *Smart Photonic Materials, Faculty of Engineering and Natural Sciences, Tampere University, FI-33101 Tampere, Finland*

Stefan Hecht — *Department of Chemistry and IRIS Adlershof, Humboldt-Universität zu Berlin, 12489 Berlin, Germany; DWI-Leibniz Institute for Interactive Materials, 52074 Aachen, Germany; Institute of Technical and Macromolecular Chemistry, RWTH Aachen University, 52074 Aachen, Germany;* ● orcid.org/0000-0002-6124-0222

Complete contact information is available at:
https://pubs.acs.org/10.1021/acsami.0c12735

Author Contributions

A.P., St.H., and H.Z. conceived the project. M.L. carried out experiments with help of Se.H. and K.K., under supervision of H.Z. and A.P. K.K. synthesized the diarylethene molecule under supervision of St.H. M.L., H.Z., and A.P. wrote the manuscript with contributions from all authors. All authors have given approval to the final version of the manuscript.

Notes

The authors declare no competing financial interest.

■ ACKNOWLEDGMENTS

■ REFERENCES

(1) Rus, D.; Tolley, M. T. Design, Fabrication and Control of Soft Robots. *Nature* **2015**, *521*, 467−475.

(2) Nelson, B. J.; Kaliakatsos, I. K.; Abbott, J. J. Microrobots for Minimally Invasive Medicine. *Annu. Rev. Biomed. Eng.* **2010**, *12*, 55−85.

(3) McCracken, J. M.; Donovan, B. R.; White, T. J. Materials as Machines. *Adv. Mater.* **2020**, *32*, 1906564.

(4) Hines, L.; Petersen, K.; Lum, G. Z.; Sitti, M. Soft Actuators for Small-Scale Robotics. *Adv. Mater.* **2017**, *29*, 1603483.

(5) Tottori, S.; Zhang, L.; Qiu, F.; Krawczyk, K. K.; Franco-Obregon, A.; Nelson, B. J. Magnetic Helical Micromachines: Fabrication, Controlled Swimming, and Cargo Transport. *Adv. Mater.* **2012**, *24*, 811−816.

(6) Nocentini, S.; Parmeggiani, C.; Martella, D.; Wiersma, D. S. Optically Driven Soft Micro Robotics. *Adv. Opt. Mater.* **2018**, *6*, 1800207.

(7) He, Q.; Wang, Z.; Wang, Y.; Minori, A.; Tolley, M. T.; Cai, S. Electrically Controlled Liquid Crystal Elastomer-Based Soft Tubular Actuator with Multimodal Actuation. *Sci. Adv.* **2019**, *5*, No. eaax5746.

(8) Davidson, Z. S.; Shahsavan, H.; Aghakhani, A.; Guo, Y.; Hines, L.; Xia, Y.; Yang, S.; Sitti, M. Monolithic Shape-Programmable Dielectric Liquid Crystal Elastomer Actuators. *Sci. Adv.* **2019**, *5*, No. eaay0855.

(9) Chen, X.; Goodnight, D.; Gao, Z.; Cavusoglu, A. H.; Sabharwal, N.; Delay, M.; Driks, A.; Sahin, O. Scaling up Nanoscale Water-Driven Energy Conversion into Evaporation-Driven Engines and Generators. *Nat. Commun.* **2015**, *6*, 7346.

(10) del Barrio, J.; Sánchez-Somolinos, C. Light to Shape the Future: From Photolithography to 4D Printing. *Adv. Opt. Mater.* **2019**, *7*, 1900598.

(11) White, T. J.; Broer, D. J. Programmable and Adaptive Mechanics with Liquid Crystal Polymer Networks and Elastomers. *Nat. Mater.* **2015**, *14*, 1087−1098.

(12) Boelke, J.; Hecht, S. Designing Molecular Photoswitches for Soft Materials Applications. *Adv. Opt. Mater.* **2019**, *7*, 1900404.

(13) Lancia, F.; Ryabchun, A.; Katsonis, N. Life-like Motion Driven by Artificial Molecular Machines. *Nat. Rev. Chem.* **2019**, *3*, 536−551.

(14) Ahn, S. K.; Ware, T. H.; Lee, K. M.; Tondiglia, V. P.; White, T. J. Photoinduced Topographical Feature Development in Blueprinted Azobenzene-Functionalized Liquid Crystalline Elastomers. *Adv. Funct. Mater.* **2016**, *26*, 5819−5826.

(15) Ube, T.; Ikeda, T. Photomobile Polymer Materials with Complex 3D Deformation, Continuous Motions, Self-Regulation, and Enhanced Processability. *Adv. Opt. Mater.* **2019**, *7*, 1900380.

(16) Dong, L.; Zhao, Y. Photothermally Driven Liquid Crystal Polymer Actuators. *Mater. Chem. Front.* **2018**, *2*, 1932−1943.

(17) Liu, L.; Liu, M. H.; Deng, L. L.; Lin, B. P.; Yang, H. Near-Infrared Chromophore Functionalized Soft Actuator with Ultrafast Photoresponsive Speed and Superior Mechanical Property. *J. Am. Chem. Soc.* **2017**, *139*, 11333−11336.

(18) Pilz Da Cunha, M.; Van Thoor, E. A. J.; Debije, M. G.; Broer, D. J.; Schenning, A. P. H. J. Unravelling the Photothermal and Photomechanical Contributions to Actuation of Azobenzene-Doped Liquid Crystal Polymers in Air and Water. *J. Mater. Chem. C* **2019**, *7*, 13502−13509.

(19) Zhang, H.; Mourran, A.; Möller, M. Dynamic Switching of Helical Microgel Ribbons. *Nano Lett.* **2017**, *17*, 2010−2014.

(20) Verpaalen, R. C. P.; Pilz da Cunha, M.; Engels, T. A. P.; Debije, M. G.; Schenning, A. P. H. J. Liquid Crystal Networks on Thermoplastics: Reprogrammable Photo-Responsive Actuators. *Angew. Chem., Int. Ed.* **2020**, *59*, 4532−4536.

(21) Zuo, B.; Wang, M.; Lin, B. P.; Yang, H. Visible and Infrared Three-Wavelength Modulated Multi-Directional Actuators. *Nat. Commun.* **2019**, *10*, 4539.

(22) Palagi, S.; Mark, A. G.; Reigh, S. Y.; Melde, K.; Qiu, T.; Zeng, H.; Parmeggiani, C.; Martella, D.; Sanchez-Castillo, A.; Kapernaum, N.; Giesselmann, F.; Wiersma, D. S.; Lauga, E.; Fischer, P. Structured Light Enables Biomimetic Swimming and Versatile Locomotion of Photoresponsive Soft Microrobots. *Nat. Mater.* **2016**, *15*, 647−653.

(23) Wani, O. M.; Zeng, H.; Priimagi, A. A Light-Driven Artificial Flytrap. *Nat. Commun.* **2017**, *8*, 15546.

(24) Lu, X.; Zhang, H.; Fei, G.; Yu, B.; Tong, X.; Xia, H.; Zhao, Y. Liquid-Crystalline Dynamic Networks Doped with Gold Nanorods Showing Enhanced Photocontrol of Actuation. *Adv. Mater.* **2018**, *30*, 1706597.

(25) Serak, S.; Tabiryan, N.; Vergara, R.; White, T. J.; Vaia, R. A.; Bunning, T. J. Liquid Crystalline Polymer Cantilever Oscillators Fueled by Light. *Soft Matter* **2010**, *6*, 779−783.

(26) Zeng, H.; Lahikainen, M.; Liu, L.; Ahmed, Z.; Wani, O. M.; Wang, M.; Yang, H.; Priimagi, A. Light-Fuelled Freestyle Self-Oscillators. *Nat. Commun.* **2019**, *10*, 5057.

(27) Gelebart, A. H.; Vantomme, G.; Meijer, B. E. W.; Broer, D. J. Mastering the Photothermal Effect in Liquid Crystal Networks: A General Approach for Self-Sustained Mechanical Oscillators. *Adv. Mater.* **2017**, *29*, 1606712.

(28) Mirvakili, S. M.; Hunter, I. W. Artificial Muscles: Mechanisms, Applications, and Challenges. *Adv. Mater.* **2018**, *30*, 1704407.

(29) Hu, J.; Wang, W.; Yu, H. Endowing Soft Photo-Actuators with Intelligence. *Adv. Intell. Syst.* **2019**, *1*, 1900050.

(30) Van Oosten, C. L.; Corbett, D.; Davies, D.; Warner, M.; Bastiaansen, C. W. M.; Broer, D. J. Bending Dynamics and Directionality Reversal in Liquid Crystal Network Photoactuators. *Macromolecules* **2008**, *41*, 8592−8596.

(31) Zeng, H.; Wasylczyk, P.; Wiersma, D. S.; Priimagi, A. Light Robots: Bridging the Gap between Microrobotics and Photomechanics in Soft Materials. *Adv. Mater.* **2018**, *30*, 1703554.

(32) Jiang, Z. C.; Xiao, Y. Y.; Zhao, Y. Shining Light on Liquid Crystal Polymer Networks: Preparing, Reconfiguring, and Driving Soft Actuators. *Adv. Opt. Mater.* **2019**, *7*, 1900262.

(33) McBride, M. K.; Martinez, A. M.; Cox, L.; Alim, M.; Childress, K.; Beiswinger, M.; Podgorski, M.; Worrell, B. T.; Killgore, J.; Bowman, C. N. A Readily Programmable, Fully Reversible Shape-Switching Material. *Sci. Adv.* **2018**, *4*, No. eaat4634.

(34) McBride, M. K.; Hendrikx, M.; Liu, D.; Worrell, B. T.; Broer, D. J.; Bowman, C. N. Photoinduced Plasticity in Cross-Linked Liquid Crystalline Networks. *Adv. Mater.* **2017**, *29*, 1606509.

(35) Ube, T.; Kawasaki, K.; Ikeda, T. Photomobile Liquid-Crystalline Elastomers with Rearrangeable Networks. *Adv. Mater.* **2016**, *28*, 8212−8217.

(36) Wang, Z.; Tian, H.; He, Q.; Cai, S. Reprogrammable, Reprocessible, and Self-Healable Liquid Crystal Elastomer with Exchangeable Disulfide Bonds. *ACS Appl. Mater. Interfaces* **2017**, *9*, 33119−33128.

(37) Jiang, Z.; Xiao, Y.; Yin, L.; Han, L.; Zhao, Y. Self-Lockable" Liquid Crystalline Diels−Alder Dynamic Network Actuators with Room Temperature Programmability and Solution Reprocessability. *Angew. Chem.* **2020**, *132*, 4955−4961.

(38) Jiang, Z. C.; Xiao, Y. Y.; Tong, X.; Zhao, Y. Selective Decrosslinking in Liquid Crystal Polymer Actuators for Optical Reconfiguration of Origami and Light-Fueled Locomotion. *Angew. Chem., Int. Ed.* **2019**, *58*, 5332−5337.

(39) Lahikainen, M.; Zeng, H.; Priimagi, A. Reconfigurable Photoactuator through Synergistic Use of Photochemical and Photothermal Effects. *Nat. Commun.* **2018**, *9*, 4148.

(40) Nie, H.; Self, J. L.; Kuenstler, A. S.; Hayward, R. C.; Read de A] aniz, J. Multiaddressable Photochromic Architectures: From Molecules to Materials. *Adv. Opt. Mater.* **2019**, *7*, 1900224.

(41) Goulet-Hanssens, A.; Eisenreich, F.; Hecht, S. Enlightening Materials with Photoswitches. *Adv. Mater.* **2020**, *32*, 1905966.

(42) Van Oosten, C. L.; Bastiaansen, C. W. M.; Broer, D. J. Printed Artificial Cilia from Liquid-Crystal Network Actuators Modularly Driven by Light. *Nat. Mater.* **2009**, *8*, 677−682.

(43) Yu, Y.; Nakano, M.; Ikeda, T. Directed Bending of a Polymer Film by Light. *Nature* **2003**, *425*, 145.

(44) Iamsaard, S.; Anger, E.; Aßhoff, S. J.; Depauw, A.; Fletcher, S. P.; Katsonis, N. Fluorinated Azobenzenes for Shape-Persistent Liquid Crystal Polymer Networks. *Angew. Chem., Int. Ed.* **2016**, *55*, 9908−9912.

(45) Ryabchun, A.; Li, Q.; Lancia, F.; Aprahamian, I.; Katsonis, N. Shape-Persistent Actuators from Hydrazone Photoswitches. *J. Am. Chem. Soc.* **2019**, *141*, 1196−1200.

(46) Herder, M.; Schmidt, B. M.; Grubert, L.; Pätzel, M.; Schwarz, J.; Hecht, S. Improving the Fatigue Resistance of Diarylethene Switches. *J. Am. Chem. Soc.* **2015**, *137*, 2738−2747.

(47) Frigoli, M.; Welch, C.; Mehl, G. H. Design of Mesomorphic Diarylethene-Based Photochromes. *J. Am. Chem. Soc.* **2004**, *126*, 15382−15383.

(48) Leydecker, T.; Herder, M.; Pavlica, E.; Bratina, G.; Hecht, S.; Orgiu, E.; Samorì, P. Flexible Non-Volatile Optical Memory Thin-Film Transistor Device with over 256 Distinct Levels Based on an Organic Bicomponent Blend. *Nat. Nanotechnol.* **2016**, *11*, 769−775.

(49) Van Oosten, C. L.; Harris, K. D.; Bastiaansen, C. W. M.; Broer, D. J. Glassy Photomechanical Liquid-Crystal Network Actuators for Microscale Devices. *Eur. Phys. J. E: Soft Matter Biol. Phys.* **2007**, *23*, 329−336.

(50) De Haan, L. T.; Schenning, A. P. H. J.; Broer, D. J. Programmed Morphing of Liquid Crystal Networks. *Polymer* **2014**, *55*, 5885−5896.

(51) Van Nostrum, C. F.; Nolte, R. J. M.; Broer, D. J.; Fuhrman, T.; Wendorff, J. H. Photoinduced Opposite Diffusion of Nematic and Isotropie Monomers during Patterned Photopolymerization. *Chem. Mater.* **1998**, *10*, 135−145.

(52) Mamiya, J. I.; Kuriyama, A.; Yokota, N.; Yamada, M.; Ikeda, T. Photomobile Polymer Materials: Photoresponsive Behavior of Cross-Linked Liquid-Crystalline Polymers with Mesomorphic Diarylethenes. *Chem. - Eur. J.* **2015**, *21*, 3174−3177.

(53) Irie, M.; Fukaminato, T.; Matsuda, K.; Kobatake, S. Photochromism of Diarylethene Molecules and Crystals: Memories, Switches, and Actuators. *Chem. Rev.* **2014**, *114*, 12174−12277.

(54) Kumar, K.; Schenning, A. P. H. J.; Broer, D. J.; Liu, D. Regulating the Modulus of a Chiral Liquid Crystal Polymer Network by Light. *Soft Matter* **2016**, *12*, 3196−3201.

(55) Shimamura, A.; Priimagi, A.; Mamiya, J.; Ikeda, T.; Yu, Y.; Barrett, C. J.; Shishido, A. Simultaneous Analysis of Optical and Mechanical Properties of Cross-Linked Azobenzene-Containing Liquid-Crystalline Polymer Films. *ACS Appl. Mater. Interfaces* **2011**, *3*, 4190−4196.

(56) Lancia, F.; Ryabchun, A.; Nguindjel, A. D.; Kwangmettatam, S.; Katsonis, N. Mechanical Adaptability of Artificial Muscles from Nanoscale Molecular Action. *Nat. Commun.* **2019**, *10*, 4819.

(57) Yamada, M.; Kondo, M.; Mamiya, J. I.; Yu, Y.; Kinoshita, M.; Barrett, C. J.; Ikeda, T. Photomobile Polymer Materials: Towards Light-Driven Plastic Motors. *Angew. Chem., Int. Ed.* **2008**, *47*, 4986−4988.

(58) Kumar, K.; Knie, C.; Bléger, D.; Peletier, M. A.; Friedrich, H.; Hecht, S.; Broer, D. J.; Debije, M. G.; Schenning, A. P. H. J. H. J. A Chaotic Self-Oscillating Sunlight-Driven Polymer Actuator. *Nat. Commun.* **2016**, *7*, 11975.

(59) Vantomme, G.; Gelebart, A. H.; Broer, D. J.; Meijer, E. W. A Four-Blade Light-Driven Plastic Mill Based on Hydrazone Liquid-Crystal Networks. *Tetrahedron* **2017**, *73*, 4963−4967.

(60) Lan, R.; Sun, J.; Shen, C.; Huang, R.; Zhang, Z.; Ma, C.; Bao, J.; Zhang, L.; Wang, L.; Yang, D.; Yang, H. Light-Driven Liquid Crystalline Networks and Soft Actuators with Degree-of-Freedom-Controlled Molecular Motors. *Adv. Funct. Mater.* **2020**, *30*, 2000252.

(61) Gelebart, A. H.; Mulder, D. J.; Vantomme, G.; Schenning, A. P. H. J.; Broer, D. J. A Rewritable, Reprogrammable, Dual Light-Responsive Polymer Actuator. *Angew. Chem., Int. Ed.* **2017**, *56*, 13436−13439.

(62) Gimenez-Pinto, V.; Ye, F.; Mbanga, B.; Selinger, J. V.; Selinger, R. L. B. Modeling Out-of-Plane Actuation in Thin-Film Nematic Polymer Networks: From Chiral Ribbons to Auto-Origami Boxes via Twist and Topology. *Sci. Rep.* **2017**, *7*, 45370.

(63) Kobatake, S.; Takami, S.; Muto, H.; Ishikawa, T.; Irie, M. Rapid and Reversible Shape Changes of Molecular Crystals on Photo-irradiation. *Nature* **2007**, *446*, 778−781.

(64) Kitagawa, D.; Tsujioka, H.; Tong, F.; Dong, X.; Bardeen, C. J.; Kobatake, S. Control of Photomechanical Crystal Twisting by Illumination Direction. *J. Am. Chem. Soc.* **2018**, *140*, 4208−4212.

(65) Preston, D. J.; Rothemund, P.; Jiang, H. J.; Nemitz, M. P.; Rawson, J.; Suo, Z.; Whitesides, G. M. Digital Logic for Soft Devices. *Proc. Natl. Acad. Sci. U. S. A.* **2019**, *116*, 7750−7759.

(66) Duncan, P. N.; Nguyen, T. V.; Hui, E. E. Pneumatic Oscillator Circuits for Timing and Control of Integrated Microfluidics. *Proc. Natl. Acad. Sci. U. S. A.* **2013**, *110*, 18104−18109.

(67) Zhang, X.; Soh, S. Performing Logical Operations with Stimuli-Responsive Building Blocks. *Adv. Mater.* **2017**, *29*, 1606483.

(68) Qi, Z.; Malo De Molina, P.; Jiang, W.; Wang, Q.; Nowosinski, K.; Schulz, A.; Gradzielski, M.; Schalley, C. A. Systems Chemistry: Logic Gates Based on the Stimuli-Responsive Gel-Sol Transition of a Crown Ether-Functionalized Bis(Urea) Gelator. *Chem. Sci.* **2012**, *3*, 2073−2082.

(69) Komatsu, H.; Matsumoto, S.; Tamaru, S.-i.; Kaneko, K.; Ikeda, M.; Hamachi, I. Supramolecular Hydrogel Exhibiting Four Basic Logic Gate Functions to Fine-Tune Substance Release. *J. Am. Chem. Soc.* **2009**, *131*, 5580−5585.

PUBLICATION
V

**Reconfiguring Gaussian Curvature of Hydrogel Sheets with
Photoswitchable Host-Guest Interactions**

Kuenstler, A.S.; Lahikainen, M; Zhou, H.; Xu, W.; Priimagi, A.; Hayward, R.C.

Letter

Reconfiguring Gaussian Curvature of Hydrogel Sheets with Photoswitchable Host−Guest Interactions

Alexa S. Kuenstler,[§] Markus Lahikainen,[§] Hantao Zhou, Wenwen Xu, Arri Priimagi,* and Ryan C. Hayward*

Read Online

ACCESS | Metrics & More | Article Recommendations | SI Supporting Information

ABSTRACT: Photoinduced shape morphing has implications in fields ranging from soft robotics to biomedical devices. Despite considerable effort in this area, it remains a challenge to design materials that can be both rapidly deployed and reconfigured into multiple different three-dimensional forms, particularly in aqueous environments. In this work, we present a simple method to program and rewrite spatial variations in swelling and, therefore, Gaussian curvature in thin sheets of hydrogels using photoswitchable supramolecular complexation of azobenzene pendent groups with dissolved α-cyclodextrin. We show that the extent of swelling can be programmed via the proportion of azobenzene isomers, with a 60% decrease in areal swelling from the all *trans* to the predominantly *cis* state near room temperature. The use of thin gel sheets provides fast response times in the range of a few tens of seconds, while the shape change is persistent in the absence of light thanks to the slow rate of thermal *cis−trans* isomerization. Finally, we demonstrate that a single gel sheet can be programmed with a first swelling pattern via spatially defined illumination with ultraviolet light, then erased with white light, and finally redeployed with a different swelling pattern.

365 nm ↕ > 430 nm
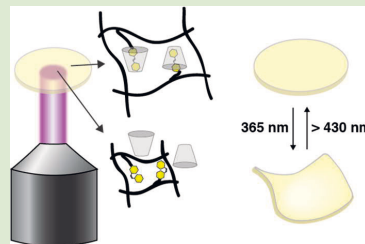
Stimuli-responsive hydrogels offer diverse applications ranging from biomedical devices[1] to soft actuators.[2] By introducing inhomogeneous in-plane swelling profiles, thin gel sheets can be programmed to buckle into shapes with essentially arbitrary distributions of Gaussian curvature, providing great flexibility for the design of targeted three-dimensional (3D) shapes.[3−5] However, the majority of work to date has focused on transformation through closely related families of shapes that are permanently programmed into the material through variations in cross-link density,[6−10] alignment of anisotropic inclusions,[11,12] or the presence of nonswelling components,[13,14] and it remains a challenge to rationally design stimuli-responsive hydrogel platforms that are amenable to adopting multiple distinct 3D configurations.[15,16]

To enable rewritable shape changes, the incorporation of photoresponsive species offers an attractive means to prescribe complex morphogenesis with a high degree of spatiotemporal control. While photothermal moieties such as carbon materials[17−19] and gold nanoparticles[20−25] have been exploited for photopatterned deswelling of thermoresponsive gels, the use of photochemical additives would offer advantages in terms of shape persistence and improved patterning resolution, due to the absence of thermal broadening and heat dissipation inherent to photothermal responses.[26] Though photochemically addressable hydrogel systems are predicted to enable robust reconfigurable shape change,[27,28] experimental demonstrations have been limited. The most promising approach to date has relied on spiropyran derivatives, where photoreversible ring-opening and -closing reactions drive large changes in hydro-

philicity and thus swelling.[29−32] However, realization of robust photochemical responses has been complicated by narrow pH operational ranges and photoswitching fatigue in these systems.
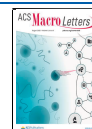
Within the broader field of photoactive soft materials, azobenzene is among the most widely employed photoswitches because it isomerizes robustly over many cycles and is highly tunable in both its absorption characteristics and thermal relaxation kinetics.[33] While azobenzene chromophores are routinely used in ordered polymer systems such as liquid crystal networks to impart large shape changes,[34,35] their effect is typically less dramatic in hydrogels and dependent on how the photoswitch is incorporated. For example, azobenzene pendent groups have been shown to drive modest isomerization-induced increases in swelling[36−38] due to the greater polarity of the *cis* isomer,[39] while azobenzene cross-linkers yielded the opposite effect.[40,41]

To enable photochemical shape morphing of hydrogels, we consider here reversible host−guest interactions with α-cyclodextrin (α-CD), wherein *trans*-azobenzene inserts into the hydrophobic cavity of α-CD while the *cis*-isomer is expelled.[42] Using this scheme, azobenzene- and α-CD-function-

alized hydrogels have been used to drive substantial volumetric changes[43−46] through on-demand changes in cross-link density. However, this work has been limited to thick gels where moderate light penetration, slow cross-linking kinetics, and diffusion-limited mass transport result in modest shape changes. As an alternative approach, α-CD complexes with *trans*-azobenzene are much more hydrophilic than free *cis*-azobenzene, providing a simple way to modulate macromolecular hydrophilicity, an effect that has been widely exploited to tune the solubility of linear macromolecules[47−49] but so far not employed for shape-programmable materials.

Herein, we introduce a facile approach to photoresponsive gels with rewritable Gaussian curvature by employing localized changes in hydrophobicity using azobenzene-functionalized poly(*N*-isopropylacrylamide) (PNIPAm) gels containing free α-CD units. Photoisomerization of azobenzene under UV light is used to impose a swelling pattern, and therefore a 3D shape, in thin gel sheets by breaking host−guest complexes. Subsequent exposure to visible light drives reisomerization to the *trans*-isomer and restoration of host−guest complexes, enabling a new 3D shape to be programmed through subsequent exposure to a different pattern of UV light, allowing for rapid and reconfigurable shape change.

Light-responsive gels are synthesized by copolymerization of *N*-isopropylacrylamide (NIPAm) and *N,N′*-methylenebis-(acrylamide) with 4-acrylamidoazobenzene (see Supporting Information for details) by free-radical polymerization to form poly(NIPAm-*co*-azobenzene) hydrogels (Scheme 1). Briefly,

Scheme 1. Synthesis of Light-Responsive Gels
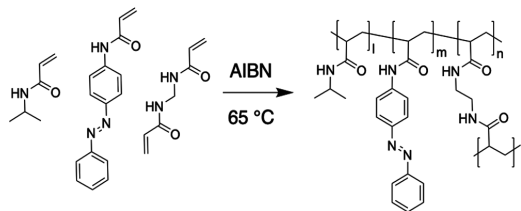
the monomer components are mixed with 5:1 tetrahydrofuran (THF):H$_2$O and purged with nitrogen. Next, the pregel solution is infiltrated between two glass slides separated by 25 μm and heated to 65 °C overnight to polymerize. Following synthesis, gels are swollen sequentially in fresh solutions of 5:1 THF:H$_2$O and deionized H$_2$O to remove unreacted monomers. After thermal equilibration in the dark, azobenzene units in the gel are in the *trans* form, and upon immersion in an aqueous solution of 15.4 mM of α-CD, gels are observed to rapidly (within tens of seconds) increase in area by ≈1.8 times. This change in size is attributed to an increase in gel hydrophilicity as the hydrophobic inner cavity of α-CD complexes with azobenzene via a host−guest interaction, leaving the hydrophilic outer portion of α-CD to interface with the surrounding water.[43]

The photoresponsive properties of the gels are studied using UV−vis spectroscopy. Initially, azobenzene units in thermally equilibrated gels are in the *trans* form as indicated by the strong π,π^* peak centered at 360 nm and a weak n,π^* at 430 nm (Figure 1A, black curve). Upon illumination with 50 mW cm^{-2} of 365 nm light, the azobenzene units are observed to switch from *trans* to *cis* and achieve a photostationary state (PSS) of >70% of *cis*, as evidenced by a decrease in intensity and blue shift of the π,π^*
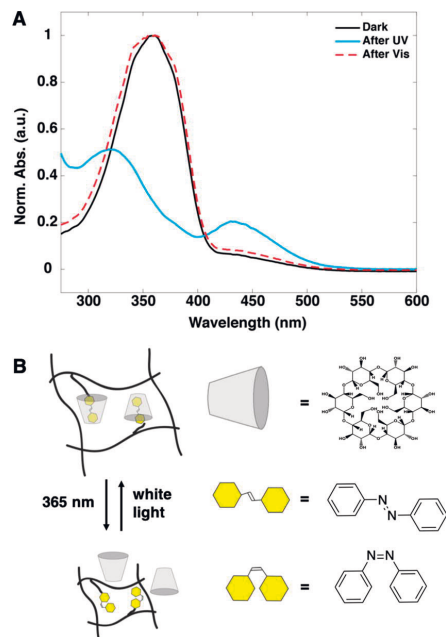

Figure 1. (A) UV−vis absorption spectra of the azobenzene-CD gel before (black) and after UV exposure (blue). The original state can be restored upon white-light exposure (red). (B) Schematic of reversible supramolecular complexation between azobenzene and α-CD in thin gel sheets upon *cis−trans* isomerization, leading to reversible changes in swelling.

peak and an increase in intensity of the n,π^* peak (Figure 1A, blue curve). While quantitative isomerization is limited by the overlap of the *cis* and *trans* spectra, the extinction coefficient at 365 nm decreases by a factor of 5 upon *trans−cis* isomerization (Figure S2). This results in an increase in the penetration depth of the gel at 365 nm from 13 to 67 μm, facilitating relatively uniform absorption through the sample thickness (25 μm) and a high *cis* content at the PSS. Isomerization is accompanied by the decrease of α-CD affinity for azobenzene due to the change in azobenzene geometry, which expels the chromophore from the α-CD cavity (Figure 1B), as previously characterized by several groups. For example, in systems where both azobenzene and α-CD are incorporated into polymer chains, the binding constant decreases from 2000 M^{-1} to 35 M^{-1} for α-CD-*trans*-azobenzene and α-CD-*cis*-azobenzene, respectively,[50] though the exact binding constants can vary based on the chemical details.[51] Additionally, isomerization is reversible by illumination with visible light (Figure 1A, red dashed curve), allowing for the formation and destruction of supramolecular complexes on demand.

The effect of photoisomerization on swelling is first investigated at room temperature under flood illumination with 50 mW cm^{-2} of 365 nm light. Prior to illumination, the gel is equilibrated in the dark to maximize *trans*-isomer content and is initially flat in the fully swollen state. When exposed to 365 nm light, the gel is observed to rapidly deswell, reaching equilibrium in ≈30 s (Video S1). The area of the gel following light exposure is reduced by ≈50% (Figure 2A), indicating that azobenzene isomerizes nearly uniformly through the thickness of the sample,
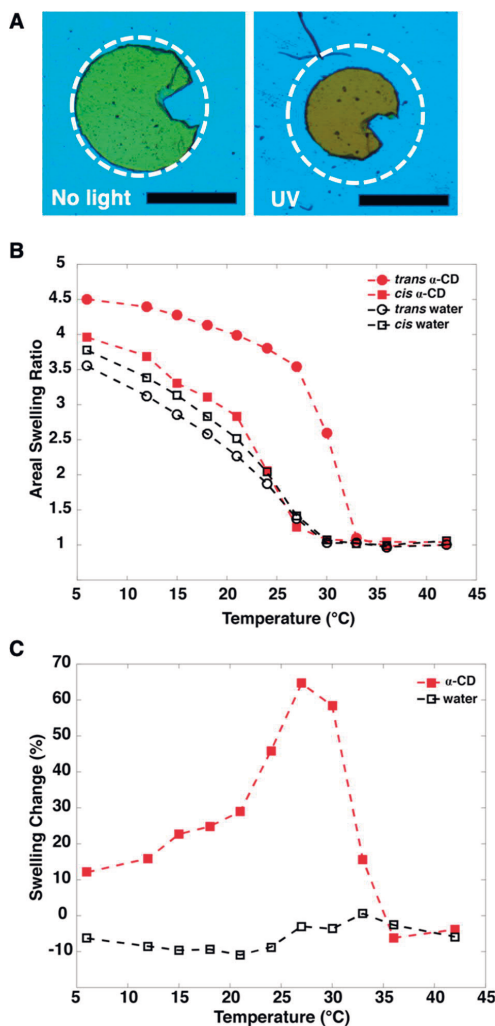
Figure 2. (A) Optical micrographs of gels with predominantly *trans*-azobenzene (left) and after photoisomerization with 365 nm light to >70% *cis*-azobenzene (right) at room temperature. Scale bar: 1 mm. (B) Equilibrium areal swelling ratios of hydrogels in pure water (black) and aqueous α-CD solution (red) as a function of temperature under different illumination conditions. While increased *cis* content slightly increases the equilibrium swelling compared to *trans* in pure water, host–guest complexation of *trans*-azobenzene with α-CD dramatically increases the swelling. (C) The percentage change in areal swelling for gels at the PSS compared to *trans* samples shows a maximum increase of ≈60%, and a 50% increase near room temperature, in α-CD solutions. Conversely, gels in deionized water show an ≈10% decrease in swelling near room temperature upon isomerization.

thickness of the gel at the PSS. Based on a typical poroelastic diffusion coefficient of $D = 1-3 \times 10^{-11}$ m^2 s^{-1},[52] the characteristic diffusion time for this system can be estimated as $\tau \approx h^2 D^{-1} \approx 20-60$ s, in close agreement with the deswelling time observed. However, this is also comparable to the time scale to reach the PSS for the light intensity used. Thus, the similar time scales coupled with the observation of transient bending under uniform illumination suggest that the deformation kinetics reflect contributions of both photoisomerization and mass transport.

To investigate how changes in isomer population—and thus supramolecular complexation—influence temperature-dependent swelling, gels are uniformly exposed to flood illumination in a bath of α-CD solution (15.4 mM) and held at a constant temperature ranging from 6 to 42 °C (Figure 2B,C). Areal swelling changes as a function of temperature and light exposure are measured by recording optical micrographs, and the areal swelling ratio is defined as the area of the gel at a given temperature normalized by the area of the gel at 42 °C. Prior to illumination, gels equilibrated in the dark show a gradual deswelling upon heating to 26 °C, followed by a sharp transition and gradual deswelling to a constant area by 42 °C (Figure 2B, filled red circles). This behavior is consistent with the classical behavior of PNIPAm gels that display lower critical solution temperature (LCST) phase behavior.[53] However, upon exposure to UV light, photoisomerization to a *cis*-rich PSS, and concomitant destruction of host–guest complexes dramatically alter the swelling characteristics due to the resulting increase in hydrophobicity that has been previously characterized by changes in water contact angle.[54] Illumination with 365 nm light (Figure 2B, filled red squares) results in a reduced extent of swelling and a shift of the deswelling transition to lower temperatures with an increased breadth of the volume transition as the concentration of *cis* isomers increases and the azobenzene–α-CD complexes are destroyed. This behavior is similar to how the choice of hydrophobic comonomer can be used to tune the swelling transition in nonphotoactive PNIPAm gels[55] and is consistent with observations in linear poly(NIPAm-*co*-azobenzene) polymers, where the LCST shifts to lower temperature upon decomplexation of azobenzene and cyclodextrin.[56] We note that this change in swelling is due to the destruction of α-CD complexes with *trans*-azobenzene and not simply due to changes in the *trans*–*cis* isomer population, which are nearly identical in both DI water and α-CD solution (Figure S4). We verify this by control experiments in deionized water, which show only a small increase (≈5%) in swelling upon *trans*–*cis* isomerization due to the moderate increase in polarity of the *cis*-isomer (Figure 2B, black curves; Figure 2C, black).[39,57] Additionally, prior work has shown that α-CD does not complex significantly with NIPAm side chains,[58] and thus it is expected that the changes in swelling are primarily dictated by azobenzene-CD complexation. Notably, the change in swelling is maximized near room temperature, with an increase in in-plane areal swelling by 50–60% relative to samples in the *trans* state (Figure 2C, red), making these materials well-suited for deployment at ambient temperatures. We note that while deformation of azo-based materials is often driven by a combination of photochemical and photothermal effects[59,60] efficient photoisomerization as monitored by UV–vis and the persistence of deswelling upon the removal of illumination indicate that volume changes in our system are due to photochemical—and not photothermal—effects.

a consequence of the fact that the penetration depth at the PSS (67 μm) is greater than the film thickness (25 μm). Notably, the sample transiently bends during the initial stages of illumination before returning to a flat state (Figure S3), consistent with an isomerization-induced increase in penetration depth that ultimately allows for nearly uniform isomerization through the
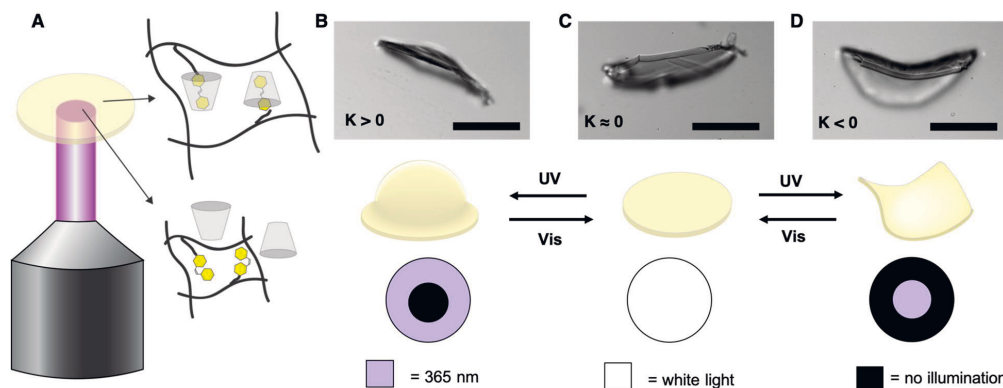
Figure 3. (A) Maskless lithography is used to locally pattern azobenzene isomerization—and therefore supramolecular complexation with α-CD— using patterns of UV light. The resulting differences in gel swelling provide a programmed shape change with Gaussian curvature K that can be erased by subsequent exposure to white light and then reprogrammed using another pattern of UV light. (B–D) Photographs of gels (top), cartoon schematic (middle), and corresponding illumination pattern (bottom). Scale bar: 1 mm.

To probe the utility of photoinduced deswelling in shape morphing, gels are illuminated with 50 mW cm^{-2} UV light patterned by a digital micromirror array and projected onto an immersed sample through an inverted microscope objective (Figure 3A). When 365 nm light is patterned in a circular annulus and projected onto a gel disk such that the center remains unilluminated, deswelling at the edges results in buckling out-of-plane into a spherical cap-like shape with positive Gaussian curvature to accommodate the in-plane strain differential (Figure 3B). Unlike photothermal systems, where gels reswell upon removal of light as heat is dissipated,[61] these gels retain their shape when illumination stops because of the long thermal relaxation time of the *cis*-isomer, which is ≈15 h at room temperature (Figure S5). Thus, even in the absence of illumination, host–guest complexes remain dissociated following light exposure. However, the gel can be returned to its initial flat state by restoring host–guest interactions via *cis–trans* photoisomerization with exposure to white light of total intensity 1.2 W cm^{-2} (with ≈100 mW cm^{-2} across the wavelengths corresponding to the n,π* transition of the *cis* isomer) for 60 s to ensure full *cis–trans* isomerization (Figure 3C). Then, the gel can be reprogrammed into another shape by shining a different pattern of UV light. For example, by patterning the gel with localized deswelling in the center of the film, a saddle-like shape with negative Gaussian curvature is formed (Figure 3C). While either type of deformation can easily be achieved with a given sample in previously reported photo-cross-linkable and photopatternable gel systems,[4] those platforms are limited to reversible transformations between preprogrammed states. In contrast, the current method allows for multiple shape transformations to be programmed and reprogrammed in a single material without the need for complex chemical reprogramming processes like ionic printing,[15] nano-particle reduction,[62] or acid–base treatment[63] as reported previously.

In summary, we have developed a simple method to pattern and deploy photoactive gels using reversible host–guest complexes. Specifically, the extent of swelling can be controlled by the isomer population of incorporated azobenzene photo-switches, thereby controlling gel hydrophilicity through *trans*-azobenzene complexation with α-cyclodextrin. Furthermore,

localized deswelling can be exploited to control Gaussian curvature using photolithographic patterning, and a single gel can be rewritten through sequential exposure to white and UV light. While Gaussian curvature was the topic of this study, this strategy could feasibly be extended to control both the Gaussian and mean curvature of a gel simultaneously through judicious selection of light intensity, wavelength, and spatial distribution. Finally, operation at room temperature with biocompatible components makes this materials platform particularly promising for use in biological systems for drug delivery or tissue engineering.

■ ASSOCIATED CONTENT

Ⓢ Supporting Information

The Supporting Information is available free of charge at https://pubs.acs.org/doi/10.1021/acsmacrolett.0c00469.

> Synthesis protocol, experimental and characterization methods, and additional UV–vis spectra (PDF)

> Video of deswelling of a gel at 22 °C in α-CD solution under flood UV illumination. Playback is at 1× speed (MP4)

■ AUTHOR INFORMATION

Corresponding Authors

Ryan C. Hayward — *Department of Polymer Science and Engineering, University of Massachusetts Amherst, Amherst, Massachusetts 01003, United States;* ◉ orcid.org/0000-0001-6483-2234; Email: hayward@umass.edu

Arri Priimagi — *Smart Photonic Materials, Faculty of Engineering and Natural Sciences, Tampere University, Tampere, Finland;* ◉ orcid.org/0000-0002-5945-9671; Email: arri.priimagi@tuni.fi

Authors

Alexa S. Kuenstler — *Department of Polymer Science and Engineering, University of Massachusetts Amherst, Amherst, Massachusetts 01003, United States*

Markus Lahikainen — *Smart Photonic Materials, Faculty of Engineering and Natural Sciences, Tampere University, Tampere, Finland;* ◉ orcid.org/0000-0002-4891-5352

Hantao Zhou − *Department of Polymer Science and Engineering, University of Massachusetts Amherst, Amherst, Massachusetts 01003, United States*

Wenwen Xu − *Department of Polymer Science and Engineering, University of Massachusetts Amherst, Amherst, Massachusetts 01003, United States*

Complete contact information is available at:
https://pubs.acs.org/10.1021/acsmacrolett.0c00469

Author Contributions

[§]A.S.K. and M.L. contributed equally

Notes

The authors declare no competing financial interest.

■ REFERENCES

(1) Brown, T. E.; Anseth, K. S. Spatiotemporal Hydrogel Biomaterials for Regenerative Medicine. *Chem. Soc. Rev.* **2017**, *46* (21), 6532−6552.

(2) Ionov, L. Hydrogel-Based Actuators: Possibilities and Limitations. *Mater. Today* **2014**, *17* (10), 494−503.

(3) Sharon, E.; Efrati, E. The Mechanics of Non-Euclidean Plates. *Soft Matter* **2010**, *6* (22), 5693−5704.

(4) Jeon, S. J.; Hauser, A. W.; Hayward, R. C. Shape-Morphing Materials from Stimuli-Responsive Hydrogel Hybrids. *Acc. Chem. Res.* **2017**, *50* (2), 161−169.

(5) Erol, O.; Pantula, A.; Liu, W.; Gracias, D. H. Transformer Hydrogels: A Review. *Adv. Mater. Technol.* **2019**, *4* (4), 1−27.

(6) Klein, Y.; Efrati, E.; Sharon, E. Shaping of Elastic Sheets by Prescription of Non-Euclidean Metrics. *Science* **2007**, *315* (5815), 1116−1120.

(7) Wu, Z. L.; Moshe, M.; Greener, J.; Therien-Aubin, H.; Nie, Z.; Sharon, E.; Kumacheva, E. Three-Dimensional Shape Transformations of Hydrogel Sheets Induced by Small-Scale Modulation of Internal Stresses. *Nat. Commun.* **2013**, *4* (1), 1−7.

(8) Kim, J.; Hanna, J. a.; Byun, M.; Santangelo, C. D.; Hayward, R. C. Designing Responsive Buckled Surfaces by Halftone Gel Lithography. *Science* **2012**, *335* (6073), 1201−1205.

(9) Zhou, Y.; Duque, C. M.; Santangelo, C. D.; Hayward, R. C. Biasing Buckling Direction in Shape-Programmable Hydrogel Sheets with Through-Thickness Gradients. *Adv. Funct. Mater.* **2019**, *29* (48), 1905273.

(10) Nojoomi, A.; Arslan, H.; Lee, K.; Yum, K. Bioinspired 3D Structures with Programmable Morphologies and Motions. *Nat. Commun.* **2018**, *9* (1), 1−11.

(11) Sydney Gladman, A.; Matsumoto, E. A.; Nuzzo, R. G.; Mahadevan, L.; Lewis, J. A. Biomimetic 4D Printing. *Nat. Mater.* **2016**, *15* (4), 413−418.

(12) Huang, L.; Jiang, R.; Wu, J.; Song, J.; Bai, H.; Li, B.; Zhao, Q.; Xie, T. Ultrafast Digital Printing toward 4D Shape Changing Materials. *Adv. Mater.* **2017**, *29* (7), 1605390.

(13) Thérien-Aubin, H.; Moshe, M.; Sharon, E.; Kumacheva, E. Shape Transformations of Soft Matter Governed by Bi-Axial Stresses. *Soft Matter* **2015**, *11* (23), 4600−4605.

(14) Wang, Z. J.; Hong, W.; Wu, Z. L.; Zheng, Q. Site-Specific Pre-Swelling-Directed Morphing Structures of Patterned Hydrogels. *Angew. Chem., Int. Ed.* **2017**, *56* (50), 15974−15978.

(15) Palleau, E.; Morales, D.; Dickey, M. D.; Velev, O. D. Reversible Patterning and Actuation of Hydrogels by Electrically Assisted Ionoprinting. *Nat. Commun.* **2013**, *4* (1), 1−7.

(16) Yu, C.; Duan, Z.; Yuan, P.; Li, Y.; Su, Y.; Zhang, X.; Pan, Y.; Dai, L. L.; Nuzzo, R. G.; Huang, Y.; et al. Electronically Programmable, Reversible Shape Change in Two- and Three-Dimensional Hydrogel Structures. *Adv. Mater.* **2013**, *25* (11), 1541−1546.

(17) Wang, E.; Desai, M. S.; Lee, S. W. Light-Controlled Graphene-Elastin Composite Hydrogel Actuators. *Nano Lett.* **2013**, *13* (6), 2826−2830.

(18) Zhang, X.; Pint, C. L.; Lee, M. H.; Schubert, B. E.; Jamshidi, A.; Takei, K.; Ko, H.; Gillies, A.; Bardhan, R.; Urban, J. J.; et al. Optically- and Thermally-Responsive Programmable Materials Based on Carbon Nanotube-Hydrogel Polymer Composites. *Nano Lett.* **2011**, *11* (8), 3239−3244.

(19) Ma, C.; Le, X.; Tang, X.; He, J.; Xiao, P.; Zheng, J.; Xiao, H.; Lu, W.; Zhang, J.; Huang, Y.; et al. A Multiresponsive Anisotropic Hydrogel with Macroscopic 3D Complex Deformations. *Adv. Funct. Mater.* **2016**, *26* (47), 8670−8676.

(20) Zhu, Z.; Senses, E.; Akcora, P.; Sukhishvili, S. A. Programmable Light-Controlled Shape Changes in Layered Polymer Nanocomposites. *ACS Nano* **2012**, *6* (4), 3152−3162.

(21) Kim, H.; Kang, J.; Zhou, Y.; Kuenstler, A. S.; Kim, Y.; Chen, C.; Emrick, T.; Hayward, R. C. Light-Driven Shape Morphing, Assembly, and Motion of Nanocomposite Gel Surfers. *Adv. Mater.* **2019**, *31* (27), 1900932.

(22) Mourran, A.; Zhang, H.; Vinokur, R.; Moller, M. Soft Microrobots Employing Nonequilibrium Actuation via Plasmonic Heating. *Adv. Mater.* **2017**, *29* (2), 1604825.

(23) Shi, Q.; Xia, H.; Li, P.; Wang, Y. S.; Wang, L.; Li, S. X.; Wang, G.; Lv, C.; Niu, L. G.; Sun, H. B. Photothermal Surface Plasmon Resonance and Interband Transition-Enhanced Nanocomposite Hydrogel Actuators with Hand-Like Dynamic Manipulation. *Adv. Opt. Mater.* **2017**, *5* (22), 1−9.

(24) Sutton, A.; Shirman, T.; Timonen, J. V. I.; England, G. T.; Kim, P.; Kolle, M.; Ferrante, T.; Zarzar, L. D.; Strong, E.; Aizenberg, J. Photothermally Triggered Actuation of Hybrid Materials as a New Platform for in Vitro Cell Manipulation. *Nat. Commun.* **2017**, *8* (1), 1−13.

(25) Guo, H.; Liu, Y.; Yang, Y.; Wu, G.; Demella, K.; Raghavan, S. R.; Nie, Z. A Shape-Shifting Composite Hydrogel Sheet with Spatially Patterned Plasmonic Nanoparticles. *J. Mater. Chem. B* **2019**, *7* (10), 1679−1683.

(26) Kuenstler, A. S.; Hayward, R. C. Light-Induced Shape Morphing of Thin Films. *Curr. Opin. Colloid Interface Sci.* **2019**, *40*, 70−86.

(27) Kuksenok, O.; Balazs, A. C. Modeling the Photoinduced Reconfiguration and Directed Motion of Polymer Gels. *Adv. Funct. Mater.* **2013**, *23* (36), 4601−4610.

(28) Dehghany, M.; Zhang, H.; Naghdabadi, R.; Hu, Y. A Thermodynamically-Consistent Large Deformation Theory Coupling Photochemical Reaction and Electrochemistry for Light-Responsive Gels. *J. Mech. Phys. Solids* **2018**, *116* (March), 239−266.

(29) Ziółkowski, B.; Florea, L.; Theobald, J.; Benito-Lopez, F.; Diamond, D. Self-Protonating Spiropyran-Co-NIPAM-Co-Acrylic Acid Hydrogel Photoactuators. *Soft Matter* **2013**, *9* (36), 8754−8760.

(30) Stumpel, J. E.; Ziółkowski, B.; Florea, L.; Diamond, D.; Broer, D. J.; Schenning, A. P. H. J. Photoswitchable Ratchet Surface Topographies Based on Self-Protonating Spiropyran-NIPAAM Hydrogels. *ACS Appl. Mater. Interfaces* **2014**, *6* (10), 7268−7274.

(31) Satoh, T.; Sumaru, K.; Takagi, T.; Kanamori, T. Fast-Reversible Light-Driven Hydrogels Consisting of Spirobenzopyran-Functionalized Poly(N-Isopropylacrylamide). *Soft Matter* **2011**, *7* (18), 8030−8034.

(32) Li, C.; Iscen, A.; Palmer, L. C.; Schatz, G. C.; Stupp, S. I. Light-Driven Expansion of Spiropyran Hydrogels. *J. Am. Chem. Soc.* **2020**, *142* (18), 8447−8453.

(33) Bandara, H. M. D.; Burdette, S. C. Photoisomerization in Different Classes of Azobenzene. *Chem. Soc. Rev.* **2012**, *41* (5), 1809−1825.

(34) Ube, T.; Ikeda, T. Photomobile Polymer Materials with Complex 3D Deformation, Continuous Motions, Self-Regulation, and Enhanced Processability. *Adv. Opt. Mater.* **2019**, *7* (16), 1900380.

(35) White, T. J.; Broer, D. J. Programmable and Adaptive Mechanics with Liquid Crystal Polymer Networks and Elastomers. *Nat. Mater.* **2015**, *14* (11), 1087−1098.

(36) Matsubara, K.; Watanabe, M.; Takeoka, Y. A Thermally Adjustable Multicolor Photochromic Hydrogel. *Angew. Chem., Int. Ed.* **2007**, *46* (10), 1688−1692.

(37) Kamenjicki, M.; Lednev, I. K.; Mikhonin, A.; Kesavamoorthy, R.; Asher, S. A. Photochemically Controlled Photonic Crystals. *Adv. Funct. Mater.* **2003**, *13* (10), 774−780.

(38) Zhang, Q. M.; Li, X.; Islam, M. R.; Wei, M.; Serpe, M. J. Light Switchable Optical Materials from Azobenzene Crosslinked Poly(N-Isopropylacrylamide)-Based Microgels. *J. Mater. Chem. C* **2014**, *2* (34), 6961−6965.

(39) Jiang, W.; Wang, G.; He, Y.; Wang, X.; An, Y.; Song, Y.; Jiang, L. Photo-Switched Wettability on an Electrostatic Self-Assembly Azobenzene Monolayer. *Chem. Commun.* **2005**, *28*, 3550−3552.

(40) Kang, M. S.; Gupta, V. K. Photochromic Cross-Links in Thermoresponsive Hydrogels of Poly(N-Isopropylacrylamide): Enthalpic and Entropic Consequences on Swelling Behavior. *J. Phys. Chem. B* **2002**, *106* (16), 4127−4132.

(41) Mudiyanselage, T. K.; Neckers, D. C. Photochromic Super-absorbent Polymers. *Soft Matter* **2008**, *4* (4), 768−774.

(42) Wang, D.; Zhao, W.; Wei, Q.; Zhao, C.; Zheng, Y. Photo-switchable Azobenzene/Cyclodextrin Host-Guest Complexes: From UV- to Visible/Near-IR-Light-Responsive Systems. *ChemPhotoChem.* **2018**, *2* (5), 403−415.

(43) Harada, A.; Takashima, Y.; Nakahata, M. Supramolecular Polymeric Materials via Cyclodextrin-Guest Interactions. *Acc. Chem. Res.* **2014**, *47* (7), 2128−2140.

(44) Sakai, T.; Murayama, H.; Nagano, S.; Takeoka, Y.; Kidowaki, M.; Ito, K.; Seki, T. Photoresponsive Slide-Ring Gel. *Adv. Mater.* **2007**, *19* (15), 2023−2025.

(45) Takashima, Y.; Hatanaka, S.; Otsubo, M.; Nakahata, M.; Kakuta, T.; Hashidzume, A.; Yamaguchi, H.; Harada, A. Expansion-Contraction of Photoresponsive Artificial Muscle Regulated by Host-Guest Interactions. *Nat. Commun.* **2012**, *3* (1), 1−8.

(46) Zheng, Z.; Hu, J.; Wang, H.; Huang, J.; Yu, Y.; Zhang, Q.; Cheng, Y. Dynamic Softening or Stiffening a Supramolecular Hydrogel by Ultraviolet or Near-Infrared Light. *ACS Appl. Mater. Interfaces* **2017**, *9* (29), 24511−24517.

(47) Zhao, Y.-L.; Stoddart, J. F. Azobenzene-Based Light-Responsive Hydrogel System. *Langmuir* **2009**, *25* (15), 8442−8446.

(48) Tamesue, S.; Takashima, Y.; Yamaguchi, H.; Shinkai, S.; Harada, A. Photoswitchable Supramolecular Hydrogels Formed by Cyclo-dextrins and Azobenzene Polymers. *Angew. Chem., Int. Ed.* **2010**, *49* (41), 7461−7464.

(49) Schmidt, B. V. K. J.; Hetzer, M.; Ritter, H.; Barner-Kowollik, C. Modulation of the Thermoresponsive Behavior of Poly(N,N-Diethylacrylamide) via Cyclodextrin Host/Guest Interactions. *Macromol. Rapid Commun.* **2013**, *34* (16), 1306−1311.

(50) Yamaguchi, H.; Kobayashi, Y.; Kobayashi, R.; Takashima, Y.; Hashidzume, A.; Harada, A. Photoswitchable Gel Assembly Based on Molecular Recognition. *Nat. Commun.* **2012**, *3* (1), 1−5.

(51) Wang, M.; Zhang, X.; Li, L.; Wang, J.; Wang, J.; Ma, J.; Yuan, Z.; Lincoln, S. F.; Guo, X. Photo-Reversible Supramolecular Hydrogels Assembled by α-Cyclodextrin and Azobenzene Substituted Poly-(Acrylic Acid)s: Effect of Substitution Degree, Concentration, and Tethered Chain Length. *Macromol. Mater. Eng.* **2016**, *301* (2), 191−198.

(52) Yoon, J.; Cai, S.; Suo, Z.; Hayward, R. C. Poroelastic Swelling Kinetics of Thin Hydrogel Layers: Comparison of Theory and Experiment. *Soft Matter* **2010**, *6* (23), 6004−6012.

(53) Otake, K.; Inomata, H.; Konno, M.; Saito, S. Thermal Analysis of the Volume Phase Transition with N-Isopropylacrylamide Gels. *Macromolecules* **1990**, *23* (1), 283−289.

(54) Wan, P.; Jiang, Y.; Wang, Y.; Wang, Z.; Zhang, X. Tuning Surface Wettability through Photocontrolled Reversible Molecular Shuttle. *Chem. Commun.* **2008**, No. 44, 5710−5712.

(55) Roy, D.; Brooks, W. L. A.; Sumerlin, B. S. New Directions in Thermoresponsive Polymers. *Chem. Soc. Rev.* **2013**, *42* (17), 7214−7243.

(56) Luo, C.; Zuo, F.; Zheng, Z.; Ding, X.; Peng, Y. Temperature/Light Dual-Responsive Inclusion Complexes of α-Cyclodextrins and Azobenzene-Containing Polymers. *J. Macromol. Sci., Part A: Pure Appl.Chem.* **2008**, *45* (5), 364−371.

(57) Kungwatchakun, D.; Irie, M. Photoresponsive Polymers. Photocontrol of the Phase Separation Temperature of Aqueous Solutions of Poly-[N-isopropylacrylamide-co-N-(4-phenylazophenyl)-Acrylamide]. *Makromol. Chem., Rapid Commun.* **1988**, *9* (4), 243−246.

(58) Ritter, H.; Sadowski, O.; Tepper, E. Influence of Cyclodextrin Molecules on the Synthesis and the Thermoresponsive Solution Behavior of N-Isopropylacrylamide Copolymers with Adamantyl Groups in the Side-Chains. *Angew. Chem., Int. Ed.* **2003**, *42* (27), 3171−3173.

(59) Lee, K. M.; White, T. J. Photochemical Mechanism and Photothermal Considerations in the Mechanical Response of Monodomain, Azobenzene-Functionalized Liquid Crystal Polymer Networks. *Macromolecules* **2012**, *45* (17), 7163−7170.

(60) Lahikainen, M.; Zeng, H.; Priimagi, A. Reconfigurable Photo-actuator through Synergistic Use of Photochemical and Photothermal Effects. *Nat. Commun.* **2018**, *9* (1), 1−8.

(61) Hauser, A. W.; Evans, A. A.; Na, J. H.; Hayward, R. C. Photothermally Reprogrammable Buckling of Nanocomposite Gel Sheets. *Angew. Chem., Int. Ed.* **2015**, *54* (18), 5434−5437.

(62) Guo, H.; Cheng, J.; Yang, K.; Demella, K.; Li, T.; Raghavan, S. R.; Nie, Z. Programming the Shape Transformation of a Composite Hydrogel Sheet via Erasable and Rewritable Nanoparticle Patterns. *ACS Appl. Mater. Interfaces* **2019**, *11* (45), 42654−42660.

(63) Kohlmeyer, R. R.; Buskohl, P. R.; Deneault, J. R.; Durstock, M. F.; Vaia, R. A.; Chen, J. Shape-Reprogrammable Polymers: Encoding, Erasing, and Re-Encoding. *Adv. Mater.* **2014**, *26* (48), 8114−8119.